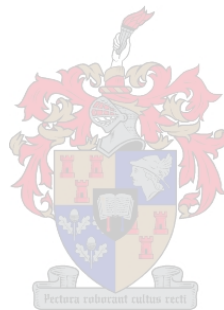# Modern-ocean ground-truthing of planktic foraminifer nitrogen isotopes: A proxy for surface ocean nutrient conditions

Sandi Smart

Dissertation approved for the degree of Doctor of Philosophy in the Faculty of Science at Stellenbosch University

March 2020

Supervisors:
Alakendra N. Roychoudhury, Stellenbosch University
Sarah E. Fawcett, University of Cape Town
Daniel M. Sigman, Princeton University

Co-supervisors & Key Collaborators:
Gerald H. Haug, Max Planck Institute for Chemistry
Ralf Schiebel, Max Planck Institute for Chemistry
Haojia Ren, National Taiwan University
Alfredo Martínez-García, Max Planck Institute for Chemistry

DECLARATION

By submitting this dissertation electronically, I declare that the entirety of the work contained therein is my own, original work, that I am the sole author thereof (save to the extent explicitly otherwise stated), that reproduction and publication thereof by Stellenbosch University will not infringe any third party rights and that I have not previously in its entirety or in part submitted it for obtaining any qualification.

This dissertation includes one original paper published in a peer-reviewed journal and two unpublished publications (one accepted for publication, one in preparation for submission). The development and writing of the papers (published and unpublished) were the principal responsibility of myself and, for each of the cases where this is not the case, a declaration is included in the dissertation indicating the nature and extent of the contributions of co-authors.

i

ABSTRACT

The nitrogen (N) isotope ratios (δ^{15}N) of organic matter trapped within the fossil shells of planktic foraminifera, upper-ocean dwelling zooplankton, are providing a new lens through which to examine the link between biological nutrient drawdown in oceanic surface waters and past global climate. This thesis uses the modern ocean as a testing ground to characterize the controls on the δ^{15}N of living and recently living foraminifera in two contrasting nutrient regimes: the nutrient-poor subtropical North Atlantic and the Southern Ocean, where surface nutrients are never completely consumed. In both environments, no systematic difference between bulk foraminifer tissue and shell-bound δ^{15}N is observed, supporting the use of shell-bound δ^{15}N as an indicator of living foraminifera.

In the nitrate-depleted Sargasso Sea, shallow-dwelling foraminifer species with dinoflagellate (algal) symbionts (average δ^{15}N ~2.3‰) approximate the δ^{15}N of the nitrate supplied to surface waters (2.6‰), while deeper dwellers without dinoflagellates have a higher δ^{15}N (~3.6‰). These findings are consistent with earlier ground-truthing efforts in the low-latitude ocean, implicating host-symbiont recycling of low δ^{15}N ammonium. Comparison between upper-ocean (living), mid-depth (sinking) and seafloor (recently deposited) foraminifer specimens reveals a weak (~0.6‰) increase in shell-bound δ^{15}N during sinking through the upper 500 m of the water column, possibly due to the loss of low-δ^{15}N shells or shell portions, but no further change in δ^{15}N upon incorporation into the sediments.

This thesis presents the first ground-truthing study conducted in the nitrate-replete high-latitude ocean. The data show spatial trends in late-summer foraminifer δ^{15}N that are consistent with the south-to-north drawdown (and δ^{15}N rise) of nitrate across the Southern Ocean. However, foraminifer δ^{15}N varies in its offset from nitrate consumed in Subantarctic surface waters, instead tracking the δ^{15}N of the foraminifer's particulate food source, which rises (due to winter decomposition) and falls (due to late-summer N recycling) with the seasons. Therefore, foraminifera do not directly record the δ^{15}N of nitrate consumed in the upper ocean (as previously thought), but rather reflect a more complex interplay of N cycling processes.

Despite all that has been learned about the foraminifer-bound δ^{15}N proxy from this and previous ground-truthing work, a major obstacle remains for its interpretation: It is not yet

known whether the magnitude of the nitrate assimilation isotope effect (the degree of isotope partitioning during nitrate consumption by phytoplankton) has varied through time. A first step towards answering this question is mapping the isotope effect of nitrate assimilation in the modern ocean to determine whether this parameter varies among environments. Preliminary estimates from a seasonally resolved biogeochemical model of the Southern Ocean suggest an isotope effect of ~8‰ for Subantarctic nitrate consumption, >2‰ higher than that determined for neighbouring Antarctic waters. As a key parameter required for reconstructing past nutrient utilization from any paleo-δ^{15}N archive, verifying this finding of a spatially variable isotope effect should be a priority.

Taken together, the modern-ocean investigations detailed in this thesis present a positive but more nuanced outlook for the foraminifer-bound δ^{15}N proxy, polishing the lens through which we view past ocean productivity and climate.

OPSOMMING

Die stikstof (N) isotoopverhoudings (δ^{15}N) van organiese materiaal wat vasgevang is in die fossielskulpe van planktoniese foraminifere, soöplankton wat die boonste lae van die oseaan bewoon, verskaf 'n nuwe perspektief waardeur die skakel tussen die afname in biologiese voedingstowwe in die oppervlakwater van die oseaan en die wêreldklimaat van die verlede bestudeer kan word. Hierdie tesis gebruik die moderne oseaan as 'n proefterrein om die bepalende faktore te karakteriseer wat die δ^{15}N bepaal van lewende en onlangs afgestorwe foraminifere in twee kontrasterende voedselstelsels: die voedingstofarme subtropiese Noord-Atlantiese Oseaan en die Suidelike Oseaan, waar die voedingstowwe in die oppervlakwater nooit heeltemal verbruik word nie. In beide hierdie omgewings is daar geen sistematiese verskil te bespeur tussen die δ^{15}N van die oorgrote meerderheid foraminifere-weefsel of net dié wat in skulpdoppe gehul is nie, wat die gebruik van die δ^{15}N, wat in skulpdoppe gehul is, as aanwyser van lewende foraminifere ondersteun.

In die Sargasso-see, waar nitraat uitgeput is, stel foraminifere spesies met dinoflagellate (alge) simbionte, wat in die oppervlakkige waters woon, by benadering die δ^{15}N vas van die nitraat wat aan die oppervlakte verskaf word (2.6‰). Daarteenoor het foraminifere spesies, wat dieper in die see woon sonder dinoflagellate, 'n hoër δ^{15}N ($\sim$3.6‰). Hierdie bevindinge stem ooreen met vorige grondslaggewende pogings in die lae breedteliggings in die oseaan, wat die gasheer-simbionte herwinning van lae δ^{15}N ammonium impliseer. Vergelykings tussen die foraminifere-monsters vanuit die oppervlakkige oseaan (lewend), middel-diepte (dalend) en die seebodem (onlangs neergedaal) onthul 'n swak ($\sim$0.6‰) toename in die δ^{15}N, wat in skulpdoppe gehul is, gedurende die neerdaling deur die boonste 500 m van die waterkolom. Dit kan moontlik toegeskryf word aan die verlies van lae δ^{15}N skulpe of skulpgedeeltes. Daar word egter geen verdere veranderinge in die δ^{15}N bespeur wanneer die foraminifere in die sedimente geïnkorporeer word nie.

Hierdie tesis bied die eerste grondslaggewende studie wat uitgevoer is in die hoë breedteliggings van die nitraatryke oseaan. Die data toon ruimtelike tendense in die laatsomer foraminifere δ^{15}N wat ooreenstem met die suid-na-noord afname (en δ^{15}N toename) in nitraat regoor die Suidelike Oseaan. Foraminifere δ^{15}N verskil egter in sy afwyking van die nitraat wat opgeneem word in die Subantarktiese oppervlakswaters. Die δ^{15}N volg eerder die deeltjies wat

iv

deur die foraminifere opgeneem word as voedsel. Die beskikbaarheid van hierdie deeltjies is seisoenaal - dit neem toe in die winter as gevolg van ontbinding en dit neem af in die somer as gevolg van laatsomer N herwinning. Dus bevat die foraminifere nie 'n direkte rekord van die δ^{15}N van nitraat wat in die boonste laag van die oseaan opgeneem word, soos voorheen vermoed is nie, maar weerspieël dit eerder 'n meer ingewikkelde wisselwerking van die N siklusprosesse.

Ten spyte van alles wat uit hierdie en ander grondslaggewende werk geleer is oor die foraminifere-gebonde δ^{15}N aanwyser, bly een van die grootste uitdagings die interpretasie daarvan – dit is nog onduidelik of die omvang van die nitraat assimilasie isotoop-effek (die graad van verdeling van die isotoop wat plaasvind wanneer die nitraat deur die fitoplankton opgeneem word) deur die tye verskil. Om hierdie vraag te beantwoord, is die opname van die isotoop-effek van nitraat assimilasie in die moderne oseaan en om vas te stel of hierdie parameter verskil tussen omgewings 'n goeie eerste stap. Voorlopige beraminge vanuit 'n biogeochemiese model van die Suidelike Oseaan, wat seisoenale faktore insluit, dui op 'n isotoop-effek van ~8 ‰ vir Subantarktiese nitraatverbruik, >2‰ hoër as wat bepaal is vir die naburige Antarktiese waters. Die bevestiging van die bevindinge van 'n ruimtelik-veranderlike isotoop-effek behoort 'n prioriteit te wees, aangesien dit 'n sleutelparameter is wat benodig word om die historiese benutting van voedingstowwe van enige paleo- δ^{15}N-argief te rekonstrueer.

Tesame bied die ondersoeke oor die modern oseaan wat in hierdie tesis gedetailleer word, 'n positiewe, maar meer genuanseerde vooruitsig vir die foraminifere-gebonde δ^{15}N aanwyser, wat die lens verskerp waardeur ons eertydse oseaanproduktiwiteit en -klimaat bestudeer.

ACKNOWLEDGEMENTS

To my surrogate home departments at Fresno State (Department of Earth & Environmental Sciences) and the University of Alabama (Department of Geological Sciences) – thank you for welcoming me into your scientific communities, for sharing your space, your microscopes, and your friendships.

To my darling husband, Alain Plattner, my partner in life and science. Thank you for celebrating with me in the ups and carrying me through the downs of life in academia.

To my parents, Jenny and Mike Smart, for supporting but never pushing, encouraging but never expecting. Mom, you inspire me with your compassion for nature, and your creative, hands-on way of problem solving (or "plan-maak-ing") -- not to mention your laboratory skills! Dad, to you I owe my love for landscapes and wide-open spaces. Thank you for stopping at every road-cutting, for the hours spent fossil-hunting in the Karoo, and for being the best example of a geologist (and dad) one could wish for.

To my grandparents, Betty Smart and Mike Heydenrych. Gran, your curiosity and love for learning is an inspiration to me. Thank you for sharing with me your love for painting and creative writing. And for keeping me on my toes with your sharp questions! Grandpa, I admire your practical, hard-working nature and your connection with the sea. To you I owe my love for big band jazz… and my sea-legs!

And lastly to Ellie, our *Canus Mississippianus*, for making me laugh every day since you adopted us, and for dragging me away from my desk even (or especially) during the final days of writing.

Table of Contents

List of Figures

List of Supplementary Figures

List of Tables

List of Supplementary Tables

CHAPTER 1: Introduction & Literature Review

1. Introduction

The last two million years of Earth history have been punctuated by ice ages, global cooling events that have shaped the surface of the planet and the fate of its inhabitants. While the pace of these events coincides with regular variations in solar radiation (set by the Earth's orbit and axial tilt relative to the sun), the amplitude of the resulting temperature swings (dropping by ~4-10°C during ice ages) implied by the geologic record is much larger than predicted (reviewed by Sigman & Boyle (2000) and Sigman et al. (2010)). Ice core records from Antarctica have revealed that the levels of carbon dioxide (CO_2, a heat-trapping "greenhouse" gas) in the atmosphere varied almost in sync with (slightly lagging behind) air temperature (Barnola et al., 1987; Petit et al., 1999), dropping by ~80-100 ppm during ice-ages (or "glacials") and reinforcing the cooling trend (Fig. 1.1). Similarly, deglaciations (the rapid transitions to warmer "interglacials") are accompanied by ~80-100 ppm increases in CO_2. Exactly how and why atmospheric CO_2 responds in this way to external solar forcing remains to be resolved (Sigman et al., 2010).
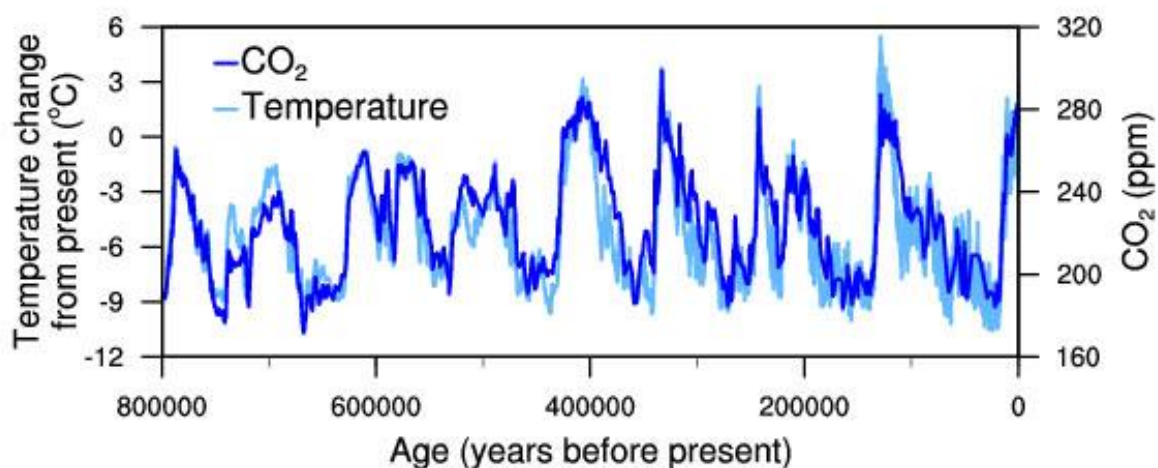
Fig. 1.1: Antarctic ice core records. Air temperature anomaly (in °C; relative to present day) and atmospheric carbon dioxide (CO_2) concentration (in parts per million; ppm) from the EPICA Dome C ice core, extending back 800 ky. [Data sources: Jouzel et al. (2007); Lüthi et al. (2008). Image source: https://www.ncdc.noaa.gov/global-warming/temperature-change].

1

It is generally agreed that the answers to these questions involve the ocean, the largest CO_2 reservoir that exchanges with the atmosphere on glacial-interglacial timescales (i.e., thousands of years) (Broecker, 1982a). But physical mechanisms alone, such as increased solubility of CO_2 in colder waters and reduced overturning circulation during ice ages (thus prolonged deep-ocean CO_2 storage), fall short of the ~80-100 ppm target (Sigman & Boyle, 2000). Another way in which the ocean interacts with the atmosphere is through biology. Marine phytoplankton, single-celled algae, take up CO_2 (together with major nutrients, nitrate (NO_3^-) and phosphate (PO_4^{3-})) during photosynthesis in the sunlit surface ocean and fix it into organic matter. When they die, some fraction of this organic material is exported, sinking into the deep ocean, where it is either decomposed back to CO_2 (and inorganic nutrients, NO_3^- and PO_4^{3-}) or buried on the seafloor. The resulting net downward transfer of CO_2 by biology is called the "biological pump". Because phytoplankton require major and trace nutrients (like iron) for growth, the amount of CO_2 they can take up ultimately depends on the availability of these nutrients in the surface ocean (Broecker, 1982a; Sigman & Boyle, 2000). Enhanced biological sequestration of CO_2 in the ocean can be achieved by increasing either the *strength* of the biological pump (via a larger total-ocean reservoir of the major nutrients, nitrate or phosphate) (Broecker, 1982a; McElroy, 1983) or its *efficiency* (by more-complete utilization of existing nutrients supplied to phytoplankton in surface waters) (Knox & McElroy, 1984; Siegenthaler & Wenk, 1984; Sarmiento & Toggweiler, 1984). The relative importance of these two mechanisms in the glacial drawdown of CO_2 is still debated.

The nitrogen (N) isotope composition (or $\delta^{15}N$; defined below in units of per mil, ‰) of organic matter has emerged as a promising indicator of past ocean nutrient conditions.

$$\delta^{15}N = \{[(^{15}N/^{14}N)_{sample}/(^{15}N/^{14}N)_{N2\ in\ air}] - 1\} \times 1000$$

The vulnerability of organic matter in bulk sediments to bacterial degradation and contamination by exogenous N has sparked the search for sedimentary archives that are robust to these effects (Altabet & Curry, 1989; Altabet & François, 1994). The calcareous shells of planktic foraminifera, a type of single-celled zooplankton, offer one such archive (Ren et al., 2009). As ubiquitous upper-ocean dwellers that feed on particulate organic matter, planktic foraminifera are well positioned to record the $\delta^{15}N$ of the organic matter produced in the surface ocean.

In the low-latitude ocean (the focus of Chapter 2), nitrate is near-completely drawn down by phytoplankton in surface waters (Fig. 1.2), such that the $\delta^{15}N$ of exported organic matter converges on that of the nitrate originally supplied (Altabet, 1988; Altabet & François, 1994). In turn, the $\delta^{15}N$ of recently deposited foraminifer shells has been found to closely track the $\delta^{15}N$ of the nitrate supply to overlying oligotrophic (nitrate-poor) surface waters (Ren et al., 2009; Ren et al., 2012b). If foraminifera indeed record the $\delta^{15}N$ of the low-latitude nitrate supply, downcore variations in shell-bound $\delta^{15}N$ would reflect past changes in mean-ocean nitrate $\delta^{15}N$, which is itself an indicator of the balance between the sinks and sources of the global nitrate reservoir (Sigman et al., 2000; Sigman et al., 2009a) (and thus, the *strength* of the biological pump). In the high-latitude ocean (the focus of Chapters 3 and 4), nitrate is not completely consumed in surface waters (Fig. 1.2), leaving the isotopic imprint of partial nitrate consumption on the $\delta^{15}N$ of the residual nitrate as well as the organic matter produced from it (Wada & Hattori, 1978; Waser et al., 1998; Sigman et al., 1999a). Therefore, foraminifer-bound $\delta^{15}N$ records from the polar/subpolar ocean should record changes in both whole-ocean nitrate $\delta^{15}N$ and in the degree of nitrate drawdown (and thus, the *efficiency* of the biological pump).
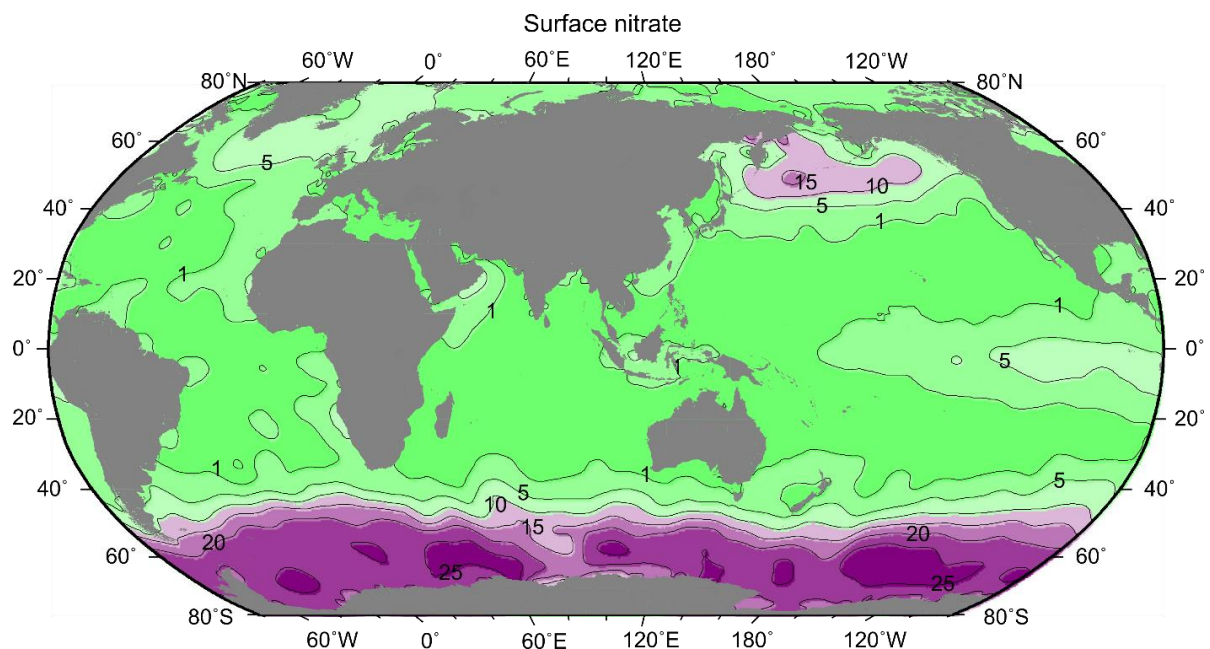
Fig. 1.2: Global sea-surface nitrate concentration (µmol/L) in the modern ocean. High concentrations in the Southern Ocean contrast with low concentrations in the subtropical ocean. [Data source: Conkright et al. (1994). Image source: Talley et al. (2011)].

3

Therefore, the foraminifer-bound $\delta^{15}N$ paleo-proxy seems poised to settle the debate over the importance of strength *vs.* efficiency of the biological pump in regulating ice age cycles. Indeed, the first foraminifer-bound $\delta^{15}N$ records have yielded promising results in this regard (Ren et al., 2009; Ren et al., 2012a; Straub et al., 2013a; Martínez-García et al., 2014; Ren et al., 2017), but the interpretation of such records relies on currently limited knowledge of foraminifer $\delta^{15}N$ in the modern ocean (Ren et al., 2012b). Open questions include:

- Does shell-bound $\delta^{15}N$ well-represent the $\delta^{15}N$ of the living organism (i.e., foraminifer tissue)?
- Is shell-bound $\delta^{15}N$ preserved during sinking and burial?
- Do living foraminifera track the $\delta^{15}N$ of nitrate consumed in surface waters?

The overarching goal of the work presented in this thesis is to address these and other uncertainties in order to support and inform the interpretation of this exciting new proxy.

2. Literature Review

2.1 Climate cycles and the ocean's biological pump

One of the outstanding questions in geoscience is why atmospheric CO_2 appears to mimic, and thus amplify, the Earth's orbitally driven temperature cycles (Fig. 1.1; Sigman & Boyle, 2000; Sigman et al., 2010). The most viable explanations to date draw on the interaction between ocean circulation and biogeochemistry, with a growing emphasis on the ocean's biological pump. One school of thought involves a *strengthening* of the biological pump at *low* latitudes during ice ages, driven by an increase in the whole-ocean reservoir of nitrate or phosphate, the major nutrients currently limiting phytoplankton growth, and thus CO_2 sequestration, across much of the low-latitude surface ocean (Broecker, 1982a; McElroy, 1983) (Fig. 1.2).

The size of the ocean's phosphorous (P) inventory is largely controlled by physical rates of weathering and riverine inputs, and its removal by burial in seafloor sediments. With a residence time of over 16 ky in the ocean, changes in the P reservoir are likely too slow to explain the rapid changes in atmospheric CO_2 during glacial-interglacial cycles (Ruttenberg,

1993; Broecker & Henderson, 1998). The ocean's N reservoir is more dynamic and is controlled by the biological rates of N_2 fixation and denitrification in the ocean (Ganeshram et al., 1995). N_2-fixing organisms called diazotrophs are able to convert N_2 from the air into a form they can take up, allowing them to thrive in N-impoverished environments such as the oligotrophic subtropical gyres (Dugdale et al., 1961; Carpenter & Capone, 1992; Karl et al., 2002). When they die and sink into subsurface waters, their biomass is remineralized (to ammonium, NH_4^+) and oxidized (to NO_2^- and then NO_3^-), adding new nitrate to the low-latitude thermocline (shallow subsurface waters). Nitrate is removed from the ocean by denitrifying microbes under low-oxygen conditions (in the water column or sediments), reducing NO_3^- to nitrogen oxides (NO and N_2O) and ultimately N_2 gas, closing the budget (Cline & Kaplan, 1975; Liu & Kaplan, 1989).

An increase in the ocean's N inventory could, therefore, be attained by either an increase in N_2 fixation or a decrease in denitrification during ice ages. Indeed, there is evidence for reduced denitrification in oxygen minimum zones during the last glacial maximum (LGM) compared to today, apparently supporting the latter mechanism (Altabet et al., 1995; Ganeshram et al., 1995; de Pol-Holz et al., 2006; Liu et al., 2008). However, if N_2 fixation rates were also lower during the LGM, the effect may be compensated. The proposed mechanism behind such a self-regulating feedback on the size of the global N reservoir is as follows: by removing nitrate, denitrification reduces the overall N:P ratio of the ocean, under which conditions N_2-fixing organisms are at an advantage compared to other phytoplankton (Schindler, 1977). The result of their boost in productivity (enhanced N_2-fixation rates) is to gradually raise the N:P ratio again until the stoichiometric ratio favorable for non-N_2 fixers (~16:1; the so-called "Redfield ratio") is restored (Redfield, 1958; Broecker, 1982a).

An alternative hypothesis for ice-age CO_2 drawdown calls for a more *efficient* biological pump at *high* latitudes during ice ages (Knox & McElroy, 1984; Siegenthaler & Wenk, 1984; Sarmiento & Toggweiler, 1984). The Southern Ocean plays a central role in this hypothesis; not only is it responsible for ventilating a large volume of the CO_2-rich waters of the ocean interior (Toggweiler, 1999), but given that nutrients are never completely exhausted in present-day Southern Ocean surface waters (Fig. 1.2), it also has great potential for increased nutrient utilization (and thus carbon fixation) (Sigman & Boyle, 2000; Sigman et al., 2010). The Antarctic Zone (AZ; south of the Polar Front) seems to have experienced diminished export

5

production during glacial periods (Mortlock et al., 1991; Kohfeld et al., 2005; Anderson et al., 2009) despite an apparent increase in the extent of nutrient consumption (François et al., 1997; Robinson & Sigman, 2008; Studer et al., 2015), suggesting a reduction in supply of these nutrients from below by weaker overturning circulation (François et al., 1997; Kemeny et al., 2018). Together with more extensive sea-ice cover during ice-age winters (acting as a physical barrier to the escape of CO_2 from upwelled deep waters; Stephens & Keeling, 2000) and the reinforcing effect of increased ocean alkalinity (the "acid-buffering capacity" of seawater, controlled chiefly by the balance between river inputs and deep-sea burial rates of calcium carbonate; Sigman & Boyle, 2000; Sigman et al., 2010), this set of conditions would have worked to lower atmospheric CO_2 by an estimated 40 ppm or more – roughly half of the observed glacial CO_2 drawdown (Toggweiler, 1999; Stephens & Keeling, 2000; Sigman et al., 2010).

The response of the Subantarctic Zone (SAZ; the northernmost domain of the Southern Ocean) to glacial conditions has been a subject of much debate (Sigman & Boyle, 2000). Paleoceanographic reconstructions suggest an increase in SAZ productivity during glacial times (Kumar et al., 1995; Kohfeld et al., 2005; Martínez-García et al., 2009), with two competing interpretations: (1) a northward migration of the productive Southern Ocean fronts into the present-day SAZ, driven by a shift in the overlying wind-field (Mortlock et al., 1991; Bard & Rickaby, 2009), or (2) fertilization of SAZ waters with iron, carried downwind from the major Southern Hemisphere dust sources by intensified westerly winds (Martin, 1990; Martínez-García et al., 2009). While the first would likely increase macronutrient (nitrate and phosphate) concentrations due to enhanced upwelling into the SAZ surface (opposing the drawdown of atmospheric CO_2 during glacials), the second would drive more complete consumption of these macronutrients (assisting in the CO_2 drawdown) (Sigman & Boyle, 2000; Martin, 1990; Martínez-García et al., 2014). Furthermore, the SAZ is largely responsible for the supply (i.e., amount and composition) of nutrients reaching the low-latitude ocean (via Antarctic Intermediate Water and Subantarctic Mode Water), augmenting its influence on the global carbon cycle through ocean alkalinity feedbacks (Kier, 1988; Matsumoto et al., 2002; Sarmiento et al., 2004). The contrary implications for atmospheric CO_2 (both locally driven within the SAZ and via positive feedbacks involving low-latitude productivity) highlight the

6

need to discern between these two interpretations, the key to which may lie in reconstructing SAZ nitrate utilization.

2.2 N isotopes as a paleo-nutrient proxy

There are two stable naturally occurring forms of nitrogen: ^{14}N (99.63% of all N) and ^{15}N (making up the remaining 0.37%). Because of their mass difference, ^{14}N and ^{15}N undergo physical and biochemical reactions at slightly different rates, leading to partitioning called kinetic isotope fractionation (Mariotti et al., 1981). For example, when nitrate is consumed by phytoplankton, the lighter ^{14}N isotope is preferentially incorporated, causing the remaining nitrate pool (and thus also the particulate organic N (PON) subsequently produced from it) to become progressively enriched in the heavier ^{15}N isotope (i.e., increasing nitrate and PON δ^{15}N as nitrate consumption proceeds) (Wada & Hattori, 1978; Pennock et al., 1996; Waser et al., 1998; Sigman et al., 1999a). The degree to which phytoplankton discriminate between the heavy and light N isotopes when taking up nitrate is known as the isotope effect (ε) of nitrate assimilation, defined as:

$$\varepsilon = [(^{14}k/^{15}k) - 1] \times 1000$$

where ^{14}k and ^{15}k are the reaction rates of ^{14}N and ^{15}N, respectively. In the simplest case of a closed system, where the reaction (nitrate assimilation) proceeds with a constant isotope effect and without any removal or replenishment of the reactant (nitrate) or product (PON), the isotopic evolution of the system can be described by the Rayleigh model (Mariotti et al., 1981) (Fig. 1.3). The δ^{15}N of nitrate undergoing consumption under such conditions can be calculated as follows:

$$\delta^{15}N_{reactant} = \delta^{15}N_{initial} - \varepsilon \times \ln(f)$$

where $\delta^{15}N_{initial}$ represents the δ^{15}N of nitrate before consumption began (i.e., the original supply), and f is the fraction of nitrate remaining. At any point in the process, the δ^{15}N of PON produced at that instant can be approximated using:

$$\delta^{15}N_{instantaneous} = \delta^{15}N_{reactant} - \varepsilon$$

such that there is a constant δ^{15}N offset (the size of the isotope effect) between the PON instantaneously produced and the nitrate remaining (the black vertical arrow in Fig. 1.3). The

δ^{15}N of the total accumulated PON pool (i.e., integrated product) increases more gradually according to:

$$\delta^{15}N_{integrated} = \delta^{15}N_{initial} + \{\varepsilon \times [f/(1-f)] \times \ln(f)\}$$
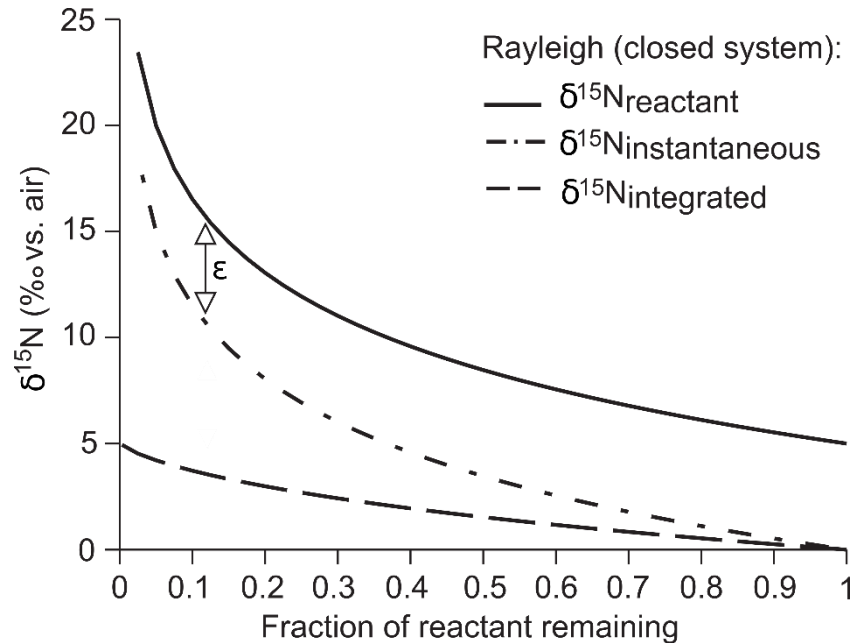
Fig. 1.3: Rayleigh model isotope systematics, illustrating changes in the δ^{15}N of reactant (solid) and product (instantaneous (dot-dashed) and integrated (dashed)) pools in a closed system as the reactant undergoes consumption with a constant isotope effect (ε). [Image source: adapted from Sigman et al. (2009b)]

If the nitrate pool is completely consumed (i.e., $f = 0$), the isotope effect is not expressed and the δ^{15}N of the total accumulated PON converges on that of the initial nitrate supply (i.e., $\delta^{15}N_{integrated} = \delta^{15}N_{initial}$; as all the isotopes, ^{14}N and ^{15}N, have been transferred from the reactant to the product pool). Thus, in oligotrophic environments like the subtropical gyres where nitrate consumption in surface waters is essentially complete, δ^{15}N variations in underlying sediments would be expected to predominantly reflect changes in the δ^{15}N of the nitrate source (i.e., $\delta^{15}N_{initial}$) (Altabet, 1988; François et al., 1992). If nitrate is not completely consumed in surface waters (i.e., $f > 0$), as in the modern Southern Ocean, the δ^{15}N of organic matter sinking to the

8

seafloor additionally reflects both the magnitude of the isotope effect (ε) and the degree of nitrate consumption (*f*) in overlying waters (Altabet & François, 1994; Sigman et al., 1999a).

The first attempts at leveraging these relationships between sedimentary $\delta^{15}N$ and surface nitrate conditions were based on the analysis of bulk sedimentary N (François et al., 1992; François et al., 1997). For example, in the Atlantic SAZ (the sector exhibiting the most prominent rise in LGM export production; Kumar et al., 1995; François et al., 1997; Kohfeld et al., 2005), bulk $\delta^{15}N$ was found to be lower during the LGM than today (François et al., 1997). Taken at face value, this implies less-complete nitrate consumption during glacial periods (François et al., 1997; Martínez-García et al., 2014), favoring the frontal-shift interpretation for the SAZ (Mortlock et al., 1991; Bard & Rickaby, 2009; (1) outlined in section 2.1 above). On the whole, however, SAZ bulk $\delta^{15}N$ records lack a clear glacial-interglacial structure; instead, they appear to be negatively correlated with the magnitude of the sinking flux (François et al., 1993; Lourey et al., 2003; Robinson et al., 2005) (e.g., compare open circles with pluses in Fig. 1.4). Remineralization, the bacterially mediated oxidation of organic matter, preferentially removes ^{14}N, leaving bulk surface sediments elevated in $\delta^{15}N$ relative to sinking PON (Saino & Hattori, 1980; Altabet, 1988; Altabet & François, 1994; Galbraith et al., 2008). The effect of this biochemical alteration, known as early diagenesis, seems to be most pronounced in low particle-flux, open-ocean settings (like the Southern Ocean and the subtropical gyres) where slowly accumulating sediments are exposed to oxygen at the seafloor for extended periods (François et al., 1992; Galbraith et al., 2008; Robinson et al., 2012). It follows that the down-core variations observed in SAZ bulk $\delta^{15}N$ might reflect the changes in remineralization in response to time-varying sinking fluxes, rather than changes in nutrient status (Mortlock et al., 1991; Kumar et al., 1993; Lourey et al., 2003; Robinson et al., 2005). Furthermore, marine sediments with a low organic N content (whether due to low flux or poor preservation) are vulnerable to contamination by organic and inorganic (e.g., clay-bound) forms of terrestrial N (Schubert & Calvert, 2001; Galbraith et al., 2008; Ren et al., 2009).

9
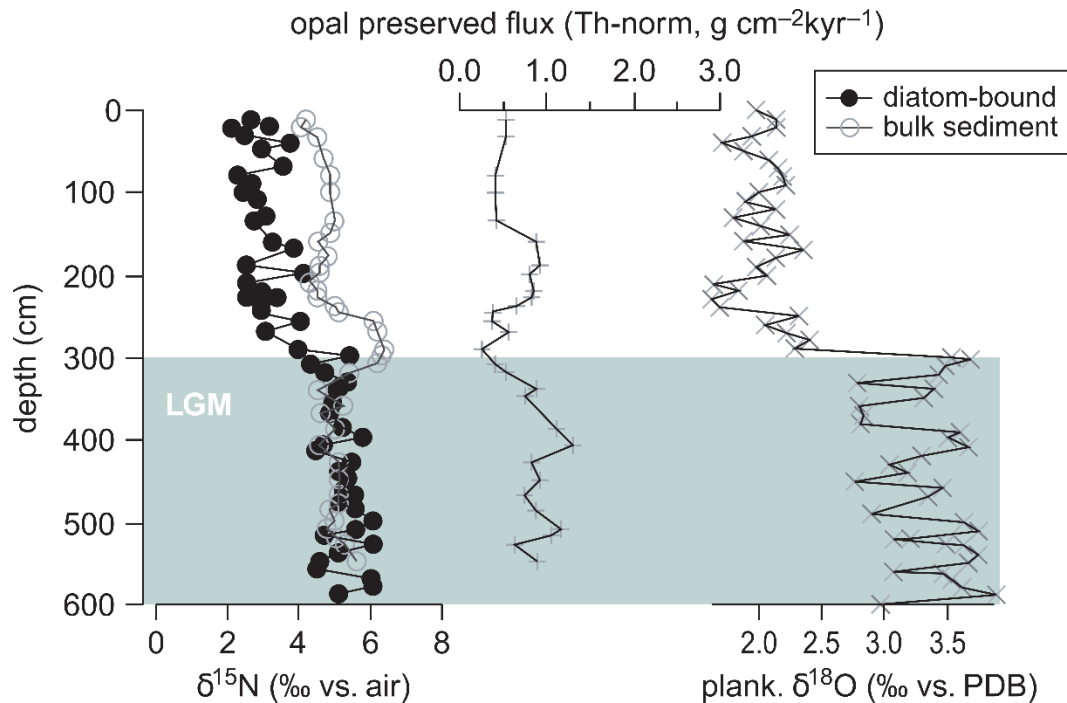
Fig. 1.4: Paleoceanographic records from the southern Subantarctic Ocean. Bulk sediment and diatom-bound $\delta^{15}N$ records (open and filled circles, respectively) spanning the last deglaciation are shown together with ^{230}Thorium-normalized opal flux (a proxy for diatom export production) and planktic foraminiferal $\delta^{18}O$ (a proxy for global ice volume) from the same sediment core (site MD84-527 in the Indian sector). The blue shaded band represents the last glacial maximum (LGM). [Data source: Robinson et al. (2005). Image source: adapted from Capone et al. (2008)].

Such concerns have cast doubt on the reliability of bulk sedimentary $\delta^{15}N$ as a proxy for nitrate utilization (Altabet & François, 1994; François et al., 1997) and prompted a shift to analysis of specific N pools that might escape these effects (Galbraith et al., 2008; Robinson et al., 2012). Much attention has been given to measuring the $\delta^{15}N$ of fossilized diatoms, phytoplankton whose resilient silica frustules offer protection of bound organic matter from diagenetic alteration (Shemesh et al., 1993; Sigman et al., 1999b; Crosta & Shemesh, 2002; Robinson et al., 2004; Robinson et al., 2005; Robinson & Sigman, 2008). Unlike bulk measurements, diatom frustule-bound $\delta^{15}N$ records from all sectors of the southern SAZ show an *increase* during glacial periods (Robinson et al., 2005; Robinson & Sigman, 2008) (e.g., filled circles in Fig. 1.4), supporting the iron fertilization explanation (Martin, 1990; Martínez-García et al., 2009; (2) outlined in section 2.1 above). Interpretation of diatom-bound $\delta^{15}N$, however, is complicated by glacial-interglacial changes in diatom assemblage and environmental conditions (e.g., mixed-layer depth or sea ice), which can alter the relationship between nitrate

10

uptake and diatom-bound $\delta^{15}N$ (Jacot Des Combes et al., 2008; DiFiore et al., 2010); this is due to the fact that different diatom species may assimilate nitrate with a different isotope effect (Needoba et al., 2003; Horn et al., 2011), and that the assimilation isotope effect of a given species appears to vary depending on its growth conditions, including light availability (Needoba & Harrison, 2004; Needoba et al., 2004). The existence of a $\delta^{15}N$ offset between diatom biomass (i.e., bulk algal tissue) and frustule-bound N adds an extra layer of complexity to interpretation of downcore records, particularly if the offset varies through time (Robinson et al., 2004; Brunelle et al., 2007; Morales et al., 2013; Morales et al., 2014). Furthermore, diatom-bound $\delta^{15}N$ measurements are inherently limited to silicate-rich waters, preventing the application of this proxy to most of the global ocean equatorward of the subpolar fronts (with the exception of upwelling regions) (Ren et al., 2012b; Martínez-García et al., 2014).

Recently, a new method has been developed for the analysis of organic N encased within the shells of planktic foraminifera (Ren et al., 2009; Ren et al., 2012b; Straub et al., 2013a), a type of calcifying zooplankton. Apart from being more widely distributed (and thus applicable to silicate-poor regions), foraminifera are large enough for individual species to be separated for analysis, avoiding any bias associated with assemblage changes. The section that follows, provides a brief introduction to foraminifer ecology, focusing on aspects that are relevant to shell-bound N. The development of the foraminifer-bound $\delta^{15}N$ proxy is then reviewed, along with its application to two contrasting nutrient regimes, demonstrating both the potential of this proxy as an archive of the past ocean N cycle and the need to ground-truth it in the modern ocean.

2.3 Ecology of planktic foraminifera

2.3.1 Classification and morphology

Foraminifera are a class of single-celled heterotrophic protists, characterized by an external shell or 'test' with one or multiple chambers (d'Orbigny, 1826; Dujardin, 1835; Loeblich & Tappan, 1992). The cell is composed of a clear ectoplasm (a mobile film that coats the test and gives rise to "pseudopodia" (seen radiating from the spines in Fig. 1.5a), which are used for capturing food) and a darker endoplasm (internal to the test, containing the nucleus (or nuclei), food vacuoles and numerous organelles). The endoplasm and ectoplasm are in constant communication via one or more apertures in the test (reviewed by Schiebel & Hemleben

11

(2017)). The test itself can vary in size, complexity and composition, although calcium carbonate ($CaCO_3$, or calcite) tests are the most common (Armstrong & Brasier, 2005).
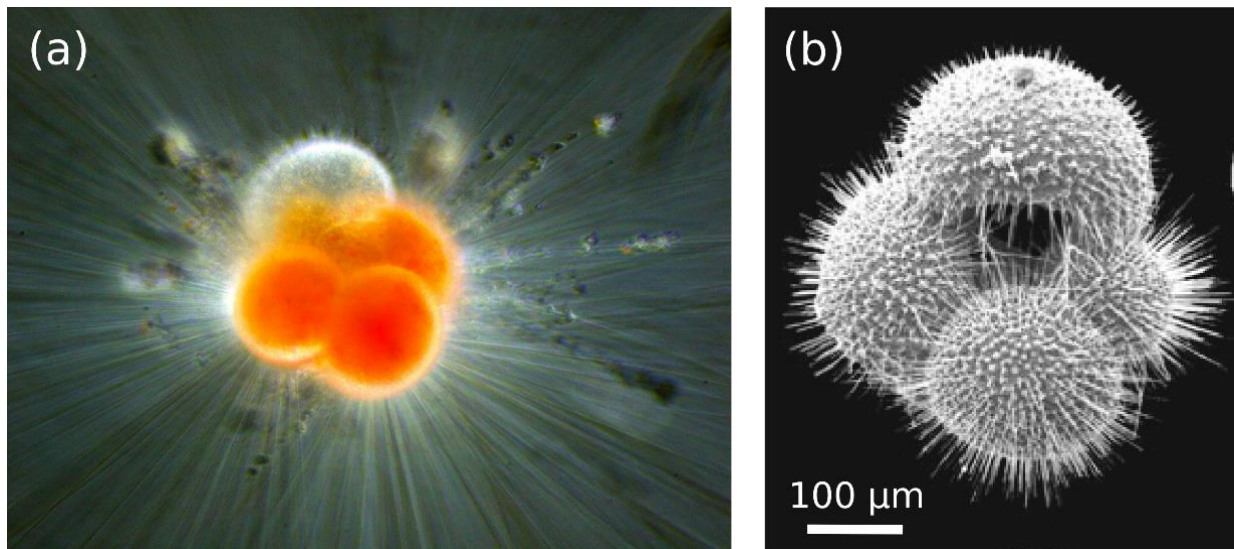
Fig. 1.5: Morphology of the planktic foraminifer, *Globigerina bulloides*. (a) Living specimen photographed using incident-light microscopy [Image source: http://www.jamstec.go.jp/res/ress/kimopy/foraminifera/e/G_bulloides/index.html] and (b) details of the test imaged by scanning electron microscopy [Image source: adapted from Schiebel & Hemleben (2017)].

Species are typically identified based on their shell morphology (i.e., morphospecies), using chamber architecture, shell-wall texture and pores, the number and shape of apertures, and other distinctive features like spines (Fig. 1.5b), "lips" and "keels" (Schiebel & Hemleben, 2017). There are around 50 morphospecies of planktic (water-column dwelling) foraminifera in the modern ocean and many more benthic (seafloor-dwelling) species (Loeblich & Tappan, 1988). Planktic foraminifera have likely evolved from benthic foraminifera multiple times (Darling et al., 2009; Arenillas & Arz, 2017) since their emergence in the Early-Mid Jurassic around 170 Ma ago (Caron & Homewood, 1983). Although benthic foraminifera are valuable indicators of past deep-sea temperature and chemistry (Zachos et al. (2001) and references therein), the focus here is on the planktic variety for their potential as recorders of upper-ocean nutrient conditions.

Observations of living planktic foraminifera with light and later electron microscopy have revealed that chamber formation is preceded by the extrusion of a balloon-like organic sheet,

12

which acts a template for mineralization (Bé & Hemleben, 1970; Bé et al., 1979; Spero, 1988). Using calcium (Ca^{2+}) and carbonate (CO_3^{2-}) ions derived from seawater, foraminifera secrete calcite (de Nooijer et al. (2014) and references therein) or a metastable precursor (e.g., vaterite; Jacob et al., 2017), covering the organic sheet and sequestering it within the shell wall. This "primary organic sheet" (Fig. 1.6) is made up of N-rich proteins which, together with the (less well-characterized) non-laminar forms of organic matter (Branson et al., 2016), constitute foraminifer-bound N. Shell-bound N (another name for foraminifer-bound N) is further protected by subsequent chamber addition and by shell-wall thickening, which can happen actively during gametogenesis (reproduction) in the water column (Bé, 1980; Schiebel et al., 1997) or passively during post-mortem encrustation in the sediments (Hemleben et al., 1989; Lohmann, 1995). The effects of partial dissolution on shell-bound N and potential for contamination (e.g., incorporation of exogenous N during encrustation) remain unknown.
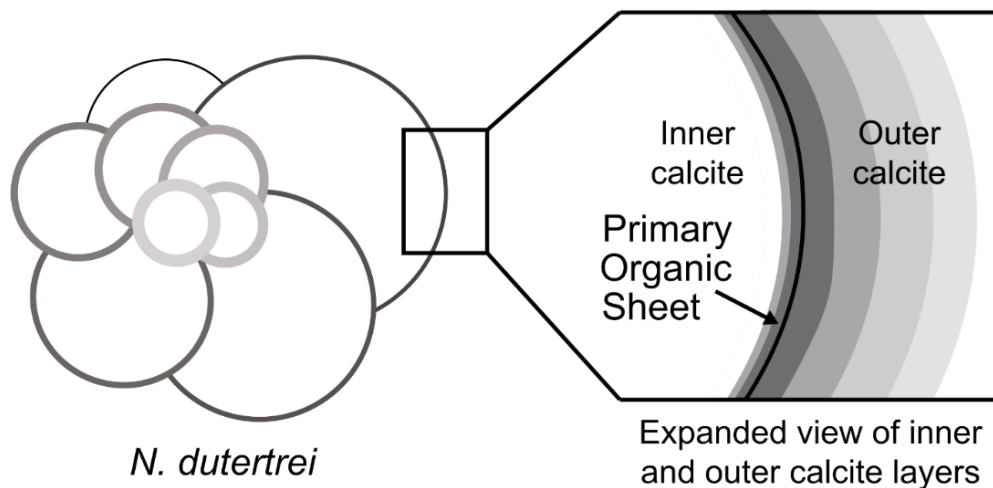
Fig. 1.6: Schematic shell structure of the planktic foraminifer, *Neogloboquadrina dutertrei.* The black line in the expanded view (right) represents the organic sheet used as the original template for calcification; grey layers represent sequential additions of calcite during growth. [Figure source: adapted from Fehrenbacher et al. (2017)].

2.3.2 Distribution, nutrition and reproduction

Planktic foraminifera inhabit an array of environments from polar to tropical regions (Fig. 1.7), with species diversity peaking in the subtropics and decreasing polewards (Bé & Tolderlund, 1971; Hemleben et al., 1989). Their distribution is primarily governed by hydrography such

13

that, on a global scale, each species occupies a particular latitudinal and depth range based on its temperature and salinity tolerance (reviewed by Armstrong & Brasier (2005)). Overall foraminiferal abundance depends on food availability, which can include phytoplankton, zooplankton and/or organic detritus, depending on the species (Anderson et al., 1979; Spindler et al., 1984). As all these potential food sources derive from primary production, foraminifera rely on there being adequate sunlight and nutrient supply to support phytoplankton growth in surface waters, even if they dwell deeper in the water column (Schiebel et al., 2001; Schiebel & Hemleben, 2017). The abundance of any one species in an environment depends on its specific ecology, including diet and symbiotic status (Erez, 1983; Spindler et al., 1984), which is discussed in detail below.
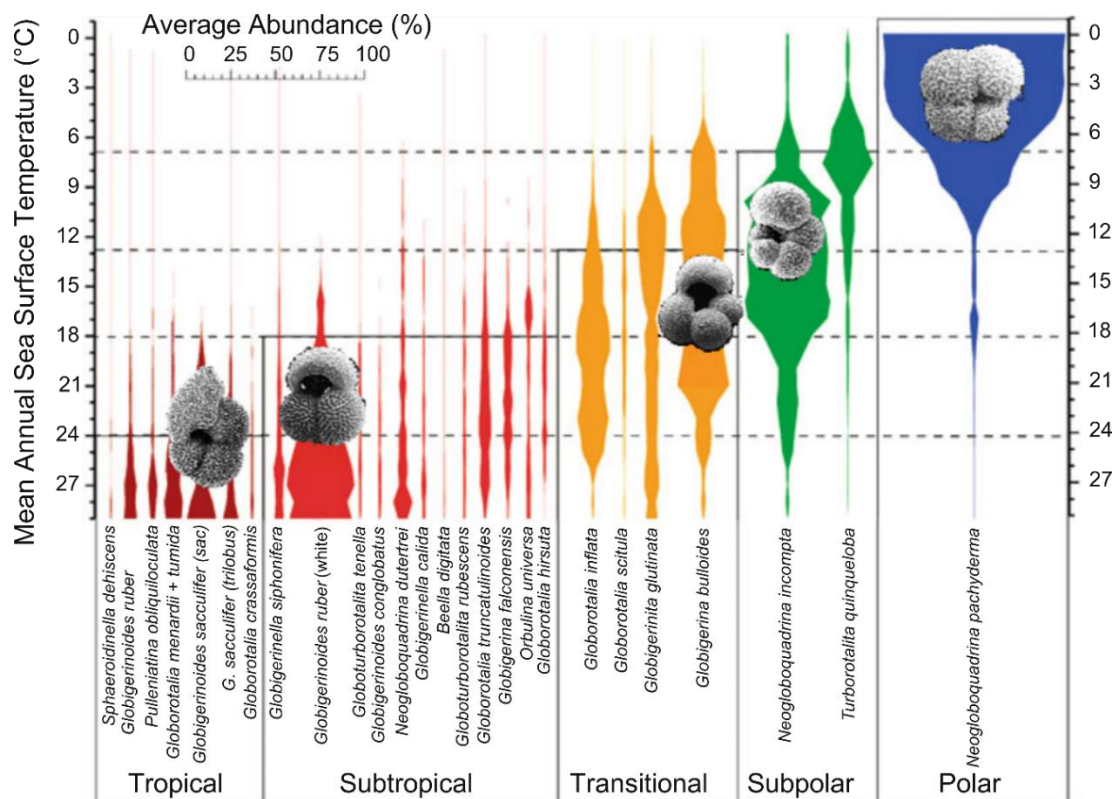
Fig. 1.7: Regional distribution of species within the Atlantic basin. Relative abundance (%) of planktic foraminifer species in surface sediments from the Atlantic basin related to annual average sea-surface temperature (averaged at 1°C intervals). Note that the temperature axis is inverted, with low temperatures at the top. [Figure source: Schiebel & Hemleben (2017); adapted from Kucera (2007)].

14

Many modern planktic foraminifera have been found to undertake mutually beneficial relationships with photosynthesizing algae, termed "(photo)symbionts". These algae can often be seen living on the spines or inside the cytoplasm of foraminifera collected by net tows or scuba divers (Bé et al., 1977; Hemleben et al., 1989). Foraminiferal symbioses are typically classified as either "obligatory" (necessary for the host's survival) or "facultative" (not required for survival) (Hemleben et al., 1989), although recent work (e.g., using active chlorophyll fluorometry; Kolber & Falkowski, 1993; Fujiki et al., 2014) suggests more of a continuum for photosymbiosis (Stoecker et al., 2009; Takagi et al., 2019). Perhaps the best-characterized relationship is the obligatory symbiosis between dinoflagellate algae and the spinose, shallow-dwelling foraminifera (e.g., *Orbulina universa*, *Globigerinoides sacculifer*, *Globigerinoides ruber*) (Spero & Parker, 1985; Jørgensen et al., 1985; Spero, 1987; Hemleben et al., 1989). From the association, dinoflagellates gain access to ammonium (the reduced, and thus preferred, N-containing nutrient) excreted by the host foraminifer; In return, the foraminifer makes use of organic compounds produced by the dinoflagellates during photosynthesis, supplementing those acquired by feeding (Uhle et al., 1997; Uhle et al., 1999). As such, the shallow-dwelling, dinoflagellate-bearing species could be considered mixotrophs (reviewed by Stoecker et al. (2017)) rather than heterotrophs. The photosynthetic requirements of the symbionts dictate a shallower (and generally, lower-latitude) habitat for dinoflagellate-bearing foraminifera (Erez, 1983; Takagi et al., 2019).

A number of intermediate-depth dwellers (e.g., *Globorotalia inflata*, *Globigerinita glutinata*, *Neogloboquadrina dutertrei*) are suspected to host chrysophytes or pelagophytes, although symbiosis appears to be facultative (Gastrich, 1987; Faber et al., 1988; Bird et al., 2018). The generally higher light-absorption efficiency of pelagophyte- (compared to dinoflagellate-) bearing foraminifera may explain the preference of these species for lower-light (intermediate-depth) environments (Takagi et al., 2016; Takagi et al., 2019). Other species have been confirmed as non-symbiotic (or symbiont-barren), including *Globorotalia truncatulinoides*, the deepest-dwelling planktic foraminifer, and *Neogloboquadrina pachyderma*, which dominates polar assemblages (Hemleben et al., 1989; Takagi et al., 2019). As yet, *G. bulloides* has not been found to contain functional chlorophyll (Takagi et al., 2019) but may have associations with free-swimming (rather than intracellular) dinoflagellates (Spero & Angel, 1991). At least one genotype (a genetically distinct subgroup or grouping of morphospecies; e.g., Darling &

15

Wade (2008)), *G. bulloides* Type IId occurring in the California Current, has been found to harbor cyanobacterial symbionts (Bird et al., 2017).

The diets of the shallow-dwelling, dinoflagellate-bearing species, *O. universa*, *G. sacculifer* and *G. ruber* (Bé et al., 1977; Spero, 1987), and the shallow- (Type I) or intermediate- (Type II) dwelling, chrysophyte-bearing *Globigerinella siphonifera* (Faber et al., 1988; Faber et al., 1989; Bijma et al., 1998) consist mostly of zooplankton and sometimes larger phytoplankton (Anderson et al., 1979; Spindler et al., 1984). Most other species feed on phytoplankton and/or detrital organic matter suspended in the water column (e.g., *G. inflata*, *G. truncatulinoides*; Anderson et al., 1979; Spindler et al., 1984), with bacteria as a potential food source for some (e.g., *G. bulloides*, *N. incompta*; Bird et al. (2017); Bird et al. (2018)). The diversity of photosymbiotic and feeding strategies employed by planktic foraminifera likely contributes to their ubiquity across the world's oceans and their evolutionary resilience (Stoecker et al., 2009; Seears et al., 2012; Fenton et al., 2016; Schiebel et al., 2018; and references therein).

Most shallow-to-intermediate depth dwelling foraminifera reproduce monthly (lunar), except for *G. ruber* and *G. siphonifera*, which reproduce twice per month (semi-lunar) (Bijma et al., 1990; Jonkers et al., 2015). Based on its population dynamics, the deep-dwelling *G. truncatulinoides* seems to reproduce only once per year (Hemleben et al., 1989). Gametogenesis is timed with the lunar cycle and occurs at a specific depth in the water column to maximize the chances of successful gamete fusion (Schiebel & Hemleben, 2017). Shallow dwellers descend to the chlorophyll maximum (typically the base of the mixed-layer) to provide ample food for their offspring (Bijma et al., 1990; Erez et al., 1991). Likely for the same reason, the deep-dwelling *G. truncatulinoides* is found abundantly in surface waters during spring (Hemleben et al., 1985; Schiebel, 2002). If feeding and calcification at different depths during different life stages incorporate organic matter with distinct compositions into the shell, these processes could complicate interpretation of the whole-shell N isotopes.

2.4 Development and application of the foraminifer-bound $\delta^{15}N$ proxy

Early investigations into the organic matrix of planktic foraminifera in deep-sea sediments found recently deposited shells and fossils of the same species as old as 300 ka to have similar amino acid compositions, despite the lower organic content of the older samples (King & Hare, 1972; Robbins & Brew, 1990). Measuring the $\delta^{15}N$ of this shell-bound organic N was first

16

attempted by Altabet & Curry (1989), but the sheer quantity of foraminifera required for each analysis (≥250 mg, taking more than 2 days to "pick", i.e., sort and separate specimens under a microscope using a picking brush) limited the number (and resolution) of species-specific measurements possible. Thanks to improvements in the techniques used for cleaning and oxidation (conversion of organic N to nitrate) of low-N microfossils (Ren et al., 2009; Ren et al., 2012a; Straub et al., 2013a; Martínez-García et al., 2014; Ren et al., 2017), together with the development of the denitrifier method (for the bacterial conversion of nitrate to N_2O) and its coupling with mass spectrometry (Sigman et al., 2001; Weigand et al., 2016), it is now possible to measure much smaller samples (~10 mg of foraminifera, yielding ~2-5 mg of cleaned calcite) with higher $\delta^{15}N$ reproducibility (~0.2‰).

2.4.1 The low-nitrate low latitude ocean
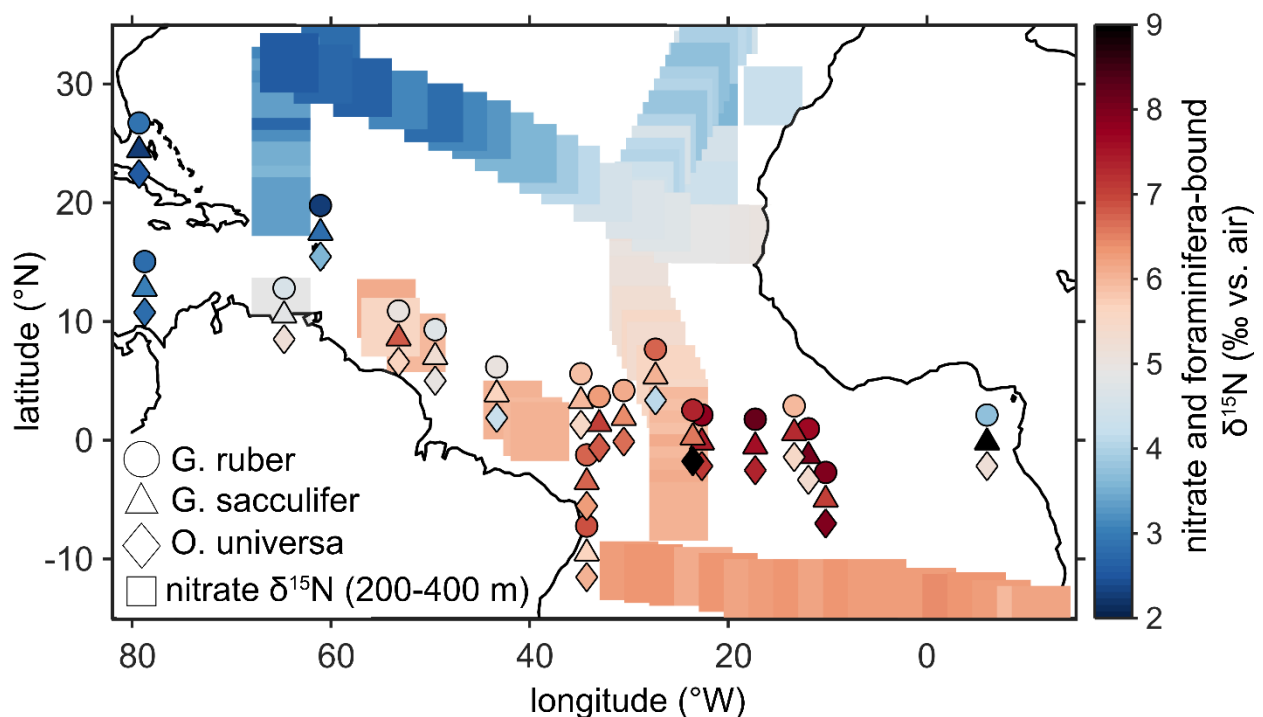
Fig. 1.8: Map relating the $\delta^{15}N$ of thermocline nitrate to foraminifera in surface sediments across the tropical/subtropical Atlantic. Subsurface (200-400 m) nitrate $\delta^{15}N$ (shaded squares; Marconi et al. (2017)) and seafloor-sediment foraminifer-bound $\delta^{15}N$ (filled symbols; Ren et al. (2009, 2012b; 2015, and unpublished results)) are indicated by the colours (in ‰ *vs.* air). All three species, *G. ruber* (circles), *G. sacculifer* (triangles) and *O. universa* (diamonds), are shallow dwelling and contain dinoflagellate-symbionts. [Figure source: Schiebel et al. (2018)].

17

In the oligotrophic subtropical ocean, the shell-bound $\delta^{15}N$ of recently deposited foraminifera (i.e., in surface sediments) is well correlated with the $\delta^{15}N$ of overlying thermocline nitrate (Fig. 1.8) (Ren et al., 2009; Ren et al., 2012b), the primary source of new N to the euphotic (sunlit) zone (Altabet, 1988; Knapp et al., 2005). On this basis, foraminifer-bound $\delta^{15}N$ records from regions of complete surface-nitrate consumption have been interpreted as reflecting changes in the $\delta^{15}N$ of the low-latitude nitrate source. For instance, measurements of *G. ruber* from the Caribbean (gold record; Fig. 1.9) and *O. universa* from the South China Sea (green record; Fig. 1.9), both shallow-dwelling dinoflagellate-bearing species, show higher shell-bound $\delta^{15}N$ for glacial-aged than recent sediments (Ren et al., 2012a; Straub et al., 2013a; Ren et al., 2017). The low $\delta^{15}N$ of nitrate in the modern subtropical thermocline (compared to that of nitrate deeper in the water column) is caused by N_2-fixing organisms adding low-$\delta^{15}N$ nitrate (closer to the value of atmospheric N_2, $\delta^{15}N \sim 0‰$) to subsurface waters during their decomposition (Knapp et al., 2005; Knapp et al., 2008; Marconi et al., 2015). Therefore, a reduction in the N_2 fixation rate is proposed to explain the higher $\delta^{15}N$ of ice-age foraminifera in the Caribbean and South China Sea records (Ren et al., 2009; Ren et al., 2012a; Straub et al., 2013a; Ren et al., 2017). Together with pre-existing evidence for reduced denitrification rates during the last glacial period (Altabet et al., 1995; de Pol-Holz et al., 2006; Liu et al., 2008) (e.g., red record of bulk $\delta^{15}N$; Fig. 1.9), the foraminifer-$\delta^{15}N$ proxy provides support for the long-standing hypothesis of a self-regulating global N reservoir (Redfield, 1958; Schindler, 1977; Broecker, 1982b; Tyrrell, 1999; Deutsch et al., 2004). The major implication of this finding is that a change in the size of the total N inventory (i.e., a *stronger* biological pump) is not likely responsible for the glacial-interglacial cycles of CO_2 drawdown, because changes in N_2-fixation fluxes over time are balanced by changes in denitrification.

18
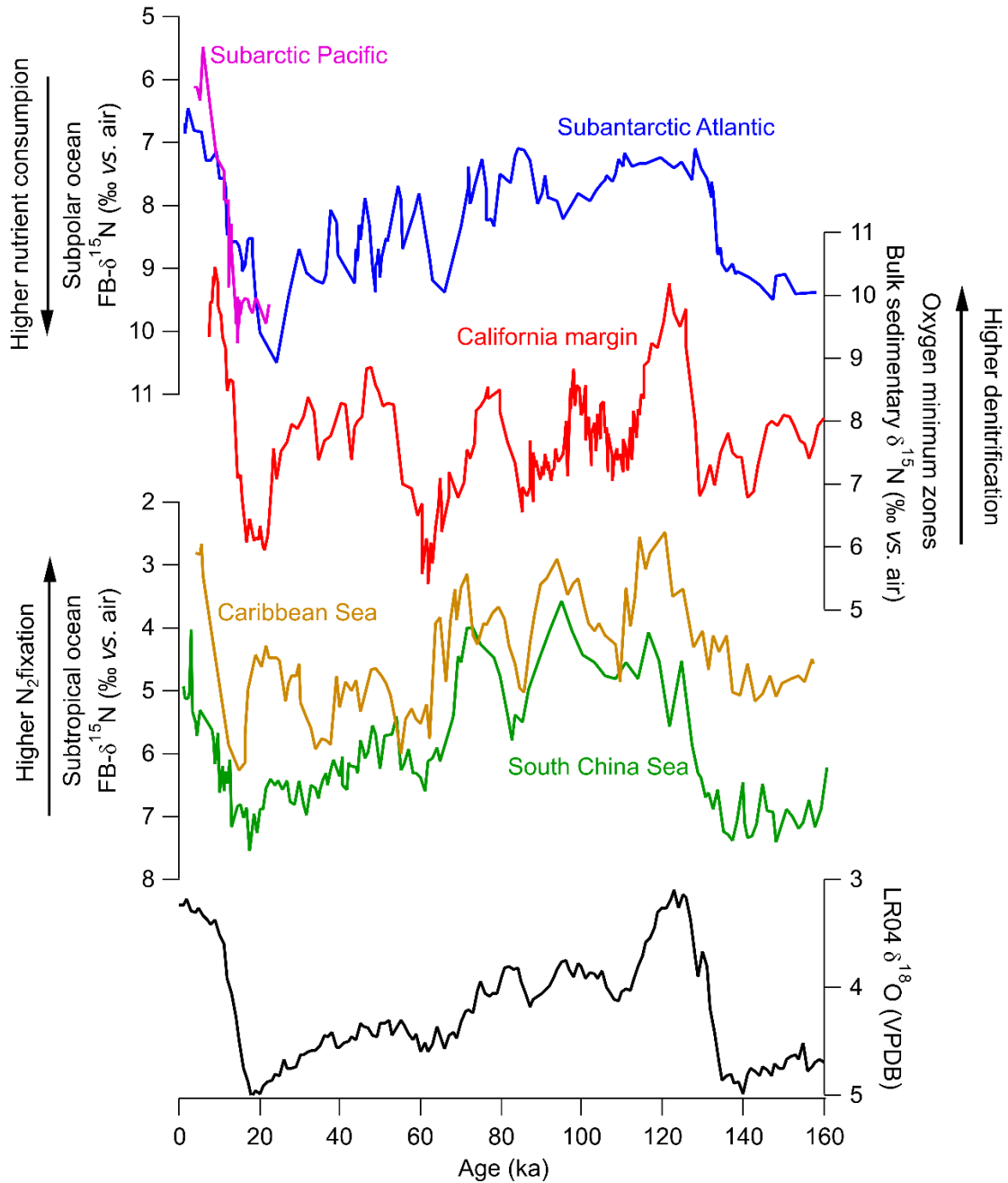
Fig. 1.9: Selection of foraminifer-bound (FB-) $\delta^{15}N$ paleo-records from the nitrate-poor low latitudes (*G. ruber* from the Caribbean (gold; Straub et al., 2013a); *O. universa* from the South China Sea (green; Ren et al., 2017)) and from the nitrate-rich high latitudes (*N. pachyderma* from the Subarctic Pacific (magenta; Ren et al., 2015); *G. bulloides* from the Subantarctic Atlantic (blue; Martínez-García et al., 2014)) plus a bulk sediment $\delta^{15}N$ record from a water-column denitrification zone in the Northeast Pacific (red; Liu et al., 2008). Benthic $\delta^{18}O$ (LR04 (black); Lisiecki & Raymo, 2005), a proxy for global temperature is shown for the 160 ky period, the last major glacial cycle. [Figure source: Schiebel et al. (2018)].

The only modern-ocean ground-truthing study (prior to the work presented in this thesis) generally supports the interpretation of foraminifer-bound δ^{15}N as a recorder of the subtropical nitrate supply, but also suggests a more complex picture (Ren et al., 2012b). While shallow-dwelling, dinoflagellate-bearing foraminifera were found to have a δ^{15}N similar to thermocline nitrate, deeper-dwelling species (either chrysophyte-bearing or symbiont-barren) were found to be elevated by 1-2‰. Heterotrophs are typically ~3‰ elevated in δ^{15}N relative to their food source due to the preferential excretion of low-δ^{15}N ammonium; this is known as the "trophic effect" or "trophic elevation" (Checkley & Miller, 1989). Therefore, one might have expected the "largely carnivorous" shallow-dwellers (feeding on higher-δ^{15}N zooplankton) to have a higher δ^{15}N than the "largely herbivorous" intermediate-to-deep dwellers (feeding on lower-δ^{15}N phytoplankton). Two different mechanisms were proposed to explain this discrepancy: (1) deep-dwellers feed on more degraded, higher-δ^{15}N particles available in the subsurface (Altabet, 1988), and/or (2) dinoflagellate symbionts consume low-δ^{15}N ammonium excreted by the shallow-dwelling foraminifera (Uhle et al., 1999), retaining low-δ^{15}N N within the host-symbiont system and thus weakening the trophic effect (Ren et al., 2012b).

The initial ground-truthing effort outlined above raises a number of questions about the foraminifer-bound δ^{15}N proxy. For one, why would foraminifera track the δ^{15}N of dissolved nitrate when they consume particulate food? Is it just a co-incidence that dinoflagellate-bearing foraminifera approximate the δ^{15}N of the modern low-latitude nitrate supply? And what do the results from the low latitudes mean for the applicability of the proxy to the high-latitude ocean, where dinoflagellate-bearing species are less abundant?

2.4.2 The high-nitrate high latitude ocean

Prior to the investigations described in this thesis, no ground-truthing work had been undertaken on foraminiferal N in the modern polar/subpolar ocean. The only high-latitude foraminifer-bound δ^{15}N paleo-records to date have been interpreted based on low-latitude ground-truthing, knowledge of N isotope dynamics in regions of incomplete nitrate consumption, and auxiliary paleo-data (Straub et al., 2013b; Martínez-García et al., 2014; Ren et al., 2015). For example, measurements of *N. pachyderma* (symbiont-barren) from the Subarctic Pacific (magenta record; Fig. 1.9) show a sharp decline in shell-bound δ^{15}N during the last deglaciation, consistent with a decrease in the δ^{15}N of nitrate consumed in surface

waters and thus, a decline in the extent of nitrate utilization into the current interglacial (Ren et al., 2015). More complete nitrate consumption during the last ice age combined with evidence for lower productivity (Kienast et al., 2004; Kohfeld & Chase, 2011) imply a reduction in the supply of nitrate to surface waters (Jaccard et al., 2005; Brunelle et al., 2007; Brunelle et al., 2010; Ren et al., 2015).

The first foraminifer-bound $\delta^{15}N$ record from the Southern Ocean has yielded some exciting results. *G. bulloides* (symbiont-barren) from the Subantarctic Atlantic (blue record; Fig. 1.9) also exhibits higher shell-bound $\delta^{15}N$ during glacial periods than during interglacials (Martínez-García et al., 2014). But in this case, elevated foraminiferal $\delta^{15}N$ coincides with higher productivity and peak dust fluxes (Kumar et al., 1995; Kohfeld et al., 2005; Martínez-García et al., 2009; Martínez-García et al., 2011). All these data are consistent with wind-blown dust alleviating iron-limited phytoplankton, leading to higher productivity (i.e., carbon fixation) and an enhanced degree of nitrate drawdown in the SAZ (Martin, 1990; Martínez-García et al., 2014), supporting the iron fertilization hypothesis over the frontal shift hypothesis (outlined in section 2.1). If this pattern of enhanced ice-age nitrate consumption applies to the whole of the SAZ, this domain of the Southern Ocean may be responsible for around half (~40 ppm) of the 80-100 ppm CO_2 decline that characterized glacial periods (Martínez-García et al., 2014; Hain et al., 2010).

In principle, however, the observed increase in ice-age foraminifer-bound $\delta^{15}N$ could alternatively be explained by: (a) a ~3‰ increase in the $\delta^{15}N$ of source nitrate; (b) a ~4‰ decrease in the isotope effect of nitrate assimilation; or (c) a ~3‰ increase in the $\delta^{15}N$ difference between *G. bulloides* and the nitrate consumed by phytoplankton during glacial times (Martínez-García et al., 2014). Below, the feasibility of mechanisms (a) to (c) are discussed in turn.

The modern SAZ is supplied with nitrate from two main sources: the SAZ thermocline (via vertical mixing, especially during winter) and Antarctic surface waters (via lateral mixing and northward Ekman (i.e., wind-driven) transport across the Polar Front Zone (PFZ), largely during summer) (Sigman et al., 1999a; DiFiore et al., 2006). While the former dominates supply on an annual basis (providing around 85% of the nitrate consumed in the more northern SAZ during summer) (DiFiore et al., 2006; Martínez-García et al., 2014), the latter dominates

21

the replenishment of fixed N that is biologically removed from the surface and thermocline of the SAZ and subtropics on longer (i.e., multi-annual to decadal) timescales (Palter et al., 2010). If nitrate consumption were more complete in the glacial AZ, as paleo-records suggest (François et al., 1997; Robinson & Sigman, 2008; Studer et al., 2015), this would have raised the δ^{15}N of nitrate supplied to the SAZ from the south, and thus also the δ^{15}N of foraminifera at the SAZ core site. However, the associated lowering of the nitrate concentration would simultaneously have lessened the contribution of the AZ endmember to the mixture, limiting its isotopic influence on the integrated SAZ nitrate supply (in accordance with isotope mass balance; Sigman et al., 2000; DiFiore et al., 2006). Mixing calculations demonstrate a maximum isotopic elevation of SAZ nitrate by ~1.2‰ via this mechanism (achieved by doubling present-day PFZ consumption; Martínez-García et al., 2014). Further increases in PFZ nitrate consumption (beyond double today's levels) would only weaken the polar endmember in its ability to elevate SAZ nitrate δ^{15}N (i.e., by less than 1.2‰). This is corroborated by the observation that SAZ foraminifer-bound δ^{15}N falls to almost interglacial values during low dust flux intervals of glacial periods (i.e., when nitrate consumption is unlikely to be enhanced, such that any changes in foraminifer-bound δ^{15}N must be driven by other mechanisms), indicating that the influence of AZ consumption changes alone can account for no more than 1‰ of the observed 3‰ elevation during glacial periods (Martínez-García et al., 2014). There is also the possibility that ~3‰ variations in the δ^{15}N of the SAZ nitrate source could result from whole-ocean nitrate δ^{15}N changes (due to an ice-age imbalance between global denitrification and N_2-fixation; Deutsch et al., 2004) but, as outlined above (section 2.4.1), this is not supported by the available low-latitude sedimentary records (François et al., 1992; François et al., 1997; Sigman et al., 1999b; Ren et al., 2012a; Galbraith et al., 2013; Straub et al., 2013a; Ren et al., 2017).

If the isotope effect of nitrate assimilation in the SAZ were lower during ice ages (i.e., weaker discrimination against the heavier ^{15}N-bearing nitrate), the biomass produced would have a higher δ^{15}N at the same degree of nitrate consumption (Wada & Hattori, 1978; Pennock et al., 1996; Waser et al., 1998; Sigman et al., 1999a; Martínez-García et al., 2014). Uncertainty regarding the isotope effect (both in terms of its magnitude and temporal variability) is a challenge common to all paleo-δ^{15}N proxies that are applied to regions of incomplete nitrate consumption (François et al., 1992; Altabet & François, 1994). The uncertainty is even greater

22

for the SAZ where traditional isotope models fail to capture the modern nitrate supply and consumption dynamics, leading to widely varying estimates for the nitrate assimilation isotope effect (from ~5‰ to ~11‰) (Sigman et al., 1999a; DiFiore et al., 2006). Narrowing this range for the modern SAZ is, therefore, an important step towards improving paleo-nutrient reconstructions from foraminifer-bound $\delta^{15}N$.

To investigate the feasibility of a glacial increase in the $\delta^{15}N$ offset between *G. bulloides* and the nitrate assimilated by phytoplankton, the shell-bound $\delta^{15}N$ of *O. universa* (a dinoflagellate-bearing species) was measured from the same core and found to be consistently ~3.4‰ lower than that measured for *G. bulloides* (Martínez-García et al., 2014). The $\delta^{15}N$ of *O. universa* has been observed to closely match the $\delta^{15}N$ of the nitrate consumed in surface waters across a range of low-latitude environments (Ren et al., 2009; Ren et al., 2012b). Assuming the same relationship holds in the high-latitude ocean, the relatively constant $\delta^{15}N$ offset (and thus the ~1:1 relationship) between *G. bulloides* and *O. universa* in the SAZ record suggests that the N isotopic relationship between *G. bulloides* and nitrate has not changed appreciably through glacial/interglacial cycles (Martínez-García et al., 2014). Measurements of living foraminifera, nitrate and particulate food source $\delta^{15}N$ from the modern Southern Ocean are critical for validating such interpretations.

2.5 Scope of the thesis

The N isotopic composition of microfossil-bound organic matter in seafloor sediments is providing new insight into the relationship between biological nutrient drawdown and global climate. The work presented in this thesis is focused on the modern ocean, tackling uncertainties that currently limit the potential of N isotope proxies, particularly foraminifer-bound $\delta^{15}N$, one of the latest additions to the paleo-$\delta^{15}N$ tool box.

Chapter 2 expands on initial ground-truthing efforts in the low-latitude ocean, where the "complication" of partial nitrate consumption is avoided. Using measurements of living, sinking, and recently buried foraminifera from the Sargasso Sea (subtropical North Atlantic), the following questions are addressed:

- What is the relationship between foraminifer tissue $\delta^{15}N$ and shell-bound $\delta^{15}N$?
- What are the drivers of seasonality in foraminiferal $\delta^{15}N$ in the Sargasso Sea?

- Is shell-bound $\delta^{15}N$ preserved during sinking and burial?

Chapter 3 presents the first attempt to ground-truth the foraminifer-bound $\delta^{15}N$ proxy in the modern high-latitude ocean. Living foraminifera were collected for $\delta^{15}N$ analysis from the Southern Ocean south of Africa during winter and late summer for comparison with the $\delta^{15}N$ of nitrate, bulk and size-fractionated particles in the same environment. Key questions include:

- Do living foraminifera in the Subantarctic track the $\delta^{15}N$ of nitrate consumed in surface waters?
- What are the drivers of seasonal differences in foraminiferal $\delta^{15}N$ in the Southern Ocean?
- What effect is seasonality expected to have on the $\delta^{15}N$ of foraminifera accumulating in seafloor sediments?

Chapter 4 addresses uncertainties regarding the nitrate assimilation isotope effect in the modern Subantarctic Ocean. Using a multi-annual, seasonally resolved geochemical box model of the Southern Ocean along with nitrate isotope observations from the Indo-Pacific sector, the following questions are addressed:

- What set of model parameters can recreate the seasonal cycle of nitrate drawdown and resupply observed in the modern Southern Ocean?
- What nitrate assimilation isotope effect best fits upper-ocean nitrate and export $\delta^{15}N$ observations from the Subantarctic?

Chapter 5 provides an overview of the conclusions that can be drawn from this work and proposes future directions for ground-truthing the foraminifer-bound $\delta^{15}N$ paleo-proxy.

3. References

Altabet, M.A. 1988. Variations in nitrogen isotopic composition between sinking and suspended particles: Implications for nitrogen cycling and particle transformation in the open ocean. *Deep-Sea Res. Pt I*, **35**, 535–554.

Altabet, M.A., & Curry, W.B. 1989. Testing models of past ocean chemistry using foraminifera ^{15}N/^{14}N. *Global Biogeochem. Cycles*, **3**(2), 107–119.

Altabet, M.A., & François, R. 1994. Sedimentary nitrogen isotopic ratio as a recorder for surface ocean nitrate utilization. *Global Biogeochem. Cycles*, **8**(1), 103–116.

Altabet, M.A., Francois, R., Murray, D.W., & Prell, W.L. 1995. Climate-related variations in denitrification in the Arabian Sea from sediment ^{15}N/^{14}N ratios. *Nature*, **373**, 506–509.

Anderson, O.R., Spindler, M., Bé, A.W.H., & Hemleben, C. 1979. Trophic activity of planktonic foraminifera. *J. Mar. Biol. Assoc. U. K.*, **59**(3), 791–799.

Anderson, R.F., Ali, S., Bradtmiller, L.I., Nielsen, S.H.H., Fleisher, M.Q., Anderson, B.E., & Burckle, L.H. 2009. Wind-driven upwelling in the Southern Ocean and the deglacial rise in atmospheric CO_2. *Science*, **323**, 1443–1448.

Arenillas, I., & Arz, J.A. 2017. Benthic origin and earliest evolution of the first planktonic foraminifera after the Cretaceous/Palaeogene boundary mass extinction. *Historical Biology*, **29**(1), 25–42.

Armstrong, H.A., & Brasier, M.D. 2005. *Microfossils*. 2nd edn. Malden, Oxford, Carlton: Blackwell Publishing Ltd.

Bard, E., & Rickaby, R.E.M. 2009. Migration of the subtropical front as a modulator of glacial climate. *Nature*, **460**, 380–384.

Barnola, J.M., Raynaud, D., Korotkevich, Y.S., & Lorius, C. 1987. Vostok ice core provides 160,000-year record of atmospheric CO_2. *Nature*, **329**, 408–414.

Bé, A.W.H. 1980. Gametogenic calcification in a spinose planktonic foraminifer, Globigerinoides sacculifer (Brady). *Mar. Micropaleontol.*, **5**, 283–310.

Bé, A.W.H., & Hemleben, C. 1970. Calcification in a living planktonic foraminifer, Globigerinoides sacculifer (BRADY). *N. Jb. Geol. Paläont. Abh.*, **134**(3), 221–234.

Bé, A.W.H., & Tolderlund, D.S. 1971. *The micropalaeontology of oceans*. Cambridge: University Press. Chap. Distribution and ecology of living planktonic Foraminifera in surface waters of the Atlantic and Indian Oceans, page 105–149.

Bé, A.W.H., Hemleben, C., Anderson, O.R., Spindler, M., Hacunda, J., & Tuntivate-Choy, S. 1977. Laboratory and Field Observations of Living Planktonic Foraminifera. *Micropaleontology*, **23**(2), 155–179.

Bé, A.W.H., Hemleben, C., Anderson, O.R., & Spindler, M. 1979. Chamber formation in planktonic Foraminifera. **25**(3), 294–307.

Bijma, J., Erez, J., & Hemleben, C. 1990. Lunar and semi-lunar reproductive cycles in some spinose planktonic foraminifers. *J. Foraminifer Res.*, **20**, 117–127.

Bijma, J., Hemleben, C., Huber, B.T., Erlenkeuser, H., & Kroon, D. 1998. Experimental determination of the ontogenetic stable isotope variability in two morphotypes of Globigerinella siphonifera (d'Orbigny). *Mar. Micropaleontol.*, **35**, 141–160.

Bird, C., Darling, K.F., Russell, A.D., Davis, C.V., Fehrenbacher, J., Free, A., Wyman, M., & Ngwenya, B.T. 2017. Cyanobacterial endobionts within a major marine planktonic calcifier (Globigerina bulloides, Foraminifera) revealed by 16S rRNA metabarcoding. *Biogeosciences*, **14**, 901–920.

Bird, C., Darling, K.F., Russell, A.D., Fehrenbacher, J.S., Davis, C.V., Free, A., & Ngwenya, B.T. 2018. 16S rRNA gene metabarcoding and TEM reveals different ecological strategies within the genus Neogloboquadrina (planktonic foraminifer). *PLoS ONE*, **13**(1), e0191653.

Branson, O., Bonnin, E.A., Perea, D.E., Spero, H.J., Zhu, Z., Winters, M., Hönisch, B., Russell, A.D., Fehrenbacher, J.S., & Gagnon, A.C. 2016. Nanometer-Scale Chemistry of a Calcite Biomineralization Template: Implications for Skeletal Composition and Nucleation. *Proc. Natl. Acad. Sci.*, **113**(46), 12934–12939.

Broecker, W.S. 1982a. Glacial to Interglacial Changes in Ocean Chemistry. *Prog. Oceanogr.*, **2**, 151–197.

Broecker, W.S. 1982b. Ocean chemistry during glacial time. *Geochim. Cosmochim. Acta*, **46**, 1689–1706.

Broecker, W.S., & Henderson, G.M. 1998. The sequence of events surrounding Termination II and their implications for the cause of glacial-interglacial CO_2 changes. *Paleoceanography*, **13**, 352–364.

Brunelle, B.G., Sigman, D.M., M.S., Cook, Keigwin, L.D., Haug, G.H., Plessen, B., Schettler, G., & Jaccard, S.L. 2007. Evidence from diatom-bound nitrogen isotopes for subarctic Pacific stratification during the last ice age and a link to North Pacific denitrification changes. *Paleoceanography*, **22**, PA1215.

Brunelle, B.G., Sigman, D.M., Jaccard, S.L., Keigwin, D.L., Plessen, B., Schettler, G., Cook, M.S., & G.H., Haug. 2010. Glacial/interglacial changes in nutrient supply and stratification in the western subarctic North Pacific since the penultimate glacial maximum. *Quat. Sci. Rev.*, **29**, 2579–2590.

Capone, D.G., Bronk, D.A., Mulholland, M.R., & Carpenter, E.J. (eds). 2008. *Nitrogen in the marine environment*. Burlington, MA: Academic Press.

Caron, M., & Homewood, P. 1983. Evolution of early planktic foraminifers. *Mar. Micropaleontol.*, **7**, 453–462.

Checkley, D.M., & Miller, C.A. 1989. Nitrogen isotope fractionation by oceanic zooplankton. *Deep-Sea Res. Pt A*, **36**, 1449–1456.

Cline, J.D., & Kaplan, I.R. 1975. Isotopic fractionation of dissolved nitrate during denitrification in the eastern tropical North Pacific Ocean. *Mar. Chem.*, **3**, 271–299.

Conkright, M.E., Levitus, S., & Boyer, T.P. 1994. World Ocean Atlas 1994 vol 1: Nutrients. NOAA Atlas NESDIS 1. U.S. Department of Commerce, Washington, D.C., 150 pp.

Crosta, X., & Shemesh, A. 2002. Reconciling down core anticorrelation of diatom carbon and nitrogen isotopic ratios from the Southern Ocean. *Paleoceanography*, **17**(1), 1–8.

Darling, K.F., & Wade, C.M. 2008. The genetic diversity of planktic foraminifera and the global distribution of ribosomal RNA genotypes. *Mar. Micropaleontol.*, **67**, 216–238.

Darling, K.F., Thomas, E., Kasemann, S.A., Seears, H.A., Smart, C.W., & Wade, C.M. 2009. Surviving mass extinction by bridging the benthic/planktic divide. *Proceedings of the National Academy of Sciences*, **106**(31), 12629–12633.

de Nooijer, L.J., Spero, H.J., Erez, J., Bijma, J., & Reichart, G.J. 2014. Biomineralization in perforate foraminifera. *Earth-Science Reviews*, **135**, 48–58.

de Pol-Holz, R., Ulloa, O., Dezileau, L., Kaiser, J., Lamy, F., & Hebbeln, D. 2006. Melting of the Patagonian Ice Sheet and deglacial perturbations of the nitrogen cycle in the eastern South Pacific. *Geophys. Res. Lett.*, **33**, L04704.

Deutsch, C., Sigman, D.M., Thunell, R.C., Meckler, A.N., & Haug, G.H. 2004. Isotopic constraints on glacial/interglacial changes in the oceanic nitrogen budget. *Global Biogeochem. Cycles*, **18**(GB4012).

DiFiore, P.J., Sigman, D.M., Trull, T.W., Lourey, M.J., Karsh, K., Cane, G., & Ho, R. 2006. Nitrogen isotope constraints on Subantarctic biogeochemistry. *J. Geophys. Res.*, **111**(C08016).

DiFiore, P.J., Sigman, D.M., Karsh, K.L., Trull, T.W., Dunbar, R.B., & Robinson, R.S. 2010. Poleward decrease in the isotope effect of nitrate assimilation across the Southern Ocean. *Geophys. Res. Lett.*, **37**(L17601).

d'Orbigny, A.D. 1826. Tableau méthodique de la classe des Céphalopodes. *Annales des Sciences Naturelles*, **7**, 96–169, 245–314.

Dujardin, F. 1835. Observations nouvelles sur les Céphalopodes microscopiques. *Annales des Sciences Naturelles, Paris (Seconde Série, Zoologie)*, **3**, 108–9.

Erez, J. 1983. *Biomineralization and biological metal accumulation*. Dordrecht: Reidel Publishing Company. Chap. Calcification rates, photosynthesis and light in planktonic Foraminifera, page 307–312.

Erez, J., Almogi-Labin, A., & Avraham, S. 1991. On the life history of planktonic Foraminifera: lunar reproduction cycle in Globigerinoides sacculifer (Brady). *Paleoceanography*, **6**, 295–306.

Faber, W.W., Anderson, O.R., Lindsey, J.L., & Caron, D.A. 1988. Algal-foraminiferal symbiosis in the planktonic foraminifer Globigerinella aequilateralis: I. Occurrence and stability of two mutually exclusive chrysophyte endosymbionts and their ultrastructure. *J. Foramin. Res.*, **18**, 334–343.

Faber, W.W., Anderson, O.R., & Caron, D.A. 1989. Algal-foraminiferal symbiosis in the planktonic foraminifer Globigerinella aequilateralis: II. Effects of two symbiont species on foraminiferal growth and longevity. *J. Foramin. Res.*, **19**(3), 185–193.

Fehrenbacher, J.S., Russell, A.D., Davis, C.V., Gagnon, A.C., Spero, H.J., Cliff, J.B., Zhu, Z., & Martin, P. 2017. Link between light-triggered Mg-banding and chamber formation in the planktic foraminifera Neogloboquadrina dutertrei. *Nat. Commun.*, **8**.

Fenton, I.S., Pearson, P.N., Dunkley Jones, T., & Purvis, A. 2016. Environmental predictors of diversity in recent planktonic foraminifera as recorded in marine sediments. *PLoS ONE*, **11**(11), e0165522.

François, R., Altabet, M.A., & Burckle, L.H. 1992. Glacial to interglacial changes in surface nitrate utilization in the Indian sector of the Southern Ocean as recorded by sediment δ^{15}N. *Paleoceanography*, **7**(5), 589–606.

François, R., Bacon, M.P., Altabet, M.A., & Labeyrie, L.D. 1993. Glacial/interglacial changes in sediment rain rate in the SW Indian sector of sub-Antarctic waters as recorded by Th-230, Pa-231, U, and δ^{15}N. *Paleoceanography*, **8**(5), 611–629.

François, R., Altabet, M.A., Yu, E.F., Sigman, D.M., Bacon, M.P., Frank, M., Bohrmann, G., Bareille, G., & Labeyrie, L.D. 1997. Contribution of Southern Ocean surface-water stratification to low atmospheric CO_2 concentrations during the last glacial period. *Nature*, **389**, 929–935.

Fujiki, T., Takagi, H., Kimoto, K., Kurasawa, A., Yuasa, T., & Mino, Y. 2014. Assessment of algal photosynthesis in planktic foraminifers by fast repetition rate fluorometry. *J. Plankton Res.*, **36**, 1403–1407.

Galbraith, E.D., Sigman, D.M., Robinson, R.S., & Pedersen, T.F. 2008. *Nitrogen in the Marine Environment*. 2nd edn. Academic Press, Burlington, Mass. Chap. Nitrogen in past marine environments, pages 1497–1535.

Galbraith, E.D., Kienast, M., Albuquerque, A.L., Altabet, M.A., Batista, F., Bianchi, D., Calvert, S.E., Contreras, S., Crosta, X., De Pol-Holz, R., Dubois, N., Etourneau, J., François, R., Hsu, T.-C., Ivanochko, T., Jaccard, S.L., Kao, S.-J., Kiefer, T., Kienast, S., Lehmann, M.F., Martinez, P., McCarthy, M., Meckler, A.N., Mix, A., Möbius, J., Pedersen, T.F., Pichevin, L., Quan, T.M., Robinson, R.S., Ryabenko, E., Schmittner, A., Schneider, R., Schneider-Mor, A., Shigemitsu, M., Sinclair, D., Somes, C., Studer, A.S., Tesdal, J.-E., Thunell, R., & Yang, J.-Y.T. 2013. The acceleration of oceanic denitrification during deglacial warming. *Nat. Geosci.*, **6**, 579–584.

Ganeshram, R.S., Pedersen, T.F., Calvert, S.E., & Murray, J.W. 1995. Large changes in oceanic nutrient inventories from glacial to interglacial periods. *Nature*, **376**, 755–758.

Gastrich, M. D. 1987. Ultrastructure of a new intracellular symbiotic alga found within planktonic foraminifera. *J. Phycol.*, **23**, 623–632.

Hain, M., Sigman, D.M., & Haug, G.H. 2010. Carbon dioxide effects of Antarctic stratification, North Atlantic Intermediate Water formation, and subantarctic nutrient drawdown during the last ice age: Diagnosis and synthesis in a geochemical box model. *Global Biogeochem. Cycles*, **24**(GB4023).

Hemleben, C., Spindler, M., Breitinger, I., & Deuser, W.G. 1985. Field and laboratory studies on the ontogeny and ecology of some globorotaliid species from the Sargasso Sea off Bermuda. *J. Foramineferal Res.*, **15**(4), 254–272.

Hemleben, C., Spindler, M., & Anderson, O.R. 1989. *Modern Planktonic Foraminifera*. Springer-Verlag.

Horn, M.G., Robinson, R.S., Rynearson, T.A., & Sigman, D.M. 2011. Nitrogen isotopic relationship between diatom-bound and bulk organic matter of cultured polar diatoms. *Paleoceanography*, **26**(PA3208).

Jaccard, S.L., Haug, G.H., Sigman, D.M., Pedersen, T.F., Thierstein, H.R., & Rohl, U. 2005. Glacial/interglacial changes in subarctic North Pacific stratification. *Science*, **308**(5724), 1003–1006.

Jacob, D.E., Wirth, R., Agbaje, O.B.A., Branson, O., & Eggins, S.M. 2017. Planktic foraminifera form their shells via metastable carbonate phases. *Nat. Commun.*, **8**.

Jacot Des Combes, H., Esper, O., De La Rocha, C.L., Abelmann, A., Gersonde, R., Yam, R., & Shemesh, A. 2008. Diatom δ^{13}C, δ^{15}N, and C/N since the Last Glacial Maximum in the Southern Ocean: Potential impact of Species Composition. *Paleoceanography*, **23**(PA4209).

Jonkers, L., Reynolds, C.E., Richey, J., & Hall, I.R. 2015. Lunar periodicity in the shell flux of planktonic Foraminifera in the Gulf of Mexico. *Biogeosciences*, **12**, 3061–3070.

Jørgensen, B.B., Erez, J., Revsbech, N.P., & Cohen, Y. 1985. Symbiotic photosynthesis in a planktonic foraminiferan Globigerinoides sacculifer (Brady), studied with microelectrodes. *Limnol. Oceanogr.*, **30**, 1253–1267.

Jouzel, J., Masson-Delmotte, V., Cattani, O., Dreyfus, G., Falourd, S., Hoffmann, G., Minster, B., Nouet, J., Barnola, J.M., Chappellaz, J., Fischer, H., Gallet, J.C., Johnsen, S., Leuenberger, M., Loulergue, L., Luethi, D., Oerter, H., Parrenin, F., Raisbeck, G., Raynaud, D., Schilt, A., Schwander, J., Selmo, E., Souchez, R., Spahni, R., Stauffer, B., Steffensen, J.P., Stenni, B., Stocker, T.F., Tison, J.L., M., Werner, & E.W.., Wolff. 2007. Orbital and Millennial Antarctic Climate Variability over the Past 800,000 Years. *Science*, **317**(5839), 793–797.

Kemeny, P.C., Kast, E.R., Hain, M.P., Fawcett, S.E., Fripiat, F., Studer, A.S., Martínez-García, A., Haug, G.H., & Sigman, D.M. 2018. A Seasonal Model of Nitrogen Isotopes in the Ice Age Antarctic Zone: Support for Weakening of the Southern Ocean Upper Overturning Cell. *Paleoceanography and Paleoclimatology*.

Kienast, S.S., Hendy, I.L., Crusius, J., Pedersen, T.F., & Calvert, S.E. 2004. Export production in the subarctic North Pacific over the last 800 kyrs: No evidence for iron fertilization? *J. Oceanogr.*, **60**(1), 189–203.

Kier, R.S. 1988. On the late Pleistocene ocean geochemistry and circulation. *Paleoceanography*, **3**, 413–445.

King, K., Jr., & Hare, P.E. 1972. Amino Acid Composition of the Test as a Taxonomic Character for Living and Fossil Planktonic Foraminifera. *Micropaleontology*, **18**(3), 285–293.

Knapp, A.N., Sigman, D.M., & Lipschultz, F. 2005. N isotopic composition of dissolved organic nitrogen and nitrate at the Bermuda Atlantic Time-series Study site. *Global Biogeochem. Cycles*, **19**, 1–15.

Knapp, A.N., DiFiore, P.J., Deutsch, C., Sigman, D.M., & Lipschultz, F. 2008. Nitrate isotopic composition between Bermuda and Puerto Rico: Implications for N_2 fixation in the Atlantic Ocean. *Global Biogeochem. Cycles*, **22**, 1–14.

Knox, F., & McElroy, M.B. 1984. Changes in atmospheric CO_2: influence of the marine biota at high latitude. *J. Geophys. Res.*, **89**, 4629–4637.

Kohfeld, K.E., & Chase, Z. 2011. Controls on deglacial changes in biogenic fluxes in the North Pacific Ocean. *Quat. Sci. Rev.*, **30**, 3350–3363.

Kohfeld, K.E., Le Quere, C., Harrison, S.P., & Anderson, R.F. 2005. Role of marine biology in glacial-interglacial CO_2 cycles. *Science*, **308**, 74–78.

Kolber, Z.S., & Falkowski, P.G. 1993. Use of active fluorescence to estimate phytoplankton photosynthesis in situ. *Limnol. Oceanogr.*, **38**, 1646–1665.

Kucera, M. 2007. *Developments in marine geology*. Elsevier. Chap. Chapter six: Planktonic Foraminifera as tracers of past oceanic environments, page 213–262.

Kumar, N., Gwiazda, R., Anderson, R.F., & Froelich, P.N. 1993. ^{231}Pa/^{230}Th ratios in sediments as a proxy for past changes in Southern Ocean productivity. *Nature*, **362**, 45–48.

Kumar, N., Anderson, R.F., Mortlock, R.A., Froelich, N., Kubik, P., Dittrich-Hannen, B., & Suter, M. 1995. Increased biological productivity and export production in the glacial Southern Ocean. *Nature*, **378**, 675–680.

Lisiecki, L.E., & Raymo, M.E. 2005. A Pliocene-Pleistocene stack of 57 globally distributed benthic $\delta^{18}O$ records. *Paleoceanography*, **20**, PA1003.

Liu, K.-K., & Kaplan, I.R. 1989. The eastern tropical Pacific as a source of ^{15}N-enriched nitrate in seawater off southern California. *Limnol. Oceanogr.*, **34**(5), 820–830.

Liu, Z., Altabet, M.A., & Herbert, T.D. 2008. Plio-Pleistocene denitrification in the eastern tropical North Pacific: Intensification at 2.1 Ma. *Geochem. Geophys. Geosyst.*, **9**(11), Q11006.

Loeblich, A.R., & Tappan, H. 1988. *Foraminiferal genera and their classification*. New York: van Nostrand Reinhold, New York.

Loeblich, A.R., & Tappan, H. 1992. *Studies in benthic Foraminifera*. Tokyo: Tokai University Press. Chap. Present status of foraminiferal classification, page 93–102.

Lohmann, G.P. 1995. A model for variation in the chemistry of planktonic foraminifera due to secondary calcification and selective dissolution. *Paleoceanography*, **10**(3), 445–457.

Lourey, M.J., Trull, T.W., & Sigman, D.M. 2003. Sensitivity of $\delta^{15}N$ of nitrate, surface suspended and deep sinking particulate nitrogen to seasonal nitrate depletion in the Southern Ocean. *Global Biogeochem. Cycles*, **17**(3), 1–18.

Lüthi, D., Le Floch, M., Bereiter, B., Blunier, T., Barnola, J.-M., Siegenthaler, U., Raynaud, D., Jouzel, J., Fischer, H., Kawamura, K., & Stocker, T.F. 2008. High-resolution carbon dioxide concentration record 650,000-800,000 years before present. *Nature*, **453**, 379–382.

Marconi, D., Weigand, M.A., Rafter, P.A., McIlbin, M.R., Forbes, M., Casciotti, K.L., & Sigman, D.M. 2015. Nitrate isotope distributions on the US GEOTRACES North Atlantic cross-basin section: Signals of polar nitrate sources and low latitude nitrogen cycling. *Marine Chemistry*, **177**, 143–156.

Marconi, D., Sigman, D.M., Casciotti, K.L., Campbell, E.C., Weigand, M.A., Fawcett, S.E., Knapp, A.N., Rafter, P.A., Ward, B.B., & Haug, G.H. 2017. Tropical dominance of N_2 fixation in the North Atlantic Ocean. *Global Biogeochem. Cycles*, **31**, 1608–1623.

Mariotti, A., Germon, J.C., Hubert, P., Kaiser, P., Letolle, R., Tardieux, A., & Tardieux, P. 1981. Experimental determination of nitrogen kinetic isotope fractionation: Some principles; illustration for the denitrification and nitrification processes. *Plant Soil*, **62**, 413–430.

Martin, J.H. 1990. Glacial-interglacial CO_2 Change: The Iron Hypothesis. *Paleoceanography*, **5**(1), 1–13.

Martínez-García, A., Rosell-Melé, A., Geibert, W., Gersonde, R., Masqué, P., Gaspari, V., & Barbante, C. 2009. Links between iron supply, marine productivity, sea surface temperature, and CO_2 over the last 1.1 Ma. *Paleoceanography*, **24**(PA1207).

Martínez-García, A., Rosell-Melé, A., Jaccard, S.L., Geibert, W., Sigman, D.M., & Haug, G.H. 2011. Southern Ocean dust–climate coupling over the past four million years. *Nature*, **476**, 312–315.

Martínez-García, A., Sigman, D.M., Ren, H., Anderson, R.F., Straub, M., Hodell, D.A., Jaccard, S.L., Eglinton, T.I., & Haug, G.H. 2014. Iron Fertilization of the Subantarctic Ocean During the Last Ice Age. *Science*, **343**, 1347–1350.

Matsumoto, K., Sarmiento, J.L., & Brzezinski, M.A. 2002. Silicic acid leakage from the Southern Ocean: A possible explanation for glacial atmospheric pCO_2. *Global Biogeochem. Cycles*, **16**(3), 1–23.

McElroy, M. B. 1983. Marine biological controls on atmospheric CO_2 and climate. *Nature*, **302**, 328–329.

Morales, L.V., Sigman, D.M., Horn, M.G., & Robinson, R.S. 2013. Cleaning methods for the isotopic determination of diatom-bound nitrogen in non-fossil diatom frustules. *Limnol. Oceanogr. Methods*, **11**(2), 101–112.

Morales, L.V., Granger, J., Chang, B.X., Prokopenko, M.G., Plessen, B., Gradinger, R., & Sigman, D.M. 2014. Elevated $^{15}N/^{14}N$ in particulate organic matter, zooplankton, and diatom frustule-bound nitrogen in the ice-covered water column of the Bering Sea eastern shelf. *Deep Sea Res. Part II*, **109**, 100–111. Understanding Ecosystem Processes in the Eastern Bering Sea III.

Mortlock, R.A., Charles, C.D., Froelich, P.N., Zibello, M.A., Saltzman, J., Hays, J.D., & Burckle, L.H. 1991. Evidence for lower productivity in the Antarctic Ocean during the last glaciation. *Nature*, **351**, 220–223.

Needoba, J.A., & Harrison, P.J. 2004. Influence of low light and a light:dark cycle on NO_3^- uptake, intracellular NO_3^-, and nitrogen isotope fractionation by marine phytoplankton. *J. Phycol.*, **40**, 505–516.

Needoba, J.A., Waser, N.A., Harrison, P.J., & Calvert, S.E. 2003. Nitrogen isotope fractionation in 12 species of marine phytoplankton during growth on nitrate. *Mar. Ecol. Prog. Ser.*, **225**, 81–91.

Needoba, J.A., Sigman, D.M., & Harrison, P.J. 2004. The mechanism of isotope fractionation during algal nitrate assimilation as illuminated by the $^{15}N/^{14}N$ of intracellular nitrate. *J. Phycol.*, **40**, 517–522.

Palter, J.B., Sarmiento, J.L., Gnanadesikan, A., Simeon, J., & Slater, R.D. 2010. Fueling export production: nutrient return pathways from the deep ocean and their dependence on the Meridional Overturning Circulation. *Biogeosciences*, **7**, 3549–3568.

Pennock, J.R., Velinsky, D.J., Ludlam, J.M., Sharp, J.H., & Fogel, M.L. 1996. Isotope fractionation of ammonium and nitrate during their uptake by Skeletonema Costatum: Implications for the $\delta^{15}N$ dynamics under bloom conditions. *Limnol. Oceanogr.*, **41**(3), 451–459.

Petit, J.R., Jouzel, J., Raynaud, D., Barkov, N.I., Barnola, J.-M., Basile, I., Bender, M., Chappellaz, J., Davis, M., Delaygue, G., Delmotte, M., Kotlyakov, V.M., Legrand, M., Lipenkov, V. Y., Lorius, C., Pépin, L., Ritz, C., Saltzman, E., & Stievenard, M. 1999. Climate and atmospheric history of the past 420,000 years from the Vostok ice core, Antarctica. *Nature*, **399**, 429–436.

Redfield, A.C. 1958. The biological control of chemical factors in the environment. *Amer. Sci.*, **46**(3), 205–221.

Ren, H., Sigman, D.M., Meckler, A.N., Plessen, B., Robinson, R.S., Rosenthal, Y., & Haug, G.H. 2009. Foraminiferal Isotope Evidence of Reduced Nitrogen Fixation in the Ice Age Atlantic Ocean. *Science*, **323**, 244–248.

Ren, H., Sigman, D.M., Chen, M.-T., & Kao, S.-J. 2012a. Elevated foraminifera-bound nitrogen isotopic composition during the last ice age in the South China Sea and its global and regional implications. *Global Biogeochem. Cycles*, **26**(GB1031), 1–13.

Ren, H., Sigman, D.M., Thunell, R.C., & Prokopenko, M.G. 2012b. Nitrogen isotopic composition of planktonic foraminifera from the modern ocean and recent sediments. *Limnol. Oceanogr.*, **57**(4), 1011–1024.

Ren, H., Studer, A.S., Serno, S., Sigman, D.M., Winckler, G., Anderson, R.F., Oleynik, S., Gersonde, R., & Haug, G.H. 2015. Glacial-to-interglacial changes in nitrate supply and consumption in the subarctic North Pacific from microfossil-bound N isotopes at two trophic levels. *Paleoceanography*, **30**, 1217–1232.

Ren, H., Sigman, D.M., Martínez-García, A., Anderson, R.F., Chen, M.-T., Ravelo, A.C., Straub, M., Wong, G.T.F., & Haug, G.H. 2017. Impact of glacial/interglacial sea level change on the ocean nitrogen cycle. *Proceedings of the National Academy of Sciences*, E6759–E6766.

Robbins, L.L., & Brew, K. 1990. Proteins from the organic matrix of core-top and fossil planktonic foraminifera. *Geochim. Cosmochim. Acta*, **54**, 2285–2292.

Robinson, R.S., & Sigman, D.M. 2008. Nitrogen isotopic evidence for a poleward decrease in surface nitrate within the ice age Antarctic. *Quat. Sci. Rev.*, **27**, 1076–1090.

Robinson, R.S., Brunelle, B.G., & Sigman, D.M. 2004. Revisiting nutrient utilization in the glacial Antarctic: evidence from a new diatom-bound N isotope method. *Paleoceanography*, **19**(PA3001), 1–13.

Robinson, R.S., Sigman, D.M., DiFiore, P.J., Rohde, M.M., Mashiotta, T.A., & Lea, D.W. 2005. Diatom-bound $^{15}N/^{14}N$: New support for enhanced nutrient consumption in the ice age Subantarctic. *Paleoceanography*, **20**(PA3003).

Robinson, R.S., Kienast, M., Albuquerque, A.L., Altabet, M., Contreras, S., De Pol Holz, R., Dubois, N., François, R., Galbraith, E., Hsu, T-C., Ivanochko, T., Jaccard, S., Kao, S-J, Kiefer, T., Kienast, S., Lehmann, M., Martinez, P., McCarthy, M., Möbius, J., Pedersen, T., Quan, T.M., Ryabenko, E., Schmittner, A., Schneider, R., Schneider-Mor, A., Shigemitsu, M., Sinclair, D., Somes, C., Studer, A., Thunell, R., & Yang, J-Y. 2012. A review of nitrogen isotopic alteration in marine sediments. *Paleoceanography*, **27**(PA4203).

Ruttenberg, K.C. 1993. Reassessment of the oceanic residence time of phosphorous. *Chem. Geol.*, **107**, 405–409.

Saino, T., & Hattori, A. 1980. ^{15}N natural abundance in oceanic suspended particulate matter. *Nature*, **283**, 752–754.

Sarmiento, J.L., & Toggweiler, J.R. 1984. A new model for the role of the oceans in determining atmospheric pCO_2. *Nature*, **308**, 621–624.

Sarmiento, J.L., Slater, R., Barber, R., Bopp, L., Doney, S.C., Hirst, A.C., Kleypas, J., Matear, R., Mikolajewicz, U., Monfray, P., Soldatov, V., Spall, S.A., & Stouffer, R. 2004. Response of ocean ecosystems to climate warming. *Global Biogeochem. Cycles*, **18**(GB3003), 1–23.

Schiebel, R. 2002. Planktic foraminiferal sedimentation and the marine calcite budget. *Global Biogeochem. Cycles*, **16**(4), 1–21.

Schiebel, R., & Hemleben, C. 2017. *Planktic Foraminifers in the Modern Ocean*. Springer-Verlag Berlin Heidelberg.

Schiebel, R., Bijma, J., & Hemleben, C. 1997. Population dynamics of the planktic foraminifer Globigerina bulloides from the eastern North Atlantic. *Deep-Sea Res. Pt I*, **44**, 1701–1713.

Schiebel, R., Waniek, J., Bork, M., & Hemleben, C. 2001. Planktic foraminiferal production stimulated by chlorophyll redistribution and entrainment of nutrients. *Deep Sea Res. Pt I*, **48**(3), 721–740.

Schiebel, R., Smart, S.M., Jentzen, A., Jonkers, L., Morard, R., Meilland, J., Michel, E., Coxall, H.K., Hull, P.M., de Garidel-Thoron, T., Aze, T., Quillévéré, F., Ren, H., Sigman, D.M., Vonhof, H.B., Martínez-García, A., Kucera, M., Bijma, J., Spero, H., & Haug, G.H. 2018. Advances in planktonic foraminifer research: New perspectives for paleoceanography. *Rev. Micropaleontol.*, **61**(3-4), 113–138.

Schindler, D.W. 1977. Evolution of Phosphorus Limitation in Lakes. *Science*, **195**(4275), 260–262.

Schubert, C.J., & Calvert, S.E. 2001. Nitrogen and carbon isotopic composition of marine and terrestrial organic matter in Arctic Ocean sediments: Implications for nutrient utilization and organic matter composition. *Deep-Sea Res. Pt I*, **48**, 789–810.

Seears, H.A., Darling, K.F., & Wade, C.M. 2012. Ecological partitioning and diversity in tropical planktonic foraminifera. *BMC Evolutionary Biology*, **12**(54).

Shemesh, A., Macko, S.A., Charles, C.D., & Rau, G.H. 1993. Isotopic evidence for reduced productivity in the glacial Southern Ocean. *Science*, **262**, 407–410.

Siegenthaler, U., & Wenk, T. 1984. Rapid atmospheric CO_2 variations and ocean circulation. *Nature*, **308**, 624–626.

Sigman, D.M., & Boyle, E.A. 2000. Glacial/interglacial variations in atmospheric carbon dioxide. *Nature*, **407**, 859–869.

Sigman, D.M., Altabet, M.A., McCorkle, D.C., François, R., & Fischer, G. 1999a. The $\delta^{15}N$ of nitrate in the Southern Ocean: Consumption of nitrate in surface waters. *Global Biogeochem. Cycles*, **13**(4), 1149–1166.

Sigman, D.M., Altabet, M.A., François, R., McCorkle, D.C., & Gaillard, J.F. 1999b. The isotopic composition of diatom-bound nitrogen in Southern Ocean sediments. *Paleoceanography*, **14**(2), 118–134.

Sigman, D.M., Altabet, M.A., McCorkle, D.C., François, R., & Fischer, G. 2000. The $\delta^{15}N$ of nitrate in the Southern Ocean: Nitrogen cycling and circulation in the ocean interior. *J. Geophys. Res.*, **105**(C8), 19599–19614.

Sigman, D.M., Casciotti, K.L., Andreani, M., Barford, C., Galanter, M., & Böhlke, J.K. 2001. A Bacterial Method for the Nitrogen Isotopic Analysis of Nitrate in Seawater and Freshwater. *Anal. Chem.*, **73**, 4145–4153.

Sigman, D.M., DiFiore, P.J., Hain, M.P., Deutsch, C., Wang, Y., Karl, D.M., Knapp, A.N., Lehmann, M.F., & Pantoja, S. 2009a. The dual isotopes of deep nitrate as a constraint on the cycle and budget of oceanic fixed nitrogen. *Deep-Sea Res. Pt I*, **56**, 1419–1439.

Sigman, D.M., Karsh, K.L., & Casciotti, K.L. 2009b. *Encyclopedia of Ocean Sciences*. 2nd edn. Elsevier, Amsterdam. Chap. Ocean process tracers: Nitrogen isotopes in the ocean, pages 4138–4152.

Sigman, D.M., Hain, M.P., & Haug, G.H. 2010. The polar ocean and glacial cycles in atmospheric CO_2 concentration. *Nature*, **466**, 47–55.

Spero, H. 1987. SYMBIOSIS IN THE PLANKTONIC FORAMINIFER, ORBULINA UNIVERSA, AND THE ISOLATION OF ITS SYMBIOTIC DINOFLAGELLATE, GYMNODINIUM BÉII SP. NOV.1. *J. Phycol.*, **23**, 307–317.

Spero, H.J. 1988. Ultrastructural examination of chamber morphogenesis and biomineralization in the planktonic foraminifer Orbulina universa. *Mar. Biol.*, **99**(1), 9–20.

Spero, H.J., & Angel, D.L. 1991. Planktonic sarcodines: microhabitat for oceanic dinoflagellates. *J. Phycol.*, **27**, 187–195.

Spero, H.J., & Parker, S.L. 1985. Photosynthesis in the symbiotic planktonic foraminifer Orbulina universa, and its potential contribution to oceanic primary productivity. *J. Foramin. Res.*, **15**(4), 273–281.

Spindler, M., Hemleben, C., Salomons, J., & Smit, L. 1984. Feeding behavior of some planktonic foraminifers in laboratory cultures. *J. Foramin. Res.*, **14**(4), 237–249.

Stephens, B.B., & Keeling, R.F. 2000. The influence of Antarctic sea ice on glacial-interglacial CO_2 variations. *Nature*, **404**, 171–174.

Stoecker, D.K., Johnson, M.D., de Vargas, C., & Not, F. 2009. Acquired phototrophy in aquatic protists. *Aquat. Microb. Ecol.*, **57**(3), 279–310.

Stoecker, D.K., Hansen, P.J., Caron, D.A., & Mitra, A. 2017. Mixotrophy in the Marine Plankton. *Annual Reviews of Marine Science*, **9**, 311–335.

Straub, M., Sigman, D.M., Ren, H., Martínez-García, A., Nele Meckler, A., & Haug, G.H. 2013a. Changes in North Atlantic nitrogen fixation controlled by ocean circulation. *Nature*, **501**, 200–204.

Straub, M., Tremblay, M.M., Sigman, D.M., Studer, A.S., Ren, H., Toggweiler, J.R., & Haug, G.H. 2013b. Nutrient conditions in the subpolar North Atlantic during the last glacial period reconstructed from foraminifera-bound nitrogen isotopes. *Paleoceanography*, **28**(1), 79–90.

Studer, A.S., Sigman, D.M., Martínez-García, A., Benz, V., Winckler, G., Kuhn, G., Esper, O., Lamy, F., Jaccard, S.L., Wacker, L., Oleynik, S., Gersonde, R., & Haug, G.H. 2015. Antarctic Zone nutrient conditions during the last two glacial cycles. *Paleoceanography*, **30**(7), 845–862. 2014PA002745.

Takagi, H., Kimoto, K., Fujiki, T., Kurasawa, A., Moriya, K., & Hirano, H. 2016. Ontogenetic dynamics of photosymbiosis in cultured planktic foraminifers revealed by fast repetition rate fluorometry. *Mar. Micropaleontol.*, **122**, 44–52.

Takagi, H., Kimoto, K., Fujiki, T., Saito, H., Schmidt, C., Kucera, M., & Moriya, K. 2019. Characterizing photosymbiosis in modern planktonic foraminifera. *Biogeosciences*.

Talley, L., Pickard, G., Emery, W., & Swift, J. 2011. *Descriptive Physical Oceanography: An Introduction*. 6th edn. Academic Press.

Toggweiler, J. R. 1999. Variations in atmospheric CO_2 driven by ventilation of the ocean's deepest water. *Paleoceanography*, **14**, 571–588.

Tyrrell, T. 1999. The relative influences of nitrogen and phosphorus on oceanic primary production. *Nature*, **400**, 525–531.

Uhle, M.E., Macko, S.A., Spero, H.J., Engel, M.H., & Lea, D.W. 1997. Sources of carbon and nitrogen in modern planktonic foraminifera: the role of algal symbionts as determined by bulk and compound specific stable isotopic analyses. *Org. Geochem.*, **27**(3/4), 103–113.

Uhle, M.E., Macko, S.A., Spero, H.J., Lea, D.W., Ruddiman, W.F., & Engel, M.H. 1999. The fate of nitrogen in the Orbulina universa foraminifera–symbiont system determined by nitrogen isotope analyses of shell-bound organic matter. *Limnol. Oceanogr.*, **44**(8), 1968–1977.

Wada, E., & Hattori, A. 1978. Nitrogen isotope effects in the assimilation of inorganic nitrogenous compounds by marine diatoms. *Geomicrobiol. J.*, **1**(1), 85–101.

Waser, N.A.D., Harrison, P.J., Nielsen, B., Calvert, S.E., & Turpin, D.H. 1998. Nitrogen Isotope Fractionation During the Uptake and Assimilation of Nitrate, Nitrite, Ammonium, and Urea by a Marine Diatom. *Limnol. Oceanogr.*, **43**(2), 215–224.

Weigand, M.A., Foriel, J., Barnett, B., Oleynik, S., & Sigman, D.M. 2016. Updates to instrumentation and protocols for isotopic analysis of nitrate by the denitrifier method. *Rapid Commun. Mass Spectrom.*, **30**(12), 1365–1383. RCM-15-0493.R1.

Zachos, J., Pagani, M., Sloan, L., Thomas, E., & Billups, K. 2001. Trends, Rhythms, and Aberrations in Global Climate 65 Ma to Present. *Science*, **292**(5517), 686–693.

CHAPTER 2: Ground-truthing the planktic foraminifer-bound nitrogen isotope paleo-proxy in the Sargasso Sea

Sandi M. Smart[1]*, Haojia Ren[2], Sarah E. Fawcett[3], Ralf Schiebel[4], Maureen Conte[5], Patrick A. Rafter[6], Karen K. Ellis[7], Mira A. Weigand[7], Sergey Oleynik[7], Gerald H. Haug[4], Daniel M. Sigman[7]

[1] Department of Earth Sciences, Stellenbosch University, Private Bag X1, Matieland, 7602, South Africa (*correspondence: sandi.smart@alumni.uct.ac.za)

[2] Department of Geosciences, National Taiwan University, Taipei 106, Taiwan

[3] Department of Oceanography, University of Cape Town, Rondebosch, 7700, South Africa

[4] Climate Geochemistry Department, Max Planck Institute for Chemistry, 55128 Mainz, Germany

[5] Bermuda Institute of Ocean Sciences, St.George's, GE 01, Bermuda

[6] Department of Earth System Science, University of California, Irvine, CA 92697, USA

[7] Department of Geosciences, Princeton University, Princeton, NJ 08544, USA

Presentation of a published research paper

This paper was published by the research journal *Geochimica et Cosmochimica Acta* in May 2018. I was personally responsible for the data analysis and plotting, data interpretation and writing the first draft of the manuscript. H. Ren performed the laboratory analyses and, together with D.M. Sigman, S.E. Fawcett and R. Schiebel, contributed to the data interpretation and revision of the manuscript. The remaining co-authors provided resources, sampling and/or laboratory support and gave feedback on the text.

ABSTRACT

We report the nitrogen (N) isotope ratios (δ^{15}N) of planktic foraminifera collected from upper ocean net tows (surface to 200 m), moored sediment traps, and core-top sediments at the Bermuda Time-series Site in the northern Sargasso Sea between 2009 and 2013. Consistent with previous measurements from low-latitude core-top sediments, the annually averaged δ^{15}N of organic matter bound within the shells of euphotic zone-dwelling, dinoflagellate symbiont-bearing foraminifera collected in net tows (2.3‰ on average) approximates that of shallow thermocline (~200 m) nitrate (2.6‰), the dominant source of new N to Sargasso Sea surface waters. Deeper-dwelling foraminifer species without dinoflagellate symbionts tend to have a higher δ^{15}N (3.6‰ on average). We observe no systematic difference between the bulk tissue and shell-bound δ^{15}N in net tow-collected foraminifera. A decline in shell N content is observed from net tows (6.8 nmol/mg) to sediment traps (5.4 nmol/mg) and surface sediment (3.0 nmol/mg). On average, shell-bound δ^{15}N rises from net tows (3.1‰) to sediment traps (3.7‰) but does not change further upon incorporation into the sediments (3.7‰). Together, these observations are consistent with preferential loss of shells or shell portions with lower δ^{15}N and higher N content during sinking through the upper 500 m, followed by a non-isotope fractionating decrease in N content between sinking and burial. Time-series data from sediment traps (and to a lesser extent, surface net tows) exhibit seasonal δ^{15}N variations, with a minimum in early spring, a maximum in late spring and a decline from summer to fall. These variations appear to arise from seasonal changes in the δ^{15}N of total upper ocean biomass, which are, in turn, driven by early springtime nitrate supply, subsequent nitrate drawdown, and an increase in the relative importance of ammonium recycling into the late summer and early fall. The δ^{15}N connection between total upper ocean biomass and foraminifera indicates that foraminifer-bound δ^{15}N records the δ^{15}N of the annual nitrate supply in oligotrophic (e.g., subtropical) environments but will also be sensitive to the degree of nitrate consumption in high-nutrient regions and possibly to changes in upper ocean ammonium recycling under some conditions.

1. Introduction

The accumulation of organic matter on the seafloor archives information about past ocean productivity and nutrient conditions, key factors controlling the influence of biology on atmospheric carbon dioxide concentrations and thus global climate. Organic nitrogen (N) in

marine sediments and sedimentary microfossils is a promising recorder of the N isotopic composition of nitrate (NO_3^-) supplied to phytoplankton in oligotrophic environments such as the subtropical gyres, which is in turn affected by and thus bears witness to processes such as N fixation and denitrification (Altabet & Curry, 1989). In addition, the N isotopes are a potential recorder of surface water nitrate consumption in nitrate-replete environments such as the Southern Ocean (François et al., 1992; Altabet & François, 1994).

When nitrate is consumed by phytoplankton, the lighter ^{14}N isotope is preferentially incorporated, causing the remaining nitrate pool (and thus also the particulate organic N (PON) subsequently produced from it) to become progressively enriched in the heavier ^{15}N isotope (i.e., increasing in δ^{15}N, where $\delta^{15}N = \{[(^{15}N/^{14}N)_{sample}/(^{15}N/^{14}N)_{N2\ in\ air}] - 1\} \times 1000$; in units of per mil, ‰) (Wada & Hattori, 1978; Pennock et al., 1996; Waser et al., 1998; Sigman et al., 1999a). Thus, PON sinking to the seafloor carries with it the isotopic imprint of partial nitrate consumption in overlying waters. If the surface ocean nitrate pool is completely consumed, the δ^{15}N of the total accumulated PON converges on that of the initial nitrate supply. Thus, in oligotrophic environments where nitrate consumption in surface waters is always essentially complete, the δ^{15}N of sinking PON (and thus of N in underlying sediments) would be expected to match the δ^{15}N of the nitrate supply (Altabet, 1988; Altabet & François, 1994). Diagenetic alteration and/or contamination, however, demonstrably influence the δ^{15}N of bulk sedimentary N (Altabet & François, 1994; Meckler et al., 2011) and have prompted a shift to analysis of N pools that are robust against these effects, with our focus here on microfossil-bound organic N (Sigman et al., 1999b; Robinson et al., 2004; Ren et al., 2009). With recent method developments, it is now feasible to analyse the N isotopes of the small amounts of organic N encased within the shells or 'tests' of planktic foraminifera (Ren et al., 2009; Ren et al., 2012; Straub et al., 2013), calcifying zooplankton that ubiquitously accumulate in deep-sea sediments.

Planktic foraminifera inhabit a wide range of ocean environments from the tropics to the poles and have a diversity of feeding habits. Shallow-dwelling species prey on zooplankton and larger phytoplankton, while deeper-dwelling species are sustained by detrital particles and/or the organisms that feed upon them (Bé et al., 1977; Spindler et al., 1984; Schiebel & Hemleben, 2017). Many shallower species also host algal symbionts: dinoflagellates in the case of most spinose, shallow-dwellers (Bé et al., 1977; Schiebel and Hemleben, 2017; and references therein), and other algae including chrysophytes in the case of some thermocline-dwellers (Gastrich, 1987; Faber et al., 1988). Foraminifera grow in size by adding chambers to their

shells, using an organic sheet as a template for calcification (King & Hare, 1972; Bé et al., 1979; Spero, 1988). In this way, N-rich biomineralizing proteins are added prior to each chamber addition and are sequestered within the calcite matrix (Bé et al., 1977; Hemleben et al., 1989). Additional calcification during life (ontogenic) and reproduction (gametogenic) may further protect shell-associated organic matter, while post-mortem encrustation might protect both shell-native and external organic matter. In the tropical and subtropical open ocean, there is a strong link between the $\delta^{15}N$ of thermocline nitrate, the main source of nitrate to the euphotic zone (i.e., the well-lit layer from the surface to the 1% light level) (Altabet, 1988; Knapp et al., 2005), and the shell-bound $\delta^{15}N$ of most planktic foraminifer species in underlying surface sediments (Ren et al., 2009; Ren et al., 2012), supporting the implementation of the planktic foraminifer-bound $\delta^{15}N$ proxy. However, important questions remain regarding the controls on foraminifer-bound $\delta^{15}N$. First, how does shell-bound $\delta^{15}N$ compare to the $\delta^{15}N$ of foraminiferal tissue, and is this relationship stable? Second, are there other factors besides the $\delta^{15}N$ of the annual nitrate supply to the euphotic zone that affect foraminifer-bound $\delta^{15}N$, and are these adequately important to cause significant changes through time? Third, is the $\delta^{15}N$ signal acquired in the upper ocean preserved as tests sink to the seafloor? If shell-bound $\delta^{15}N$ is altered, is the magnitude of this alteration constant and/or systematic? To address these unknowns, we present modern foraminiferal tissue and shell-bound $\delta^{15}N$ measurements for a range of species collected from the upper ocean, sediment traps, and surface sediments at the Bermuda Time-series Site in the Sargasso Sea.

The Bermuda region has a well-characterised seasonal cycle of mixing and primary production (Steinberg et al., 2001; Lomas et al., 2013). The deepest mixing occurs in late winter/early spring (down to 200-250 m), injecting thermocline nitrate into surface waters. As the surface ocean warms and the mixed layer shoals in the late spring and early summer, nitrate is drawn down rapidly by phytoplankton to less than 0.1 µM (Lipschultz, 2001), and its concentration generally remains extremely low throughout the summer and early fall stratification period (<0.01 µM) (Fawcett et al., 2015). A gradual deepening of the mixed layer occurs in late fall and winter as the surface ocean cools and wind-driven mixing erodes the strong thermal gradient. Even during the period of deepest mixing, however, nitrate concentrations typically remain well below 0.5 µM in the upper 100 m, or ~15% of the concentration present at 200-250 m (Fig. 2.1). Therefore, nitrate consumption in this region is close to complete year-round (Lipschultz, 2001; Fawcett et al., 2015) and the $\delta^{15}N$ of PON sinking out of the euphotic zone should equal the $\delta^{15}N$ of the original subsurface nitrate supply (Altabet, 1988; François et al.,

45

1992). This balance is only weakly affected by the export of organic N in dissolved or suspended particulate forms (Knapp et al., 2005). Thus, by focusing our ground-truthing efforts on the oligotrophic ocean, we have sought to initially minimize the complication of partial nitrate consumption. The Bermuda Time-series Site is typical of the oligotrophic, subtropical open ocean gyres (Steinberg et al., 2001; Lomas et al., 2013), making our findings broadly applicable to a large area of the global ocean.

In this ground-truthing study, we compare the δ^{15}N of living foraminifera caught in surface net tows, sinking shells collected in moored sediment traps and fossil shells present in core-top sediments. Together, these data capture foraminifer-bound N at important stages in its production and preservation, from incorporation of N into the living organism, through diagenesis during sinking and burial in the sediments.
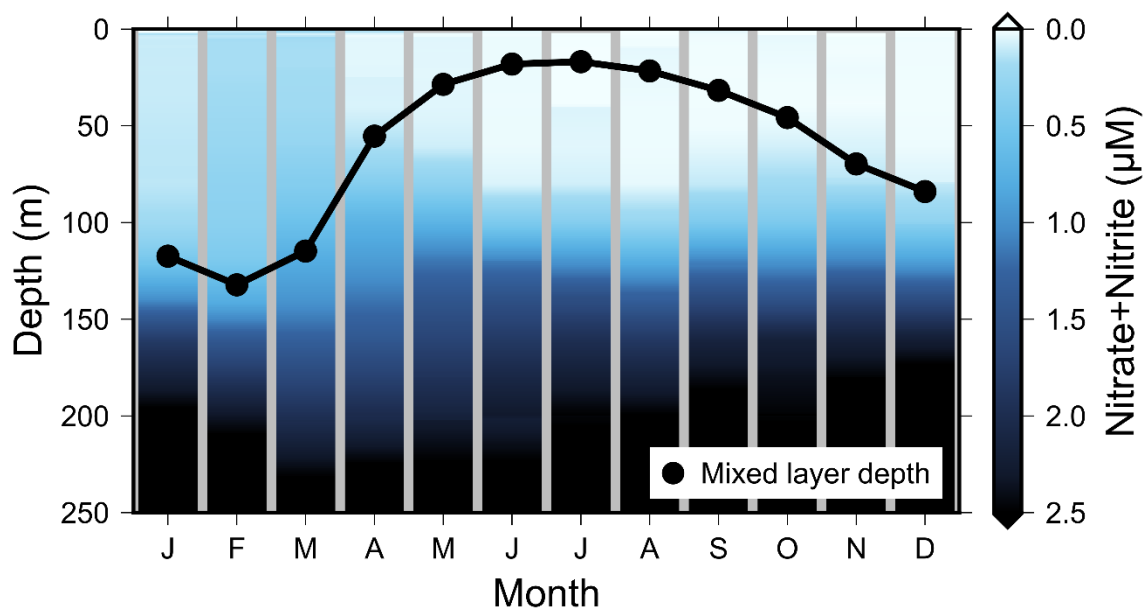
Fig. 2.1: Sargasso Sea climatology. Long-term monthly averages of upper-ocean (0-250 m) nitrate+nitrite concentration (in µM; colour shading) and mixed-layer depth (in meters; black circles) at the Bermuda Atlantic Time-series Study (BATS) site. Averages were computed using all BATS cruise data collected between October 1988 to December 2014 (available online at http://batsftp.bios.edu/BATS/). Mixed-layer depth is defined as the minimum depth at which potential temperature had decreased by ≥ 0.2°C from a reference depth of 10 m (de Boyer Montégut et al., 2004).

2. Methods

2.1 Sample collection

Living foraminifera were collected from the upper water column using a 1-m^2, 200-µm-mesh plankton net during ten cruises between July 2011 and November 2013. Each tow lasted 2–3 hours at a target depth between 0 m and 200 m (see Table S2.1 for details). Approximately 90% of the foraminifer-containing tow material was preserved in a 5–10% pH-buffered formalin solution and stored at 4°C until processing (Ren et al., 2012). The remaining 10% was size-fractionated, filtered and freeze-dried for elemental and isotopic analysis of PON. Hydrographic data for each station were acquired from a Sea-Bird conductivity-temperature-depth (CTD) sensor mounted on a Niskin bottle rosette (data available online at http://batsftp.bios.edu/BATS/). Mixed-layer depth was defined as the depth at which temperature had decreased by ≥0.2°C from a reference depth of 10 m (de Boyer Montégut et al., 2004). Seawater samples collected from the Niskin bottles on the same cruises were measured for the concentration and N isotope ratios of nitrate and nitrate+nitrite (Fawcett et al., 2011, 2014, 2015). Foraminifer tests were picked from Oceanic Flux Program (OFP) sediment traps at 500 m, 1500 m and 3200 m water depth (Conte et al., 2001; Conte & Weber, 2014). The OFP mooring was located at 31°50'N, 64°10'W between November 2009 and November 2010, with each sample representing a two-week collection. To attain sufficient N for shell-bound analysis, specimens from two or all three trap depths were combined when needed. Core-top sediments were collected using a modified Van Veen corer at a nearby site (31°44'N, 64°05'W; 4570 m water depth – shallower than the lysocline, the depth below which calcite preservation is greatly reduced; Honjo & Erez, 1978). Fossil foraminifer tests were picked from the >125 µm size fraction of the 0.5–2.0 cm depth interval. Carbon-14 dating of surface sediments from the vicinity (two cores at 31°45'N, 64°21'W; 4300±100 m water depth; Haidar et al., 2000) suggests an average age of approximately one thousand years for our sediment samples. A more precise age estimate (i.e., radiocarbon dates for our actual core-top sediments) is not necessary for our purposes of comparing modern with recently deposited shells, as downcore foraminifer-bound δ^{15}N from the Caribbean indicates no change in the region during the late Holocene (Ren et al., 2009).

2.2 N isotope methods for foraminifer tissue, shells and particulate organic N

Foraminifera were isolated from bulk tow collections by density separation (addition of a 300 g/L NaCl solution), decanted into a watch glass and left in a fume hood until the formalin-

seawater solution had evaporated. Between one and 100 individuals of the same species were picked per sample (depending on species availability and estimated N content) under a dissecting microscope using a wet picking brush. Picked samples were transferred to 5 mL Eppendorf tubes, rinsed several times with deionised water, briefly sonicated to loosen any detritus, and transferred to 12 mL pre-combusted Wheaton vials (Ren et al., 2012). After pipetting off the supernatant liquid, samples were oven-dried at 30-40°C. Dried specimens were gently crushed open with an ethanol-cleaned spatula, sonicated in deionised water and the external organic N (i.e., tissue) converted to nitrate by the persulfate oxidation method (Nydahl, 1978; Knapp et al., 2005) (described below).

After removal of the tissue N fraction, the remaining crushed shells were rinsed at least five times with deionised water and oven dried at 50°C. Approximately 1–3 mg of cleaned calcite was weighed out into 4 mL pre-combusted Wheaton vials, combining samples of the same species (from different tows and occasionally different cruises, but always the same season) where necessary. The crushed tests were dissolved in 6 N hydrochloric acid (HCl) to release calcite-bound organic N into solution, and oxidised to nitrate by adding 1 mL of a basic persulfate oxidising reagent (POR; a potassium persulfate/sodium hydroxide solution) to each vial and autoclaving for 65 min on a slow vent setting (Nydahl, 1978; Knapp et al., 2005). Blanks (containing 4 mL POR) and three amino acid reference materials (AG, USGS-40 and USGS-41) were included in every batch of samples to ensure complete oxidation and correct for the N blank associated with the POR. USGS-40 and USGS-41 are international reference materials (both glutamic acid; Qi et al., 2003), and AG is an in-house mixed amino acid standard that has been calibrated by analysis of the mixed powder with elemental analyzer-isotope ratio mass spectrometry.

All resulting nitrate samples (from tissue and shell-bound N oxidations) were adjusted to a pH of 5-7 using HCl and measured for nitrate concentration by chemiluminescence (Braman & Hendrix, 1989). Finally, nitrate was converted to nitrous oxide using the bacterial conversion technique known as the "denitrifier method" (Sigman et al., 2001; Casciotti et al., 2002), followed by $\delta^{15}N$ measurement by gas chromatography–isotope ratio mass spectrometry using a Thermo MAT 253 with purpose-built online N_2O extraction and purification system (Sigman et al., 2001; Casciotti et al., 2002; Weigand et al., 2016). All $\delta^{15}N$ measurements were referenced to atmospheric N_2 using solutions of nitrate reference materials IAEA-NO3 and USGS-34, and oxidised samples were then corrected for the POR blank using the amino acid reference materials.

Foraminifera from sediment traps were analyzed for shell-bound $\delta^{15}N$ in the same way as the tow specimens. For the core-top shells, two additional cleaning steps were undertaken (after crushing) following Ren et al. (2015): (1) 5 min ultrasonication in 2% sodium hexametaphosphate (pH 8) to remove clays, and (2) reductive cleaning using sodium bicarbonate-buffered dithionite-citrate reagent to remove metal oxides. Replicate analyses were made when possible. For tow-caught foraminifera, pooled standard deviations (1σ) of tissue $\delta^{15}N$ and shell-bound $\delta^{15}N$ cleaning-and-oxidation replicates were 0.53‰ and 0.47‰, respectively. The relatively large standard deviation for shell-bound $\delta^{15}N$ may be partly due to higher (and more variable) blank/total N ratios (averaging 10%). However, this cannot explain the tissue standard deviations, as the blank contributes only ~4% on average. Rather, the fact that fewer individuals are combined to make a $\delta^{15}N$ measurement (typically 1-20 for tissue *vs.* hundreds for shells) is a likely contributor. The limited availability of shell specimens in core-top and sediment trap collections prevented replicate oxidations, but blanks only contributed 3-4% on average of the total sample N.

The $\delta^{15}N$ of size-fractionated PON (ranging from 200 µm to >5000 µm) collected in the upper 200 m during the net tows was determined by elemental analyzer-isotope ratio mass spectrometry, referencing to atmospheric N_2 using USGS-40 and an in-house aminocaproic acid standard. The pooled standard deviation of replicate measurements was 0.07‰. The $\delta^{15}N$ of sinking PON was analyzed on the <125 µm size fraction of sediment trap samples by mass spectrometry using either a Europa 20-20 or GV Isoprime mass spectrometer. Samples were acidified prior to analysis to remove carbonates using a modification of the Verrado et al. (1990) method.

2.3 Averaging foraminifer $\delta^{15}N$ and N content

Foraminifer $\delta^{15}N$ and N content averages (e.g., for each type of collection) were calculated using three different methods: first, the arithmetic (unweighted) average, where all species are assigned equal weight; second, the "$N_{measured}$-weighted" average, where each species is weighted by its contribution to the total amount of foraminifera N picked and measured; and third, the "$N_{present}$-weighted" average, where each species is weighted by its estimated contribution to the total amount of foraminiferal N (>100 µm) actually present in that environment. On the one hand, the second method does not account for the actual abundance of each species in the environment (i.e., it assumes that the picked specimens represent the

species proportions in the original collection). On the other hand, the third method relies on estimations of the shell weights of each species and of species abundances from other studies.

For the net tows, contributions to $N_{present}$ were estimated from the mean annual species compositions of Tolderlund and Bé (1971) (from 0-10 m and 0-500 m plankton tows at Bermuda Station S) together with the average shell weights of Movellan (2013) (from 0-200 m tows in the North Atlantic, Caribbean, Arabian Sea and Red Sea) and Takahashi and Bé (1984) (from near-surface tows in the North Atlantic and Caribbean). For the sediment traps, N contributions were estimated from the annual test fluxes measured in the 1500 m OFP sediment trap during 2009-2010 (the same period as our trap-caught foraminifera) (Salmon et al., 2015) together with our own measurements of N per shell. For the core-top sediments, the contribution of each species was estimated from foraminifera counts at a nearby core site (V007067; 34°40'N, 61°27'W; 4308 m water depth; CLIMAP Project Members, 1981, 1994) and average shell weights from North Atlantic and Caribbean deep-sea sediments (Takahashi and Bé, 1984). In the two cases where core-top shell-weight data were unavailable (*G. truncatulinoides* and *G. conglobatus*), weights were approximated using the average shell-weight of all the other species.

In the results section below, the $\delta^{15}N$ averages from all three calculation methods are presented: unweighted, $N_{measured}$-weighted, and $N_{present}$-weighted. However, given the focus of this study on N transfer and turnover and based on our assessment of uncertainties, we refer only to the $N_{measured}$-weighted average in the following discussion.

3. Results

3.1 Overview of foraminifer $\delta^{15}N$ and N content

The $\delta^{15}N$ of foraminiferal tissue collected from net tows ranges from 1.5‰ to 4.7‰, while foraminifer shells from the same tows have a $\delta^{15}N$ ranging from 1.8‰ to 7.8‰. We note that the large size of the error bars for some species derives mainly from $\delta^{15}N$ variability between cruises (pooled cruise standard deviation of 1.09‰ for tissue, 1.33‰ for shell), which is larger than the variability between tows on the same cruise (pooled tow standard deviation of 0.82‰ for tissue, unavailable for shell) and, in turn, larger than the variability between measurements within a tow (pooled measurement standard deviation of 0.57‰ for tissue, 0.59‰ for shell;

Table S2.2). The unweighted averages of all the tow data (light grey triangles in Fig. 2.2a) indicate a higher $\delta^{15}N$ for shells (3.6‰; n = 72) than for tissue (2.9‰; n = 452). Weighting the $\delta^{15}N$ of each species by its N contribution yields tissue and shell-bound $\delta^{15}N$ averages that are more similar to each other; 3.2‰ *vs.* 3.1‰, respectively, using $N_{measured}$ (black triangles) and 3.2‰ *vs.* 3.0‰, $\delta^{15}N$ respectively, using $N_{present}$ (dark grey triangles). The $\delta^{15}N$ of sinking shells (n = 86) ranges from 2.6‰ to 5.3‰ with an unweighted average of 4.0‰, and weighted averages of 3.7‰ and 4.1‰ for $N_{measured}$ and $N_{present}$, respectively. Core-top shells (n = 11) range from 1.9‰ to 6.5‰ with an unweighted average $\delta^{15}N$ of 3.7‰, and weighted averages of 3.7‰ and 4.2‰ for $N_{measured}$ and $N_{present}$, respectively (Fig. 2.2a).
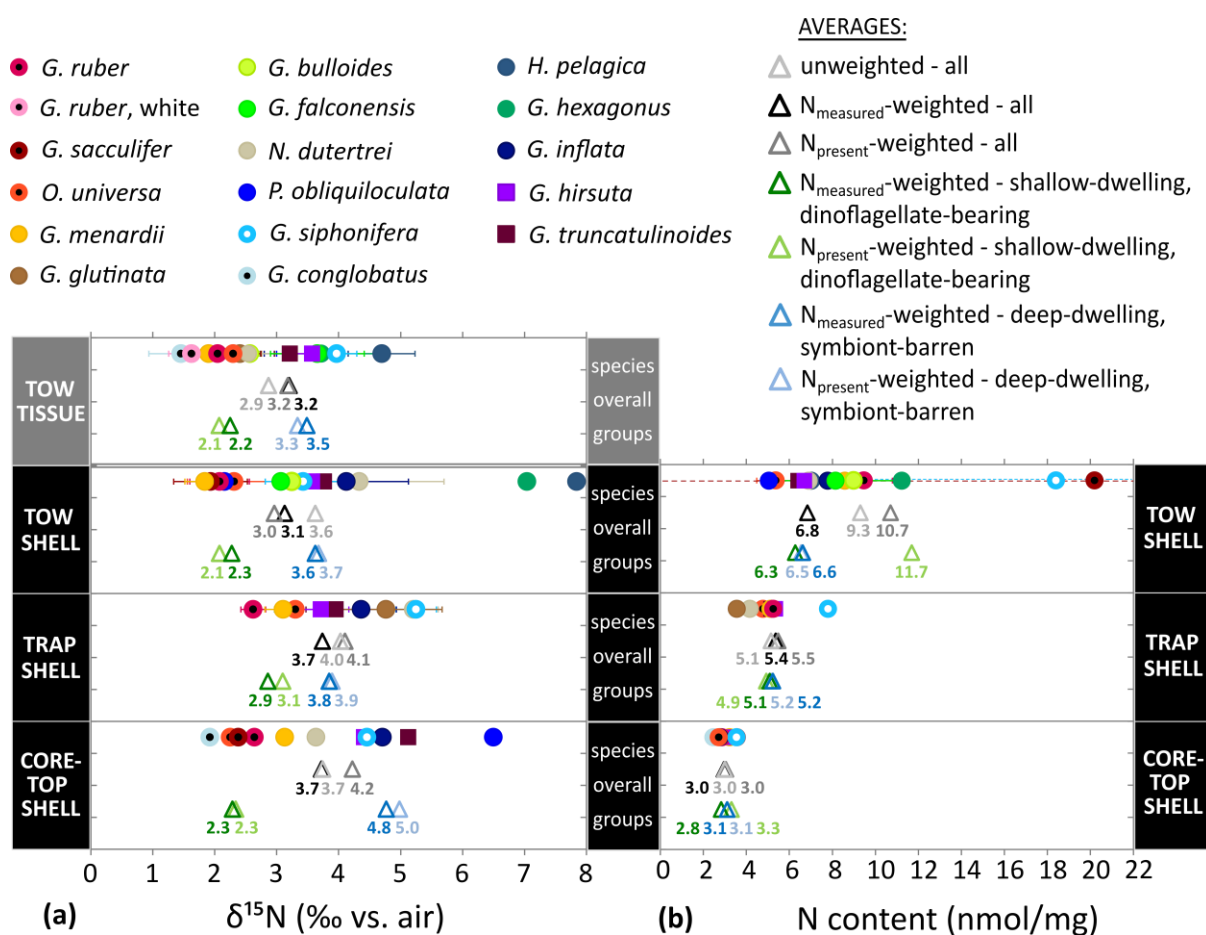
Fig. 2.2: Overview of foraminifer measurements at the Bermuda Time-series Site. (a) $\delta^{15}N$ (in ‰ *vs.* N_2 in air) and (b) N content (nmol/mg) of foraminifera collected from upper ocean net tows (surface to 200 m), moored sediment traps (500 m, 1500 m and 3200 m) and core-top sediments (4570 m water depth). For each collection type, coloured circles (shallow-to-intermediate dwellers) and squares (deep dwellers) show the average for each foraminifer species, with the fill colour indicating the type of symbiont hosted (black fill for dinoflagellates, white fill for chrysophytes), if any symbiosis has been confirmed. Error bars show standard error. Black and grey triangles average over all species for each type of collection (light grey for unweighted averages; black where species are weighted by contribution to the total amount of N measured ($N_{measured}$-weighted); dark grey where species are weighted by

contribution to the estimated amount of N (>100 µm) present in the environment ($N_{present}$-weighted); see section 2.3 for details). Green and blue triangles show group averages for dinoflagellate-bearing, shallow-dwellers and symbiont-barren, deep-dwelling species, respectively; bright green/blue for $N_{measured}$-weighted and pastel green/blue for $N_{present}$-weighted averages. For an expanded view of sinking shell-bound $\delta^{15}N$ (for the cases where we have measurements from multiple sediment trap depths), refer to Fig. S2.4.

The N content of tow-collected shells (n = 72) generally ranges from 5.0 to 11.2 nmol/mg (except for *Globigerinella siphonifera* and *Globigerinoides sacculifer*, which exceed 18 nmol/mg) with an unweighted average of 9.3 nmol/mg (Fig. 2.2b). Weighting species by contribution to $N_{measured}$ and $N_{present}$ yields averages of 6.8 nmol/mg and 10.7 nmol/mg, respectively. Sinking shells (n = 86) have a lower N content than tow-caught shells and a smaller range of 3.5 to 5.4 nmol/mg (with a higher value of 7.8 nmol/mg for *G. siphonifera*). On average, the N content of sinking shells is 5.1 nmol/mg (unweighted), 5.4 nmol/mg ($N_{measured}$-weighted) and 5.5 nmol/mg ($N_{present}$-weighted). Core-top shell N content (n = 11) has a still narrower range (2.5 to 3.5 nmol/mg) and lower average value (3.0 nmol/mg, both weighted and unweighted).

We proceed by comparing the $\delta^{15}N$ of foraminiferal tissue with shell-bound $\delta^{15}N$ in the upper ocean, and then present a time-series view of foraminifer-bound $\delta^{15}N$ to address whether this proxy captures the seasonal cycle and/or other temporal signals. Finally, we trace the journey of foraminifer shells as they sink through the water column, highlighting any changes in shell-bound $\delta^{15}N$ along the way.

3.2 Foraminifer tissue *vs.* shell-bound $\delta^{15}N$ from net tows

For most species, tissue $\delta^{15}N$ is similar between the two years of sampling, albeit with a tendency for lower average $\delta^{15}N$ in the first year (Fig. 2.3). This comparison suggests that, despite the potential for interannual variability and for biases associated with unavoidable irregularities in sampling schedule, our sampling and analyses have captured the characteristic $\delta^{15}N$ of the different species. A species-level comparison of all available data pairs (from a range of individual tows or cruises; n = 33) shows a pervasive positive correlation between tissue and shell-bound $\delta^{15}N$ (Fig. 2.4a). All species except *Globigerina falconensis* exhibit positive regression slopes (Table 2.1), indicating that a large portion of shell-bound $\delta^{15}N$ variation is associated with variation in the $\delta^{15}N$ of foraminiferal tissue. Of the nine species with positive slopes, seven (or six when outliers are excluded) have slopes less than 1,

indicating greater δ^{15}N variability in tissue than in shell-bound N. Most species averages fall within 0.5‰ (*Globigerinoides ruber*, *G. sacculifer*, *Globorotalia hirsuta*, *Globorotalia inflata*, *Globorotalia menardii*, *Globorotalia truncatulinoides*) or 1‰ (*Orbulina universa*, *G. siphonifera*, *Globigerina bulloides*, *G. falconensis*) of a 1:1 line in a plot of tissue *vs.* shell-bound δ^{15}N, while others exhibit a 1-2‰ deviation above (*Neogloboquadrina dutertrei*) or below (*Pulleniatina obliquiloculata*) the 1:1 line (Fig. 2.4b). The most extreme deviations from 1:1 are observed for *Hastigerina pelagica* and *Globorotaloides hexagonus*, with shell-bound δ^{15}N values 2-3‰ higher than their tissue. Nevertheless, both weighted (black and dark grey triangles) and unweighted averages of all species (light grey triangle) fall close to (i.e., within 0.6‰ of) the 1:1 line. On the whole, while there is a fair amount of scatter around a 1:1 relationship, there is no consistent offset between foraminifer tissue and shell-bound δ^{15}N.
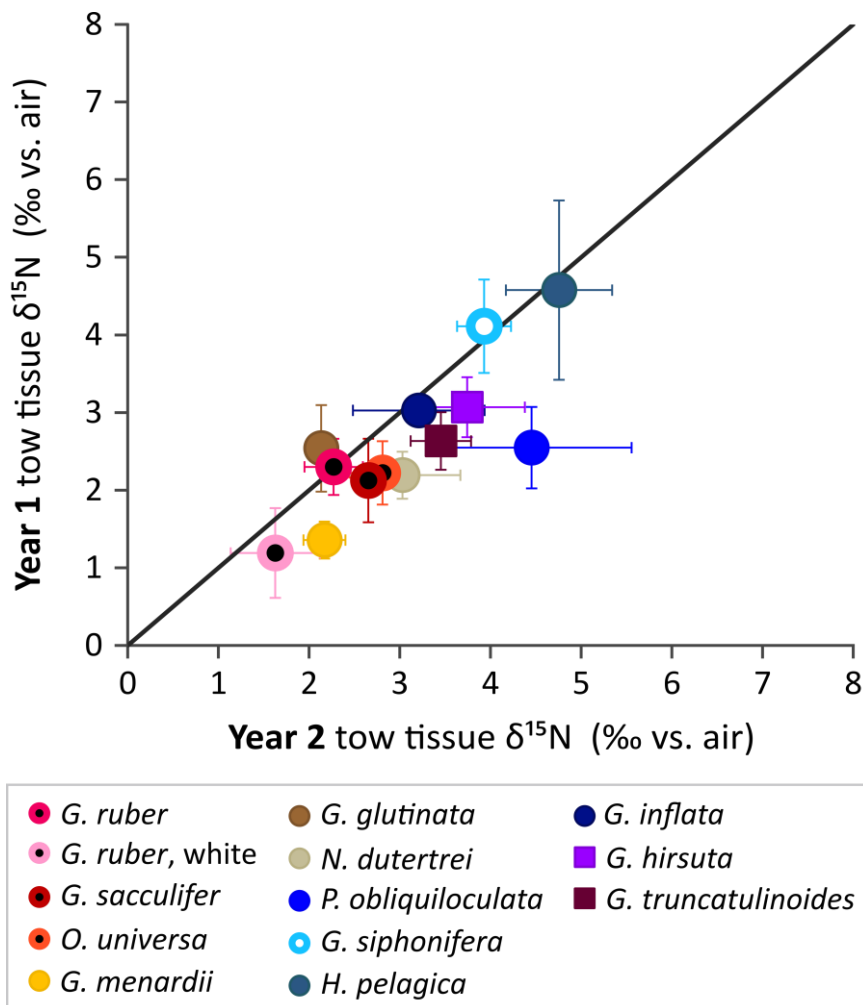
Fig. 2.3: Interannual comparison of foraminifer tissue δ^{15}N for each species between the two years of net tow sampling. Year 1 includes Jul 2011, Oct 2011, Apr 2012 and Jul 2012 (i.e., excludes Feb 2012), and Year 2 includes Aug 2012, Nov 2012, Apr 2013 and Jul 2013 (i.e., excludes Nov 2013) to ensure even seasonal coverage of both years. Error bars show standard error.

53
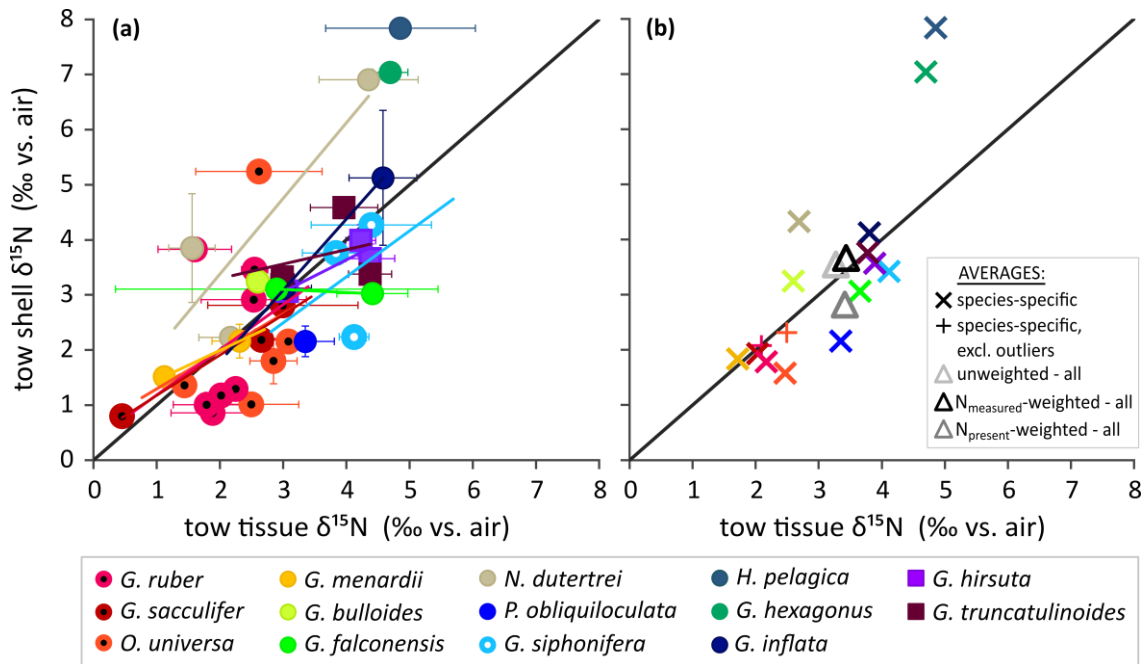
Fig. 2.4: Direct, species-level comparison between foraminifer tissue $\delta^{15}N$ and corresponding shell-bound $\delta^{15}N$ from tow collections in the upper ocean (0-200 m), with 1:1 lines (black diagonals) for reference. (a) Simple regression lines (based on the monthly averages i.e., the average of all measurements from all tows on a cruise; coloured circles and squares) are plotted for each species. Regression slopes and correlation coefficients, including and excluding outliers (one *O. universa* (orange) and one *G. ruber* (dark pink) measurement), are presented in Table 2.1. Error bars in panel (a) show standard deviation. (b) Average tissue $\delta^{15}N$ *vs.* shell-bound $\delta^{15}N$ for each species, incorporating only the paired data shown in panel (a), including ('+' symbols) and excluding ('x' symbols) outliers. Triangles indicate overall averages; unweighted (light grey), $N_{measured}$-weighted (black) and $N_{present}$-weighted (dark grey). The large standard error (shown by the error bars in panel (b)) for some species derives mainly from $\delta^{15}N$ variability between cruises (rather than variability between measurements, or variability between different tows from the same cruise).

Table 2.1: Regression lines resulting from plotting tissue $\delta^{15}N$ *vs.* shell-bound $\delta^{15}N$ for each foraminifer species with n ≥2 (see Fig. 2.3a).

	regression line		
species	slope	R^2	n
O. universa	0.68	0.06	5
- excluding outlier	0.41	0.35	4
G. ruber	0.82	0.06	7
- excluding outlier	3.10	0.84	6
G. sacculifer	0.73	0.97	3
G. siphonifera	0.83	0.05	3
N. dutertrei	1.37	0.72	3
G. hirsuta	0.58	0.80	3
G. inflata	1.29	(1.00)	2
G. menardii	0.54	(1.00)	2
G. truncatulinoides	0.26	0.07	3
G. falconensis	-0.06	(1.00)	2
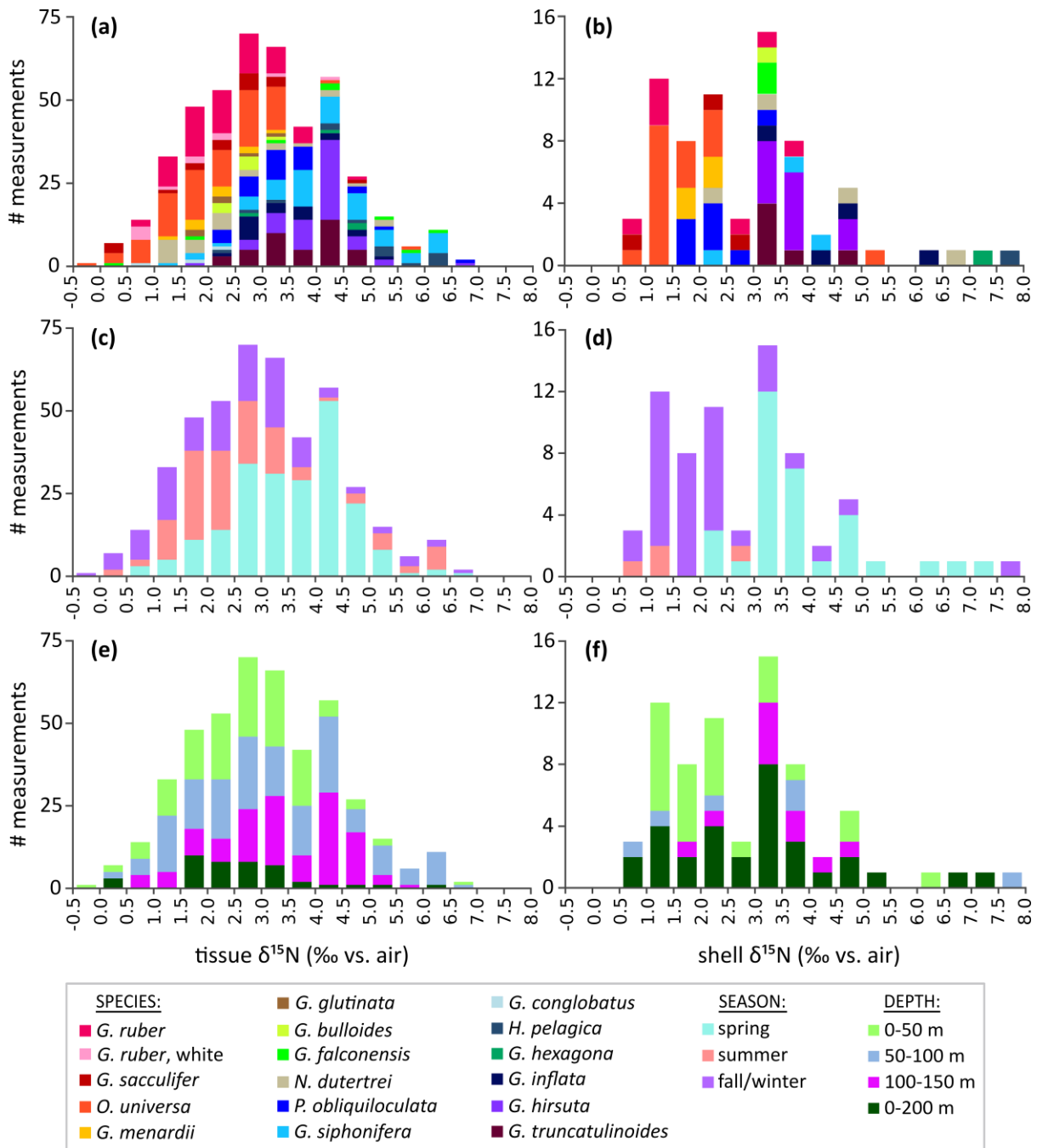
Fig. 2.5: Histograms showing the distribution of foraminifer δ^{15}N measurements obtained from the tissue (a, c, e) and shells (b, d, f) of tow-collected specimens, coloured by species (a, b), season (c, d) and collection depth (e, f).

In histograms of the compiled δ^{15}N measurements (Fig. 2.5), a pattern common to both tissue and shell measurements is a clustering of *O. universa* (orange), *G. ruber* (dark pink) and *G. sacculifer* (dark red) at the lower end of the δ^{15}N distribution (typically <3.5‰), and a

clustering of *G. hirsuta* (purple), *G. truncatulinoides* (plum) and *G. inflata* (navy blue) at the higher end (typically >3‰) (Fig. 2.5a&b). The δ^{15}N difference between these two groups is significant in both tissue and shell-bound N (p<<0.05 based on a two-sample, unequal variances t-test (Welch, 1947); see Table S2.3 for details). For other species (particularly *G. siphonifera* (sky blue) and *N. dutertrei* (tan)), measurements are more evenly distributed across a wide range of δ^{15}N values. Looking across seasons (Fig. 2.5c&d), summer and fall δ^{15}N values are both significantly lower than springtime δ^{15}N and not statistically different from each other (Table S2.3). This pattern exists in both tissue δ^{15}N (averaging 2.7‰ and 2.6‰ *vs.* 3.5‰, respectively) and shell-bound δ^{15}N (averaging 1.5‰ and 2.1‰ *vs.* 3.9‰, respectively). The tissue δ^{15}N data also reveal significant increases with tow depth (Table S2.3), from an average of 2.7‰ at 0-50 m to 3.3‰ at 50-100 m and 3.4‰ at 100-150 m (Fig. 2.5e). While the pattern is less clear in the shell-bound measurements (for which different tow depths often had to be combined; 0-200 m category (dark green bars)), there is a significant increase between the 0-50 m and 100-150 m intervals (Table S2.3), averaging 2.4‰ and 3.4‰, respectively (Fig. 2.5f). Similarly, the δ^{15}N of size-fractionated (200-5000 µm) PON from these tows increases with depth, from an average of 3.2‰ at 0-50 m to 3.8‰ at 50-100 m to 4.2‰ at 100-150 m (where n = 31, 26, and 17, respectively; Fig. S2.1). In addition, the larger PON size fractions are generally higher in δ^{15}N than the smaller size fractions (e.g., 2.7‰ (n = 16) for 200-500 µm and 4.4‰ (n = 21) for 2000-5000 µm PON, on average).

3.3 Time-series of δ^{15}N in foraminifera from sediment traps and net tows

In the foraminifer-bound δ^{15}N of sinking shells measured from fall 2009 to fall 2010, the dominant pattern that emerges for most species (*G. siphonifera*, *G. hirsuta*, *G. truncatulinoides*, *G. inflata*) is a δ^{15}N minimum in late winter/early spring (after the period of deepest mixing) followed by a δ^{15}N maximum in late spring (coinciding with the rapid shoaling of the mixed layer) (Fig. 2.6). Thereafter, the species for which we have data show a gradual decline in δ^{15}N over the course of the summer (as surface waters become increasingly thermally stratified), with a clear δ^{15}N offset between species (i.e., *O. universa* and *G. ruber* remaining ~2‰ lower than *G. siphonifera*). The δ^{15}N of bulk sinking PON collected in the sediment trap at 500 m shows a similar progression (with a minimum in early spring, a maximum in early summer and a gradual decline through the summer). While the δ^{15}N of bulk PON in the 500 m, 1500 m and 3200 m traps (ranging from -0.6‰ to 5.1‰) is generally lower than that of the foraminifer-bound fraction (0.8‰ to 6.6‰), the amplitude of the seasonal δ^{15}N change is very similar

(5.7‰ *vs.* 5.8‰). The presence/absence of foraminifer species through the trap time-series is consistent with previous observations of seasonal changes in species composition in the Sargasso Sea (e.g., Bé, 1960; Deuser et al., 1981; Deuser, 1987; Salmon et al., 2015). While *G. ruber* and *G. siphonifera* occur throughout the year, *O. universa* shows a marked decrease in abundance during winter. Species like *G. truncatulinoides*, *G. inflata* and *G. hirsuta* peak in winter and spring, while *N. dutertrei* is confined to a brief period in winter or spring (the latter in our case). The scarcity of *H. pelagica* in sinking and seafloor material (despite being one of the most abundant species in surface waters year-round) is likely due to extensive structural weakening of their monolamellar and thin-walled tests during gametogenesis, which reduces their preservation (Deuser et al., 1981).
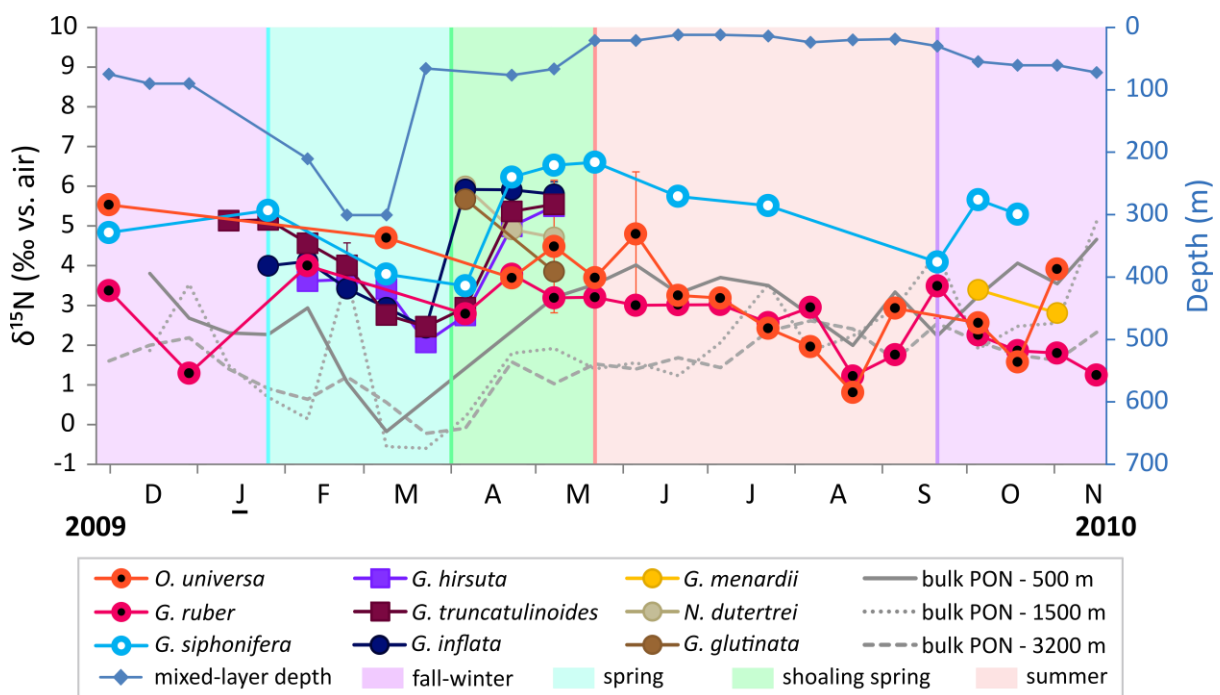
Fig. 2.6: Sediment trap δ^{15}N time-series. Foraminifer-bound δ^{15}N (coloured circles and squares) collected at 500 m, 1500 m and 3200 m between November 2009 and November 2010. Where more than one measurement was possible, error bars show standard deviation. The δ^{15}N of bulk PON collected in each trap over the same period is also shown (dashed and dotted lines). Mixed-layer depth (blue diamonds) is plotted on the secondary y-axis, and background colours denote seasons (blue for spring, green for shoaling spring, pink for summer, purple for fall/winter).

The time-series of upper ocean net tow samples (tissue and shell-bound δ^{15}N) from summer 2011 to fall 2013 (Fig. S2.2) shows a similar range of δ^{15}N variability to the sinking shells (varying by ~5-6‰ overall) and exhibits similar relationships between species (e.g., *O. universa* and *G. ruber* at the lower end and *G. siphonifera* at the upper end of the foraminifer

57

δ^{15}N spectrum). Roughly in parallel with the sediment trap observations, the δ^{15}N of tow-collected PON (>200 µm) also peaks in late spring and declines in late summer, illustrated here by the 200-1000 µm fraction from the upper 0-100 m (thick, mauve line in Fig. S2.2) (mostly copepods in the Bermuda region; Deevey and Brooks, 1971). While the timing of response across different foraminifer species in the net tows is not as consistent as for sinking shells, the δ^{15}N of most net tow foraminifer species varies in concert with the δ^{15}N of tow-collected PON.

Fig. S2.3 shows the δ^{15}N of nitrate (and nitrate+nitrite) at 200 m and 250 m water depth (near the base of the thermocline), spanning both tow and trap sampling periods (Fawcett et al., 2011, 2014, 2015). These data indicate no significant nitrate (or nitrate+nitrite) δ^{15}N difference between the two periods (p>0.05 based on a two-sample, unequal variances t-test; Welch, 1947) with a δ^{15}N of 2.6±0.2‰ (2.5±0.2‰) during the trap period (n = 6) and a δ^{15}N of 2.6±0.1‰ (2.5±0.2‰) during the tow period (n = 20).

3.4 Shell-bound δ^{15}N from net tows to sediment traps and the seafloor

A comparison between foraminifer-bound δ^{15}N of shells from upper ocean net tows (collected between July 2011 and November 2013) and those collected in sediment traps (between November 2009 and November 2010) shows sinking shells to be elevated in δ^{15}N by 0.1‰ to 1.8‰ (Fig. 2.7a). This elevation appears to be species-dependent. While some species (*G. hirsuta*, *G. truncatulinoides*, *G. inflata*) show almost no offset (falling within 0.2‰ of the 1:1 line), on average, trap-caught shells are between 0.6‰ (using $N_{measured}$) and 1.3‰ (using $N_{present}$) higher in δ^{15}N than tow-caught shells (as indicated by the deviations of the triangle symbols from the 1:1 line). The δ^{15}N difference between tow- and trap-collected shells is strongly significant (p<<0.05; based on a two-sample, unequal variances t-test; Welch, 1947), regardless of whether (or with which method) measurements are weighted by N contribution (n = 61-94 for tow shells and n = 77-92 for trap shells). Between 500 m and 3200 m (the depth interval spanned by the three OFP traps), there is no change evident in the δ^{15}N of sinking shells, except for *O. universa*, which increases by ~2‰ (Fig. S2.4). Comparison of foraminifer-bound δ^{15}N of sinking shells with that of shells from core-top sediments shows no consistent offset from the 1:1 line (Fig. 2.7b). The δ^{15}N offset ranges from -1.6‰ to 1.2‰, with an unweighted average of 0.1‰ (light grey triangle) and weighted averages of -0.1‰ (black triangle) and -0.3‰ (dark grey triangle), for $N_{measured}$ and $N_{present}$, respectively. We note that the average offsets reported here differ slightly from the offsets implied by the triangles in

summary Fig. 2.2a. This is because the triangles in Fig. 2.2 average over all available data, not only those species for which we have paired (x, y) measurements (as in Fig. 2.7a&b).
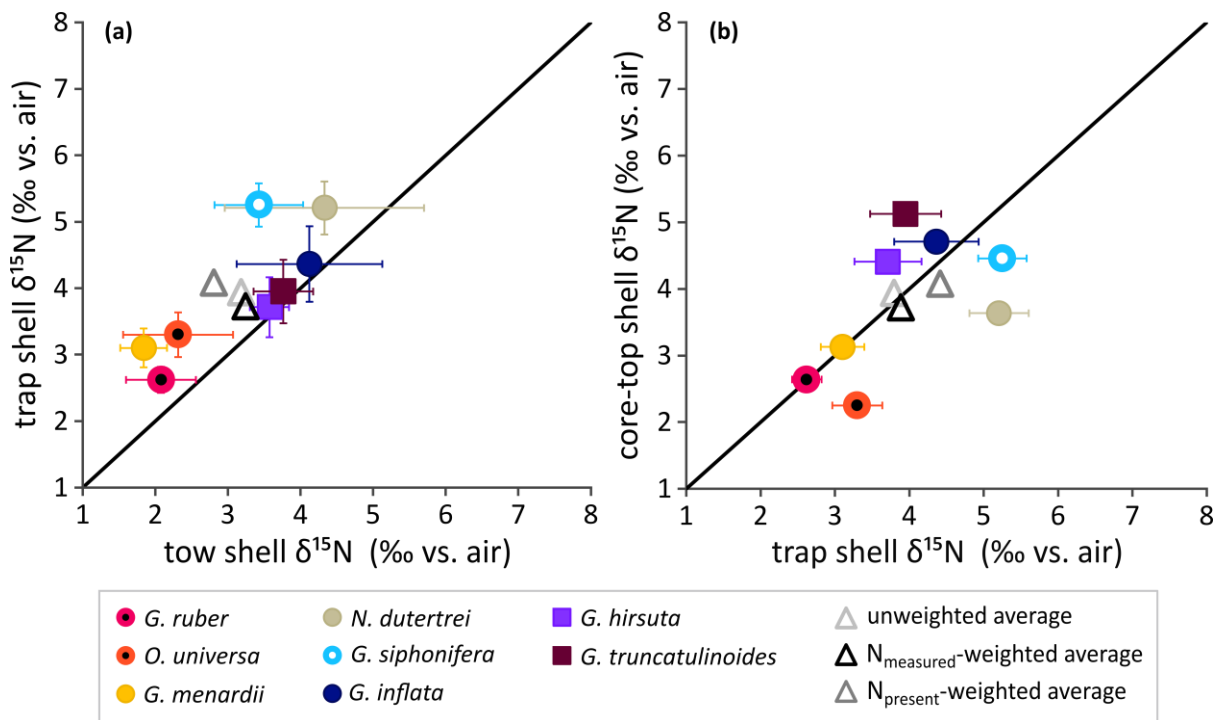
Fig. 2.7: Changes in foraminifer-bound δ^{15}N through the water column as revealed through a comparison of the δ^{15}N of (a) tow-caught *vs.* sinking shells and (b) sinking *vs.* core-top shells. Coloured circles and squares represent species averages, and triangles mark the weighted (black and dark grey) and unweighted (light grey) averages over all species shown in a panel. Standard error is shown by error bars, except for core-top shell δ^{15}N (the y-axis in panel (b)) where measurements derive from a single collection (i.e., the seasonal δ^{15}N range is unknown).

4. Discussion

4.1 Relationship between foraminifer tissue and shell-bound δ^{15}N in the upper subtropical ocean

On the whole, there is no systematic offset in δ^{15}N between tissue and shell-bound N in living foraminifera at the Bermuda Time-series Site (Fig. 2.4). This implies that the compounds used by foraminifera for shell building are not isotopically distinct from their bulk tissue. A similarity in δ^{15}N has been observed between the coral-bound N and tissue of symbiotic corals (Muscatine et al., 2005), but not in diatoms, where frustule-bound δ^{15}N differs substantially from diatom tissue δ^{15}N (Sigman et al., 1999b; Horn et al., 2011; Morales et al., 2013; Morales et al., 2014). This difference may be due to the fact that the N bound within foraminifer tests

and coral skeletons is mainly comprised of amino acids (King & Hare, 1972; Drake et al., 2017), a significant constituent of the tissue, whereas the organic N in diatom frustules is largely composed of long-chain polyamines (Kröger et al., 2000; Sumper et al., 2005), specialized compounds for building opal frustules that are not widely used in the bulk tissue. Thus, differences in the δ^{15}N of biosynthetic compounds might produce an offset in δ^{15}N between frustule-bound and diatom tissue, whereas this is not expected for foraminifera and other calcifiers. A significant offset would increase the range of mechanisms by which the tissue/fossil δ^{15}N relationship might vary through time, and variation in this relationship would greatly complicate interpretation of paleo-proxy records. Thus, it is both practically convenient and fundamentally beneficial that foraminiferal tissue and shell-bound δ^{15}N are not distinctly different. At the same time, given the variability that we observe in this study, more work on this question is called for.

While the δ^{15}N relationship between foraminifer shell and tissue N appears to be characterized by a relatively high degree of variability, inter-season variation in foraminiferal tissue δ^{15}N is positively correlated with variation in shell δ^{15}N for all species for which we have adequate data to undertake the comparison (Fig. 2.4a). From this we conclude that most of the variation in shell-bound δ^{15}N has the same cause as tissue δ^{15}N variation (discussed below). For most species, we observe slopes that are less than 1, implying a greater δ^{15}N range in tissue than in shells. This observation is consistent with shell-bound N integrating over the lifetime of the organism (i.e., weeks to months), while tissues like cytoplasm (including food-containing vacuoles) record recent activity, allowing for greater variation between individuals of the same species living in the same environment. Details aside, the positive correlation and lack of a pervasive δ^{15}N offset between shell-bound and tissue N are auspicious for the foraminifer paleo-proxy, as they suggest that the δ^{15}N of organic matter trapped within fossil shells (as long as it is preserved) largely reflects the δ^{15}N of the organism over the course of its life.

4.2 Factors affecting foraminifer tissue and shell-bound δ^{15}N

From the distributions of net tow δ^{15}N measurements (Fig. 2.5), it emerges that species, season, and depth play a role in determining foraminifera tissue and shell-bound δ^{15}N. The dominant δ^{15}N distinction is between the spinose, dinoflagellate-bearing shallow dwellers, which dominate the lower end of the δ^{15}N range (*O. universa* (orange), *G. ruber* (dark pink) and *G. sacculifer* (dark red); Fig. 2.5a&b), and the non-spinose, non-dinoflagellate-bearing deeper dwellers, which tend to be higher in δ^{15}N (*G. hirsuta* (purple) and *G. truncatulinoides* (plum)).

60

A similar $\delta^{15}N$ offset (of 0.5-2.0‰) between these two groups of species has previously been observed in sinking and core-top shells (Ren et al., 2012). Our data confirm an upper ocean origin for this signal. Two potential mechanisms were put forward by Ren et al. (2012) to explain the group-specific $\delta^{15}N$ difference. First, the lower $\delta^{15}N$ of spinose, euphotic zone-dwelling foraminifera (despite their dietary preference for high-$\delta^{15}N$ zooplankton) may result from their dinoflagellate symbionts consuming (and therefore reducing the excretion of) low-$\delta^{15}N$ ammonium. Second, the higher $\delta^{15}N$ of non-spinose, deeper-dwelling foraminifera (despite being predominantly herbivorous) may reflect their partial dependence on subeuphotic-zone PON, the $\delta^{15}N$ of which increases with depth (Fig. S2.1) (Altabet, 1988). Intermediate-dwelling species (including the spinose, chrysophyte-hosting *G. siphonifera* (sky blue) and the non-spinose (possibly chrysophyte-bearing) *N. dutertrei* (tan), *P. obliquiloculata* (blue) and *G. inflata* (navy)), exhibit a range of $\delta^{15}N$ values intermediate between the low-$\delta^{15}N$ dinoflagellate-bearing and high-$\delta^{15}N$ symbiont-barren groups, but most occupy a higher $\delta^{15}N$ range, more similar to the symbiont-barren species. The $\delta^{15}N$ in foraminiferal tissue and shells in summer/fall tends to be lower than in spring (Fig. 2.5c&d). This may reflect the advantage that some symbiont-bearing foraminifera have under the oligotrophic conditions of seasonal (e.g., summertime in the mid-latitudes) or near-permanent (as in the subtropical gyres) stratification. Photosynthesising endosymbiotic algae use metabolized N forms (mostly ammonium) respired by their host and fix them into amino acids that are then available to foraminifera for biosynthesis. Consistent with this explanation, previous work indicates that dinoflagellate symbionts are primarily sustained by ammonium from the host foraminifer (Uhle et al., 1999). A similar observation has been made for symbiotic corals, which also appear to be low-productivity specialists (Muscatine et al., 2005). Thus, the shallow, well-lit mixed layers and low euphotic-zone nutrient concentrations at the Bermuda Time-series Site in late summer provide favourable growth conditions for dinoflagellate-bearing, surface-dwelling species (Tolderlund & Bé, 1971). This seasonality in on-site production (although modulated by current-transported tests) is reflected in the seasonality of shell fluxes in the OFP sediment traps. For example, the dinoflagellate-bearing *G. ruber* and *G. sacculifer* peak between July and October (Salmon et al., 2015), whereas fluxes of the symbiont-barren deep-dwellers (*G. truncatulinoides* and *G. hirsuta*) and (possibly chrysophyte-bearing) intermediate-dwellers (*G. inflata* and *N. dutertrei*) peak in late winter and spring, respectively, when phytoplankton production and export (and thus food availability) are at a maximum (Lomas et al., 2013; Salmon et al., 2015). In addition to the seasonal shift in the dominant foraminifer group (i.e., from symbiont-barren to dinoflagellate-bearing), enhanced symbiotic activity of (and thus

61

reduced efflux of low-δ^{15}N ammonium from) dinoflagellate-bearing species may contribute to the spring-to-summer decline in foraminifer δ^{15}N. However, at least part of this summertime δ^{15}N decline must be due to the observed decrease in the baseline δ^{15}N of available food sources (Fig. S2.2). Seasonality is examined further in section 4.3 below.

The data indicate an increase in the δ^{15}N of foraminiferal tissue (and to a lesser extent, shells) with depth within the upper 150 m (Fig. 2.5e&f). Depth stratification has been observed previously in foraminifer species distributions and in their shell carbon and oxygen isotopic compositions (Fairbanks et al., 1980; Fairbanks et al., 1982; Ravelo & Fairbanks, 1992; Mulitza et al., 1997; Mulitza et al., 2004). Thus, one might suspect that the observed δ^{15}N increase derives from partitioned depth habitats, with lower-δ^{15}N dinoflagellate-bearing species dominating the euphotic zone and higher-δ^{15}N symbiont-barren/chrysophyte-bearing species dwelling deeper in the water column. However, the common occurrence of "deep-typical" *G. truncatulinoides* and *G. hirsuta* in shallow tow collections and "shallow-typical" *G. ruber* and *O. universa* in deeper tow collections argues against strong partitioning of species over this depth interval, particularly when averaged over the year. Indeed, many of the species analysed here have overlapping depth habitats within the upper 150 m (e.g., *O. universa* and *G. bulloides*), and others undergo large depth changes during ontogeny (e.g., *G. truncatulinoides*). Therefore, collection depth should not be expected to represent the primary depth habitat. Rather, the depth gradient in the δ^{15}N of bulk suspended (>0.7 µm) PON below ~100 m in the Sargasso Sea (Saino and Hattori, 1980; Altabet, 1988), as well as in the larger (>200 µm) PON size fractions measured here (increasing by ~1.0‰ between the surface and 150 m; Fig. S2.1) suggest that the ~0.9‰ increase in foraminifer tissue over the same interval may reflect an increase in the δ^{15}N of their diet.

An alternative (but not necessarily contradictory) hypothesis for the observed group-specific δ^{15}N differences is that different species have distinct compositions of amino acids (King & Hare, 1972; Stathoplos & Hare, 1989; Robbins & Brew, 1990), which undergo varying degrees of isotopic fractionation during synthesis and/or translocation (Uhle et al., 1997; McClelland & Montoya, 2002). For instance, the apparently greater trophic enrichment of symbiont-barren foraminifera compared to dinoflagellate-bearers might be explained as deriving from a greater proportion of "trophic" (e.g., glutamic acid) *vs.* "source" (e.g., phenylanaline) amino acids (Popp et al., 2007; McCarthy et al., 2007) in the symbiont-barren group. While the existing amino acid content data from core-top planktic foraminifera do not support this interpretation (King & Hare, 1972; Robbins & Brew, 1990), amino-acid-specific δ^{15}N measurements would

62

help to robustly test this. As implied by the histograms (Fig. 2.5), averaging across euphotic zone-dwelling, dinoflagellate-bearing species (green triangles in Fig. 2.2a) yields a lower $\delta^{15}N$ than averaging across deeper-dwelling, symbiont-barren species (blue triangles in Fig. 2.2a). The resulting group averages reveal similar shell *vs.* tissue $\delta^{15}N$ relationships: the shells of both euphotic zone, dinoflagellate-bearing species and deep-dwelling, symbiont-barren species are only 0.1‰ elevated relative to their respective tissues. From this observation, we infer that the organic components employed by both symbiont-bearing and symbiont-barren foraminifera in biomineralization resemble their respective bulk tissues in amino acid composition. In this way, foraminifera may differ from corals: Muscatine et al. (2005) found that symbiont-barren corals exhibit a significantly higher $\delta^{15}N$ for skeletal N than for tissue N while symbiont-bearing corals do not.

4.3 Seasonal signals in foraminifer-bound $\delta^{15}N$

Here, we consolidate and extend our discussion of the seasonality of foraminifer-bound $\delta^{15}N$ and its underlying drivers. While our tow collections exhibit modest seasonal variation in $\delta^{15}N$ (with foraminifer tissue, shell-bound, and bulk PON $\delta^{15}N$ generally being lowest in late summer/fall and highest in spring), the trend in sinking shells is more apparent (compare Fig. 2.6 with Fig. S2.2). This is not surprising, as sediment traps remain in place year-round, sampling at regular intervals and integrating over longer timescales (~14 days) than net tows. By contrast, 120-190 minute net tows only provide a snapshot of foraminifer $\delta^{15}N$, and thus capture shorter term variations and small-scale features (e.g., storms, short-lived eddies or filaments) that may blur or overwhelm the seasonal signal (Schiebel et al., 1995; Beckmann et al., 1987; Schmuker & Schiebel, 2002) .

The $\delta^{15}N$ of sinking shells shows a distinctive minimum in late winter/early spring (Fig. 2.6). This follows closely after the period of deepest mixing (down to ~300 m in late February 2010), when deep nitrate is supplied to surface waters and the $\delta^{15}N$ of nitrate is 'reset' to the thermocline value (~2.6‰; Fig. S2.3) (Knapp et al., 2005; Fawcett et al., 2015). The late-spring maximum in foraminifer-bound $\delta^{15}N$ follows the rapid shoaling of the mixed layer (to ~20 m in May 2010) and the peak of the spring phytoplankton bloom (Lomas et al., 2013). During this time, nitrate in surface waters is drawn down rapidly, driving an increase in the $\delta^{15}N$ of the nitrate pool being consumed (due to isotopic fractionation during nitrate assimilation) (Knapp et al., 2005; Fawcett et al., 2015) and thus also the $\delta^{15}N$ of any PON subsequently produced from it (Altabet et al., 1991; Sigman et al., 1999a). Given that all foraminifera consume a

63

component of the PON pool, it seems reasonable that shell-bound $\delta^{15}N$ in sinking shells also records this $\delta^{15}N$ increase (depicted by panels 1-2 in Fig. 2.8). In short, even though it was not our intention to focus on seasonal nitrate drawdown at this study of a subtropical gyre site, this signal was recovered.
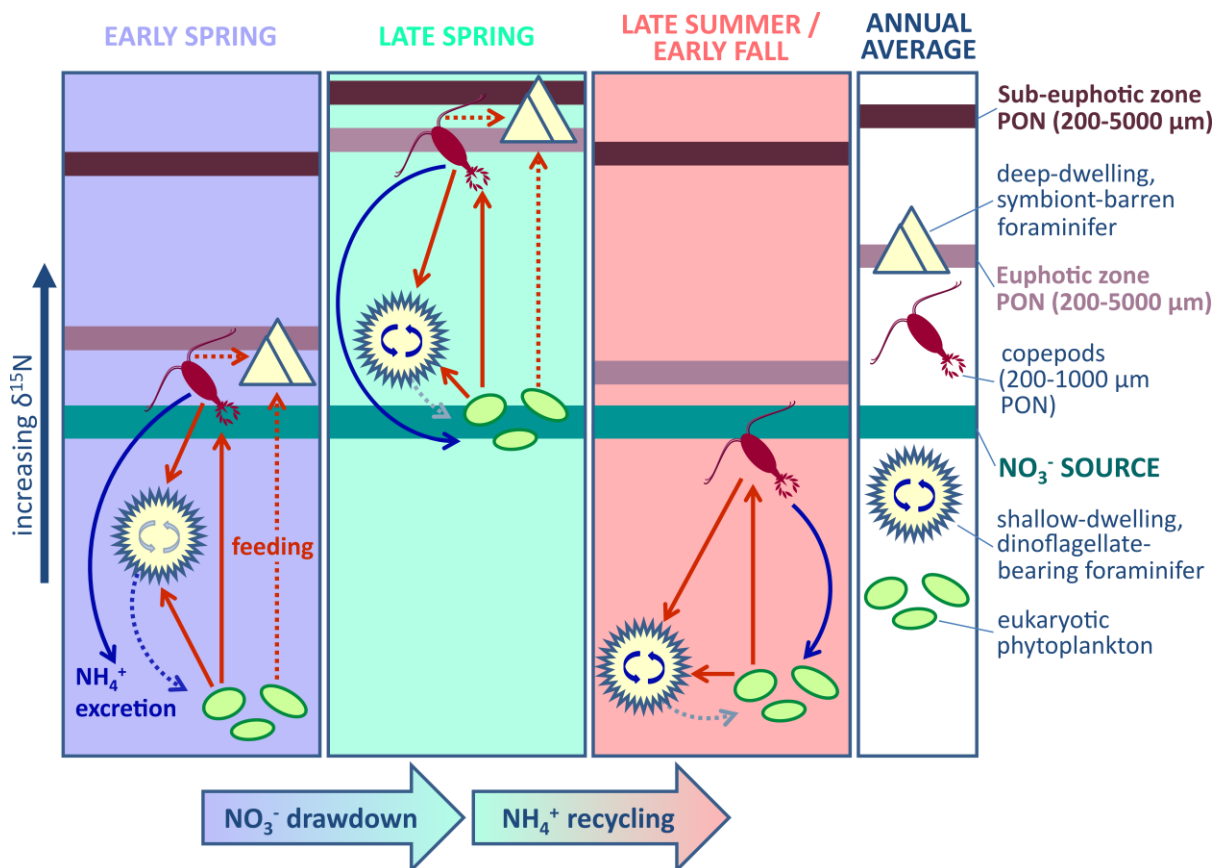
Fig. 2.8: Cartoon summary depicting the seasonal progression in $\delta^{15}N$ (panels 1-3) and the annual average state (panel 4) of dinoflagellate-bearing/shallow-typical and symbiont-barren/deep-typical foraminifera in relation to copepods, eukaryotic phytoplankton (both primary components of the sinking flux) and the mean annual nitrate supply to the euphotic zone at the Bermuda Time-series Site. Red arrows indicate feeding (solid arrows showing a preference for fresh prey, dashed arrows showing a preference for detrital particles and/or the organisms that feed upon them), which raises the $\delta^{15}N$ of heterotrophs relative to their diet). Blue arrows indicate ammonium excretion, which indirectly lowers the $\delta^{15}N$ of the entire system when consumed by phytoplankton. Circular arrows inside the shallow-typical foraminifer represents internal ammonium recycling between the host and photosymbionts, which lowers the $\delta^{15}N$ (and trophic level) of the host when active.

The decrease in $\delta^{15}N$ observed in sinking shells through the summer and fall coincides with the period of intense stratification when the nitrate supply from below is severely impeded (Steinberg et al., 2001; Lomas et al., 2013). Previous studies have found this to be a period of enhanced recycling of N within the shallow mixed layer (Menzel & Ryther, 1960; Lipschultz,

2001). Because recycled ammonium is lower in $\delta^{15}N$ than nitrate (Checkley & Miller, 1989; Lehmann et al., 2002), as the phytoplankton community becomes more dependent on ammonium, the $\delta^{15}N$ of PON suspended in the euphotic zone (including eukaryotic phytoplankton (Fawcett et al., 2014) and thus also the zooplankton that prey upon them) decreases (Fig. S2.2). Foraminifera, representing a subset of the zooplankton in the system, would also be expected to record this signal, explaining the decrease in shell-bound $\delta^{15}N$ during the summer and fall (as illustrated in panels 2-3 of Fig. 2.8). Thus, the data argue that the shells of individual foraminifer species capture seasonal changes in the $\delta^{15}N$ of phytoplankton and zooplankton biomass. At the same time, there is evidence for enhanced internal N cycling within the foraminifer-dinoflagellate system during late spring and summer from the changing $\delta^{15}N$ offset between dinoflagellate-bearing *vs.* symbiont-barren species, as well as between dinoflagellate-bearing species and their food sources (Fig. 2.8). In February/March, the sinking shells of dinoflagellate-bearing *G. ruber* and *O. universa* are similar in $\delta^{15}N$ to those of symbiont-barren species (e.g., *G. truncatulinoides*) (Fig. 2.6). By the end of April, *O. universa* and *G. ruber* shell-bound $\delta^{15}N$ have decreased slightly, despite sharp $\delta^{15}N$ increases in their primary food sources: copepods (200-1000 µm PON in Fig. 2.8 and Fig. S2.2) and eukaryotic phytoplankton (Fawcett et al., 2014). The resulting divergence of *O. universa* and *G. ruber* $\delta^{15}N$ below that of symbiont-barren foraminifera (by 1-3‰ in late spring; Fig. 2.6) may thus reflect more active or efficient retention of low-$\delta^{15}N$ ammonium within the host-symbiont system under improving light conditions of a shallower mixed layer (Fig. 2.8). Evaluating this possibility further might be pursued by measuring the $\delta^{15}N$ relationship between the symbionts and foraminifer host tissue on a seasonal basis.

Curiously, we also observe a significant $\delta^{15}N$ offset (2-3‰) between sinking shells of *G. ruber* / *O. universa* and *G. siphonifera* in early spring and summer, despite all three species being symbiont-bearing and largely carnivorous (Fig. 2.6). However, by late fall through early spring, this $\delta^{15}N$ difference is no longer apparent. This may represent additional evidence that the chrysophyte symbiosis of *G. siphonifera* is not as active in N cycling as the dinoflagellate symbioses of *G. ruber* and *O. universa* (Hemleben et al., 1989; Spero, 1998; Bijma et al., 1998), such that *G. siphonifera* is more similar in its N isotope characteristics to symbiont-barren foraminifera. If this is the case, the convergence of $\delta^{15}N$ in *G. ruber* / *O. universa* and *G. siphonifera* in late fall to early spring could result from a decrease in activity of host-dinoflagellate recycling, effectively raising the trophic levels (and thus shell-bound $\delta^{15}N$) of *G. ruber* and *O. universa* during this period. However, an additional consideration is that *G.*

siphonifera has two genotypes, each with a different type of chrysophyte symbiosis: type I (facultative) and type II (obligatory) (Faber et al., 1988; Faber et al., 1989; Bijma et al., 1998). The two are morphologically similar (and thus were not separated here), but exhibit distinct growth, feeding and reproductive behaviour (Faber et al., 1988; Faber et al., 1989). In the future, types I and II should be measured separately (at least from net tow collections) to evaluate their contributions (if different) to the observed seasonal signal in *G. siphonifera* δ^{15}N.

4.4 Changes in shell-bound δ^{15}N with depth

An important consideration for the application of the foraminifer δ^{15}N paleo-proxy is whether the δ^{15}N of foraminifer-bound N changes as a test sinks through the water column and is ultimately incorporated into the seafloor sediments. Between the net tows in the upper 200 m of the water column and the sediment traps at mid-depths, the δ^{15}N of shells increases by 0.6‰, while the N content decreases by 1.4 nmol/mg ($N_{measured}$-weighted averages; black triangles in Fig. 2.7a&b). Between the sediment traps and the seafloor, shell N content continues to decrease by an average of 2.4 nmol/mg, while average δ^{15}N remains unchanged. Below, we investigate the potential reasons for these observations.

4.4.1 Alteration in the upper water column

There are several possible explanations for the δ^{15}N rise from the tows to the traps: environmental differences between the two sampling periods, addition to or alteration of the test structure or composition during gametogenesis, and alteration of shell-bound N during early diagenesis (with or without shell dissolution and the associated exposure of previously protected organic N). Based on the available nitrate+nitrite data (Fig. S2.3) (Fawcett et al., 2011, 2014, 2015), we observe no significant δ^{15}N difference (p>0.05) between the two sampling periods (Jul 2011–Nov 2013 for the tows and Nov 2009–Nov 2010 for the traps), nor from the δ^{15}N measured for nitrate+nitrite (2.65±0.32‰) at 250 m between June 2000 and May 2001 (Knapp et al., 2005). These data argue that a difference in the δ^{15}N of the thermocline nitrate source is not responsible for the observed increase in foraminifer-bound δ^{15}N of sinking shells.

The remaining possible explanations for the tow-to-trap δ^{15}N difference would have implications for our interpretation of fossil foraminiferal δ^{15}N. First, the tow-to-trap δ^{15}N difference might result from alteration during gametogenesis, the final stage of a foraminifer's life cycle. During this stage, some species migrate to a different depth in the water column and

may form gametogenic calcite (and/or additional chambers) before releasing their gametes into the surrounding water (Deuser et al., 1981; Deuser, 1987; Schiebel et al., 1997a; Schiebel et al., 2002). Even within the same species, the degree of gametogenic calcification may vary substantially between specimens (Hemleben et al., 1989; Schiebel & Hemleben, 2017). Shallow-dwelling species like *O. universa* typically descend to the deep chlorophyll maximum (near the base of the euphotic zone at the Bermuda Time-series Site) for reproduction, while deep-dwellers like *G. truncatulinoides* and *G. hirsuta* ascend and proliferate in near-surface waters in early spring (Schiebel et al., 2002; Schiebel & Hemleben, 2005). If the gametogenic calcite encapsulates organic N with a $\delta^{15}N$ that is different from that of the shell-bound N laid down during the foraminifer's juvenile and adult life, this might explain at least part of the difference between foraminifer-bound $\delta^{15}N$ in the surface ocean and ocean interior. Because gametogenic calcification (unlike chamber-building) does not require a new structural template, the added calcite lacks the N-rich primary organic sheet of ontogenic calcite. While very little is known about the distribution of non-laminar organics in gametogenic calcite (Branson et al., 2016), we generally expect this calcite to be organic-poor and thus to contribute to the decline in shell N content from tows to traps.

However, our N content data combined with previously published data on the mass and/or thickness of gametogenic calcite do not make a compelling case for gametogenesis as the main explanation for the tow-to-trap differences in shell-bound N content or $\delta^{15}N$. Given that gametogenic calcite typically contributes 4-20% of the mass in post-gametogenic *O. universa* shells (Hamilton et al., 2008), the observed decrease in N content from tows to traps (from 5.4 nmol/mg to 4.8 nmol/mg, respectively) would require gametogenic calcite to have an N content of -9.9 to +1.8 nmol/mg. The negative values indicate that the mass of added calcite is generally too low for it to explain the N content decrease. Similarly, *N. dutertrei* (with an average gametogenic layer 46% of the total shell-wall thickness (Steinhardt et al., 2015), and assuming a range of ±10%) would require the added calcite to have an N content of -3.5 to -0.7 nmol/mg to reproduce the observed N content decline (from 6.9 to 4.2 nmol/mg). For the remaining four species with sufficient data to undertake the calculation (all *Globoratalia*), we assume the thickness of gametogenic calcite in *Globorotalia scitula* shells (47% (Steinhardt et al., 2015), ±10%) to be a reasonable approximation. Of these four, only *G. truncatulinoides* and *G. hirsuta* yield non-negative N contents (between 1.7 and 3.0 nmol/mg). From the calculated N contents, the $\delta^{15}N$ of gametogenic calcite in these two species is inferred to be between 5.2 and 7.9‰. It is unclear why gametogenic calcite would have a $\delta^{15}N$ so different from the rest of the shell

and tissue. As with the N content calculations, this argues against the gametogenic calcite N as the driver of the changes from net tows to sediment traps. These apparent failings of an explanation focused on gametogenesis compel us to consider N loss from shells (or the shell assemblage) during early diagenesis.

If a low-δ^{15}N N pool were preferentially lost from sinking shells post-mortem, it would leave the remaining shell-bound N elevated in δ^{15}N. As foraminifer tests sink, any external (i.e., non-calcified) N is accessible (to bacteria, predators, etc.) and the δ^{15}N of the remaining tissue is vulnerable to alteration. Indeed, the preferential removal of ^{14}N during remineralization (i.e., bacterially mediated oxidation of organic matter) is thought to drive the observed increase in the δ^{15}N of bulk suspended PON with depth in the Sargasso Sea (Saino & Hattori, 1980; Altabet & McCarthy, 1986; Altabet, 1988). However, before our foraminifer-bound δ^{15}N measurements are made, the tests undergo harsh chemical cleaning (see section 2.2 above) to ensure that any accessible and potentially compromised organic matter is removed (Ren et al., 2009). Thus, the tow-to-trap increase in foraminifer-bound δ^{15}N is not easily explained by bacterially mediated diagenesis of the foraminifer-native N. It is possible that shell-bound organic matter degrades chemically, without being exposed to environmental fluids and bacterial processes. Indeed, such degradation very likely occurs. As a well-documented example, biomineral matrix-bound amino acids racemize over time, with impacts on the proteins in which they occur (Bada, 1982; Collins et al., 1998). However, it seems unlikely that such degradation would provide a mechanism by which the associated N would be released from the mineral matrix, absent changes in the mineral matrix itself. Thus, especially with regard to the changes in shell-bound N from net tow- to sediment trap-collected foraminifera, we focus our attention on diagenesis of the mineral matrix that protects the shell-bound N.

Partial dissolution of settling foraminifer shells may be an important process in general. It is evident from the size distribution of sinking and sedimentary tests (compared with living fauna) that larger, faster-sinking tests are preferentially preserved over smaller, slower-sinking tests (Peeters et al., 1999). The shells of juveniles are thinly calcified (Fehrenbacher et al., 2017), such that the larger shells of foraminifera that have completed their life cycle (undergone ontogenic and/or gametogenic thickening) are preferentially preserved through the water column and into the sediments (Schiebel and Hemleben, 2017; and references therein). Moreover, substantial (19%) weight-loss in shells of the same size has been observed between 100 m and 1000 m depth in the North Atlantic, despite the super-saturated state of carbonate in ambient seawater and the addition of gametogenic calcite (Schiebel et al., 2007). One

68

explanation is that, as exposed organic tissues (including cytoplasm and any organic coatings e.g., pore linings) are remineralized by bacteria post mortem, weak organic acids are released, creating a micro-environment within and/or surrounding the test that is conducive to dissolution (i.e., under-saturated with respect to calcite) (Schiebel et al., 1997b; Milliman et al., 1999; Schiebel, 2002; Schiebel et al., 2007; Schiebel & Hemleben, 2017). Alternatively, this shallow dissolution might entail the loss of vaterite, the unstable (and more soluble) polymorph of calcium carbonate, as its protective organic membrane decays post mortem (Jacob et al., 2017). For any of these scenarios to explain our observations, the dissolution would need to expose N-bearing organic matter with a low $\delta^{15}N$ to remineralization, causing shell-bound N to rise in $\delta^{15}N$ as its N content declines.

If dissolution alone were responsible for the tow-to-trap differences in $\delta^{15}N$ and N content of shell-bound N, the $\delta^{15}N$ of the lost organic matter would be roughly 0.9‰. If the smaller, thinly calcified (thus, high N content) shells of all species are the main casualties of upper water column dissolution, the low $\delta^{15}N$ implied for smaller shells might reflect the lower trophic level of juveniles (feeding on smaller phytoplankton and detritus) relative to adults (preying upon larger phytoplankton and zooplankton). At the same time, weight loss in shells of the same size-class (observed by Schiebel et al., 2007) indicates partial dissolution of the shells that do survive sinking through the upper water column. Indeed, shells collected below this zone often show signs of dissolution within chambers of the final whorl (e.g., peeling of the chamber wall and corroded pores; Constandanche et al., 2013). The outermost (and normally the largest) chambers are generally more vulnerable to dissolution and breakage, as they are not as sheltered as the innermost chambers. Thus, if the largest (most recently formed) chambers and/or their inner walls are the primary sites of dissolution in the upper 500 m, we might infer that the low-$\delta^{15}N$ of constituent organic matter reflects an increasing reliance on symbiont photosynthesis toward the end of the foraminiferal life span (i.e., enhanced cyclic N flow). This is consistent with the observed strong correlation between test size and symbiont density (Spero & Parker, 1985), with greater retention of low-$\delta^{15}N$ ammonium within the host-symbiont system to support the increasing photosynthetic rates of dinoflagellates as the foraminifer grows. Repeating the above calculation, but separating species by symbiotic state, reveals that the $\delta^{15}N$ of calcite lost from the dinoflagellate-bearing group is notably lower than their tow shell average (-0.2‰ and 2.3‰, respectively), while the $\delta^{15}N$ of calcite lost from the symbiont-barren group is only slightly lower than their average (2.8‰ and 3.6‰). This distinction is also evident from paired measurements (where only species appearing in both tows and traps are

compared; Fig. 2.7a): while symbiont-bearing species are offset by 0.5-1.8‰ above the 1:1 line, symbiont-barren species (*G. hirsuta* (purple), *G. truncatulinoides* (plum)) fall only slightly (by 0.1-0.2‰) above the 1:1 line. These observations may indicate the preferential dissolution of the most recently formed chambers from dinoflagellate-hosting foraminifera, bearing the strongest low-δ^{15}N imprint of symbiont N cycling, as the main driver of the tow-to-trap δ^{15}N increase.

4.4.2 Preservation in the sediments

The average foraminifer-bound δ^{15}N of core-top sediments is nearly identical to sinking shells (Fig. 2.2a), despite a further 2.4 nmol/mg decrease in N content (Fig. 2.2b) from sinking to burial, with this transition representing a much longer period of time than from living to sinking. During this phase, there is no net effect on shell-bound δ^{15}N. Passive encrustation of shells is unlikely to incorporate much organic matter and thus represents a possible mechanism for lowering N content. However, substantial shell weight gain by encrustation is unlikely (Lohmann, 1995). For such overgrowth alone to explain the 45% decrease in average N content from traps to core-tops, an increase in shell weight of at least an 80% would be required. Yet shell-weight data show neither a consistent increase nor decrease (Takahashi & Bé, 1984). Thus, the best explanations for the N content decrease are (1) the dissolution of N-rich shells or N-rich portions of shells, or (2) chemical degradation of the shell-bound organic matter that then somehow ends its protection by the mineral matrix.

Close inspection of the trap-to-seafloor change in shell-bound δ^{15}N suggests a distinction between the δ^{15}N of calcite lost from symbiont-bearing and symbiont-barren species, with the dinoflagellate-bearing group losing N with a higher δ^{15}N than their sinking shell average (3.6‰ and 2.9‰, respectively), while the δ^{15}N of calcite lost from the symbiont-barren group appears to be lower than their average (2.5‰ and 3.8‰, respectively). This weak distinction, if real, may reflect the interaction between changes in the δ^{15}N of calcite-bound N added during growth with the differential vulnerability of different parts of the shell (or shells of different size and/or maturity) to dissolution on the seafloor. In general, though, our essential finding is that seafloor alteration appears to have only very minor effects on shell-bound δ^{15}N.

4.4.3 Overview of depth changes

In summary, the observations discussed above suggest a role for dissolution-driven N loss as shells sink through the water column and are incorporated into the sediments. In the early

phase, as shells sink through the upper 500 m, low-δ^{15}N calcite is lost, perhaps because this calcite derives from the lowest-δ^{15}N chambers of dinoflagellate-bearing foraminifera. At the same time, empty shells of foraminifera that have undergone active gametogenic thickening (and thus should have less N per unit mass) might preferentially escape dissolution, raising the average weight and thus lowering the average N content of shells reaching the sediment traps. In the deeper water column and sediments, a second phase of dissolution appears to remove calcite that is less isotopically distinct from shell-bound N as a whole. Most likely, the two phases of dissolution-driven N loss are continuous, with the loss of the most dissolution-prone calcite/vaterite (e.g., small, slowly sinking, perhaps cytoplasm-containing tests, as well as the outermost chambers of individual tests) transitioning gradually to dissolution of calcite that is less distinct from that of the total shell assemblage. Future measurements of the organic N in separate size fractions and specific shell components (e.g., ontogenic *vs.* gametogenic calcite) would help to test the explanations proposed here.

5. Implications for the foraminifer-bound δ^{15}N paleo-proxy

Given the near-complete consumption of nitrate in Sargasso Sea surface waters, the mean annual δ^{15}N of living foraminifera in this environment should converge on the δ^{15}N of the nitrate supply. Indeed, we find the annually averaged δ^{15}N (weighted by $N_{measured}$) of the bulk tissue (3.2‰) and shell-bound N (3.1‰) from tow-caught foraminifera to be within 0.6‰ of shallow thermocline (~200 m) nitrate (2.6‰). The individual species reveal two distinct groupings. Dinoflagellate-bearing, euphotic zone-dwelling foraminifera have tissue δ^{15}N (2.2‰) and shell-bound δ^{15}N (2.3‰) that are similar to the δ^{15}N of the annual nitrate supply from the thermocline. In contrast, symbiont-barren, deep-dwelling foraminifera record a higher δ^{15}N than thermocline nitrate for both tissue and shell-bound N (3.5‰ and 3.6‰, respectively). A potential concern is the subsequent rise in shell-bound δ^{15}N by 0.6‰ on average (weighted by $N_{measured}$) as foraminifera sink through the upper water column. Further work is called for to address whether this δ^{15}N increase is robust, widespread, or variable. Despite the changes that occur as foraminifer shells sink and settle on the seafloor, the distinction between low-δ^{15}N euphotic zone-dwelling, dinoflagellate-bearing and high-δ^{15}N deeper-dwelling, symbiont-barren species holds throughout the water column and into the sediments (compare green *vs.* blue triangles from surface tows with deeper sinking and core-top values; Fig. 2.2a). Thus,

knowledge of the basic ecology of the chosen foraminifer species is important for accurately inferring past nitrate $\delta^{15}N$ from downcore fossil shells.

Time-series of foraminifer $\delta^{15}N$ appear to follow the seasonal variation in $\delta^{15}N$ of autotrophic biomass and PON in general. This is consistent with the expectation that foraminifera acquire most, if not all, of their N from feeding and not directly from the nitrate supply. On a seasonal basis, PON $\delta^{15}N$ varies for reasons other than the $\delta^{15}N$ of the nitrate supply, including the isotopically fractionating drawdown of nitrate in the spring and the onset of intense N cycling in the late summer and early fall, and foraminifer $\delta^{15}N$ appears to track these seasonal PON $\delta^{15}N$ changes. This raises the concern that, at times in the past, foraminifer $\delta^{15}N$ might stray from the current relationship with subsurface nitrate $\delta^{15}N$ if, for example, N recycling in surface waters was more or less important (relative to nitrate-based production). This basic concern is inherent to using as a proxy any one N pool in the sinking flux, as opposed to the integrated sinking flux itself. Only the integrated N export is ensured by mass balance to record the $\delta^{15}N$ of the nitrate consumed in the euphotic zone.

We have shown here that, despite an imprint of N recycling on the seasonality of foraminifera, the shell-bound $\delta^{15}N$ of the euphotic zone-dwelling, dinoflagellate-bearing foraminifera, in particular, approximates the $\delta^{15}N$ of the mean annual nitrate supply, as has been found at other sites based mostly on foraminifer shells from surface sediments (Ren et al., 2009; Ren et al., 2012). This supports the expectation that, at least for the subtropical ocean, the $\delta^{15}N$ of the nitrate consumed in the euphotic zone (equivalent to the annual nitrate supply) is the underlying control on foraminifer-bound $\delta^{15}N$. The isotopic similarity between foraminifera (especially the dinoflagellate-bearing, shallow-dwellers) and the annual mean nitrate supply is consistent with their typical reliance on zooplankton and eukaryotic phytoplankton as their prey (Fig. 2.8). Eukaryotic phytoplankton and small zooplankton together appear to account for most of the sinking flux at the Bermuda Time-series Site (Fawcett et al., 2011), so that their consumption by foraminifera ties the annually integrated foraminifer $\delta^{15}N$ to the $\delta^{15}N$ of export production. The linkage exists despite the isotopic fractionation during N metabolism that causes heterotrophs to be higher in $\delta^{15}N$ than their prey. This isotopic fractionation also returns low $\delta^{15}N$ ammonium to surface waters, which drives a compensatory decline in phytoplankton $\delta^{15}N$, eventually lowering the $\delta^{15}N$ of zooplankton as well (Fig. 2.8). Over the annual cycle, the net effect is for the $\delta^{15}N$ of grazing zooplankton to approximate that of the sinking flux, as long as heterotrophs are responsible for most of the N export; our data and previous measurements are consistent with this view of the system. In the case of dinoflagellate-bearing

72

foraminifera, their consumption of both eukaryotic phytoplankton and heterotrophs weakens the significance of any isotopic distinctions between the two, potentially making these species a particularly reliable measure of the δ^{15}N of the N export in the subtropical ocean.

On the whole, our findings also bode well for the implementation of the foraminifer-bound δ^{15}N paleo-proxy at high latitudes. Foraminifer shells in polar environments should record variations in the δ^{15}N of upper-ocean nitrate, in response to both changes in the δ^{15}N of the subsurface nitrate supply and the degree of nitrate consumption by phytoplankton. At the same time, the evidence for a role of upper ocean N recycling in the seasonality of foraminifer δ^{15}N raises the possibility that the effect of recycling on foraminifera δ^{15}N may be important in paleoceanographic studies of polar ocean regions, which appear to have undergone large changes in nitrate supply and export production over time. Changes in the δ^{15}N offset between different foraminifer species have been observed (Ren et al., 2015), and the seasonally varying processes of nitrate drawdown and N recycling may be responsible. Ground-truthing of the foraminifer-bound δ^{15}N proxy in the modern polar ocean will be critical for identifying and testing such possibilities.

6. Acknowledgements

7. References

Altabet M.A. (1988). Variations in nitrogen isotopic composition between sinking and suspended particles: Implications for nitrogen cycling and particle transformation in the open ocean. *Deep-Sea Res. Pt I*, **35**, 535–554.

Altabet M.A. and Curry W.B. (1989). Testing models of past ocean chemistry using foraminifera $^{15}N/^{14}N$. *Global Biogeochem. Cycles*, **3**(2), 107–119.

Altabet M.A. and François R. (1994). Sedimentary nitrogen isotopic ratio as a recorder for surface ocean nitrate utilization. *Global Biogeochem. Cycles*, **8**(1), 103–116.

Altabet M.A. and McCarthy J.J. (1986). Vertical patterns in ^{15}N natural abundance in PON from the surface waters of warm-core rings. *J. Mar. Res.*, **44**, 185–201.

Altabet M.A., Deuser W.G., Honjo S. and Stienen S. (1991). Seasonal and depth-related changes in the source of sinking particles in the N. Atlantic. *Nature*, **354**, 136–139.

Altieri K.E., Hastings M.G., Gobel A.R., Peters A.J. and Sigman D.M. (2013). Isotopic composition of rainwater nitrate at Bermuda: The influence of air mass source and chemistry in the marine boundary layer. *J. Geophys. Res. Atmos.*, **118**, 11,304–11,316.

Altieri K.E., Fawcett S.E., Peters A.J., Sigman D.M. and Hastings M.G. (2016). Marine biogenic source of atmospheric organic nitrogen in the subtropical North Atlantic. *Proc. Natl. Acad. Sci. U.S.A.*, **113**(4), 925–930.

Bada J.L. (1982). Racemization of Amino Acids in Nature. *Interdisciplinary Science Reviews*, **7**(1), 30–46.

BATS Contributors. (2016). *Bermuda Atlantic Time-series Study CTD*. Available online: http://batsftp.bios.edu/BATS/. [dataset].

Bé A.W.H. (1960). Ecology of Recent Planktonic Foraminifera: Part 2: Bathymetric and Seasonal Distributions in the Sargasso Sea off Bermuda. *Micropaleontology*, **6**(4), 373–392.

Bé A.W.H., Hemleben C., Anderson O.R., Spindler M., Hacunda J. and Tuntivate-Choy S. (1977). Laboratory and Field Observations of Living Planktonic Foraminifera. *Micropaleontology*, **23**(2), 155–179.

Bé A.W.H., Hemleben C., Anderson O.R. and Spindler M. (1979). Chamber formation in planktonic Foraminifera. **25**(3), 294–307.

Beckmann W., Auras A. and Hemleben C. (1987). Cyclonic cold-core eddy in the eastern North Atlantic. III. Zooplankton. *Mar. Ecol. Prog. Ser.*, **39**, 165–173.

Bijma J., Hemleben C., Huber B.T., Erlenkeuser H. and Kroon D. (1998). Experimental determination of the ontogenetic stable isotope variability in two morphotypes of Globigerinella siphonifera (d'Orbigny). *Mar. Micropaleontol.*, **35**, 141–160.

Braman R.S. and Hendrix S.A. (1989). Nanogram nitrite and nitrate determination in environmental and biological materials by Vanadium(III) reduction with chemiluminescence detection. *Anal. Chem.*, **61**, 2715–2718.

Branson O., Bonnin E.A., Perea D.E., Spero H.J., Zhu Z., Winters M., Hönisch B., Russell A.D., Fehrenbacher J.S. and Gagnon A.C. (2016). Nanometer-Scale Chemistry of a Calcite Biomineralization Template: Implications for Skeletal Composition and Nucleation. *Proc. Natl. Acad. Sci.*, **113**(46), 12934–12939.

Casciotti K.L., Sigman D.M., Galanter Hastings M., Böhlke J.K. and Hilkert A. (2002). Measurement of the Oxygen Isotopic Composition of Nitrate in Seawater and Freshwater Using the Denitrifier Method. *Anal. Chem.*, **74**, 4905–4912.

Checkley D.M. and Miller C.A. (1989). Nitrogen isotope fractionation by oceanic zooplankton. *Deep-Sea Res. Pt A*, **36**, 1449–1456.

CLIMAP Project Members. (1981). Seasonal reconstruction of the Earth's surface at the last glacial maximum. *Geol. Soc. Am., Map and Chart Series*, 1–18.

CLIMAP Project Members. (1994). *CLIMAP 18K Database. IGBP PAGES/ World Data Center-A for Paleoclimatology Data Contribution Series # 94-001*. Available online: ftp://ftp.ncdc.noaa.gov/pub/data/paleo/paleocean/climap/climap18/. [dataset].

Collins M.J., Walton D. and King A. (1998). *Nitrogen-Containing Macromolecules in the Bio- and Geosphere*. ACS Symposium Series, vol. 707. American Chemical Society. Chap. The Geochemical Fate of Proteins, pages 74–87.

Constandanche M., Yerly F. and Spezzaferri S. (2013). Internal pore measurements on macroperforate planktonic foraminifera as an alternative morphometric approach. *Swiss J. Geosci.*, **106**, 179–186.

Conte M.H. and Weber J.C. (2014). Particle flux in the deep Sargasso Sea: The 35-year Oceanic Flux Program time series. *Oceanography*, **27**(1), 142–147.

Conte M.H., Ralph N. and E. Ross E. (2001). Seasonal and interannual variability in deep ocean particle fluxes at the Oceanic Flux Program/Bermuda Atlantic Time-series (BATS) site in the western Sargasso Sea near Bermuda. *Deep-Sea Res. Pt II*, **48**, 1471–1505.

de Boyer Montégut C., Madec G., Fischer A.S., Lazar A. and Iudicone D. (2004). Mixed layer depth over the global ocean: An examination of profile data and a profile-based climatology. *J. Geophys. Res.*, **109**(C12003).

Deevey G.B. and Brooks A.L. (1971). The annual cycle in quantity and composition of the zooplankton of the Sargasso Sea off Bermuda. 2. The surface to 2000 m. *Limnol. Oceanogr.*, **16**(6), 927–943.

Deuser W.G. (1987). Seasonal variations in isotopic composition and deep-water fluxes of the test of perennially abundant planktonic foraminifera of the Sargasso Sea: results from sediment-trap collections and their paleoceanographic significance. *J. Foramin. Res.*, **17**(1), 14–27.

Deuser W.G., Ross E.H., Hemleben C. and Spindler M. (1981). Seasonal changes in species composition, numbers, mass, size, and isotopic composition of planktonic foraminifera settling into the deep Sargasso Sea. *Palaeogeogr. Palaeoclimatol. Palaeoecol.*, **33**, 103–127.

Drake J.L., Schaller M.F., Mass T., Godfrey L., Fu A., Sherrell R.M., Rosenthal Y. and Falkowski P.G. (2017). Molecular and geochemical perspectives on the influence of CO_2 on calcification in coral cell cultures. *Limnol. Oceanogr.*, 1–15.

Duce R.A., LaRoche J., Altieri K., Arrigo K.R., Baker A.R., Capone D.G., Cornell S., Dentener F., Galloway J., Ganeshram R.S., Geider R.J., Jickells T., Kuypers M.M., Langlois R., Liss P.S., Liu S.M., Middelburg J.J., Moore C.M., Nickovic S., Oschlies A., Pedersen T., Prospero J., Schlitzer R., Seitzinger S., Sorensen L.L., Uematsu M., Ulloa O., Voss

M., Ward B. and Zamora L. (2008). Impacts of Atmospheric Anthropogenic Nitrogen on the Open Ocean. *Science*, **320**, 893–897.

Faber W.W., Anderson O.R., Lindsey J.L. and Caron D.A. (1988). Algal-foraminiferal symbiosis in the planktonic foraminifer Globigerinella aequilateralis: I. Occurrence and stability of two mutually exclusive chrysophyte endosymbionts and their ultrastructure. *J. Foramin. Res.*, **18**, 334–343.

Faber W.W., Anderson O.R. and Caron D.A. (1989). Algal-foraminiferal symbiosis in the planktonic foraminifer Globigerinella aequilateralis: II. Effects of two symbiont species on foraminiferal growth and longevity. *J. Foramin. Res.*, **19**(3), 185–193.

Fairbanks R.G., Wiere P.H. and Bé A.W.H. (1980). Vertical Distribution and Isotopic Composition of Living Planktonic Foraminifera in the Western North Atlantic. *Science*, **207**(4426), 61–63.

Fairbanks R.G., Sverdlove M., Free R., Wiebe P.H. and Bé A.W.H. (1982). Vertical distribution and isotopic fractionation of living planktonic foraminifera from the Panama Basin. *Nature*, **298**, 841–844.

Fawcett S.E., Lomas M.W., Casey J.R., Ward B.B. and Sigman D.M. (2011). Assimilation of upwelled nitrate by small eukaryotes in the Sargasso Sea. *Nat. Geosci.*, **4**, 717–722.

Fawcett S.E., Lomas M.W., Ward B.B. and Sigman D.M. (2014). The counterintuitive effect of summer-to-fall mixed layer deepening on eukaryotic new production in the Sargasso Sea. *Global Biogeochem. Cycles*, **28**, 86–102.

Fawcett S.E., Ward B.B., Lomas M.W. and Sigman D.M. (2015). Vertical decoupling of nitrate assimilation and nitrification in the Sargasso Sea. *Deep-Sea Res. Pt I*, **103**, 64–72.

Fehrenbacher J.S., Russell A.D., Davis C.V., Gagnon A.C., Spero H.J., Cliff J.B., Zhu Z. and Martin P. (2017). Link between light-triggered Mg-banding and chamber formation in the planktic foraminifera Neogloboquadrina dutertrei. *Nat. Commun.*, **8**.

François R., Altabet M.A. and Burckle L.H. (1992). Glacial to interglacial changes in surface nitrate utilization in the Indian sector of the Southern Ocean as recorded by sediment δ^{15}N. *Paleoceanography*, **7**(5), 589–606.

Gastrich M. D. (1987). Ultrastructure of a new intracellular symbiotic alga found within planktonic foraminifera. *J. Phycol.*, **23**, 623–632.

Gobel A.R., Altieri K.E., Peters A.J., Hastings M.G. and Sigman D.M. (2013). Insights into anthropogenic nitrogen deposition to the North Atlantic investigated using the isotopic composition of aerosol and rainwater nitrate. *Geophys. Res. Lett.*, **40**, 5977–5982.

Haidar A.T., Thierstein H.R. and Deuser W.G. (2000). Calcareous phytoplankton standing stocks, fluxes and accumulation in Holocene sediments off Bermuda (N. Atlantic). *Deep-Sea Res. Pt II*, **47**, 1907–1938.

Hamilton C.P., Spero H.J., Bijma J. and Lea D.W. (2008). Geochemical investigation of gametogenic calcite addition in the planktonic foraminifera Orbulina universa. *Mar. Micropaleontol.*, **68**, 256–267.

Hemleben C., Spindler M. and Anderson O.R. (1989). *Modern Planktonic Foraminifera*. Springer-Verlag.

Honjo S. and Erez J. (1978). Dissolution rates of calcium carbonate in the deep ocean; an in-situ experiment in the North Atlantic Ocean. *Earth Planet. Sci. Lett.*, **40**(2), 287–300.

Horn M.G., Robinson R.S., Rynearson T.A. and Sigman D.M. (2011). Nitrogen isotopic relationship between diatom-bound and bulk organic matter of cultured polar diatoms. *Paleoceanography*, **26**(PA3208).

Hottinger L. and Dreher D. (1974). Differentiation of protoplasm in nummulitidae (Foraminifera) from Elat, Red Sea. *Mar. Biol.*, **25**(1), 41–61.

Jacob D.E., Wirth R., Agbaje O.B.A., Branson O. and Eggins S.M. (2017). Planktic foraminifera form their shells via metastable carbonate phases. *Nat. Commun.*, **8**.

Jickells T.D., Buitenhuis E., Altieri K., Baker A.R., Capone D., Duce R.A, Dentener F., Fennel K., Kanakidou M., LaRoche J., Lee K., Liss P., Middelburg J.J., Moore J.K., Okin G., Oschlies A., Sarin M., Seitzinger S., Sharples J., Singh A., Suntharalingam P., Uematsu M. and Zamora L.M. (2017). A reevaluation of the magnitude and impacts of anthropogenic atmospheric nitrogen inputs on the ocean. *Global Biogeochem. Cycles*, **31**(2), 289–305.

King, K. Jr. and Hare P.E. (1972). Amino Acid Composition of the Test as a Taxonomic Character for Living and Fossil Planktonic Foraminifera. *Micropaleontology*, **18**(3), 285–293.

Knapp A.N., Sigman D.M. and Lipschultz F. (2005). N isotopic composition of dissolved organic nitrogen and nitrate at the Bermuda Atlantic Time-series Study site. *Global Biogeochem. Cycles*, **19**, 1–15.

Kröger N., Deutzmann R., Bergsdorf C. and Sumper M. (2000). Species-specific polyamines from diatoms control silica morphology. *Proc. Natl. Acad. Sci. U.S.A.*, **97**(26), 14133–14138.

Langer M.R. (1992). Biosynthesis of glycosaminoglycans in foraminifera: A review. *Mar. Micropaleontol.*, **19**, 245–255.

Lehmann M.F., Bernasconi S.M., Barbieri A. and McKenzie J.A. (2002). Preservation of organic matter and alteration of its carbon and nitrogen isotope composition during simulated and in situ early sedimentary diagenesis. *Geochim. Cosmochim. Acta*, **66**(20), 3573–3584.

Lipschultz F. (2001). A time-series assessment of the nitrogen cycle at BATS. *Deep-Sea Res. Pt II*, **48**, 1897–1924.

Lohmann G.P. (1995). A model for variation in the chemistry of planktonic foraminifera due to secondary calcification and selective dissolution. *Paleoceanography*, **10**(3), 445–457.

Lomas M.W., Bates N.R., Johnson R.J., Knap A.H., Steinberg D.K. and Carlson C.A. (2013). Two decades and counting: 24-years of sustained open ocean biogeochemical measurements in the Sargasso Sea. *Deep-Sea Res. Pt II*.

Martínez-García A., Sigman D.M., Ren H., Anderson R.F., Straub M., Hodell D.A., Jaccard S.L., Eglinton T.I. and Haug G.H. (2014). Iron Fertilization of the Subantarctic Ocean During the Last Ice Age. *Science*, **343**, 1347–1350.

McCarthy M.D., Benner R., Lee C. and Fogel M.L. (2007). Amino acid nitrogen isotopic fractionation patterns as indicators of heterotrophy in plankton, particulate, and dissolved organic matter. *Geochimica et Cosmochimica Acta*, **71**, 4727–4744.

McClelland J.W. and Montoya J.P. (2002). Trophic Relationships and the Nitrogen Isotopic Composition of Amino Acids in Plankton. *Ecology*, **83**(8), 2173–2180.

Meckler A.N., Ren H., Sigman D.M., Gruber N., Plessen B., Schubert C.J. and Haug G.H. (2011). Deglacial nitrogen isotope changes in the Gulf of Mexico: evidence from bulk sedimentary and foraminifera-bound nitrogen in Orca Basin sediments. *Paleoceanography*, **26**(PA4216), 1–13.

Menzel D.W. and Ryther J.H. (1960). The annual cycle of primary production in the Sargasso Sea off Bermuda. *Deep Sea Res.*, **6**, 351–367.

Milliman J.D., Troy P.J., Balch W.M., Adams A.K., Li Y.H. and Mackenzie F.T. (1999). Biologically mediated dissolution of calcium carbonate above the chemical lysocline? *Deep-Sea Res. Pt I*, **46**, 1653–1669.

Morales L.V., Sigman D.M., Horn M.G. and Robinson R.S. (2013). Cleaning methods for the isotopic determination of diatom-bound nitrogen in non-fossil diatom frustules. *Limnol. Oceanogr. Methods*, **11**(2), 101–112.

Morales L.V., Granger J., Chang B.X., Prokopenko M.G., Plessen B., Gradinger R. and Sigman D.M. (2014). Elevated $^{15}N/^{14}N$ in particulate organic matter, zooplankton, and diatom frustule-bound nitrogen in the ice-covered water column of the Bering Sea eastern shelf. *Deep Sea Res. Part II*, **109**, 100–111. Understanding Ecosystem Processes in the Eastern Bering Sea III.

Movellan A. (2013). *La biomasse des foraminifères planctoniques actuels et son impact sur la pompe biologique de carbone*. Ph.D. thesis, Sciences de la Terre, Université d'Angers, Français.

Mulitza S., Dürkoop A., Hale W., Wefer G. and Niebler H.S. (1997). Planktonic foraminifera as recorders of past surface-water stratification. *Geology*, **25**, 335–338.

Mulitza S., Donner B., Fischer G., Paul A., Pätzold J., Rühlemann C. and Segl M. (2004). *The South Atlantic in the late quaternary: reconstruction of material budgets and current systems*. Springer, Berlin. Chap. The South Atlantic oxygen isotope record of planktic foraminifera, pages 121–142.

Muscatine L., Goiran C., Land L., Jaubert J., Cuif J.P. and Allemand D. (2005). Stable isotopes (δ^{13}C and δ^{15}N) of organic matrix from coral skeleton. *Proc. Natl. Acad. Sci. U.S.A.*, **102**, 1525–1530.

Nydahl F. (1978). On the peroxodisulphate oxidation of total nitrogen in waters to nitrate. *Water Res.*, **12**, 1123–1130.

Peeters F., Ivanova E., Conan S., Brummer G.-J., Ganssen G., Troelstra S. and van Hinte J. (1999). A size analysis of planktic foraminifera from the Arabian Sea. *Mar. Micropaleontol.*, **36**(1), 31–63.

Pennock J.R., Velinsky D.J., Ludlam J.M., Sharp J.H. and Fogel M.L. (1996). Isotope fractionation of ammonium and nitrate during their uptake by Skeletonema Costatum: Implications for the δ^{15}N dynamics under bloom conditions. *Limnol. Oceanogr.*, **41**(3), 451–459.

Popp B.N., Graham B.S., Olson R.J., Hannides C.C.S., Lott M.J., López-Ibarra G.A., Galván-Magaña F. and Fry B. (2007). Insight into the Trophic Ecology of Yellowfin Tuna, Thunnus albacares, from Compound-Specific Nitrogen Isotope Analysis of Proteinaceous Amino Acids. *Terrestrial Ecology*, **1**, 173–190.

Qi H., Coplen T.B., Geilmann H., Brand W.A. and Böhlke J.K. (2003). Two new organic reference materials for δ^{13}C and δ^{15}N measurements and a new value for the δ^{13}C of NBS 22 oil. *Rapid Commun. Mass Spectrom.*, **17**, 2483–2487.

Ravelo A.C. and Fairbanks R.G. (1992). Oxygen Isotopic Composition of Multiple Species of Planktonic Foraminifera: Recorders of the Modern Photic Zone Temperature Gradient. *Paleoceanography*, **7**(6), 815–831.

Ren H., Sigman D.M., Meckler A.N., Plessen B., Robinson R.S., Rosenthal Y. and Haug G.H. (2009). Foraminiferal Isotope Evidence of Reduced Nitrogen Fixation in the Ice Age Atlantic Ocean. *Science*, **323**, 244–248.

Ren H., Sigman D.M., Thunell R.C. and Prokopenko M.G. (2012). Nitrogen isotopic composition of planktonic foraminifera from the modern ocean and recent sediments. *Limnol. Oceanogr.*, **57**(4), 1011–1024.

Ren H., Studer A.S., Serno S., Sigman D.M., Winckler G., Anderson R.F., Oleynik S., Gersonde R. and Haug G.H. (2015). Glacial-to-interglacial changes in nitrate supply and consumption in the subarctic North Pacific from microfossil-bound N isotopes at two trophic levels. *Paleoceanography*, **30**, 1217–1232.

Robbins L.L. and Brew K. (1990). Proteins from the organic matrix of core-top and fossil planktonic foraminifera. *Geochim. Cosmochim. Acta*, **54**, 2285–2292.

Robinson R.S., Brunelle B.G. and Sigman D.M. (2004). Revisiting nutrient utilization in the glacial Antarctic: evidence from a new diatom-bound N isotope method. *Paleoceanography*, **19**(PA3001), 1–13.

Saino T. and Hattori A. (1980). ^{15}N natural abundance in oceanic suspended particulate matter. *Nature*, **283**, 752–754.

Salmon K.H., Anand P., Sexton P.F. and Conte M. (2015). Upper ocean mixing controls the seasonality of planktonic foraminifer fluxes and associated strength of the carbonate pump in the oligotrophic North Atlantic. *Biogeosciences*, **12**(1), 223–235.

Schiebel R. (2002). Planktic foraminiferal sedimentation and the marine calcite budget. *Global Biogeochem. Cycles*, **16**(4), 1–21.

Schiebel R. and Hemleben C. (2005). Modern planktic Foraminifera. *Paläontologische Zeitschrift*, **79**(1), 135–148.

Schiebel R. and Hemleben C. (2017). *Planktic Foraminifers in the Modern Ocean*. Springer-Verlag Berlin Heidelberg.

Schiebel R., Hiller B. and Hemleben C. (1995). Impacts of storms on Recent planktic foraminiferal test production and $CaCO_3$ flux in the North Atlantic at 47°N, 20°W (JGOFS). *Mar. Micropaleontol.*, **26**(1), 115–129.

Schiebel R., Bijma J. and Hemleben C. (1997a). Population dynamics of the planktic foraminifer Globigerina bulloides from the eastern North Atlantic. *Deep-Sea Res. Pt I*, **44**, 1701–1713.

Schiebel R., Zeltner A. and Hemleben C. (1997b). Produktion und vertikaler FluX kalkigen Planktons im NE-Atlantik und der Arabischen See. *Page 47–48 of:* Giese M. and Wefer

G. (eds), *Bericht über den 5. JGOFS-Workshop. 27/28 November 1996 in Bremen, Berichte aus dem Fachbereich Geowissenschaften Universität Bremen*, vol. 89.

Schiebel R., Waniek J., Zeltner A. and Alves M. (2002). Impact of the Azores front on the distribution of planktic foraminifers, shelled gastropods, and coccolithophorids. *Deep-Sea Res. Pt II*, **49**, 4035–4050.

Schiebel R., Barker S., Lendt R., Thomas H. and Bollmann J. (2007). Planktic foraminiferal dissolution in the twilight zone. *Deep-Sea Res. Pt II*, **54**, 676–686.

Schiebel R., Spielhagen R.F., Garnier J., Hagemann J., Howa H., Jentzen A., Martínez-García A., Meilland J., Michel E., Repschläger J., Salter I., Yamasaki M. and Haug G. (2017). Modern planktic foraminifers in the high-latitude ocean. *Mar. Micropaleontol.*, **136**, 1–13.

Schmuker B. and Schiebel R. (2002). Planktic foraminifers and hydrography of the eastern and northern Caribbean Sea. *Mar. Micropaleontol.*, **46**(3-4), 387–403.

Sigman D.M., Altabet M.A., McCorkle D.C., François R. and Fischer G. (1999a). The δ^{15}N of nitrate in the Southern Ocean: Consumption of nitrate in surface waters. *Global Biogeochem. Cycles*, **13**(4), 1149–1166.

Sigman D.M., Altabet M.A., François R., McCorkle D.C. and Gaillard J.F. (1999b). The isotopic composition of diatom-bound nitrogen in Southern Ocean sediments. *Paleoceanography*, **14**(2), 118–134.

Sigman D.M., Casciotti K.L., Andreani M., Barford C., Galanter M. and Böhlke J.K. (2001). A Bacterial Method for the Nitrogen Isotopic Analysis of Nitrate in Seawater and Freshwater. *Anal. Chem.*, **73**, 4145–4153.

Spero H.J. (1988). Ultrastructural examination of chamber morphogenesis and biomineralization in the planktonic foraminifer Orbulina universa. *Mar. Biol.*, **99**(1), 9–20.

Spero H.J. (1998). *Isotope Paleobiology and Paleoecology*. Special publication edn. Paleontological Society Papers, vol. 4. The Paleontological Society. Chap. Life History and Stable Isotope Geochemistry of Planktonic Foraminifera.

Spero H.J. and Parker S.L. (1985). Photosynthesis in the symbiotic planktonic foraminifer Orbulina universa, and its potential contribution to oceanic primary productivity. *J. Foramin. Res.*, **15**(4), 273–281.

Spindler M., Hemleben C., Salomons J. and Smit L. (1984). Feeding behavior of some planktonic foraminifers in laboratory cultures. *J. Foramin. Res.*, **14**(4), 237–249.

Stathoplos L. and Hare P.E. (1989). Amino acids in planktonic foraminifera: are they phylogenetically useful? *Pages 329–338 of:* Crick R.E. (ed), *Origin, Evolution, and Modern Aspects of Biomineralization in Plants and Animals*. Proc. 5th Intl. Symp. Biomineral. University of Texas, Arlington, Texas: Springer Science & Business Media.

Steinberg D.K., Carlson C.A., Bates N.R., Johnson R.J., Michaels A.F. and Knap A.H. (2001). Overview of the US JGOFS Bermuda Atlantic Time-series Study (BATS): a decade-scale look at ocean biology and biogeochemistry. *Deep-Sea Res. Pt II*, **48**, 1405–1447.

Steinhardt J., de Nooijer L.L.J, Brummer G.-J. and Reichart G.-J. (2015). Profiling planktonic foraminiferal crust formation. *Geochem. Geophys. Geosyst.*, **16**, 2409–2430.

Straub M., Sigman D.M., Ren H., Martínez-García A., Nele Meckler A. and Haug G.H. (2013). Changes in North Atlantic nitrogen fixation controlled by ocean circulation. *Nature*, **501**, 200–204.

Sumper M., Brunner E. and Lehmann G. (2005). Biomineralization in diatoms: Characterization of novel polyamines associated with silica. *FEBS Lett.*, **579**(17), 3765–3769.

Takahashi K. and Bé A.W.H. (1984). Planktonic foraminifera: factors controlling sinking speeds. *Deep Sea Research*, **31**(12), 1477–1500.

Tolderlund D.S. and Bé A.W.H. (1971). Seasonal Distribution of Planktonic Foraminifera in the Western North Atlantic. *Micropaleontology*, **17**(3), 297–329.

Uhle M.E., Macko S.A., Spero H.J., Engel M.H. and Lea D.W. (1997). Sources of carbon and nitrogen in modern planktonic foraminifera: the role of algal symbionts as determined by bulk and compound specific stable isotopic analyses. *Org. Geochem.*, **27**(3/4), 103–113.

Uhle M.E., Macko S.A., Spero H.J., Lea D.W., Ruddiman W.F. and Engel M.H. (1999). The fate of nitrogen in the Orbulina universa foraminifera–symbiont system determined by nitrogen isotope analyses of shell-bound organic matter. *Limnol. Oceanogr.*, **44**(8), 1968–1977.

Verrado D.J., Froelich P.N. and McIntyre A. (1990). Determination of organic carbon and nitrogen in marine sediments using the Carlo Erba NA-1500 analyzer. *Deep-Sea Res.*, **37**, 157–165.

Wada E. and Hattori A. (1978). Nitrogen isotope effects in the assimilation of inorganic nitrogenous compounds by marine diatoms. *Geomicrobiol. J.*, **1**(1), 85–101.

Wang X.T, Sigman D.M, Cohen A.L., Sinclair D.J, Sherrell R.M., Weigand M.A., Erler D.V. and Ren H. (2015). Isotopic composition of skeleton-bound organic nitrogen in reef-building symbiotic corals: A new method and proxy evaluation at Bermuda. *Geochim. Cosmochim. Acta*, **148**, 179–190.

Waser N.A.D., Harrison P.J., Nielsen B., Calvert S.E. and Turpin D.H. (1998). Nitrogen Isotope Fractionation During the Uptake and Assimilation of Nitrate, Nitrite, Ammonium, and Urea by a Marine Diatom. *Limnol. Oceanogr.*, **43**(2), 215–224.

Weigand M.A., Foriel J., Barnett B., Oleynik S. and Sigman D.M. (2016). Updates to instrumentation and protocols for isotopic analysis of nitrate by the denitrifier method. *Rapid Commun. Mass Spectrom.*, **30**(12), 1365–1383. RCM-15-0493.R1.

Welch B.L. (1947). The generalization of "Student's" problem when several different population variances are involved. *Biometrika*, **34**(1–2), 28–35.

Wessel P., Smith W.H.F., Scharroo R., Luis J. and Wobbe F. (2013). Generic Mapping Tools: Improved Version Released. *Eos, Transactions American Geophysical Union*, **94**(45), 409–410.

8. Supplementary Information

8.1 Supplementary Figures
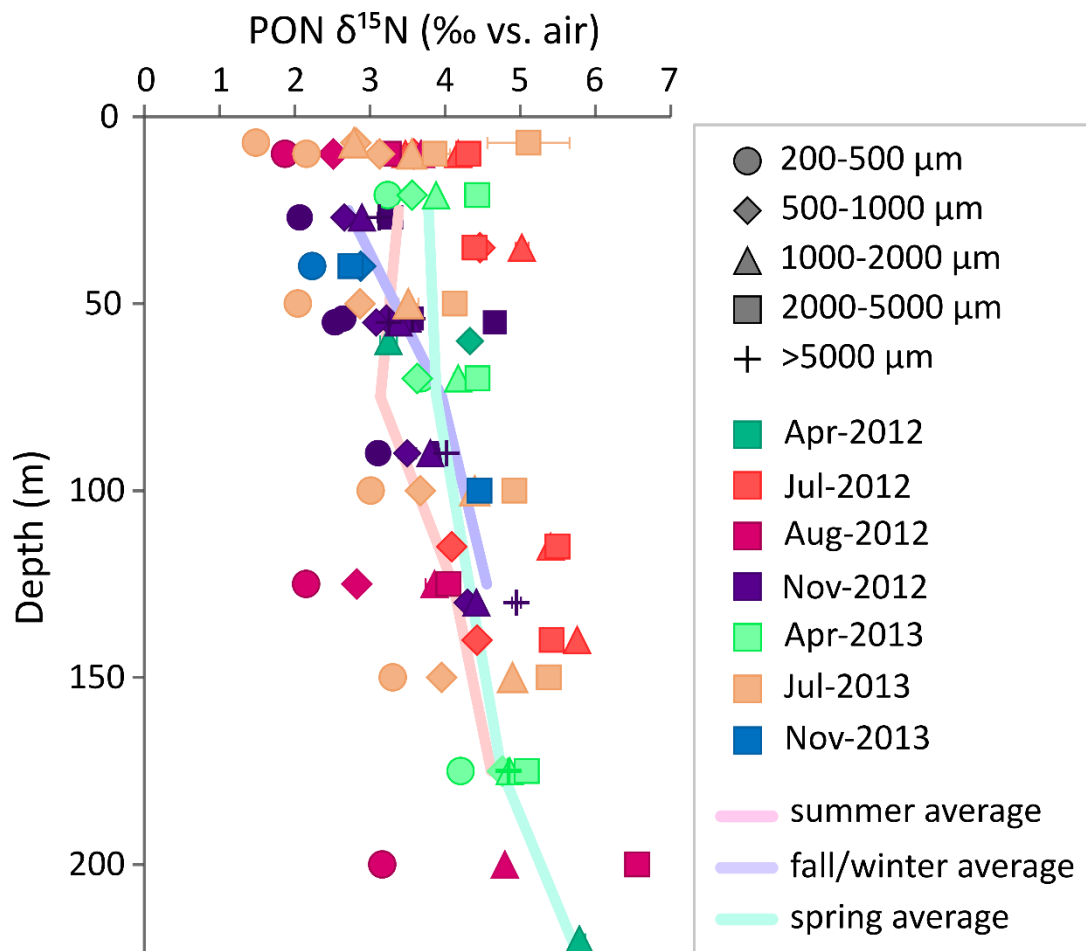
Fig. S2.1: Depth profile of size-fractionated PON δ¹⁵N in the upper ocean (0-250 m) at the Bermuda Time-series Site, sampled from net tows conducted between April 2012 and November 2013. Symbol shapes represent different size-fractions (>200 µm), and their colours represent different cruises (blue/dark purple for fall, turquoise/green for spring, and peach/magenta for summer). Error bars show measurement standard deviation (n = 2-3). Pastel-coloured profile lines show fall, spring, and summer averages, incorporating all size fractions.
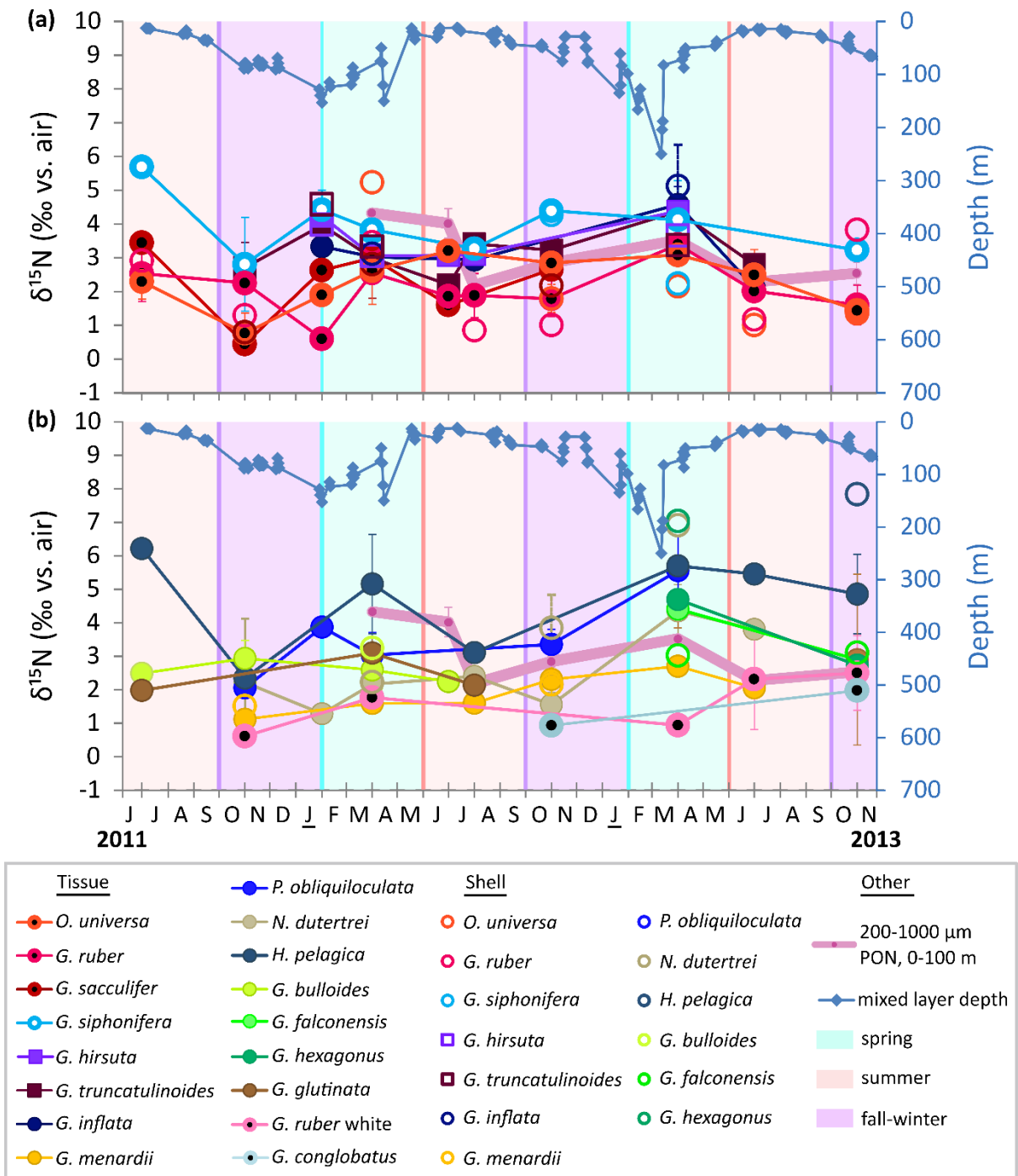
Fig. S2.2: Net tow δ^{15}N time-series. Foraminifer δ^{15}N collected via net tows during ten cruises between July 2011 and November 2013. Species are split into panels (a) and (b) for visibility. Filled circles and squares denote foraminiferal tissue, and open circles and squares denote shell-bound measurements, with error bars showing the standard deviation of all tows from a cruise. Euphotic-zone averages of (Fawcett et al., 2014) size-fractionated PON δ^{15}N (200-1000 µm from 0-100 m; broad mauve lines) are overlaid. Mixed layer depth (blue diamonds) is plotted on the secondary y-axis, and background colours denote seasons (turquoise for spring, pink for summer, purple for fall/winter).
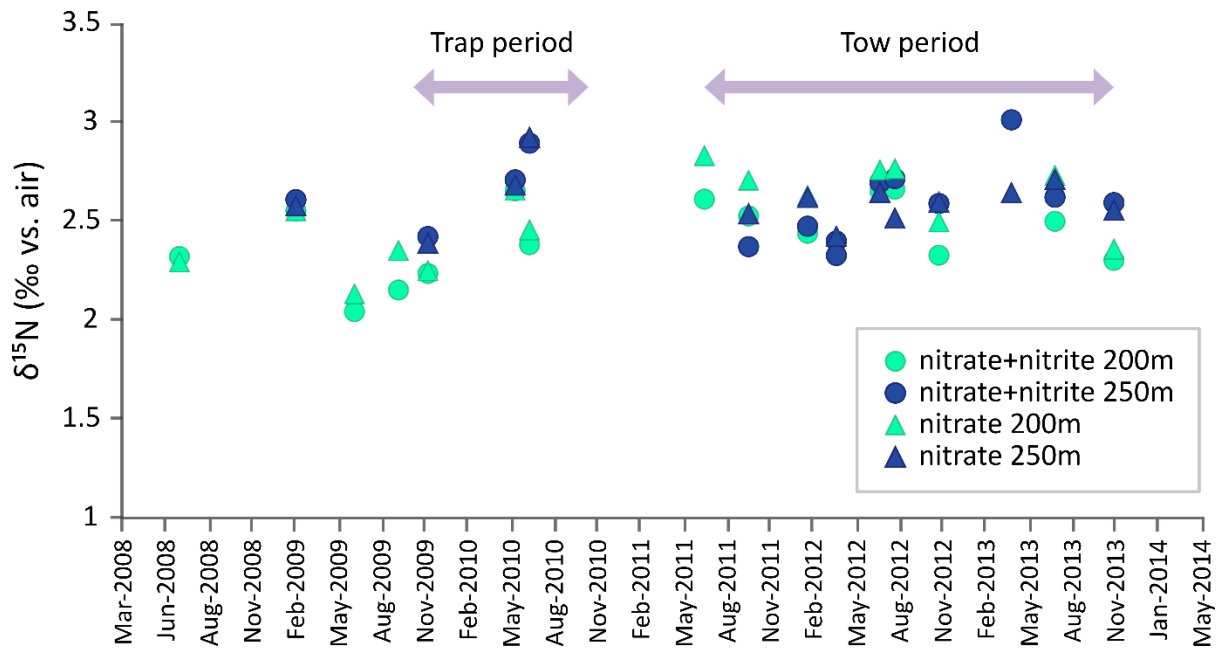
Fig. S2.3: Subsurface nitrate $\delta^{15}N$ time-series. Measurements of nitrate (triangles) and nitrate+nitrite (circles) $\delta^{15}N$ near the base of the thermocline (200 m (light blue symbols), and 250 m (dark blue symbols)) at the Bermuda Time-series Site between July 2008 and November 2013 (Fawcett et al., 2011, 2014, 2015). The time-series spans both sediment-trap and net-tow sampling periods (indicated by purple arrows). A two-sample, unequal variances t-test indicates no significant difference (p>0.05) in thermocline nitrate or nitrate+nitrite $\delta^{15}N$ between the two sampling periods, ruling out a change in the $\delta^{15}N$ of the thermocline supply as the main driver of the tow-to-trap difference in foraminifer-bound $\delta^{15}N$.
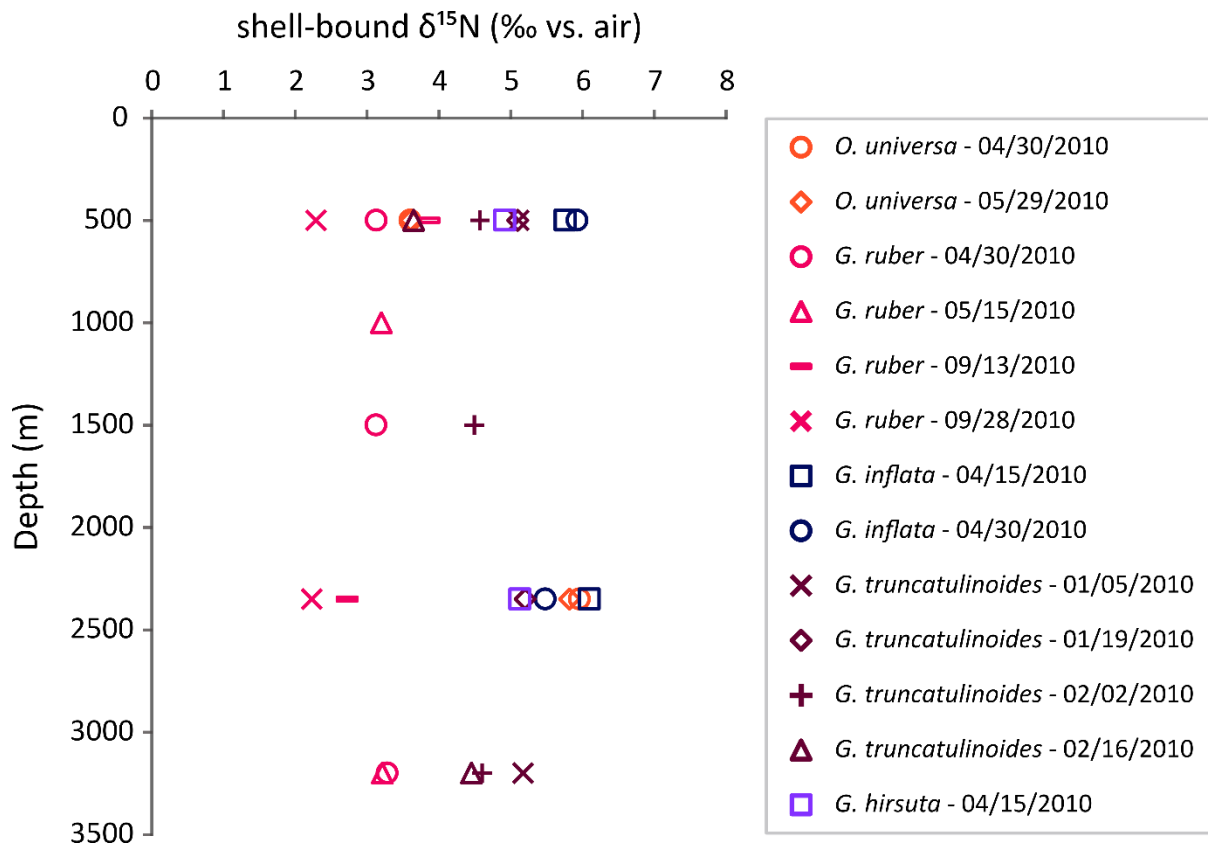
Fig. S2.4: Expanded depth profile of foraminifer-bound δ^{15}N captured by sediment traps (moored at 500 m, 1500 m and 3200 m). Only those species (colours) and collection periods (symbols) with sufficient shells for multi-depth measurements are shown. Each data point represents a two-week collection period, and is plotted at the average trap depth (i.e., the average of the two or three trap depths from which specimens were combined to make the measurement). We observe no sizeable or consistent change in the δ^{15}N of sinking shells over this depth interval, except for *O. universa*, which exhibits an increase of ~2‰ between 500 m and 1500-3200 m.

8.2 Supplementary Tables

Table S2.1: Details of foraminifer net tow collections in the Sargasso Sea.

Cruise name	Month & Year	Station site	Tow depths (m)	Tow durations (min)
HS1178	Jul 2011	Hydro Station S*	60; 100; 150; 200	150; 180; 165; 180
B274	Oct 2011	BATS**	50; 100; 150	180; 180; 180
AE1203	Feb 2012	BATS	30; 80; 150	180; 180; 185
B280	Apr 2012	BATS	150; 61; 40; 220; 60; 35	182; 190; 163; 180; 165; 180
B283	Jul 2012	BATS	35; 100	180; 170
AE1220	Aug 2012	BATS	10; 125; 200	180; 180; 180
B287	Nov 2012	BATS	80-100; 130; 55; 27; 54	180; 120; 180; 180; 180
B292	Apr 2013	BATS	175; 70; 21	180; 120; 140
B295	Jul 2013	BATS	5-10; 10; 50; 100; 150	180; 180; 180; 180; 180
B299	Nov 2013	BATS	150-175; 100; 40	185; 180; 180

* Hydro Station S (32°10'N, 64°34'W)
** BATS site (31°40'N, 64°10'W)

Table S2.2: Contributors to foraminifer δ^{15}N variability in (a) tissue, and (b) shell-bound N, for each species and overall. Variability between measurements within a tow, variability between tows on the same cruise, and variability between cruises are compared using their standard deviations (where n is number of contributing data points).

(a) TISSUE δ^{15}N	variability among measurements within a tow		variability among tows in a cruise		variability among different cruises	
species	pooled measurement standard deviation	n	pooled tow standard deviation	n	cruise standard deviation	n
O. universa	0.64	15	0.56	7	0.80	9
G. ruber	0.61	17	0.48	8	0.73	10
G. sacculifer	0.39	5	0.93	3	1.09	6
P. obliquiloculata	0.27	6	0.73	3	1.29	5
N. dutertrei	0.37	6	1.19	4	1.13	7
G. siphonifera	0.76	13	0.94	6	0.91	8
G. inflata	0.20	5	0.54	3	0.90	5
G. truncatulinoides	0.23	6	0.50	4	0.70	8
G. conglobatus	(0.09)	1	--	0	0.74	2
G. menardii	(0.87)	1	(0.44)	1	0.57	6
G. hirsuta	0.31	11	0.28	3	0.67	5
G. glutinata	0.16	2	(0.48)	1	0.60	3
H. pelagica	0.82	3	1.11	3	1.43	7
G. bulloides	0.36	2	0.38	2	0.29	4
G. falconensis	1.47	2	1.85	2	2.10	3
G. hexagonus	--	0	(0.28)	1	3.35	3
G. ruber, white	1.00	2	1.21	3	0.83	5
Overall (pooled)	**0.57**	14	**0.82**	13	**1.09**	17

(b) SHELL δ^{15}N	variability among measurements within a tow		variability among tows in a cruise		variability among different cruises	
species	pooled measurement standard deviation	n	pooled tow standard deviation	n	cruise standard deviation	n
O. universa	0.36	2	(0.41)	1	1.69	5
G. ruber	--	0	--	0	1.27	7
G. sacculifer	--	0	--	0	1.03	3
P. obliquiloculata	(0.53)	1	(0.28)	1	--	1
N. dutertrei	--	0	(0.99)	1	2.38	3
G. siphonifera	--	0	--	0	1.06	3
G. inflata	--	0	(1.22)	1	1.42	2
G. truncatulinoides	(0.28)	1	(0.10)	1	0.71	3
G. conglobatus	--	0	--	0	--	0
G. menardii	--	0	(0.31)	1	0.46	2
G. hirsuta	0.65	4	0.28	2	0.47	3
G. glutinata	--	0	--	0	--	0
H. pelagica	--	0	--	0	--	1
G. bulloides	--	0	--	0	--	1
G. falconensis	--	0	--	0	0.06	2
G. hexagonus	--	0	--	0	--	1
G. ruber, white	--	0	--	0	--	0
Overall (pooled)	**0.59**	2	**(0.28)**	1	**1.33**	10

Table S2.3: Significance testing. Results of two-sample, unequal variances t-tests (Welch, 1947), showing the significance of δ^{15}N differences between species, seasons, and collection depth in tow-caught foraminifera.

		Tissue δ^{15}N				Shell δ^{15}N			
group 1	group 2	n1	n2	p-value	significant at 5% level?	n1	n2	p-value	significant at 5% level?
universa / ruber / sacculifer	truncatulinoides / hirsuta / inflata	165	112	2.9E-37	Y	27	21	9.9E-10	Y
spring	summer	214	122	7.9E-08	Y	32	4	0.01	Y
spring	fall	214	116	4.2E-10	Y	32	37	4.5E-07	Y
summer	fall	122	116	0.37	N	4	37	0.30	N
0-50 m	50-100 m	129	164	1.5E-04	Y	25	6	0.46	N
0-50 m	100-150 m	129	117	7.3E-07	Y	25	10	0.02	Y

8.3 Supplementary References

Fawcett S.E., Lomas M.W., Casey J.R., Ward B.B. and Sigman D.M. (2011). Assimilation of upwelled nitrate by small eukaryotes in the Sargasso Sea. *Nature Geoscience*, **4**, 717–722.

Fawcett S.E., Lomas M.W., Ward B.B. and Sigman D.M. (2014). The counterintuitive effect of summer-to-fall mixed layer deepening on eukaryotic new production in the Sargasso Sea. *Global Biogeochemical Cycles*, **28**, 86–102.

Fawcett S.E., Ward B.B., Lomas M.W. and Sigman D.M. (2015). Vertical decoupling of nitrate assimilation and nitrification in the Sargasso Sea. *Deep-Sea Research I*, **103**, 64–72.

CHAPTER 3: Ground-truthing the planktic foraminifer-bound nitrogen isotope paleo-proxy in the Southern Ocean

Sandi M. Smart[1,2]*, Sarah E. Fawcett[3], Haojia Ren[4], Ralf Schiebel[2], Alfredo Martínez-García[2], Luca Stirnimann[3], Alakendra Roychoudhury[1], Gerald H. Haug[2], Daniel M. Sigman[5]

[1] Department of Earth Sciences, Stellenbosch University, Private Bag X1, Matieland, 7602, South Africa (*correspondence: sandi.smart@alumni.uct.ac.za)

[2] Climate Geochemistry Department, Max Planck Institute for Chemistry, 55128 Mainz, Germany

[3] Department of Oceanography, University of Cape Town, Rondebosch, 7700, South Africa

[4] Department of Geosciences, National Taiwan University, Taipei 106, Taiwan

[5] Department of Geosciences, Princeton University, Princeton, NJ 08544, USA

Presentation of an accepted research paper

This paper was submitted to the research journal *Geochemistry, Geophysics, Geosystems* in May 2019, and accepted for publication in January 2020 with the revised title: "The nitrogen isotopic composition of tissue and shell-bound organic matter of planktic foraminifera in Southern Ocean surface waters". I was personally responsible for sample collection, laboratory work, data analysis and interpretation, as well as writing the first draft of the manuscript. D.M. Sigman and S.E. Fawcett contributed to the data interpretation and revision of the manuscript. L. Stirnimann made bulk particle and zooplankton isotope measurements. The remaining co-authors provided resources, sampling and/or laboratory support and gave feedback on the text.

Key Points

1. Foraminifer $\delta^{15}N$ tracks bulk particulate organic N (rather than nitrate) $\delta^{15}N$ in the Southern Ocean mixed layer on a seasonal basis.

2. Particulate N $\delta^{15}N$ records early-summer nitrate consumption, late-summer ammonium recycling and winter decomposition.

3. With today's seasonality, late summer is estimated to outweigh winter in its effect on the $\delta^{15}N$ of foraminifera accumulated on the seabed.

ABSTRACT

We present the first nitrogen isotope ($\delta^{15}N$) measurements of planktic foraminifera, paleoceanographically important zooplankton, from the nutrient-rich waters of the modern Southern Ocean. Foraminifera were collected from net tows in the Subantarctic and Polar Frontal Zones (SAZ and PFZ, respectively) south of Africa during winter 2015 and late summer 2016. In late summer, consistent with preferential uptake of ^{14}N-nitrate and the progressive, northward depletion of nitrate by phytoplankton across the Southern Ocean, foraminifer tissue and shell-bound $\delta^{15}N$ of most foraminifera species rises equatorward along with nitrate $\delta^{15}N$. However, foraminifer $\delta^{15}N$ is ~3‰ lower than expected for heterotrophs relying on photosynthetic biomass generated directly from nitrate. This discrepancy appears to originate with the particulate organic N (PON) in late-summer surface waters, the $\delta^{15}N$ of which is lowered by ammonium recycling. In winter, when overall productivity and foraminifer production are reduced, foraminifer $\delta^{15}N$ is higher (by 4.4‰ for tissue and by 3.4‰ for shell-bound N compared to late summer) and exhibits no clear north-south trend. These characteristics can also be explained by the feeding-driven connection of foraminifera to PON, which is elevated in $\delta^{15}N$ by net degradation in winter. Combining our isotope data with previously reported sediment trap fluxes from the western Pacific SAZ/PFZ suggests that, under modern conditions, the late-summer ammonium recycling signal outweighs that of wintertime decomposition on the annually integrated $\delta^{15}N$ of sinking foraminifera.

95

Plain Language Summary

Shells of foraminifera, single-celled zooplankton, record information about their surroundings, making their fossils a useful tool for investigating past ocean conditions. Paleoceanographers have begun to use the ratio of heavy-to-light-nitrogen isotopes in fossil foraminifer shells as a measure of past biological nitrate consumption in the Southern Ocean. But the link between living foraminifera and nitrate consumption has only been tested in the subtropics, where surface nitrate is fully consumed by phytoplankton. In today's polar ocean, surface nitrate is only partly consumed, and mostly during the productive spring/summer. Our goal was to check whether living foraminifera record the composition of nitrate consumed in Southern Ocean surface waters. We collected living foraminifera from the region south of Africa during winter and late summer, using a net towed by the ship. We found that, during these (less productive) seasons, the nitrogen in foraminifer shells and tissues tracks the foraminifer's particulate nitrogen food. While nitrate and particulate nitrogen in surface waters are closely linked during spring/summer, the two can diverge because of nitrogen recycling in late summer and winter. Therefore, when interpreting foraminifer-bound nitrogen paleo-records, we must consider the effects of these "off-peak" seasons, as their influence may have been greater in the past.

1. Introduction

The Southern Ocean is the world's largest surface-ocean reservoir of unused nitrate, a major nutrient for phytoplankton, and it has the capacity for far greater productivity and carbon sequestration than occurs today (Knox & McElroy, 1984; Sarmiento & Toggweiler, 1984; Siegenthaler & Wenk, 1984). One way to monitor the degree of nitrate (and, indirectly, carbon) drawdown by phytoplankton is through the use of nitrogen (N) isotopes. During its consumption by phytoplankton, nitrate containing the lighter ^{14}N isotope is preferentially consumed over ^{15}N-bearing nitrate, causing an increase in both reactant (nitrate) and product (particulate organic N, PON) δ^{15}N (where δ^{15}N = $\{[(^{15}N/^{14}N)_{sample}/(^{15}N/^{14}N)_{N2\ in\ air}] - 1\} \times 1000$; in units of per mil, ‰) (Wada & Hattori, 1978; Pennock et al., 1996; Waser et al., 1998; Sigman et al., 1999a). In theory, this relationship could be used to infer past changes in surface-ocean nitrate drawdown from the δ^{15}N of PON buried in seafloor sediments (François et al., 1992; Altabet & François, 1994). However, bulk PON is poorly preserved in Southern Ocean sediments, compromising its use for paleo-δ^{15}N reconstructions (Altabet & François, 1994).

96

Microfossil-bound organic matter offers an alternative, physically protected pool of organic matter for $\delta^{15}N$ analysis. In the Antarctic Zone (AZ), south of the Polar Front (PF), the silica frustules of diatoms (single-celled algae) have been used for this purpose (Sigman et al., 1999b; Robinson et al., 2004; Studer et al., 2015; Studer et al., 2018). In more northern latitudes of the Southern Ocean, which are the focus of our study, a promising microfossil candidate is the planktic foraminifer, a single-celled zooplankton with a calcium carbonate shell or 'test'. Foraminifera use N-rich proteins to construct new chambers, which are added periodically to the shell during its lifetime (ranging from two weeks to one year, depending on the species) (King & Hare, 1972; Bé et al., 1979; Spero, 1988; Hemleben et al., 1989). Additional calcite added either actively during development (ontogenesis) and reproduction (gametogenesis), or passively during burial (i.e., post-mortem encrustation) (Bé & Hemleben, 1970; Hemleben et al., 1985) can further protect this shell-bound organic matter from bacterial decomposition.

Planktic foraminifera do not migrate diurnally (Siccha et al., 2012; Schiebel & Hemleben, 2017; Meilland et al., 2019), but many species may undertake large depth changes during a specific stage of life (e.g., for reproduction; Hemleben et al., 1985; Schiebel, 2002; Schiebel & Hemleben, 2017). The diet of planktic foraminifera varies between species. In laboratory feeding experiments, most spinose species (e.g., *Orbulina universa, Trilobatus sacculifer*) readily accept zooplankton prey like copepods and sometimes also larger phytoplankton like diatoms, while most non-spinose species (e.g., *Globorotalia truncatulinoides, Globorotalia inflata, Globorotalia hirsuta*) appear to prefer algal prey and/or detrital organic matter (Anderson et al., 1979; Spindler et al., 1984). Bacterial food sources might be important for some species, including the spinose *Globigerina bulloides* (Bird et al., 2017) and the non-spinose *Neogloboquadrina incompta* (Bird et al., 2018).

In low-to-mid-latitude oceans, many spinose, shallow-dwelling species (e.g., *O. universa, T. sacculifer, Globigerinoides ruber*) are known to host intracellular dinoflagellate symbionts (e.g., Bé et al., 1977; Spero, 1987; and references therein). These symbionts photosynthesize and fix organic N (probably mostly from the host's metabolic ammonium), which is then available to the foraminifer for biosynthesis (Uhle et al., 1999), supplementing that obtained from its largely-carnivorous diet (Anderson et al., 1979; Spindler et al., 1984). These dinoflagellate-bearing foraminifera appear to depend on their photosymbionts for survival (i.e., "obligatory" symbiosis; Hemleben et al., 1989), such that they are functionally mixotrophic rather than heterotrophic (Stoecker et al., 2009; Stoecker et al., 2017). Some of these

97

(sub)tropical foraminifer species (e.g., *O. universa*) also occur in the Subantarctic Zone (SAZ; between the Subantarctic Front, SAF, and the Subtropical Front, STF) (King & Howard, 2003; Mortyn & Charles, 2003). In the Polar Frontal Zone (PFZ; between the PF and the SAF), elevated foraminiferal abundances (of *G. bulloides*, in particular) have been observed at the depth of the sub-surface chlorophyll maximum (Mortyn & Charles, 2003). Unlike the (sub)tropical spinose species discussed above, *G. bulloides* and *Turborotalita quinqueloba quinqueloba* (temperate/subpolar and polar/subpolar species, respectively, and both spinose) have not been reported to host dinoflagellate endosymbionts (Gastrich, 1987; Hemleben et al., 1989; Schiebel & Hemleben, 2017) or to contain functional (i.e., non-food derived) chlorophyll (Takagi et al., 2019). While associations of *G. bulloides* with cyanobacterial endobionts (Bird et al., 2017) and free-swimming dinoflagellates (Spero & Angel, 1991) have been documented, it is not yet clear how pervasive these relationships are. Several intermediate depth-dwellers (including *G. inflata*, *Globigerinita glutinata* and *G. hirsuta*) are suspected to host chrysophyte symbionts, while the deepest-dwelling planktic foraminifer (*G. truncatulinoides*) and native polar/subpolar species (*Neogloboquadrina pachyderma* and *Neogloboquadrina incompta*) appear to be symbiont-barren (Gastrich, 1987; Faber et al., 1988; Bird et al., 2018; Takagi et al., 2019). In terms of $\delta^{15}N$, a clear distinction has been observed between species that host dinoflagellate endosymbionts and those that do not; the former group has a significantly lower $\delta^{15}N$, explained as deriving from the recycling of low-$\delta^{15}N$, metabolic ammonium from the host (Ren et al., 2012; Smart et al., 2018).

In the tropical and subtropical oceans, spatial variations in the shell-bound $\delta^{15}N$ of recently deposited foraminifera appear to track the $\delta^{15}N$ of the thermocline nitrate supplied annually to overlying surface waters (Ren et al., 2009; Ren et al., 2012). This is consistent with the complete or near-complete consumption of nitrate in the modern euphotic zone of these regions on an annual basis (Altabet, 1988; François et al., 1992). On shorter (i.e., seasonal) timescales, however, the $\delta^{15}N$ of bulk tissue (i.e., the non-calcified biomass of living foraminifera caught in surface net tows) and sinking shells (intercepted by sediment traps) also reflects changes in upper ocean N recycling (Smart et al., 2018). In the Southern Ocean, nitrate supplied to the mixed layer is not fully consumed by phytoplankton, so we expect the degree of nitrate consumption to represent a major influence on the $\delta^{15}N$ of the biomass produced in surface waters and thus to also affect foraminifer $\delta^{15}N$. In addition to the degree of nitrate consumption by phytoplankton, the $\delta^{15}N$ of nitrate in the mixed layer depends on the $\delta^{15}N$ of the nitrate

98

supply and the isotope effect of nitrate assimilation (Altabet & François, 1994; Sigman et al., 1999a). Based on these expectations, a foraminifer-bound $\delta^{15}N$ record from the SAZ has been generated to reconstruct nitrate consumptions through the last glacial cycle (Martínez-García et al., 2014), but the link between foraminifer $\delta^{15}N$ and nitrate $\delta^{15}N$ has not yet been demonstrated in the modern Southern Ocean.

Here, through $\delta^{15}N$ measurements of foraminifera (tissue and shells), nitrate and various particulate N forms, we seek to determine whether upper ocean-dwelling foraminifera in the modern PFZ and SAZ track the $\delta^{15}N$ of the nitrate and thus the degree of nitrate consumption. We find that foraminifer $\delta^{15}N$ is tied to the $\delta^{15}N$ of PON in the mixed layer, a predictable result given that foraminifera are known to feed on this material. The $\delta^{15}N$ of PON is largely controlled by nitrate consumption in the early and mid-summer (Lourey et al., 2003), but we confirm previous findings that ammonium cycling and decomposition cause significant overprints on PON $\delta^{15}N$ in late summer and winter, respectively (Altabet & François, 2001; Lourey et al., 2003). These overprints are also recorded in foraminifer $\delta^{15}N$, causing them to deviate from recording nitrate consumption alone during the low-flux late-summer and winter periods. We provide an initial exploration of the significance of these findings for the foraminifer-bound $\delta^{15}N$ proxy in the Southern Ocean.

2. Methods

2.1 Sample collection at sea

Planktic foraminifera were collected from the Southern Ocean using a double 1-m^2-opening, 200-µm-mesh plankton net in Jul-Aug (winter) 2015 (Atlantic sector, between South Africa and the Antarctic sea-ice edge at 56.4°S, 0.3°E; Fig. 3.1a) and in Apr-May (late summer) 2016 (Indian sector, between South Africa and Marion Island at 46.9°S, 37.7°E; Fig. 3.1b) aboard the R/V *S.A. Agulhas II* (VOY016 and VOY019, respectively). The positions of the major Southern Ocean fronts were determined from expendable bathythermograph temperature and salinity profiles (using the criteria of Belkin & Gordon (1996) and Holliday & Read (1998)) in winter 2015. On the late-summer 2016 voyage, the fronts were identified from gradients in continuous surface temperature and salinity (underway thermosalinograph) measurements and altimetry (Aviso Absolute Dynamic Topography; https://www.aviso.altimetry.fr). Before net

99

deployment, hydrographic profile data and seawater nitrate samples were collected from a Niskin bottle rosette mounted with Sea-Bird conductivity-temperature-depth (CTD) and florescence sensors. Mixed layer depth (MLD) was defined as the minimum depth at which potential density ($\sigma\theta$, calculated from temperature and salinity profiles) increased by ≥ 0.03 kg.m^{-3} from a reference depth of 11 m, the shallowest depth common to all CTD stations (de Boyer Montégut et al., 2004).
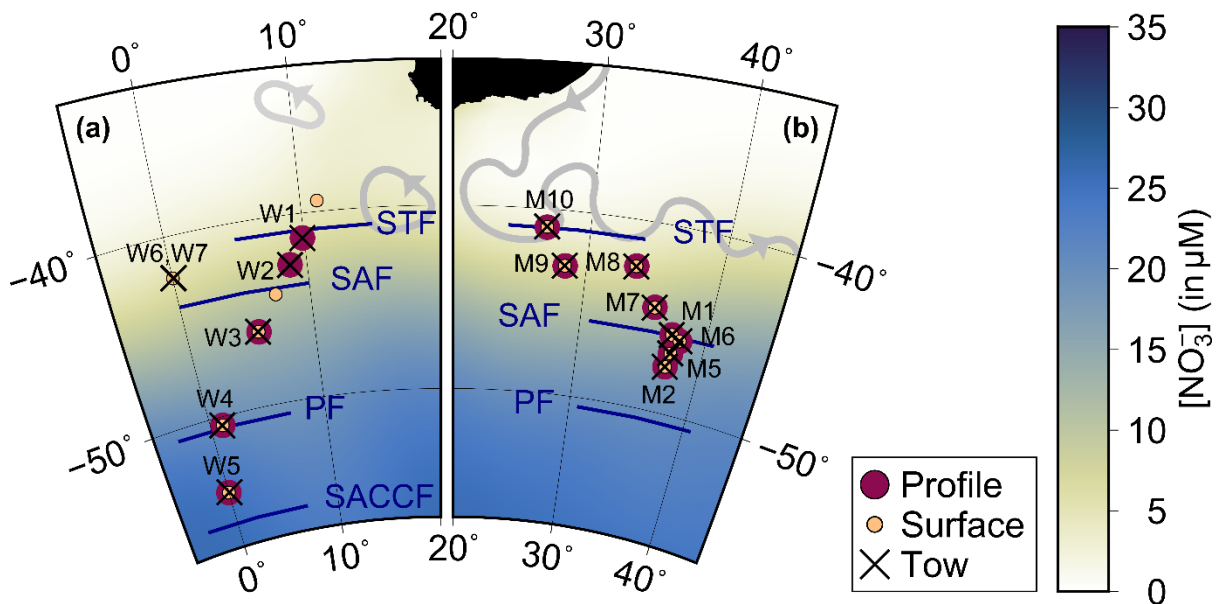
Fig. 3.1: Southern Ocean sampling locations. Cruise tracks of the R/V *S.A. Agulhas II* during (a) winter 2015 along the Good Hope Line (0°E) and (b) late summer 2016 to Marion Island (46.9°S, 37.7°E). Each net tow is marked by a black 'x' and named by cruise ('W' for winter, 'M' for Marion) and tow number. Stations sampled for seawater nitrate and particulate organic N are indicated by filled circles (underway surface stations in orange and depth profile stations in maroon). Each cruise track is overlaid on its monthly climatology (July and April, respectively) of surface nitrate concentration (in µM; colour shading) from World Ocean Atlas 2013 (Garcia et al., 2014; online at https://www.nodc.noaa.gov/OC5/woa13/). The relevant oceanic fronts at the time of sampling are indicated (STF: Subtropical Front, SAF: Subantarctic Front, PF: Polar Front, and SACCF: Southern Antarctic Circumpolar Current Front). Thick grey lines show the approximate circulation of the Agulhas Current (western boundary of the south Indian Ocean), Agulhas Retroflection (eastward return flow) and rings (warm-core eddies shed into the southeast Atlantic) based on altimetry at the time of each cruise. This figure was created using GMT (Wessel et al., 2013).

Each net tow lasted approximately 90 min, with the net towed at 1-1.5 kn at a depth between 25 m and 90 m (see Table S3.1 for details), targeting the chlorophyll maximum (or the middle of the mixed layer if no single peak was present in the fluorescence profile). Once retrieved,

approximately 90% of the foraminifer-containing tow material was preserved in a 5–10% formalin-seawater solution (pH-buffered with sodium borate) and kept at 4°C until processing (following Ren et al., 2012). The remaining 10% was sieved (through 5000-, 2000-, 1000-, 500-, 250- and 150-µm-mesh sieves), filtered (onto pre-combusted 0.7-µm-pore-size GF/Fs) and frozen at −20°C for elemental and isotopic analysis of size-fractionated PON. For the duration of the tow, seawater from the ship's underway intake (at ~7 m depth) was filtered through a pre-combusted 0.3-µm-pore-size GF/F for collecting bulk PON and filtered nitrate from surface waters. GF/Fs were frozen at −80°C and all nitrate samples (from profile and underway collections) were frozen at −20°C until analysis. Additional bulk PON samples from the region (35°S-57°S and 0°E-42°E) come from underway surface and CTD profile collections in Jul-Aug (winter) 2012 (VOY03; R/V *S.A. Agulhas II*), Feb-Mar (late summer) 2013 (SOSCEx I; R/V *S.A. Agulhas I*), Dec-Mar (midsummer) 2016/2017 (ACE; R/V *Akademik Treshnikov*), and Jun-Jul (winter) 2017 (VOY025; R/V *S.A. Agulhas II*).

2.2 Foraminifer sample preparation, cleaning and oxidation

Foraminifera were separated from bulk formalin-preserved tow material by sieving (using a 500- or 1000-µm-mesh sieve and rinsing with deionized water), density separation (addition of a 200 g/L sodium chloride solution), decanting into petri dishes, and allowing the diluted formalin solution to evaporate in a fume hood (adapted from Smart et al., 2018). For some tows, an additional separation step was needed; dried material was resuspended (in tap water, adjusted to pH ~8 using 2-3 drops of 1 N sodium hydroxide) and gently disaggregated in a recrystallizing dish, swirled and allowed to settle. Foraminifera and other dense particles, which accumulate at the centre, could be pipetted off under a microscope and transferred to a clean petri dish to dry at room temperature. This swirl-and-pipette step was repeated until no more foraminifera were visible at the centre of the dish. Nine different species were identified and picked from the dried material in the petri dishes under a microscope using a wet picking brush. Depending on their abundance, size and estimated N content (based on preceding measurements), specimens were earmarked for tissue (typically 1-50 individuals) and/or shell-bound (typically 50-150 individuals) N isotope analysis, and if possible, sorted into size fractions using a microscope reticle.

Subsequent laboratory work was undertaken during three different sessions: in 2016, 2017 (at Princeton University, USA) and 2018 (at the Max Planck Institute for Chemistry (MPIC), Germany). During each session, different protocols were tested for the processing (i.e., rinsing,

transferring and crushing) and oxidation (conversion from organic N to nitrate) of "tissue" samples (i.e., foraminifer shells with cytoplasm). Each protocol is described in detail in the supporting information (Text S1). While the resulting $\delta^{15}N$ values were similar between protocols, the 2017 protocol was found to be the least reliable, yielding the largest standard deviations (for replicate oxidations) and the largest number of incomplete ("failed") oxidations (all of which have been excluded). Below we describe the 2018 protocol, which was the most successful (yielding the smallest standard deviations and no "failed" oxidations).

"Tissue" specimens were transferred to a 4 mL pre-combusted Wheaton vial and briefly rinsed with Milli-Q (Ren et al., 2012) inside the vial to loosen detritus and dilute any residual nitrate or formalin. After pipetting off the supernatant liquid under a microscope, samples were dried in a dessicator (with silica gel) for 10-16 h. Once dry, specimens were crushed open with an ethanol-cleaned spatula to expose the foraminiferal tissue for oxidation. This (non-shell-bound) organic N was converted to nitrate by a 1 mL addition of a basic persulfate oxidizing reagent (POR; 1 g potassium persulfate and 0.7 g sodium hydroxide dissolved in 100 mL Milli-Q) and autoclaving on a slow vent setting for 65 min (Nydahl, 1978; Knapp et al., 2005). Blanks (containing POR only) and standards (containing POR plus an amino acid reference material) were included in every batch to correct for the POR-associated N blank and to ensure complete oxidation. At the MPIC, USGS-40 and USGS-41 were used as references (Qi et al., 2003). Analyses carried out at Princeton included (in addition to USGS-40 and/or USGS-41) an in-house mixed alanine-glycine (AG) amino acid standard calibrated by analysis with elemental analyzer-isotope ratio mass spectrometry.

"Shell" specimens were cleaned using the same persulfate oxidation method described above (Nydahl, 1978; Knapp et al., 2005), but scaling up the POR recipe (to 2 g potassium persulfate and 2 g sodium hydroxide in 100 mL Milli-Q) and volume addition (to 3 mL) to match the larger number of individuals. After removing the high-nitrate supernatant (from oxidation of the tissue fraction), the crushed shell material was rinsed six times with Milli-Q and oven dried at 50°C. Shell-bound N was released by dissolution of calcite with a 50 µL addition of 4 N hydrochloric acid (HCl), and oxidized to nitrate by a 1 mL addition of POR (in this case, 0.7 g potassium persulfate and 1 g sodium hydroxide dissolved in 100 mL Milli-Q; a more basic recipe to compensate for the HCl addition). Where possible, additional shell-bound N measurements were obtained by combining the POR-cleaned shell material (from the same species and tow, or occasionally neighbouring tows) leftover from tissue oxidations.

Auxiliary data were obtained from morphometric analysis (using an Olympus SZX16 incident light microscope (planapochromatic), and an Olympus UC90 camera with a resolution of 1.32 x 1.32 µm per pixel) and weighing (using a Mettler Toledo XP6U comparator 7-digit microbalance). Due to the time required for these steps and the risks of contamination and sample loss (particularly for cleaned shell samples), these measurements were undertaken on only a selection of (mostly tissue) specimens (approximately 14% of all (n = 1039) samples measured).

2.3 N isotope analyses

All nitrate samples resulting from tissue and shell-bound N oxidation were adjusted to a pH of 5–7 using HCl and measured for nitrate concentration by chemiluminescence (Braman & Hendrix, 1989). Nitrate was quantitatively converted to nitrous oxide (N_2O) using the denitrifier method, followed gas chromatography–isotope ratio mass spectrometry (GC-IRMS; using a Thermo MAT 253 with online N_2O extraction and purification) (Sigman et al., 2001; Casciotti et al., 2002; Weigand et al., 2016). The $\delta^{15}N$ measurements were referenced to N_2 in air using nitrate reference materials USGS-34 and IAEA-NO3. Oxidized samples were corrected for the POR blank (on average, 2% and 5% of the total N in tissue and shell samples, respectively) using the measured $\delta^{15}N$ and N content of the blanks associated with each batch and calibrated using the amino acid standards. The pooled standard deviations (1σ) of all foraminifer tissue $\delta^{15}N$ and shell-bound $\delta^{15}N$ cleaning-and-oxidation replicates were 1.0‰ (n = 77) and 1.2‰ (n = 14), respectively, if the 2017 analyses are included or 0.5‰ (n = 47) and 0.8‰ (n = 6), respectively, when the 2017 analyses are excluded.

Seawater nitrate samples collected from the Niskin bottles and underway intake were treated with sulfamic acid to remove nitrite (Granger & Sigman, 2009). Nitrate and nitrate+nitrite concentrations were then measured by chemiluminescence (Braman & Hendrix, 1989), and the $\delta^{15}N$ of nitrate and nitrate+nitrite determined using the denitrifier method in conjunction with GC-IRMS (Sigman et al., 2001; Casciotti et al., 2002; Weigand et al., 2016) as described above. The pooled standard deviations (1σ) of seawater nitrate+nitrite $\delta^{15}N$ and nitrate-only $\delta^{15}N$ denitrifier replicates were 0.09‰ and 0.06‰, respectively. For brevity, we focus our attention on the nitrate+nitrite data, which is suggested to be the more "stable" pool (i.e., robust to potential nitrate-nitrite interconversion; Kemeny et al., 2016) and thus possibly a better reflection of the pool available for assimilation by phytoplankton in the Southern Ocean (Fripiat et al., 2019)). Regardless, our conclusions are unaffected by the choice of nitrate-only

or nitrate+nitrite. Bulk and size-fractionated PON samples were analysed for $\delta^{15}N$ by elemental analyser–isotope ratio mass spectrometry (Thermo Scientific FLASH 2000 elemental analyzer coupled to a Thermo Scientific Delta V Plus mass spectrometer) and referenced to atmospheric N_2 using three in-house organic standards (Choc, Merck Gel and Valine). The pooled standard deviation of replicate analyses was 0.3‰ for bulk and 0.9‰ for size-fractionated samples.

2.4 Additional estimations and assumptions

It should be noted that the number of foraminifer specimens picked may not accurately represent the abundance of foraminifera in the ocean. The heterogeneous nature of the tow-collected material (particularly the tendency of some specimens, often small and/or spinose ones, to clump together with algal material and/or detritus) hindered representative sub-sampling for exact species counts. However, all tow collections underwent the same sieving and density separation procedures and should, thus, be inter-comparable (i.e., all being subject to the same potential biases). We therefore do not rely on absolute abundances (i.e., number of individuals of a particular species or size fraction; Fig. 3.2a), but rather focus on the relative abundances (as a percentage of the total foraminifera picked; Fig. 3.2b).

In addition, we consider the first two sets of analyses (2016 and 2017) to more closely resemble the relative species and size proportions within the original tow collection, as foraminifera were picked at random before sorting by species and size. For the last set of analyses (2018), some tows and species were specifically targeted for reanalysis, and their inclusion in the abundance dataset (Fig. 3.2) would artificially elevate their contributions; we, therefore, exclude these from the abundance dataset. We do, however, draw on the detailed morphometric data obtained during the 2018 set of analyses (Fig. S3.1) to test the robustness of observations from the cruder size data (only 3 to 4 size fractions) obtained from visually separating specimens using a microscope reticle (i.e., the only size data available for the 2016 and 2017 analyses).

(a) # specimens picked

(b) % specimens picked

Legend:
bul mix, bul <250, bul >250, bul >350, glu mix, glu <150, glu 150-250, glu >250
hir <300, hir 300-500, hir>500, inc mix, inf mix, inf <250, inf 250-350, inf >350
pac mix, pac <150, pac 150-200, pac >200, qui mix, qui <150, qui 150-200, qui >200
tru mix, tru <250, tru 250-350, tru >350, uni mix, uni <250, uni 250-250, uni >350
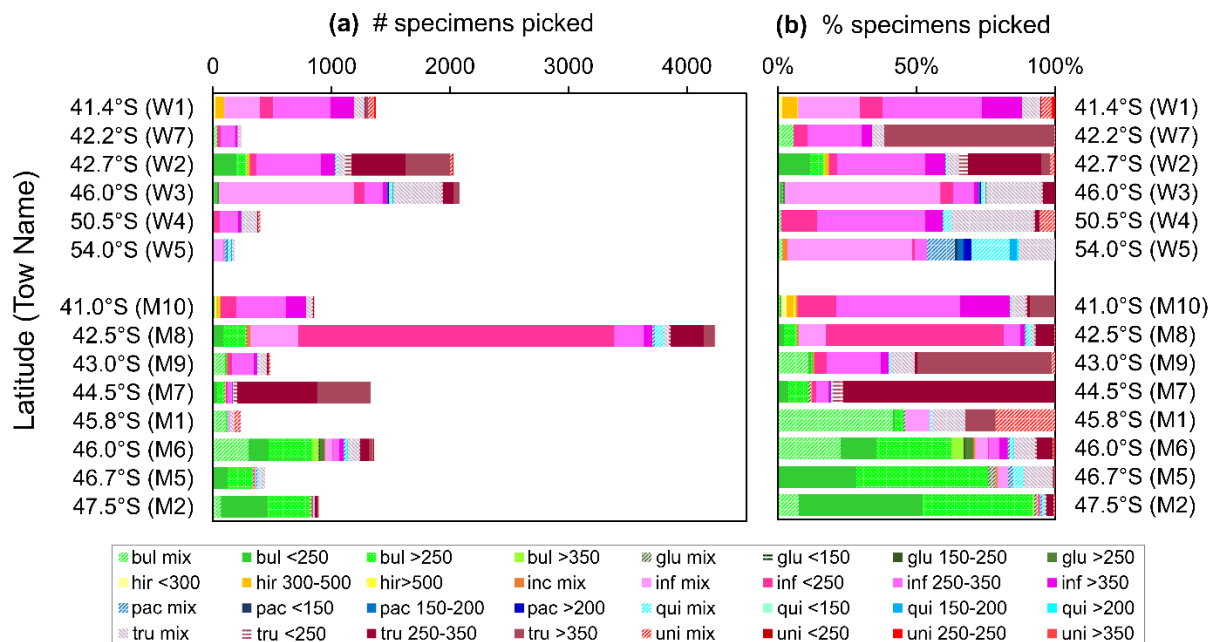
Fig. 3.2: Net tow species assemblages. The (a) absolute and (b) relative abundances of foraminifera specimens picked from net tow collections in winter 2015 (top set) and late summer 2016 (bottom set). Colours represent different foraminifer species (bul: *G. bulloides*, glu: *G. glutinata*, hir: *G. hirsuta*, inc: *N. incompta*, inf: *G. inflata*, 'pac': *N. pachyderma*, 'qui': *T. quinqueloba*, 'tru': *G. truncatulinoides*, 'uni': *O. universa*). Variations in hue and texture indicate different size fractions (as per the figure legend, in μm). Only the 2016 and 2017 analyses are shown here (as our most representative subset of the original collections) where size fractions were separated by eye using a microscope reticle. Morphometric measurements made during the 2018 analyses are shown in Fig. S3.1. The legend label "mix" indicates a sample of mixed specimen size, where there were not enough individuals for size-fractionated N measurements.

3. Results

3.1 Hydrographic and nitrate+nitrite conditions

During the winter 2015 voyage (Fig. 3.1a), the sub-surface core of the STF was located at 40.7°S with its surface expression between 39.7°S and 40.9°S. The SAF, the PF and the Southern Antarctic Circumpolar Current Front were located at 43.8°S, 50.6°S and 55.7°S, respectively. Along the late-summer 2016 transect (Fig. 3.1b), the core of the Agulhas Current was located at 36-38°S, and the Agulhas Retroflection was encountered at 38-41°S. The northern branch of the STF was near 41.0°S, while the southern branch was at around 41.5°S. The SAF was divided into northern (~42.5°S), middle (~45.8°S) and southern (~46.8°S) branches. The PF was located well south of Marion Island at ~50.5°S at the time of sampling. Mixed-layer depth was 110-147 m at the winter tow stations and between 92 m and 107 m in

late-summer at all but station M10 where it was shallower than 60 m. Comparing only the SAZ/PFZ stations (i.e., excluding the southernmost winter tow W5 and the northernmost summer tow M10), mixed layers were ~30 m deeper on average for the winter 2015 transect.
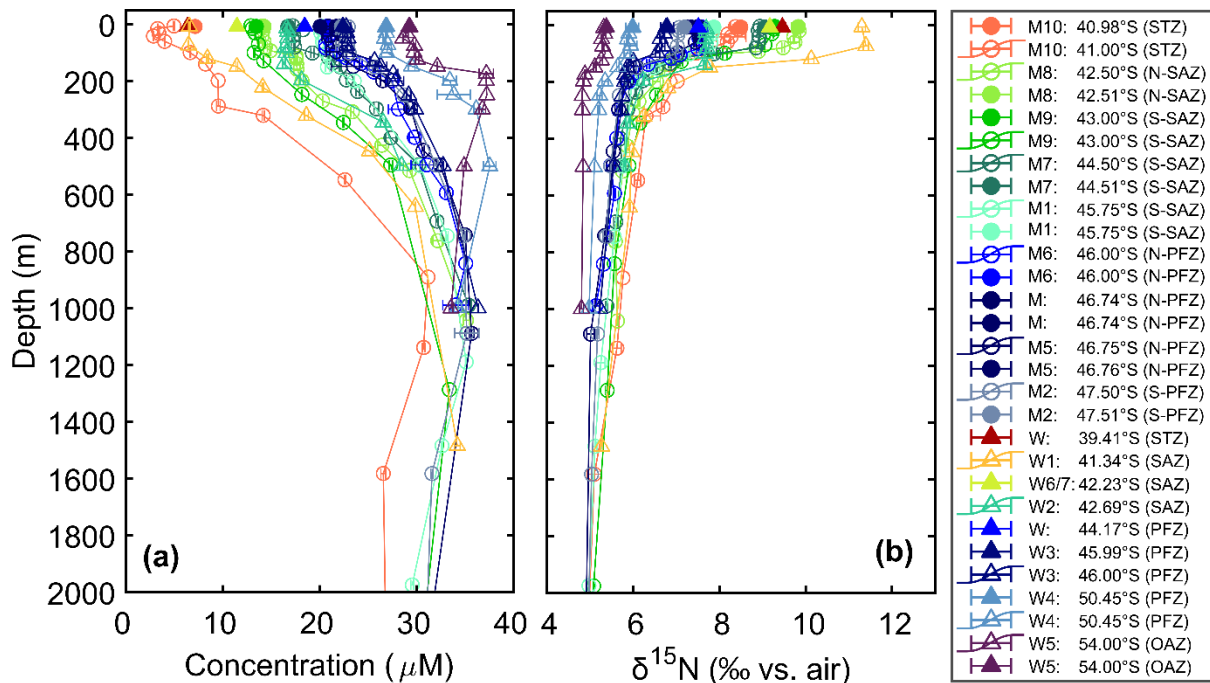
Fig. 3.3: Water-column nitrate+nitrite. Depth profiles (open symbols) and surface (filled symbols) measurements of nitrate+nitrite (a) concentration (in μM), and (b) $\delta^{15}N$ (in ‰ *vs.* N_2 in air), for the upper 2000 m from the winter (triangles) and late summer (circles) transects south of Africa. Data are coloured by latitude zone, with the Subtropical Zone (STZ) and Subtropical Front (STF) in warm colours, the Subantarctic Zone (SAZ) in greens, Polar Frontal Zone (PFZ) in blues and the Open Antarctic Zone (OAZ) in purple. Legend labels give the associated tow name where applicable (or cruise code (M or W) where no tow was performed), followed by the latitude and zone of the depth profile. Error bars indicate the measurement standard deviation (n ≥ 2). For a comparison with nitrate-only (i.e., when nitrite is removed), see Fig. S3.2 in the supporting information.

In the open AZ, nitrate-rich Upper Circumpolar Deep Water (UCDW) upwells year-round (due to Ekman divergence; Nowlin and Klinck, 1986) and references therein) through the base of the winter mixed layer (which underlies a shallower mixed layer during summer) and is incorporated into surface waters by the homogenization of the two (former summer and winter) mixed layers during wintertime cooling and mixed layer deepening (Toole, 1981; Sigman et al., 1999a). Both the PFZ and SAZ mixed layers are supplied laterally by equatorward Ekman transport (with nitrate from the adjacent polar mixed layer) and vertically by mixing with the

underlying thermocline (McCartney, 1977; Sigman et al., 1999a; DiFiore et al., 2006). From south to north along the winter transect, mixed-layer nitrate+nitrite concentrations (triangles in Fig. 3.3a) decrease from ~29 µM at the southernmost station in the Open Antarctic Zone, to 18-27 µM at the PFZ stations, to 6-17 µM in the SAZ, and remain between 6 µM and 7 µM north of the STF. Over the same area, nitrate+nitrite $\delta^{15}N$ (triangles in Fig. 3.3b) increases from ~5.4‰ in the Open Antarctic Zone to ~6.0-7.5‰ in the PFZ to 7.7-11.4‰ in the SAZ and then decreases to ~9.5‰ into the STZ. Along the late-summer transect, surface nitrate+nitrite concentrations (circles in Fig. 3.3a) decrease from 20-23 µM in the PFZ (the southernmost stations on the voyage), to 13-20 µM in the SAZ, to 5-7 µM just north of the STF in the Agulhas Retroflection. Over the same area, nitrate+nitrite $\delta^{15}N$ (circles in Fig. 3.3b) increases from ~7.0-7.5‰ in the PFZ to ~7.8-9.8‰ in the SAZ before decreasing to ~8.4‰ at the northernmost station. In both the winter and late summer profiles, the nitrate+nitrite concentration decreases upwards through the water column from the sub-surface maximum of UCDW (which shoals poleward from ~1100-1500 m in the SAZ to ~200 m in the Open Antarctic Zone, along the 1027.6 kg.m^{-3} isopycnal), and reaches minimum values within the surface mixed layer. This trend is qualitatively mirrored by nitrate+nitrite $\delta^{15}N$, which increases from deep to shallow, particularly through the thermocline (between ~100 m and 200 m). The magnitude of the deep-to-shallow changes in nitrate+nitrite concentration and $\delta^{15}N$ generally increases with decreasing latitude, except north of the STF. Nitrate-only concentration and $\delta^{15}N$ (from seawater samples with nitrite removed; dotted profiles in Fig. S3.2 in the supporting information) exhibit similar patterns to nitrate+nitrite (described above), but generally have higher $\delta^{15}N$ values (typically by ~0.3-1.0‰) in the mixed layer.

The average nitrate+nitrite concentration and $\delta^{15}N$ of UCDW (identified by its characteristic potential density (~1027.6 kg.m^{-3}) and low oxygen content (~3.7 mL/L); not shown) on the winter transect are 36.5±1.4 µM and 5.1±0.2‰ (n = 5), respectively, compared to 34.7±0.9 µM and 5.2±0.1‰ (n = 6) on the late-summer transect. Using only data from the core of the SAZ/PFZ yields a slightly different nitrate+nitrite concentration and $\delta^{15}N$ for winter UCDW (36.9±0.9 µM and 5.2±0.1‰ (n = 2), respectively), but makes no difference to the late-summer values. In either case, UCDW nitrate+nitrite is significantly different between transects in terms of concentration (p < 0.05), but not in terms of $\delta^{15}N$ (p > 0.05 based on a two-sample, equal variances t-test). AAIW is identified by pronounced sub-surface salinity minima (<34.3 psu) and weak local oxygen maxima (~5 mL/L) north of the SAF (not shown) and is roughly

bounded by the 1027.05 kg.m^{-3} and 1027.4 kg.m^{-3} isopycnals. The average nitrate+nitrite concentration and δ^{15}N of AAIW are 29.1±1.0 µM (n = 2) and 5.9±0.1‰ (n = 2), respectively, for the winter transect and 29.8±2.4 µM (n = 9) and 5.7±0.1‰ (n = 10), respectively, for the late-summer transect. Neither concentration nor δ^{15}N differences in AAIW between cruises are significant (p > 0.05). Directly beneath the SAZ mixed layer and above AAIW lies SAMW, identified by its high salinity (>34.3 psu) and relatively low oxygen content in a density range of approximately 1026.7-1027.05 kg.m^{-3}. The average nitrate+nitrite concentration and δ^{15}N of SAMW on the winter transect are 20.5±5.2 µM and 6.2±0.4‰ (n = 5), respectively, not significantly different from 21.6±2.6 µM and 6.3±0.3 (n = 12) on the late-summer transect (p >> 0.05). The average nitrate+nitrite concentration and δ^{15}N given here for UCDW, AAIW and SAMW are typically within 1-3 µM and 0.0-0.4‰, respectively, of those reported previously for the Atlantic (Smart et al., 2015), and Indo-Pacific Sectors (Sigman et al., 2000; Rafter et al., 2012; Rafter et al., 2013).

Combining data from the SAZ and PFZ stations only shows that the late-summer mixed layer (with n = 44 samples) has a lower nitrate+nitrite concentration (19.1±3.4 µM) and higher nitrate+nitrite δ^{15}N (8.1±0.9‰) than the winter mixed layer (20.0±6.5 µM and 7.3±1.6‰, respectively; with n = 18). The δ^{15}N difference is significant (p < 0.05), but the concentration difference is not (p > 0.05). Mixed-layer nitrate-only (dotted profiles in Fig. S3.2) at the same stations has higher δ^{15}N values than nitrate+nitrite (solid profiles in Fig. S3.2), by 0.4±0.2‰ (n = 18; p > 0.05, i.e., not significantly higher) for winter and by 0.8±0.1‰ (n = 44; p << 0.05, i.e., significantly higher) for late summer on average, implying low δ^{15}N values for mixed-layer nitrite of −10±11‰ (n = 18) and −34±25‰ (n = 36), respectively, based on mass balance calculations. The lowest mixed-layer nitrite δ^{15}N values are calculated for the late summer PFZ (−50±28‰; n = 15), significantly lower than for the winter PFZ (−7±6‰; n = 9). Within the SAZ, mixed-layer nitrite δ^{15}N is also lower in late summer (−22±15‰; n = 21) than in winter (−14±15‰; n = 8), although this difference is not significant.

3.2 Species and size distributions of foraminifera and other zooplankton

Based on microscope observations made ship-board, the smallest net tow size-fraction (<150 µm) consisted mostly of detritus, with very few smaller foraminifera. Foraminifera were most common in the 150-250 µm and 250-500 µm size fractions, which also contained small crustaceans (mostly amphipods, isopods and ostracods) and, in some tows, pteropods (pelagic sea snails). Intermediate size fractions (500-1000 µm and 1000-2000 µm) were dominated by

108

crustaceans (including krill, amphipods, copepods and ostracods), pteropods and fish larvae. The largest size fractions (2000-5000 µm and >5000 µm) were typically dominated by gelatinous species (including salps and chaetognaths), and/or larger crustaceans, with the occasional fish or fish larvae.

On average, late-summer tows yielded double the number of foraminifer specimens obtained from winter tows (Fig. 3.2a). Winter assemblages contain primarily *G. inflata* and *G. truncatulinoides* (averaging 60% and 20% of the total picked foraminifera, respectively), while late-summer assemblages are dominated by *G. bulloides*, *G. inflata* and/or *G. truncatulinoides* (averaging 40%, 30% and 20%, respectively) (Fig. 3.2a&b). Near the STF, the total abundance and species compositions of foraminifera are similar in winter (W1) and late summer (M10), with *G. inflata* contributing 80-90% and *G. hirsuta* contributing 6-8%. *O. universa* is present at low abundances (<3%) in most summertime collections and some winter tows, with peak abundances (24%) at station M1 (45.8°S) near the M-SAF. *G. glutinata* generally occurs in low numbers but appears more commonly in tows where *G. bulloides* dominates the assemblage. *N. incompta* is present in most summer and some winter tows, but typically makes up <2% of the total assemblage. *N. pachyderma* and *T. quinqueloba* are generally scarce, only contributing substantially (12% and 16%, respectively) to the total foraminifer assemblage in the southernmost winter tow, in the Open Antarctic Zone.

In general, most *G. bulloides* specimens collected in late-summer tows were large (>250 µm), while those collected during winter were in the 150-250 µm size range (Fig. 3.2 and Fig. S3.1a). *G. truncatulinoides* was particularly abundant at stations M7 (44.5°S; late summer) and W2 (42.7°S; winter) in the SAZ, making up around 90% and 50% of the total foraminifer assemblage, respectively. While the 250-350 µm size fraction dominates numerically in all tows where *G. truncatulinoides* are present (Fig. 3.2), the larger (>350 µm) size fraction contributes proportionally more to the total *G. truncatulinoides* assemblage in winter tows than in late-summer tows (e.g., compare W2/W3 with M6/M8; Fig. 3.2 and Fig. S3.1b). The abundance of foraminifera at station M8 (42.5°S, near the N-SAF; collected late summer) is notably high (Fig. 3.2a) and dominated by small (<250 µm) *G. inflata* (Fig. 3.2b). This contrasts with the 250-350-µm-dominated size distribution of *G. inflata* in every other tow collection.

3.3 $\delta^{15}N$ and N content of foraminifer tissue and shells

The $\delta^{15}N$ of foraminifer tissue is significantly higher (by 4.0‰) in the winter (5.3 ± 0.2‰; n = 59; all circles in Fig. 3.4a) than in the late summer (1.3±0.2‰; n = 94; all circles in Fig. 3.4b) tow collections (p << 0.05 based on a two-sample, equal variances t-test). The $\delta^{15}N$ of foraminifer shells (triangles in Fig. 3.4a&b) is more variable (within and among species), but generally shows the same tendencies described above for tissue $\delta^{15}N$. Shell-bound $\delta^{15}N$ is significantly higher (by 3.2‰; p < 0.05) in winter (5.2±1.0‰; n = 17) than in late summer (1.9±0.6‰; n = 24).   Undertaking the same comparison for SAZ/PFZ tows only (excluding tows near the STF (M10) and those south of the PF (W5), which fall in the shaded margins of Fig. 3.4), yields the same key results. The $\delta^{15}N$ of foraminifer tissue is significantly higher (by 4.4‰; Table 3.1) in the winter (5.4±0.2‰; n = 56) than in the late summer (1.0±0.2‰; n = 84) tow collections (p << 0.05 based on a two-sample, equal variances t-test). This late-summer-$vs.$-winter difference is significant (p < 0.05) in five of the seven species for which we have tissue data for both seasons (all except $N.$ $pachyderma$ and $T.$ $quinqueloba$, which have very few measurements). Late-summer tissue $\delta^{15}N$ exhibits a south-to-north increase by ~3.1‰ (Fig. 3.4b), while the winter trend shows the opposite: a ~2.9‰ decrease across the SAZ/PFZ (Fig. 3.4a). Excluding the 2017 analyses raises the winter and summer tissue $\delta^{15}N$ averages slightly to 6.1±0.3‰ (n = 28) and 1.5±0.3‰ (n = 35), respectively, but has little effect on the magnitude of late-summer-$vs.$-winter difference (4.6‰ instead of 4.4‰) or its significance (p << 0.05). The effect on latitudinal changes (from south to north) is to strengthen the late-summer trend (to a 4.3‰ rise) but weaken the winter trend (to a 2.4‰ decline) across the SAZ/PFZ. We explore these trends further in section 3.5 below. The $\delta^{15}N$ of foraminifer shells is still more variable than tissue (within and among species) in the SAZ/PFZ, but generally shows the same tendencies described for SAZ/PFZ tissue $\delta^{15}N$. Again, shell-bound $\delta^{15}N$ is significantly higher (by 3.4‰ (Table 3.1); p < 0.05) in winter (4.8±1.0‰; n = 16) than in late summer (1.4±0.6‰; n = 21). At the species level, the late-summer-$vs.$-winter difference is only significant (p < 0.05) for $G.$ $truncatulinoides$ (one of the five species with shell data for both seasons). Excluding the 2017 analyses raises the winter and summer shell $\delta^{15}N$ averages (to 7.0±0.3‰ (n = 5) and 3.3±1.0‰ (n = 6), respectively), thereby increasing the late-summer-$vs.$-winter difference (3.7‰ instead of 3.4‰), which remains significant (p < 0.05).

Table 3.1: Overview of tow-caught foraminifer tissue and shell-bound $\delta^{15}N$.

Note. $\delta^{15}N$ values are in ‰ *vs.* N_2 in air. Winter and late-summer averages (with n = number of oxidations) are shown in separate columns, and the simple $\delta^{15}N$ difference between the two seasons alongside.

| | Tissue $\delta^{15}N$ (‰) | | | | | | | Shell-bound $\delta^{15}N$ (‰) | | | | | | |
| | LATE SUMMER | | | WINTER | | | winter minus late summer | LATE SUMMER | | | WINTER | | | winter minus late summer |
Species	avg	std err	n	avg	std err	n	diff	avg	std err	n	avg	std err	n	diff
G. bulloides	**0.8**	0.2	25	**3.3**	0.8	5	2.6	**0.3**	0.9	10	**-1.1**	-	1	-1.4
G. inflata	**2.5**	0.4	22	**5.9**	0.3	22	3.4	**2.9**	1.1	6	**4.3**	1.5	9	1.4
G. truncatulinoides	**1.1**	0.2	19	**5.9**	0.6	13	4.8	**2.9**	0.6	4	**6.5**	1.2	5	3.6
O. universa	**-0.8**	0.8	5	**4.3**	1.1	5	5.1	**-**	-	0	**-**	-	0	-
G. hirsuta	**-**	-	0	**5.6**	0.2	7	-	**-**	-	0	**7.1**	-	1	-
G. glutinata	**-0.7**	0.6	6	**7.4**	-	1	8.1	**-3.2**	-	1	**-**	-	0	-
N. incompta	**-0.2**	1.3	2	**-**	-	0	-	**-**	-	0	**-**	-	0	-
T. quinqueloba	**-1.1**	2.2	3	**3.0**	0.9	2	4.1	**-**	-	0	**-**	-	0	-
N. pachyderma	**0.7**	1.1	2	**6.0**	-	1	5.3	**-**	-	0	**-**	-	0	-
ALL	**1.0**	0.2	84	**5.4**	0.2	56	**4.4**	**1.4**	0.6	21	**4.8**	1.0	16	**3.4**
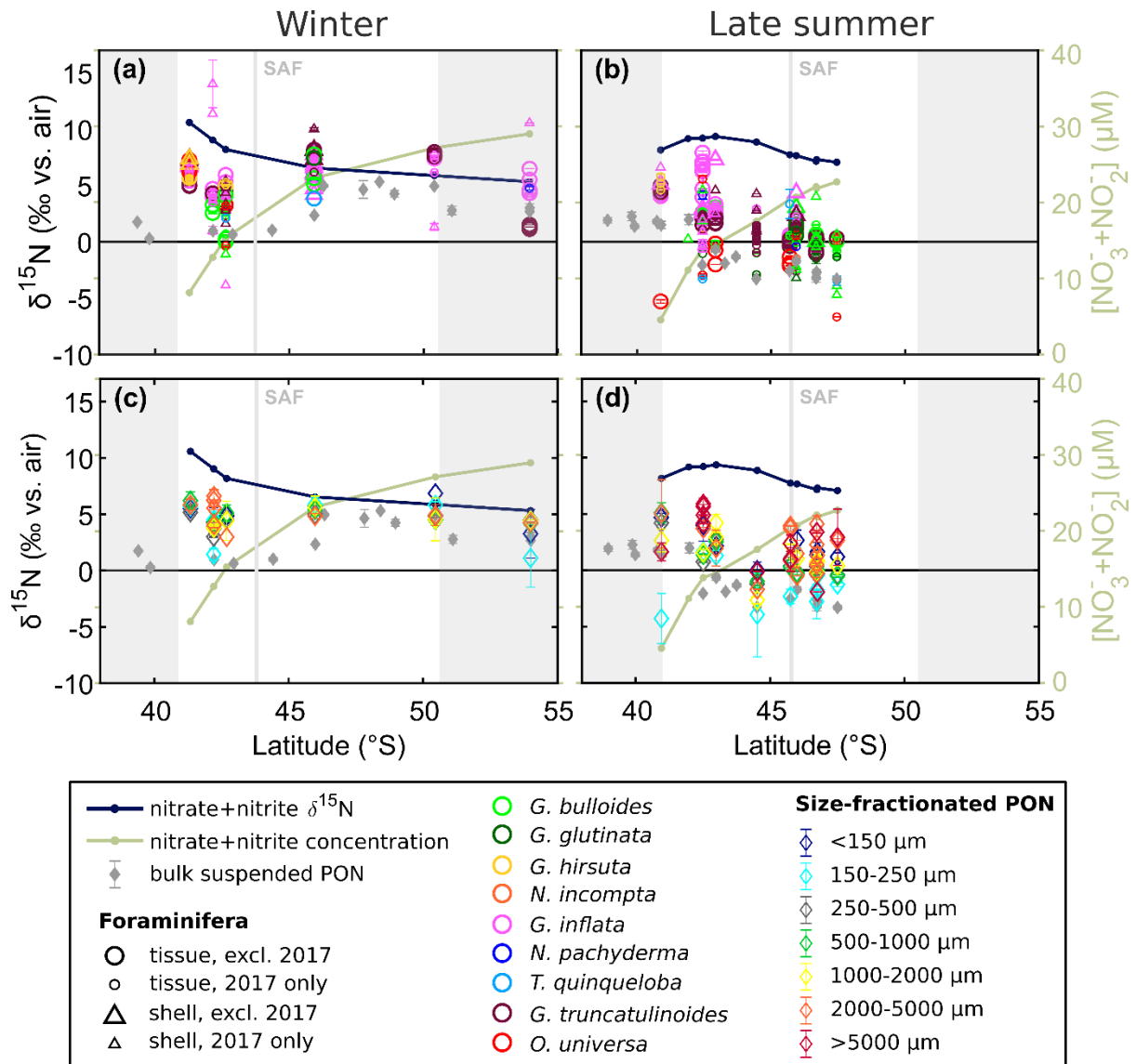
Fig. 3.4: Foraminifer, particulate N and nitrate+nitrite transects. Upper panels show transects of foraminifer tissue (circles) and shell (triangles) $\delta^{15}N$ from mixed-layer net tow collections during (a) winter and (b) late summer, where each colour represents a different foraminifer species. The 2017 analyses are denoted by small symbols (circles and triangles), for comparison with the rest (large symbols, where 2017 analyses are excluded from sample averages). Lower panels show transects of size-fractionated PON $\delta^{15}N$ (open, colour diamonds) from the same net tows, during (c) winter and (d) late summer, where each colour represents a different size fraction (from <150 μm to >5000 μm). In all panels, in situ (i.e., tow-depth) nitrate+nitrite concentration (light green line; secondary y-axis) and $\delta^{15}N$ (dark blue line; primary y-axis) are shown, as well as surface-water bulk (>0.7 µm) suspended PON $\delta^{15}N$ (filled, grey diamonds). Light grey shaded areas fall outside of the core PFZ/SAZ (the focus of this study), and the vertical grey line denotes the latitude of the Subantarctic Front (SAF), which divides the PFZ from the SAZ. Error bars indicate the standard deviation of replicate isotope measurements (typically n = 2-3).

112

Overall, there is a strong ($R^2 = 0.6$) and significant ($p \ll 0.05$) positive relationship between foraminifer tissue and shell-bound $\delta^{15}N$ with a slope of 1.0 (dashed black line in Fig. 3.5), based on all available data pairs (n = 33; i.e., where tissue and shell measurements were made of the same species, from the same net tow, but not necessarily of the same individuals). The three species with sufficient data for comparison have positive regression slopes (between 0.4 and 0.9), but the relationship is only significant for *G. truncatulinoides* (with $p \ll 0.05$ and $R^2 = 0.95$; n = 9). The intermediate-dwelling *G. bulloides* (and possibly *G. glutinata*) cluster at lower $\delta^{15}N$ (typically <2‰), while deeper-dwelling *G. inflata*, *G. truncatulinoides* and *G. hirsuta* span a higher $\delta^{15}N$ range (typically >2‰). Using all data pairs from both transects, the average $\delta^{15}N$ of foraminifera is 3.8±0.4‰ for tissue and 3.8±0.6‰ for shells (n = 33).
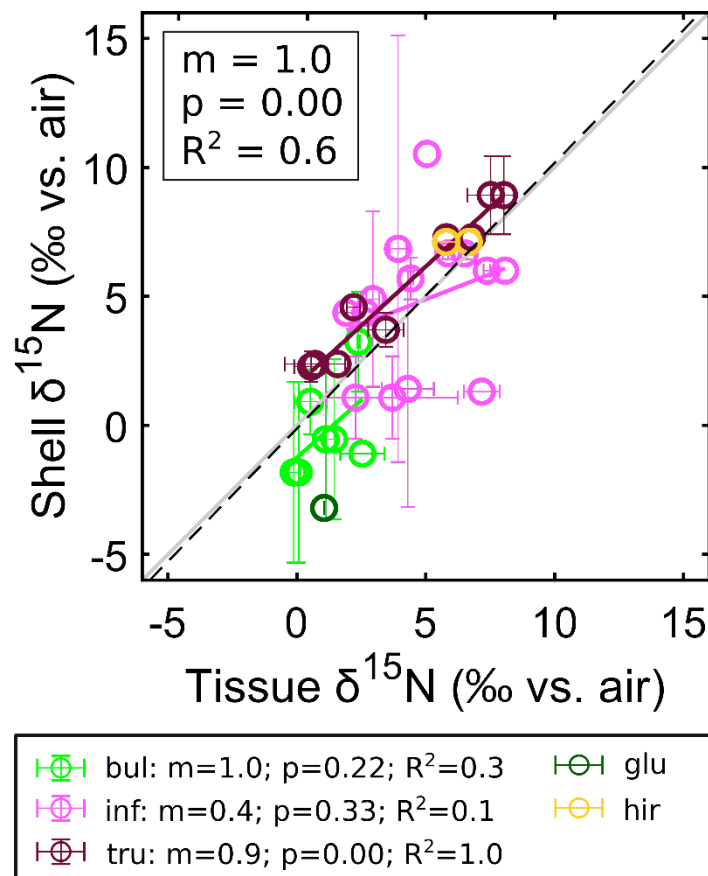
Fig. 3.5: Foraminifer tissue $\delta^{15}N$ *vs.* shell-bound $\delta^{15}N$. Cross-plot of all available data pairs (i.e., measurements of the same species from the same tow collection), with colour denoting species. Regression lines are shown for individual species (solid, colour lines) and overall (dashed, black line), with a 1:1 line (solid, grey diagonal) for reference. Error bars indicate the standard deviation of repeat (oxidation) measurements of the same species from the same tow.

113

The average N content of foraminifer tissue (i.e., all non-shell-bound organic matter) is 3.6±0.2 nmol/indiv (n = 140), or 397±17 nmol/mg (n = 91) (Table 3.2). These overall and species-specific averages are approximately 3 to 4 times lower than the N contents of the same species caught in upper-ocean net tows in the Sargasso Sea (15.1±1.0 nmol/indiv (n = 128), or 1208±131 nmol/mg (n = 128); shown alongside in Table 3.2). A factor of 3 to 4 difference for both N per individual and N per milligram (which are both volume-dependent measures) would be consistent with subtropical specimens being approximately 1.4 to 1.6 times the size (i.e., diameter) of the subpolar specimens. In both regions (sub-polar and subtropical), *O. universa* has the highest tissue N content per individual (approximately double that of most other species), but the tissue N per milligram is similar to or even below the average. The N contents of *N. incompta*, *N. quinqueloba* and *N. pachyderma* tissue, on the other hand, appear to be lower than those of the other the species. While we have fewer measurements of shell-bound N content and the results are less conclusive, the shell N content of most species (whether in terms of nmol/indiv or nmol/mg) does not appear to differ substantially between the SAZ/PFZ and the Sargasso Sea (Table 3.2).

Table 3.2: Comparison between Southern Ocean and Sargasso Sea foraminifer tissue N content.

Note. Averages and standard error (with n = number of oxidations) are given for each species and overall (bottom row). *estimated based on the average shell weights of Movellan (2013) and Takahashi and Bé (1984) from upper ocean net tows.

	SAZ/PFZ						Sargasso Sea					
	Tissue N content (nmol/indiv)			Tissue N content (nmol/mg)			Tissue N content (nmol/indiv)			*Estimated tissue N content (nmol/mg)		
Species	avg	std err	n	avg	std err	n	avg	std err	n	avg	std err	n
G. bulloides	**2.6**	0.3	30	**499**	43	23	**6.6**	0.9	8	**1878**	245	8
G. inflata	**4.1**	0.3	44	**432**	24	32	**11.2**	2.1	20	**1541**	286	20
G. truncatulinoides	**3.4**	0.2	32	**309**	15	21	**15.3**	2.0	24	**1047**	140	24
O. universa	**7.4**	1.6	10	**331**	37	4	**21.6**	2.6	38	**868**	103	38
G. hirsuta	**4.5**	0.7	7	**274**	46	6	**12.8**	1.2	32	**678**	64	32
G. glutinata	**3.2**	0.2	7	**367**	52	3	**8.8**	3.6	6	**4820**	1971	6
N. incompta	**1.2**	0.3	2	**-**	-	0	**-**	-	0	**-**	-	0
T. quinqueloba	**0.9**	0.2	5	**153**	-	1	**-**	-	0	**-**	-	0
N. pachyderma	**0.8**	0.0	3	**118**	-	1	**-**	-	0	**-**	-	0
ALL	**3.6**	0.2	140	**397**	17	91	**15.1**	1.0	128	**1208**	131	128

Table 3.3: Comparison between Southern Ocean and Sargasso Sea foraminifer shell N content.

Note. Averages and standard error (with n = number of oxidations) are given for each species and overall (bottom row). *estimated based on the average shell weights of Movellan (2013) and Takahashi and Bé (1984) from upper ocean net tows.

| | SAZ/PFZ | | | | | | Sargasso Sea | | | | | |
| | Shell N content (nmol/indiv) | | | Shell N content (nmol/mg) | | | *Estimated shell N content (nmol/indiv) | | | Shell N content (nmol/mg) | | |
Species	avg	std err	n	avg	std err	n	avg	std err	n	avg	std err	n
G. bulloides	**0.05**	0.01	10	**26.8**	-	1	**0.03**	-	1	**9.0**	-	1
G. inflata	**0.07**	0.01	13	**10.8**	-	1	**0.06**	0.01	4	**7.9**	0.7	4
G. truncatulinoides	**0.08**	0.01	9	-	-	0	**0.10**	0.01	6	**6.9**	0.6	6
O. universa	-	-	0	-	-	0	**0.13**	0.03	17	**5.3**	1.1	17
G. hirsuta	**0.10**	-	1	-	-	0	**0.13**	0.01	11	**6.7**	0.3	11
G. glutinata	**0.08**	-	1	-	-	0	-	-	0	-	-	0
N. incompta	-	-	0	-	-	0	-	-	0	-	-	0
T. quinqueloba	-	-	0	-	-	0	-	-	0	-	-	0
N. pachyderma	-	-	0	-	-	0	-	-	0	-	-	0
ALL	**0.07**	0.01	34	**18.8**	8.0	2	**0.11**	0.01	39	**6.3**	0.5	39

3.4 δ^{15}N of size-fractionated and bulk particulate organic N

The δ^{15}N of size-fractionated tow material is similar in absolute value and follows the same overall patterns described for foraminifera (increasing from south-to-north in late summer but not in winter), with significantly ($p \ll 0.05$) higher values in winter (4.7±0.2‰; n = 42; Fig. 3.4c) than in late summer (1.1±0.3‰; n = 54; Fig. 3.4d). Excluding data outside of the core SAZ/PFZ yields similar averages of 4.8±0.2‰ (n = 36) for winter and 0.9±0.3‰ (n = 48) for late summer (also with $p \ll 0.05$). This significant difference between winter and late summer applies to the bulk tow material (i.e., combining all size fractions from <150 µm to 5000 µm) as well as to each individual size fraction. We exclude the >5000 µm fraction from the comparison, as it was only collected on the late-summer cruise. On average, there is a δ^{15}N increase from smaller (150-250 µm or 250-500 µm) to larger (2000-5000 µm) size fractions in both seasons (although this trend is less consistent for the winter tows), with a larger range of values in late summer (from −0.8±0.8‰ (n = 7) to 1.9±0.6‰ (n = 12), respectively) than in winter (from 4.4±0.3‰ (n = 6) to 5.1±0.4‰ (n = 8), respectively). A notable exception is the smallest size fraction (<150 µm), which has a high δ^{15}N that is comparable to the medium-to-large size fractions from the same tow.

The overall δ^{15}N of bulk PON collected in surface waters (grey filled diamonds in Fig. 3.4) is also significantly ($p \ll 0.05$) higher for the winter transect (2.8±0.3‰, n = 26) than for the

115

late-summer transect (0.4±0.5‰, n = 25). Considering only the core of the SAZ/PFZ, the difference between cruises is even larger, with PON $\delta^{15}N$ averaging 3.2±0.7‰ (n = 9) and −2.0±0.4‰ (n = 12) respectively. In both cases, surface-ocean bulk PON is generally lower in $\delta^{15}N$ than both foraminifer tissue (by 2.9±0.3‰ (n = 13) for all tows; by 3.2±0.2‰ (n = 10) for the SAZ/PFZ tows) and size-fractionated tow material (by 2.8±0.4‰ (n = 14) for all tows; by 3.2±0.5‰ (n = 10) for the SAZ/PFZ tows) from the same site. Bulk PON $\delta^{15}N$ rises by ~7‰ from south-to-north across the entire late-summer transect (from 47.5°S to 35.5°S), ~4‰ of which occurs across the SAZ/PFZ. In winter, the overall trend in bulk PON $\delta^{15}N$ (between 55.7°S and 34.5°S) is not linear: increasing from the Antarctic Zone to PFZ, decreasing across the PFZ and SAZ (by ~5‰), and then increasing again into the subtropics.

3.5 Trends in foraminifer tissue $\delta^{15}N$ with latitude, nitrate+nitrite $\delta^{15}N$ and PON $\delta^{15}N$

Below, we focus on trends in foraminifer tissue $\delta^{15}N$ (rather than shell-bound $\delta^{15}N$, as these data are sparse and more variable) within the SAZ/PFZ (the zones in which our two transects overlap).

In late summer, foraminifer tissue $\delta^{15}N$ shows a significant northward increase overall (i.e., negative slope and p << 0.05), with a slope of −0.5 ($R^2 = 0.2$; Fig. 3.6e) when the 2017 analyses are included, and a slope of −0.7 ($R^2 = 0.4$; not shown) when the 2017 analyses are excluded. This trend is evident in six of the eight species and is significant for those with the most data (*G. bulloides*, *G. inflata* and *G. truncatulinoides*). *G. glutinata* and *T. quinqueloba*, on the other hand, exhibit weak, non-significant, southward increases in $\delta^{15}N$ in late summer (i.e., small positive regression slopes with p >> 0.05). In winter, the relationship between foraminifer tissue $\delta^{15}N$ and latitude is reversed, with a significant northward decrease (i.e., positive slope and p < 0.05), with (slope = 0.4; $R^2 = 0.3$; Fig. 3.6a) or without (slope = 0.3; $R^2 = 0.2$; not shown) the 2017 analyses. Considering each species separately produces a range of (positive and negative) regression slopes, largely depending on the latitudinal distribution of the species, but with a consistent local minimum in tissue $\delta^{15}N$ at W7 (42.2°S), common to all species measured. The relationship between foraminifer tissue $\delta^{15}N$ and in situ nitrate+nitrite $\delta^{15}N$ is significant in both seasons, but strongly positive in late summer (slope = 0.9; $R^2 = 0.2$; Fig. 3.6f), and weakly negative in winter (slope = −0.3; $R^2 = 0.1$; Fig. 3.6b). Excluding the 2017 analyses further strengthens the late-summer trend (slope = 1.3; $R^2 = 0.4$) and lessens the significance of the winter trend (p > 0.05) (not shown). The species-specific trends generally

conform to the overall trends, with mostly positive slopes in late summer (between 0.5 and 1.7; excluding the under-sampled *G. glutinata* and *T. quinqueloba*) and a variety of positive and negative slopes in winter (between −1.5 and +1.7).
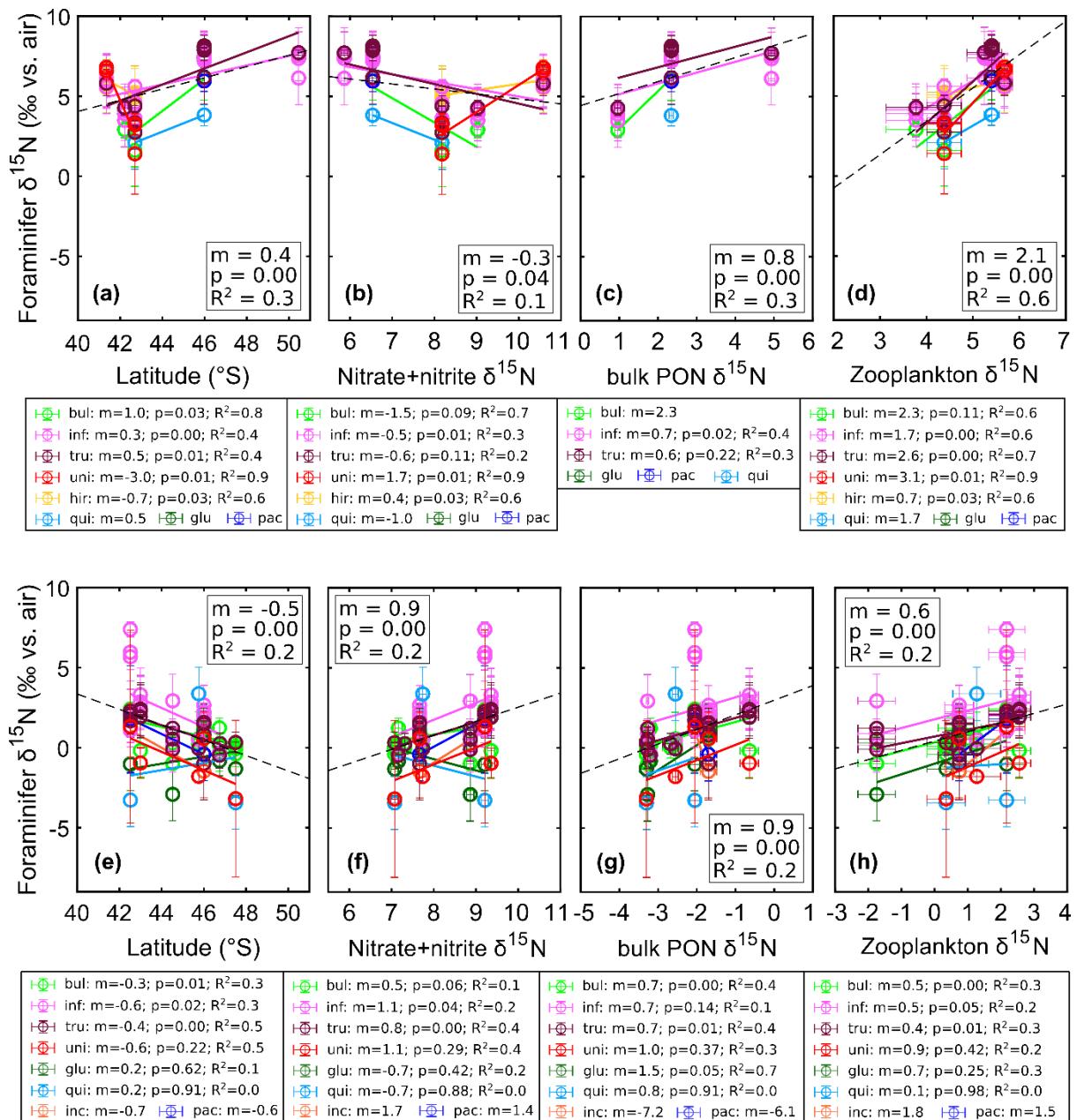
Fig. 3.6: Investigating controls on foraminifer tissue $\delta^{15}N$. Relationships with (a, e) latitude, (b, f) nitrate+nitrite $\delta^{15}N$, (c, g) bulk (>0.7 μm) suspended PON $\delta^{15}N$, and (d, h) zooplankton (i.e., size-fractionated tow PON) $\delta^{15}N$ in the African PFZ/SAZ mixed layer during winter (top row) and late summer (bottom row). Regression lines are drawn for individual species (solid, colour lines) and overall (dashed, black line). Y error bars show the standard deviation of replicate oxidations. X error bars show measurement standard deviation where applicable (c-d, g-h), and pooled standard deviation in the case of (b) and (f).

In contrast, the $\delta^{15}N$ relationship between mixed-layer foraminifer tissue and bulk surface PON is positive in both winter and late summer, with overall slopes of 0.8 ($R^2 = 0.3$; $p \ll 0.05$; Fig. 3.6c) and 0.9 ($R^2 = 0.2$; $p \ll 0.05$; Fig. 3.6g), respectively. Excluding the 2017 analyses makes little difference (not shown). In late summer, significant species-specific trends exist for *G. glutinata* (slope = 1.5; $R^2 = 0.7$), *G. bulloides* (slope = 0.7; $R^2 = 0.4$), and *G. truncatulinoides* (slope = 0.7; $R^2 = 0.4$). Interestingly, *G. inflata* exhibits a significant relationship with bulk PON in winter (slope = 0.7; $R^2 = 0.4$), but a non-significant one in late summer (slope = 0.7; $R^2 = 0.1$). This appears to be largely driven by the "unusual" conditions or population dynamics at station M8 (42.5°S). The relationship between foraminifer tissue $\delta^{15}N$ and bulk surface PON $\delta^{15}N$ is the only case tested so far where combining the winter and late-summer data strengthens the correlation (to $R^2 = 0.7$, with slope = 1.1 and intercept = 3.4). This is not the case for the correlations with latitude (Fig. 3.6a&e) or nitrate+nitrite (Fig. 3.6b&f), where winter and late-summer trends oppose each other. Even shell-bound $\delta^{15}N$ has a significant positive relationship with bulk surface PON $\delta^{15}N$ (despite fewer measurements and greater variability than tissue $\delta^{15}N$ (n = 27 *vs.* n = 109 for the core SAZ/PFZ)), yielding a similar slope (0.8) and intercept (3.3) to the tissue data. A similarly consistent relationship is observed between foraminifer $\delta^{15}N$ and tow-caught PON $\delta^{15}N$ (i.e., other zooplankton and larger detritus from the same tows as the foraminifera). The correlation is positive and significant ($p \ll 0.05$) in both winter (overall slope = 2.1; $R^2 = 0.6$; Fig. 3.6d) and late summer (overall slope = 0.6; $R^2 = 0.2$; Fig. 3.6h) and combining the two seasons strengthens the correlation (to $R^2 = 0.7$, with slope = 1.1 and intercept = 0.0). Excluding the 2017 analyses does not change the significance of the overall correlation, but makes the winter (slope = 1.8, $R^2 = 0.5$) and late-summer (slope = 1.2, $R^2 = 0.3$) trends more similar to each other (not shown). There are significant species-specific trends for *G. truncatulinoides* and *G. inflata* in both seasons, as well as for *G. hirsuta* and *O. universa* in winter, and for *G. bulloides* in late summer.

4. Discussion

Given the dominant control of nitrate assimilation on the $\delta^{15}N$ of nitrate+nitrite across the Southern Ocean (Lourey et al., 2003; Sigman et al., 1999a), it seems reasonable to predict that surface ocean-dwelling planktic foraminifera should exhibit similar trends of (1) a northward increase in $\delta^{15}N$ and (2) higher $\delta^{15}N$ values in summer than in winter. These patterns would be congruent with the progressive south-to-north and winter-to-summer drawdown of nitrate by

phytoplankton, which elevates the $\delta^{15}N$ of mixed-layer nitrate+nitrite and thus the $\delta^{15}N$ of net biomass production and export (i.e., export production). The first prediction appears to be upheld by the latitudinal gradients in foraminifer $\delta^{15}N$ in late summer. However, this prediction fails in winter when foraminifer $\delta^{15}N$ increases poleward. The prediction of higher foraminifer $\delta^{15}N$ in summer also fails, with significantly higher tissue and shell-bound $\delta^{15}N$ in winter than in summer.

Therefore, the $\delta^{15}N$ of foraminifera in the Southern Ocean mixed-layer does not simply track the $\delta^{15}N$ of ambient nitrate+nitrite, at least not year-round. The divergence of foraminifer $\delta^{15}N$ from nitrate+nitrite $\delta^{15}N$ appears to be related to a similar divergence of upper-water-column PON $\delta^{15}N$ from nitrate+nitrite $\delta^{15}N$. However, in order to best interpret the seasonal and latitudinal patterns in living foraminifer $\delta^{15}N$ and assess their implications for the paleo-proxy, we must first address the contributions of spatial differences (i.e., sampling different regions with potentially different nitrate source properties, N isotope dynamics and/or PON properties) and foraminifer assemblage differences (i.e., the prevalence of different species and/or size-fractions) to the apparent "winter *vs.* summer" differences. Because different latitudinal bands or "zones" of the Southern Ocean are characterized by different hydrodynamic regimes and nitrate sources, and possibly different isotope effects of nitrate assimilation (Sigman et al., 1999a; Altabet & François, 2001; DiFiore et al., 2006; DiFiore et al., 2010), we focus our analysis on the zones where the two cruises overlap: the PFZ and the SAZ.

4.1 Disentangling seasonal signals from regional and assemblage differences in foraminifer $\delta^{15}N$

While all our foraminifer samples were collected from the Southern Ocean south of Africa, the winter and late-summer voyages are separated by 17-38° longitude, falling into different sectors (Atlantic and Indian, respectively). The complex frontal geometry (e.g., branching) and proximity of the Agulhas retroflection (Fig. 3.1b) make for a more dynamic hydrographic setting in the late-summer (i.e., Indian sector) transect (Belkin & Gordon, 1996; Lutjeharms & Valentine, 1984). This raises the question: how much of the winter foraminifer $\delta^{15}N$ elevation (by 4.4‰ for tissue and 3.4‰ for shells; Table 3.1) relative to late summer can be explained by spatial differences? For one, the higher $\delta^{15}N$ of foraminifera on the winter transect could be caused by a higher-$\delta^{15}N$ nitrate source feeding the PFZ/SAZ mixed layer in the Atlantic relative to the Indian sector. However, we observe no such difference in UCDW or SAMW properties between the two transects.

119

The meridional gradient in mixed-layer nitrate $\delta^{15}N$ on the Indian/late-summer transect appears weak compared to winter/Atlantic gradient (compare dark blue lines in Fig. 3.4a&b). Late-summer nitrate $\delta^{15}N$ plateaus into the northern SAZ and decreases across the STF, despite the continued and steepening northward decline in nitrate concentration along the same transect (light green line in Fig. 3.4b). One possible explanation is the lowering of Indian SAZ mixed-layer nitrate $\delta^{15}N$ by cross-frontal mixing with low-$\delta^{15}N$ Agulhas nitrate. Our own measurements of mixed-layer nitrate in the Agulhas Retroflection (station M10 at 41.0°S; Fig. 3.1b) exhibit anomalously low $\delta^{15}N$ values for the low nitrate concentration, deviating from the equatorward rise in $\delta^{15}N$ expected for progressive nitrate assimilation (northernmost station in Fig. 3.4b; orange profile in Fig. 3.2). This low-$\delta^{15}N$ signature has been observed previously in Agulhas rings (Campbell, 2016; Smart, 2014; Smart et al., 2015) and in the Agulhas current itself (Sinyanya et al., 2020) and may derive from near-complete consumption of relatively low-$\delta^{15}N$ thermocline nitrate, possibly lowered by N_2-fixation (implied by excess nitrate relative to phosphate, i.e., high N* concentrations; Gruber and Sarmiento, 1997), in the western subtropical Indian Ocean. A consequence of mixing with this low-$\delta^{15}N$, low-concentration Agulhas nitrate would be to weaken the $\delta^{15}N$ gradient (at least slightly) but strengthen the concentration gradient across the SAZ mixed layer, potentially masking part of the summertime assimilation signal in this region. While cross-frontal exchange with the subtropics (via eddy mixing; Speer et al., 2000; McNeil et al., 2001) has been estimated to contribute minimally to SAZ mixed-layer nitrate south of Australia, the contribution may be more significant in this dynamic region south of Africa. Regardless of any potential Agulhas influence, the SAZ and PFZ mixed layers of the late-summer/Indian transect host higher nitrate $\delta^{15}N$ than those of the winter/Atlantic transect, as would be expected from the increased ratio of nitrate consumption relative to supply in the summertime Southern Ocean.

Hypothetically, the $\delta^{15}N$ of the food sources available to foraminifera could be higher in the Atlantic sector than in the Indian sector. Assuming that nitrate is the dominant control on the $\delta^{15}N$ of PON, such a difference in food $\delta^{15}N$ is unlikely in the absence of substantial longitudinal differences in the nitrate source or isotope effect of nitrate assimilation. However, different environmental conditions could favor different plankton assemblages and thus bulk PON properties. We test this using the bulk suspended PON data (Fig. 3.7). We observe very little difference in the $\delta^{15}N$ of PON (Fig. 3.7a) between the Atlantic (triangles) and Indian (circles) sectors (divided at 20°E) in winter (3.2±0.9‰ (n = 4; blue triangles) *vs.* 4.0±0.3‰ (n

120

= 6; turquoise circles)), midsummer (0.6±1.2‰ (n = 3; orange triangles) *vs.* 0.8±0.4‰ (n = 7; red circles)) or late summer (−2.1±0.4‰ (n = 13; pink triangles) *vs.* −2.0±0.4‰ (n = 12; purple circles)); for this comparison, averages are calculated from PON samples that were collected within the latitudinal range of our net tows (indicated by filled symbols), and cover both the Indian and Atlantic sectors (i.e., where filled circles and triangles overlap in latitude). Even the broader latitudinal patterns in PON δ^{15}N are remarkably similar between sectors, excluding those collected nearshore and downstream of Marion Island (circles within the vertical grey bar), where we have no foraminifer data. Interestingly, the concentration of PON (Fig. 3.7b) does differ between the Atlantic and Indian sectors in the winter (0.8±0.0µM (n = 4; blue triangles) *vs.* 0.3±0.0µM (n = 6; turquoise circles)) and late summer (0.7±0.0µM (n =13; pink triangles) *vs.* 1.1±0.1µM (n = 12; purple circles)) but not in midsummer (1.0±0.0µM (n = 3; orange triangles) *vs.* 1.0±0.1µM (n = 7; red circles)).
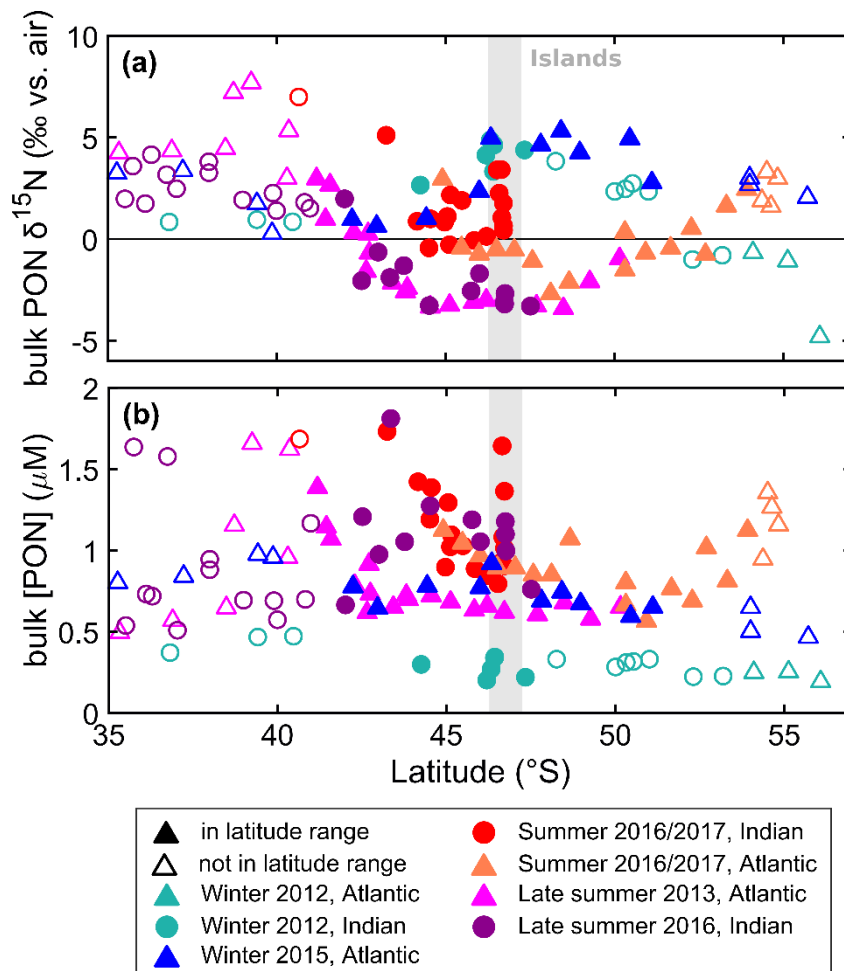
Fig. 3.7: Compilation of bulk suspended PON data from the Southern Ocean south of Africa (0-42°E). Measurements of (a) δ^{15}N (‰ *vs.* N_2 in air) and (b) concentration (µM) from underway surface collections of bulk (>0.7 µm) particles. Triangles denote data from the Atlantic Sector (west of 20°E)

121

and circles denote those from the Indian Sector (east of 20°E). Blue symbols are used for winter, orange/red symbols for midsummer and pink/purple for late summer. Symbols are filled if they fall within the same latitude range as our foraminifer tow collections in that sector. Circles within the vertical grey bar are excluded from our calculations, as these samples were collected nearshore and downstream of Marion Island, where we have no foraminifer data.

Another possibility is that the observed winter *vs*. summer differences in foraminifer δ^{15}N are the result of seasonal changes in foraminifer species assemblage and size distribution. In order to avoid overinterpretation of data with large gaps, we focus our discussion on the three most abundant and commonly occurring species in our collections: *G. inflata*, *G. truncatulinoides* and *G. bulloides*. For example, the lower average δ^{15}N of foraminifer tissue and shells in late summer could be due to the abundance of *G. bulloides* in the late-summer tow collections, which typically have a lower δ^{15}N than *G. inflata* and *G. truncatulinoides* in the same tow (by 1.0‰ and 0.4‰ on average, respectively). Similarly, *G. bulloides* dominates the more polar tows on the late-summer transect (Fig. 3.2), which could steepen the meridional gradient in foraminifer δ^{15}N. While such effects may contribute to the overall average seasonal differences (black trendline in Fig. 3.6e), we observe the same patterns (i.e., a higher δ^{15}N in winter than in summer, and equatorward δ^{15}N rise in summer) within the same species (colour trendlines in Fig. 3.6e). In terms of test size, the prevalence of larger (>350 µm) *G. truncatulinoides* in winter (more so than in late summer; Fig. S3.1b), raises the possibility that a higher average "apparent trophic level" of the *G. truncatulinoides* population in winter (potentially feeding on higher-δ^{15}N PON) could contribute to the elevated δ^{15}N of *G. truncatulinoides* in winter than in summer. On the other hand, the mean size (and expected trophic level) of *G. bulloides* was higher in late summer (>250 µm) than in winter (150-250 µm) and would have the opposite effect (raising the summertime average δ^{15}N for *G. bulloides*). Regardless, our data indicate a weak positive relationship ($R^2 \leq 0.1$ overall) between foraminifer δ^{15}N and specimen size (not shown), that is only significant ($p < 0.05$) during late summer for *G. bulloides* ($R^2 = 0.15$) and *G. inflata* ($R^2 = 0.08$). In summary, differences in regional nitrate sources, PON properties and foraminifer assemblages appear to contribute little to the observed Atlantic/winter *vs*. Indian/late-summer differences in N isotope properties of the PFZ and SAZ mixed-layers. We thus conclude that the differences between cruises primarily reflect seasonal changes in the PFZ/SAZ and refer to them as such below.

4.2 Control of foraminifer $\delta^{15}N$ by PON $\delta^{15}N$

The inconsistent relationship between foraminifer $\delta^{15}N$ and ambient seawater nitrate+nitrite $\delta^{15}N$ (Fig. 3.6b&f), in terms of correlation (positive in winter, negative in late summer) and absolute offset (small in winter, large in late summer), leads us to more closely consider the immediate N sources to foraminifera and their reflection in foraminifer $\delta^{15}N$. The most consistent relationship we observe, regardless of season, is between foraminifer $\delta^{15}N$ and bulk suspended PON $\delta^{15}N$ (Fig. 3.6c&g). Whether tissue or shell data are used, the bulk PON-foraminifer relationship is close to 1:1 and the offset around 3‰, the typical $\delta^{15}N$ difference between heterotrophs and their diet (Minagawa & Wada, 1984; Checkley & Miller, 1989). The $\delta^{15}N$ difference between foraminifer tissue and bulk suspended PON (3.2±0.2‰; n = 10) is similar to that observed in the subtropical North Atlantic (2.5±0.6‰; n = 5) (Table 3.4). The bulk suspended PON with which we compare our foraminifera contains all particles larger than the pore size of the filter and, therefore, includes phytoplankton (from the larger diatoms and coccolithophores through to small cyanobacteria like *Synechoccocus*), detritus and the occasional zooplankton, but excludes bacteria smaller than 0.7 µm unless they are particle-associated. In terms of biomass, large phytoplankton likely contribute the most to both living and detrital organic matter in the Southern Ocean mixed-layer (Buitenhuis et al., 2013, and references therein). While there is also a strong correlation between PFZ/SAZ foraminifera (dominated by non-dinoflagellate bearing species) and larger size fractions of PON (caught by the same net tow; Fig. 3.6d&h), the small $\delta^{15}N$ offset (0.2±0.3‰; n = 12) between the two groups suggests that the relationship is driven largely by a common food source rather than by foraminifera feeding heavily on zooplankton and/or their detritus. We return to this at the end of section 4.2. The consistent positive correlation between foraminifer $\delta^{15}N$ and bulk suspended PON suggests that foraminifera more closely resemble their diet than ambient seawater nitrate+nitrite in $\delta^{15}N$, which is consistent with foraminifera acquiring N mostly from their particulate food (Bé et al., 1977; Spindler et al., 1984; Uhle et al., 1997), rather than from seawater (dissolved nitrate+nitrite) directly. This interpretation relies on two assumptions: (1) the $\delta^{15}N$ of bulk suspended PON in surface waters approximates the $\delta^{15}N$ of bulk suspended PON at the depth of the tow collection, and (2) bulk suspended PON is a reasonable measure of the PON consumed by foraminifera.

First, the $\delta^{15}N$ of suspended PON has been found to increase with depth in the open ocean, particularly through the upper 500 m of the water column (by ~6-10‰), due to the preferential

123

removal of ^{14}N from particles during heterotrophic degradation (Saino & Hattori, 1980; Altabet & McCarthy, 1986; Altabet et al., 1991; Hannides et al., 2013). This δ^{15}N increase is typically accompanied by a decrease in the concentration and an increase in the C:N ratio of suspended PON with depth, signaling the more rapid decomposition of labile, N-rich components like proteins (Altabet & McCarthy, 1986; Lehmann et al., 2002). However, all of our tow collections were made within the upper 100 m of the water column, usually within a uniformly high chlorophyll mixed layer (although local sub-surface maxima were targeted when present, i.e., at M2, M9, and W1), suggesting a relatively even distribution of phytoplankton particles through the mixed layer at most stations. Depth-profiles of suspended PON δ^{15}N from the PFZ/SAZ south of Africa exhibit an overall increase in δ^{15}N from near the surface to 100 m depth of ~1‰ in midsummer (2016/2017 profiles between 0 and 40°E; warm colours in Fig. S3.3) and of <0.5‰ in winter (2017 profiles along 30°E; cool colours in Fig. S3.3). In addition, existing late-summer measurements from the Indian sector (high-nutrient, low-chlorophyll off-plateau sites near Kerguelen (Trull et al., 2008)) indicate minimal increases of ≤0.5‰ in PON-δ^{15}N with depth in the upper 100 m of the water column. Furthermore, the average C:N ratios of suspended PON increase by less than 0.5 over the same interval in these profiles (Trull et al., 2008) and show no consistent depth trend in the Atlantic sector (Martiny et al., 2014). Therefore, we consider our underway collections of suspended PON to be a reasonable approximation for the δ^{15}N of suspended PON at tow depth, at least during winter and late summer when foraminifera were collected.

Second, some foraminifer species feed preferentially on specific types of PON, which may differ in δ^{15}N from bulk suspended PON. In high-nutrient waters like the Southern Ocean, *G. bulloides* appears to follow the chlorophyll maximum (Mortyn & Charles, 2003). *G. inflata* and *G. truncatulinoides* are thought to rely mostly on detrital particles due to their deeper average depth habitat (with peak abundances observed at 50-300 m and 100-600 m, respectively, in the summertime Atlantic sector; Mortyn & Charles, 2003). Clearly, they do spend some portion of their life cycle within the mixed layer (evident from their abundance in our net tows), but these periods may coincide with reproduction and be relatively short-lived, at least for *G. truncatulinoides* which appears to only reproduce annually (Weyl, 1978; Schiebel et al., 2002). The partial dependence on more degraded PON with a higher δ^{15}N is one explanation for the higher δ^{15}N of *G. inflata*, *G. truncatulinoides* and *G. hirsuta* relative to

124

shallow-dwellers like *O. universa* in subtropical environments (the other being the absence of dinoflagellate symbionts, which we discuss below) (Ren et al., 2012).

Table 3.4: Comparison between Southern Ocean and Sargasso Sea foraminifer $\delta^{15}N$ relationships with PON and nitrate consumed.

Note. Here we compare the $\delta^{15}N$ offset of foraminifer tissue from bulk (>0.7 µm) suspended PON (left-hand side) and from nitrate consumed (right-hand side) in two different nutrient regimes, the African PFZ/SAZ (where surface nitrate is partially consumed) and the Sargasso Sea (where surface nitrate is fully consumed). Averages and standard error (with n = number of stations, i.e., tows) are given for each species and overall (bottom row).

[a] Here we use surface collections to approximate mixed-layer average suspended PON-$\delta^{15}N$.

[b] Here we use euphotic-zone-averaged bulk PON-$\delta^{15}N$.

[c] In the case of incomplete nitrate consumption (PFZ/SAZ), we estimate (using a simple mixing model) the $\delta^{15}N$ of nitrate consumed during the productive summer season from the $\delta^{15}N$ and concentration at the start (calculated) and end (measured) of the growing season. The properties of mixed-layer nitrate at the start of spring are calculated using two end-member isotope models as described in section 4.3. We average the results (0.7‰ for the Rayleigh case, 1.4‰ for steady-state) to get a $\delta^{15}N$ of 1.0‰ for nitrate consumed in the SAZ/PFZ.

[d] In the case of complete nitrate consumption (Sargasso Sea), we take the $\delta^{15}N$ of thermocline source (~2.5‰ for nitrate+nitrite) as the $\delta^{15}N$ of nitrate consumed annually in the euphotic zone.

| | Foraminifer minus PON $\delta^{15}N$ difference (‰) | | | | | | Foraminifer minus nitrate-consumed $\delta^{15}N$ difference (‰) | | | | | |
| | SAZ/PFZ[a] | | | Sargasso Sea[b] | | | SAZ/PFZ[c] | | | Sargasso Sea[d] | | |
Species	avg	std err	n	avg	std err	n	avg	std err	n	avg	std err	n
G. bulloides	**3.1**	0.3	9	**2.2**	0.2	3	**0.7**	0.6	10	**0.1**	0.1	4
G. inflata	**3.8**	0.4	9	**3.3**	0.8	3	**2.5**	0.8	11	**0.7**	0.4	5
G. truncatulinoides	**3.4**	0.3	10	**2.6**	0.7	5	**1.9**	0.9	12	**0.7**	0.2	8
O. universa	**1.2**	0.7	5	**2.0**	0.6	5	**-0.3**	1.2	7	**-0.2**	0.3	9
G. hirsuta	**-**	-	0	**3.1**	0.4	3	**4.5**	0.5	2	**1.1**	0.3	5
G. glutinata	**2.3**	0.7	6	**1.9**	0.6	2	**-0.6**	1.5	6	**-0.1**	0.3	3
N. incompta	**1.7**	1.5	2	**-**	-	0	**-1.2**	1.3	2	**-**	-	0
T. quinqueloba	**1.5**	1.6	4	**-**	-	0	**-0.5**	1.6	5	**-**	-	0
N. pachyderma	**2.9**	0.8	3	**-**	-	0	**1.4**	1.9	3	**-**	-	0
ALL	**3.2**	0.2	10	**2.5**	0.6	5	**1.7**	0.8	12	**0.2**	0.2	10

In contrast, *O. universa* is believed to be mostly carnivorous, preying upon other zooplankton like copepods (Bé et al., 1977; Spindler et al., 1984), and would, therefore, be expected to have a higher-$\delta^{15}N$ diet than that of herbivorous foraminifera. At the same time, this species has dinoflagellate endosymbionts, which act to weaken their host's trophic elevation by taking up low-$\delta^{15}N$ ammonium that would otherwise be excreted by the foraminifer (Uhle et al., 1999).

It has been proposed that this internal N recycling (and thus lack of ammonium efflux) explains the lower δ^{15}N of *O. universa* relative to symbiont-barren species, at least in the (sub)tropical ocean (Ren et al., 2012; Smart et al., 2018). In the SAZ/PFZ, *O. universa* are, on average, 1.3±0.5‰ (n = 7) lower in δ^{15}N than (i.e., approximately half a trophic level below) non-dinoflagellate bearers from the same tow. While the scarcity of *O. universa* in our tow collections prevents us from drawing more robust conclusions about this species in the Southern Ocean, their symbionts might contribute either directly (as a major constituent of the cytoplasm we measure as foraminifer "tissue"; Spero, 1987) or indirectly (via biochemical exchanges) to their lower measured δ^{15}N relative to other species. Given the lower temperature bound of ~10°C for *O. universa* (Bé, 1977; Darling & Wade, 2008), it is also possible that these individuals were transported into subpolar waters by warm-core eddies or by mixing across the STF and that local conditions are not representative of their primary habitat. A similar mechanism was proposed to explain the abundance of *O. universa* (up to 7%) in sediment traps during winter in the central SAZ (47°S) south of Tasmania (King & Howard, 2003).

The δ^{15}N elevation that we observe for *G. bulloides* relative to surface suspended PON (at the same station) remains fairly constant from winter (2.9±0.9‰; n = 2) to late summer (3.2±0.3‰; n = 7), suggesting a close coupling between this species and phytoplankton in the surface ocean. On average, the δ^{15}N of *G. bulloides* is lower than that of *G. inflata* and *G. truncatulinoides* (by 1.0±0.3‰ (n = 9) and 0.4±0.3‰ (n = 10), respectively) from the same tows. Given that none of these species have dinoflagellate endosymbionts, the differences might imply a higher-δ^{15}N diet for the latter two species (i.e., feeding on more degraded PON below 100 m depth and/or on zooplankton-derived PON). Our measured offsets are in line with observations from the Sargasso Sea, where the tissue δ^{15}N of tow-caught *G. bulloides* is ~0.6‰ lower than the annual averages for *G. inflata* and *G. truncatulinoides* (Smart et al., 2018). While our *G. inflata*−*G. bulloides* offset is similar between seasons (1.4±0.2‰ in winter and 0.8±0.4‰ in late summer), the *G. truncatulinoides*−*G. bulloides* offset varies from 1.3±0.2‰ in winter to 0.0±0.3‰ in late summer. The late-summer convergence of *G. truncatulinoides* δ^{15}N on *G. bulloides* δ^{15}N may reflect a dietary shift in *G. truncatulinoides* from more degraded/zooplankton-derived PON to a phytoplankton-based diet, perhaps due to seasonal/annual migration into shallow waters (e.g., for reproduction) or, alternatively, the arrival of "fresher" phytoplankton-derived material at depth (>100 m) following the productive summer season. This is supported by consistently higher δ^{15}N values (by 1.2‰ on average; n

126

= 9) for *G. truncatulinoides* shells (recording long-term conditions at their primary habitat) compared to tissue (capturing recent activity such as feeding at the tow collection depth) from the same net tows.

In summary, the $\delta^{15}N$ of foraminifera appears to be more closely tied to the $\delta^{15}N$ of particulate N forms than to that of dissolved nitrate. On the whole, the observed $\delta^{15}N$ relationships (among different foraminifer species, as well as between foraminifera, other zooplankton and bulk suspended PON) point to a similar, largely phytoplankton- (and detritus-) based diet for non-dinoflagellate bearing foraminifera living in the SAZ/PFZ.

4.3 Seasonality in bulk PON

If PON is indeed the main control on foraminifer $\delta^{15}N$, then processes affecting spatial patterns and seasonality in PON $\delta^{15}N$ warrant our attention. The first process we consider is nitrate assimilation. Nitrate is drawn down rapidly (although not to completion) during the productive season, fueling the phytoplankton blooms that characterize spring and summer in the Southern Ocean. Depending on the rate of nitrate resupply to the summertime mixed layer, the N isotope dynamics of the remaining nitrate and the PON produced can be approximated by a simple Rayleigh model (assuming no nitrate resupply) or steady-state model (assuming continuous resupply). While the PFZ and SAZ exhibit aspects of both closed- (e.g., stratification and nitrate depletion) and open- (e.g., equatorward transport) system behavior during the summer (Altabet & François, 2001; DiFiore et al., 2006), we can use these two endmember models to calculate the range of PON $\delta^{15}N$ values expected for the region south of Africa.

For each zone, we estimate the fraction of nitrate remaining at the end of summer using the average concentration difference between the surface and 150 m depth; ~0.88 for the PFZ, ~0.78 for the SAZ (Lourey et al., 2003). We then back-calculate the $\delta^{15}N$ of "initial" mixed-layer nitrate (i.e., at the start of spring) for each model, using literature values for the isotope effect of nitrate assimilation; ε ~ 4.9-6.1‰ in the PFZ (Fripiat et al., 2019) and ε ~ 7-9‰ in the SAZ (DiFiore et al., 2006; Lourey et al., 2003). Using the same parameters, we estimate the $\delta^{15}N$ of PON being produced by the end of the summer season (i.e., the instantaneous product) to be +1.2 to +2.4 ‰ or +1.2 to +2.4‰ in the PFZ, and −0.4 to +1.7‰ or −0.1 to +1.9‰ in the SAZ (for steady-state or Rayleigh models, respectively). If all the PON produced during the growing season accumulated in the mixed-layer, it would have a $\delta^{15}N$ of +0.8 to +2.1‰ in the PFZ and −1.3 to +1.0‰ in the SAZ. These values are substantially higher than what we observe

127

in late-summer surface waters, particularly for the PFZ (where PON $\delta^{15}N$ averages -2.8 ± 0.3‰; n = 5). Conversely, the calculated $\delta^{15}N$ values are well below our bulk suspended PON measurements for the winter PFZ (averaging $+3.9\pm0.6$‰; n = 7).

An investigation conducted in the Pacific sector south of Australia yielded similar results: the $\delta^{15}N$ of bulk suspended PON in the late-summer PFZ (and possibly SAZ) is too low to be explained by nitrate depletion alone (Lourey et al., 2003). The study concluded that the most likely cause is ammonium recycling in the late-summer mixed layer. Ammonium originates from two main sources: bacterial decomposition of PON (Lehmann et al., 2002) and excretion by zooplankton (Checkley & Miller, 1989). Isotopic fractionation during these processes (specifically, deamination) causes ammonium to have a low $\delta^{15}N$ relative to nitrate. Its subsequent assimilation by phytoplankton can, therefore, lower the $\delta^{15}N$ of the mixed-layer PON pool. Ultimately, the retention of ^{14}N within the mixed-layer must be linked to the preferential export of ^{15}N-rich particles (like larger, faster-sinking phytoplankton or zooplankton fecal pellets) (Altabet & Small, 1990; Möbius, 2013). The use of ammonium as an alternative N source by phytoplankton has been observed previously in the Southern Ocean (Glibert et al., 1982; Koike et al., 1986; Sambrotto & Mace, 2000; Elskens et al., 2002), including across PFZ and SAZ surface waters of the African sector (Joubert et al., 2011; Thomalla et al., 2011). In fact, the meridional gradient in suspended PON $\delta^{15}N$ (and we propose, by extension, in the $\delta^{15}N$ of foraminifera) across the late-summer Pacific PFZ/SAZ was hypothesized to be at least partly driven by more intense ammonium recycling lowering PON $\delta^{15}N$ in the PFZ relative to the SAZ (Lourey et al., 2003), rather than being solely a consequence of the south-to-north increase in nitrate consumption that causes the northward rise in nitrate $\delta^{15}N$ (Sigman et al., 1999a).

As for the wintertime, when light conditions deteriorate (due to deeper mixing and turbulence, as well as less insolation), the rate ratio of nitrate assimilation to nitrate resupply is lower, and thus nitrate and any PON produced from it would be expected to have a lower $\delta^{15}N$ than during peak (midsummer) nitrate drawdown. Yet the winter PFZ mixed layer hosts the highest-$\delta^{15}N$ PON, even compared to midsummer measurements from the same transects (compare blue *vs.* orange triangles and turquoise *vs.* red circles in Fig.7a). As with the anomalously low $\delta^{15}N$ of late-summer PON, higher-than-predicted "early season" (i.e., pre-bloom) PON $\delta^{15}N$ has been noted previously in the Southern Ocean (Altabet & François, 1994; Altabet & François, 2001; Lourey et al., 2003) and in the subarctic Pacific (Wu et al., 1997). A likely explanation for this

phenomenon is the remineralization of PON remaining in the mixed layer during the long, less-productive winter season. As described previously, bacterially mediated decomposition of suspended PON leaves remaining particles elevated in $\delta^{15}N$ (Saino & Hattori, 1980; Altabet & McCarthy, 1986; Altabet et al., 1991) and could, thus, drive at least part of the ~8‰ summer-to-winter increase in PON $\delta^{15}N$ observed in the PFZ. While remineralization within the mixed layer likely occurs year-round, the ammonium released from decomposition during summer would be re-assimilated into new biomass (i.e., PON), along with continued production of PON from nitrate. In addition, during the winter, the heterotrophic activity and packaging processes that remove partially decomposed organic matter from the surface may be at a minimum. Another contributor to the PON $\delta^{15}N$ rise might be a return to nitrate assimilation, but this switch alone could not explain more than ~3‰ of the observed ~8‰ increase, and nitrate assimilation is an energetically expensive process that seems unlikely under winter conditions. In summary, while nitrate assimilation appears to be the overarching driver of bulk PON $\delta^{15}N$ in Southern Ocean surface waters during the productive spring and summer seasons, internal mixed-layer N cycling processes seem to be important additional controls on PON (and indirectly, foraminifer) $\delta^{15}N$ during the rest of the year.

4.4 Implications for the foraminifer-bound $\delta^{15}N$ paleo-proxy

This study confirms that, for the nitrate-rich environment of the Southern Ocean, feeding causes living planktic foraminifera (tissue and shell) to track the $\delta^{15}N$ of upper-ocean PON rather than that of nitrate directly. Furthermore, the $\delta^{15}N$ of bulk PON in modern SAZ/PFZ surface waters, and therefore the foraminifera that feed upon it, does not simply reflect nitrate assimilation but also records (1) ammonium recycling in late summer and (2) microbial decomposition in winter. Here, we explore how these "non-nitrate-assimilation" processes might be reflected in the $\delta^{15}N$ of foraminifer shells accumulating in seafloor sediments.

The ability to reconstruct the degree of surface nitrate consumption from the $\delta^{15}N$ of exported PON relies on the mass balance condition: that all the N consumed by phytoplankton within the mixed layer is (eventually) exported as PON and does not accumulate indefinitely in the surface ocean or undergo substantial lateral export (as PON, ammonium, etc.) (Altabet & François, 1994; their Figure 9). The seasonal partitioning of ^{14}N and ^{15}N between different mixed-layer N pools does not violate this condition of mass balance, as long as it is applied on annual or longer timescales. A greater concern for sinking PON as a proxy for nitrate consumption is isotopic alteration of the organic matter in the water column or surface

129

sediments, which raises its $\delta^{15}N$ by 0-5‰ (François et al., 1992; Altabet & François, 1994; Thunell et al., 2004). The potential for climate-modulated, temporal variation in the degree of isotopic alteration makes this "diagenetic offset" (Altabet & François, 1994) particularly difficult to correct for (e.g., Martínez-García et al., 2014).

On the one hand, foraminifer shell-bound (not cytoplasm) organic matter is physically protected from bacterially mediated decay by the mineral matrix, thus mitigating the concern of diagenesis as shells sink through the water column and are incorporated into the sediments. Indeed, changes in shell-bound $\delta^{15}N$ from net tows to seafloor sediments are comparatively small (Ren et al., 2012), with an average increase of ~0.6‰ (Smart et al., 2018). On the other hand, foraminifera make up just one component of the total PON produced in and exported from the upper ocean and thus need not track the $\delta^{15}N$ of nitrate consumed annually (i.e., foraminifera are not constrained by the mass balance that applies to bulk sinking PON). Different species also peak in abundance at different times of year and may have different feeding preferences, depth habitats and lifespans, further complicating the picture.

In order to assess the influence of upper ocean N cycling on SAZ/PFZ foraminifera-bound $\delta^{15}N$ recorded in sediments, we combine our isotopic data with information on the relative contributions of late-summer and winter to annual foraminifer production. Our net tows provide a snapshot of mixed-layer foraminifer abundances, and from only two seasons. Furthermore, the presence of a species within the upper ocean does not require that its production and export are significant during the season of observation; the greatest fluxes of planktic foraminifera are observed during episodic mass flux events (Schiebel, 2002). We, therefore, look to sediment trap data for the seasonality of Southern Ocean foraminiferal flux, which are available from the western Pacific SAZ/PFZ (Honjo et al., 2000; Trull et al., 2001; King & Howard, 2001; King & Howard, 2003). Total mass flux and foraminiferal flux are generally lower in the SAZ and higher in the PFZ, with local maxima at the SAF (highest overall) and STF boundaries. Most traps in this region record a double peak in production, one early (in spring/midsummer) and one late (in mid/late-summer). In calculating the contribution of each season to the annual sinking flux, we take winter to be represented by the three-month period, either Jun-Jul-Aug (JJA) or Jul-Aug-Sep (JAS), depending on the site.

In the northern SAZ (45°S) east of New Zealand (just south of the STF), mass fluxes captured in a 1000 m trap (Nodder & Northcote, 2001) were dominated by spring (68% in SON), with

130

lower fluxes in midsummer (13% in DJF), late summer (5% in MAM) and winter (14% in JAS). Foraminiferal fluxes in the same collections appear largely consistent with the mass fluxes (King & Howard, 2001), but with a slight (~2 week) lag, contributing to lower foraminiferal fluxes for winter (~7%) and higher for late summer (~16%). In a collection from the central SAZ (47°S) south of Tasmania (King & Howard, 2003), spring (OND) contributed 15-22%, midsummer (JFM) contributed 34-37%, late summer (AMJ) contributed 39-42% and winter (JAS) contributed 6% to the annual total of foraminifera reaching 3800 m depth. At the SAF (51°S; 3100 m depth) and PFZ (54°S; 1500 m depth) sites south of Tasmania, the winter period was not captured, but low foraminiferal fluxes recorded in September (King & Howard, 2003) suggest an annual contribution of <6%. Total mass fluxes and inorganic carbon fluxes from a PFZ (57°S) sediment trap south of New Zealand (Honjo et al., 2000) suggest smaller contributions from late summer (9% and 13%, respectively; MAM) and winter (~1% for both; JJA) compared to the SAZ, with spring (27% and 33%, respectively; SON) and midsummer (63% and 53%, respectively; DJF) dominating the sinking flux at 1000 m.

Based on these data, the seasons in which internal mixed-layer N cycling dominates (late summer and winter) are the seasons that contribute the least to the annual total foraminifera sinking to the sediments in the PFZ. In the SAZ, winter production may contribute proportionally more shells to the sediments, but the effects of winter decomposition (on PON and foraminifer δ^{15}N) appear to be weaker here than in the PFZ mixed layer. Ammonium recycling, on the other hand, appears to be important, at least in the southern/central SAZ, and late-summer foraminifer fluxes can be substantial.
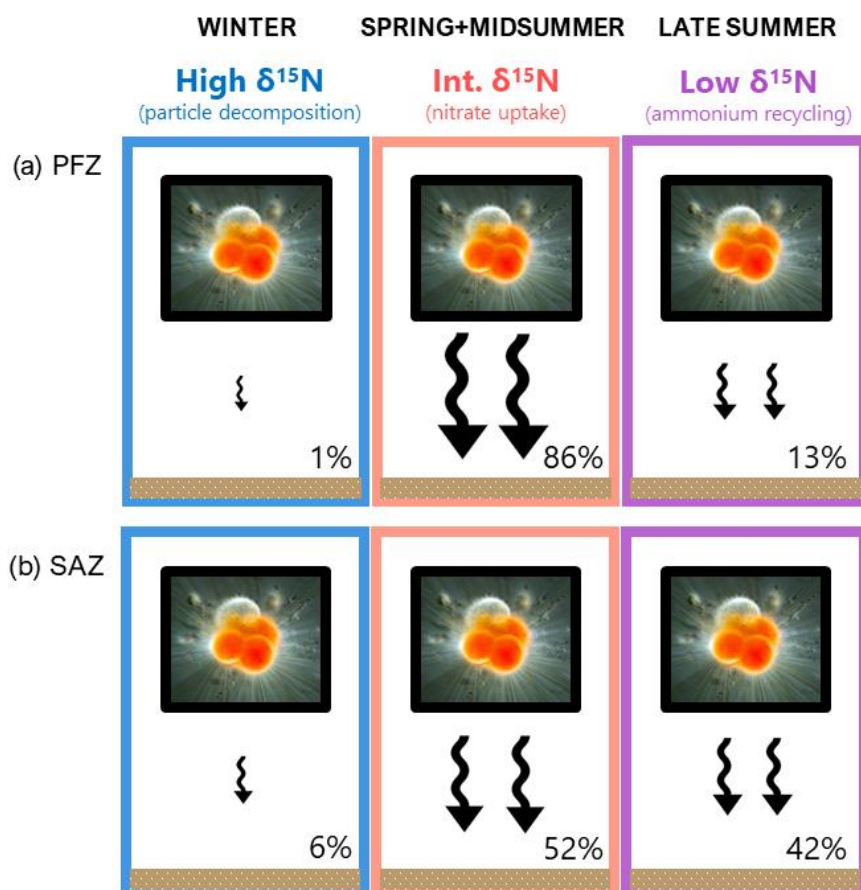
Fig. 3.8: Cartoon illustrating modern-day seasonal fluxes of foraminifer shells to the seafloor in (a) the PFZ and (b) the SAZ. Colours represent season (blue for winter, orange for spring+midsummer, purple for late summer), and arrow sizes illustrate the magnitude of the sinking shell flux. Percentage contributions to the annual total sinking flux are derived from sediment trap data from the western Pacific PFZ (Honjo et al., 2000) and SAZ (King & Howard, 2003).

To test the influence of these "peripheral" seasons on the $\delta^{15}N$ of the modern annual foraminifer flux, we calculate the expected $\delta^{15}N$ of a sediment sample from the PFZ where 86% of the foraminifera derive from spring plus midsummer, 13% derive from late summer and 1% derive from winter (based on the inorganic carbon fluxes of Honjo et al. (2000); illustrated by Fig. 3.8a). We repeat this exercise for the SAZ, assuming 52% of shells derive from spring plus midsummer, 42% are from late summer, and 6% are from winter (using the foraminiferal fluxes of King & Howard (2003); illustrated by Fig. 3.8b). In both cases, we use the overall SAZ/PFZ average foraminifer tissue $\delta^{15}N$ ("naturally weighted" towards the $\delta^{15}N$ of more abundant species; combining all the tissue $\delta^{15}N$ data from Table 3.1) as an approximation for the shell flux $\delta^{15}N$ in winter (5.4‰) and late summer (1.0‰), and estimate the spring+midsummer

132

foraminifer $\delta^{15}N$ as the average spring+midsummer PON $\delta^{15}N$ (orange and red symbols in Fig.7a) plus our average observed trophic elevation (Table 3.4) (i.e., 0.7 + 3.2 = 3.9‰). Presumably, the $\delta^{15}N$ of the foraminiferal flux corresponds to surface mixed layer conditions up to a month earlier, but we do not attempt to correct for this here.

From this calculation, we can develop a first sense of the degree to which winter and late-summer fluxes "skew" the sediment record away from the spring+midsummer nitrate consumption signal that we hope to reconstruct using foraminifer-bound $\delta^{15}N$. For the PFZ, the resulting sediment mixture has a $\delta^{15}N$ that is 0.4‰ lower than the $\delta^{15}N$ of the spring+midsummer shells alone. For the SAZ, the resulting mixture is 1.1‰ lower than the spring+midsummer $\delta^{15}N$. Perhaps a more realistic test is to use PFZ- and SAZ-specific ranges for the $\delta^{15}N$ of the foraminiferal flux in each season; 6.0 to 8.2‰ and 3.0 to 6.0‰ in winter, −0.8 to 1.8‰ and −0.6 to 3.6‰ in late summer, and 2.3 to 3.5‰ and 2.4 to 7.2‰ in spring+midsummer for the PFZ and SAZ, respectively. Using the same seasonal contributions as before, PFZ sediments are 0.2-0.4‰ lower and SAZ sediments are 1.2-1.6‰ lower than they would be if made up of spring+midsummer shells only (compare rows (a) with rows (b) in Table 3.5; or the colour difference between "Modern" and the top corners of the triangles in Fig. 3.9).

Table 3.5: Effects of varying seasonal contributions on the annual total foraminifer flux $\delta^{15}N$ in the PFZ and SAZ.

Note. For the foraminifer flux $\delta^{15}N$ ranges in each season, we use our measurements of tissue $\delta^{15}N$ where available (winter and late summer) and estimate the spring+summer range from PON $\delta^{15}N$ and the average trophic elevation as described in section 4.4. The average results are illustrated by Fig. 3.9.

* Modern PFZ seasonal flux contributions calculated from Honjo et al. (2000).

** Modern SAZ seasonal flux contributions calculated from King and Howard (2003).

Zone	Scenario	Spring+summer Foraminifer $\delta^{15}N$ (‰)	Contribution (%)	Late summer Foraminifer $\delta^{15}N$ (‰)	Contribution (%)	Winter Foraminifer $\delta^{15}N$ (‰)	Contribution (%)	Annual TOTAL Foraminifer $\delta^{15}N$ (‰)	Contribution (%)
PFZ	(a) Modern*	2.3-3.5	86	−0.8-1.8	13	6.0-8.2	1	**1.9-3.3**	100
	(b) Only spring+summer	2.3-3.5	100	-	0	-	0	**2.3-3.5**	100
	(c) No winter	2.3-3.5	87	−0.8-1.8	13	-	0	**1.9-3.3**	100
	(d) No late-summer	2.3-3.5	99	-	0	6.0-8.2	1	**2.3-3.6**	100
	(e) No spring+summer	-	0	−0.8-1.8	93	6.0-8.2	7	**−0.3-2.3**	100
SAZ	(a) Modern**	2.4-7.2	52	−0.6-3.6	42	3.0-6.0	6	**1.2-5.6**	100
	(b) Only spring+summer	2.4-7.2	100	-	0	-	0	**2.4-7.2**	100
	(c) No winter	2.4-7.2	55	−0.6-3.6	45	-	0	**1.1-5.6**	100
	(d) No late-summer	2.4-7.2	90	-	0	3.0-6.0	10	**2.5-7.1**	100
	(e) No spring+summer	-	0	−0.6-3.6	88	3.0-6.0	13	**−0.2-3.9**	100

The results confirm that, under today's conditions, the effect of non-nitrate-assimilation processes (i.e., mixed-layer N cycling) is greater in the SAZ (Fig. 3.9b) than in the PFZ (Fig. 3.9a). The lowered $\delta^{15}N$ for both PFZ and SAZ sediments suggest that, on balance, late-summer ammonium recycling (which acts to lower shell-assemblage $\delta^{15}N$; compare rows (a) with rows (d)) has a stronger influence on the sediments than does winter decomposition (which acts to raise shell-assemblage $\delta^{15}N$; compare rows (a) with rows (c)). In general, under modern conditions, the two processes oppose each other in their $\delta^{15}N$ effects, and the winter shell flux is minor. In summary, these preliminary calculations suggest that seasonality influences the annually averaged value of foraminifer-bound $\delta^{15}N$ so as to underpredict the degree of nitrate consumption. However, such a seasonality-induced bias only affects paleoceanographic reconstructions of changes in the degree of nitrate consumption if this seasonality has changed over time.
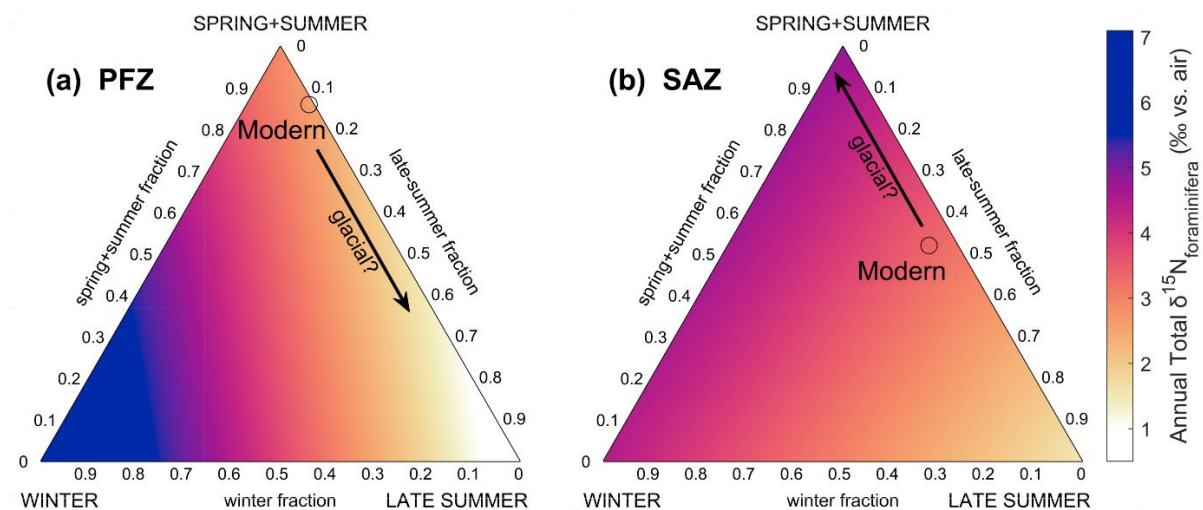
Fig. 3.9: Ternary diagrams illustrating the effects of varying seasonal contributions (and their associated $\delta^{15}N$ values) to the $\delta^{15}N$ of annually accumulated foraminifera in (a) PFZ and (b) SAZ sediments. The black circle indicates the modern situation (based on seasonal flux data from sediment traps in the western Pacific SAZ/PFZ), and the black arrow indicates the approximate direction of change we might expect during glacial periods. This figure was created using the MATLAB routine "ternplot" (Sandrock & Afshari, 2016) and the colourmap of Kovesi (2015).

Accordingly, we consider briefly how changes in the seasonality of the Southern Ocean N cycle over the glacial-interglacial transition could affect the foraminifer-bound $\delta^{15}N$ change observed in the sediment record. In the AZ, a reduced supply of nitrate (and iron) to surface waters during

134

glacial periods (François et al., 1997; Kemeny et al., 2018) could lead to an earlier switch to ammonium-based phytoplankton production in the Southern Ocean than occurs today (Studer et al., 2015). It is possible that this would then increase the contribution of "late-summer-like" foraminifera (with a low $\delta^{15}N$) to the total shell assemblage in PFZ sediments during ice ages (approximate direction indicated by the arrow in Fig. 3.9a). Indeed, under today's conditions, our data imply a larger $\delta^{15}N$ offset between foraminifera and nitrate consumed in subpolar surface waters (1.7±0.8; n = 12) than in the subtropics (0.2±0.2; n = 10) (right hand columns in Table 3.4). This appears to stem largely from a lower $\delta^{15}N$ for bulk PON relative to nitrate consumed in the Sargasso Sea, consistent with a greater dependence on ammonium by autotrophs in this subtropical ecosystem. Under the much lower nitrate supply rates calculated for the glacial Antarctic Zone (Kemeny et al., 2018; Studer et al., 2015), Antarctic PON may adopt $\delta^{15}N$ relationships more similar to the modern Sargasso Sea; that is, becoming lower relative to the $\delta^{15}N$ of nitrate consumed in surface waters (Table 3.4). The effect on a foraminifer-bound $\delta^{15}N$ record from the PFZ would be to damp the glacial-interglacial signal, leading to underestimation of the ice-age enhancement of nitrate drawdown in polar waters.

In contrast, enhanced iron bearing-dust deposition to the glacial SAZ may prolong nitrate-based production at these latitudes (Martin, 1990; Martínez-García et al., 2014), increasing the proportion of "spring/midsummer-like" shells that more strongly follow nitrate consumption (approximate direction indicated by the arrow in Fig. 3.9b). The effect on a foraminifer-bound $\delta^{15}N$ record from the SAZ would thus be to amplify the glacial-interglacial signal, leading to overestimation of the ice-age enhancement of nitrate drawdown in subpolar waters. For example, in the case of the *G. bulloides* $\delta^{15}N$ record from the Atlantic SAZ (site ODP1090; Martínez-García et al., 2014), part of the 3-4‰ rise in glacial-age shells could be explained by a reduction in ammonium-supported production compared to today. To place an upper bound on this effect, we consider the end-member case of zero ammonium recycling in the ice-age SAZ. We estimate the $\delta^{15}N$ of modern *G. bulloides* shells in spring+midsummer from the bulk PON $\delta^{15}N$ in the northern SAZ (red symbols in Fig. 3.7a) plus our average observed trophic elevation for *G. bulloides* (Table 3.4) (i.e., ~5 + 3.1 ≈ 8.1‰). The result is ~1.4‰ higher than the measured $\delta^{15}N$ of *G. bulloides* in surface sediments at ODP1090 (6.7‰), which integrates over all seasons. Therefore, "correcting" this paleo-record for the ammonium recycling effect (which lowers the measured $\delta^{15}N$ of *G. bulloides* during interglacials but, in this endmember case, not during ice ages) would reduce the observed amplitude of the 3-4‰ glacial-interglacial

signal by ~1-2‰ at most. This would leave the remaining (2-3‰) ice-age elevation in foraminifer-bound δ^{15}N to be explained by enhanced nitrate drawdown.

While climate-driven change in N cycling seasonality may appear to present a concern, there would seem to be limits to its impact on foraminifer-bound δ^{15}N records. The PON, ammonium, and dissolved organic N in Southern Ocean surface waters ultimately derives from the assimilation of nitrate. Thus, the availability of both ammonium for late-summer assimilation and of PON for wintertime degradation are tied to nitrate assimilation-sourced biological production in the preceding spring and summer seasons. Given this, the annually integrated proportions of foraminifera recording the low-δ^{15}N late-summer signal or high-δ^{15}N winter signal, relative to the quantity of foraminifera recording the spring+summer PON signal of nitrate consumption, may well be highly conserved over time. Furthermore, much of the low-δ^{15}N ammonium released during wintertime PON degradation (Lehmann et al., 2002) will ultimately be re-assimilated by phytoplankton in the following spring/summer, either directly as ammonium (Elskens et al., 2002; Glibert et al., 1982) or after nitrification to nitrate within the winter mixed layer (Smart et al., 2015), and likely help to balance the high-δ^{15}N of winter PON on an annual basis. These considerations argue against major changes in foraminifer-bound δ^{15}N over time that are independent of changes in the degree of nitrate consumption. Nevertheless, this remains to be tested, and foraminifer-bound δ^{15}N paleo-records from the Southern Ocean would clearly benefit from an improved understanding of upper-ocean particle dynamics in polar and subpolar waters.

To better constrain changes in the seasonality of the Southern Ocean N cycle, the use of multi-species foraminifer-bound δ^{15}N records may prove helpful. Sediment traps from the Pacific sector and other regions suggest a consistent seasonal succession of species for the Southern Ocean region between the STF and the PF possibly driven, at least in part, by mixed-layer depth through its influence on food availability near the surface (King & Howard, 2001; King & Howard, 2003). For example, the high abundance of *G. bulloides* in springtime sinking fluxes and its close association with the chlorophyll maximum (Mortyn & Charles, 2003) suggest that this species may best record the initial drawdown of nitrate during the growing season. *N. pachyderma* and *N. incompta* have been found to dominate midsummer foraminiferal fluxes in the Pacific PFZ and SAZ, respectively (King & Howard, 2001; King & Howard, 2003), suggesting that these species may well represent midsummer conditions in the Southern Ocean. In the case of site ODP1090 in the northern SAZ, a constant δ^{15}N offset

between *G. bulloides* and *O. universa* suggests that the $\delta^{15}N$ relationship between *G. bulloides* and assimilated nitrate has not changed appreciably through time (Martínez-García et al., 2014). In addition, coral-bound $\delta^{15}N$ records from across the SAZ (south of Tasmania and in the Drake Passage; Wang et al., 2017) exhibit a similar amplitude of glacial/interglacial $\delta^{15}N$ change to (and a relatively constant offset from) the foraminifer-bound $\delta^{15}N$ records at ODP1090. Deep sea corals rely on the flux of sinking PON into deep waters. There is no clear mechanism for their $\delta^{15}N$ to be biased by changes in the seasonality of the $\delta^{15}N$ of sinking PON, especially because corals appear to feed on suspended PON, which is produced over time from sinking PON (Wang et al., 2014). The agreement between $\delta^{15}N$ proxies provides further support for scaling of seasonal signals through glacial-interglacial transitions, at least in the SAZ.

5. Conclusions

The N isotopes have been explored extensively as a tool for reconstructing the degree of nitrate consumption in the Southern Ocean, especially over glacial/interglacial cycles. The sinking flux out of the euphotic zone is an excellent target for $\delta^{15}N$ reconstruction because, regardless of upper ocean ammonium cycling, the total N sinking out of the euphotic zone is constrained by mass balance to approximate the $\delta^{15}N$ of the nitrate consumed in the euphotic zone (Altabet & François, 1994). This mass balance helped to motivate the early focus on bulk sedimentary N as a record of the $\delta^{15}N$ of sinking N in the past. Since then, however, the evidence for variable diagenetic alteration of bulk sediment $\delta^{15}N$ has driven the field to explore N protected within the mineral matrix of microfossils and fossils, including diatoms, deep sea corals, and planktic foraminifera. While the total N sinking out of the euphotic zone is constrained by mass balance to approximate the $\delta^{15}N$ of the N supply to the euphotic zone, this does not apply to any sub-fraction of the sinking N, including N contained within planktic fossils. For such proxies, modern ocean ground-truthing is particularly important to understand the degrees to which the proxies record nitrate consumption and other N cycling processes at work in the surface ocean.

The data reported here support the utility of planktic foraminifera as recorders of nitrate consumption, but they also indicate the potential for lower-productivity periods to influence the $\delta^{15}N$ of foraminifer shells. Foraminifer $\delta^{15}N$ is more closely tied to the $\delta^{15}N$ of PON than to that of dissolved nitrate, consistent with foraminifera acquiring most (if not all) of their N

from their diet. Our sampling periods included the late summer and the winter. While the degree of nitrate consumption influences the $\delta^{15}N$ of PON throughout the year (Altabet & François, 2001; Lourey et al., 2003), during the periods that we investigated, other processes are also important. In the late-summer, bulk particles and the foraminifera that feed upon them also reflect ammonium recycling, lowering their $\delta^{15}N$; in the winter, particle decomposition raises their $\delta^{15}N$. In terms of their influence on the $\delta^{15}N$ of foraminifera sinking to the seafloor each year, late-summer ammonium recycling appears to outweigh wintertime decomposition. Both signals are likely weak compared to that of the productive spring/mid-summer (which dominates the present-day sinking flux) when bulk particle $\delta^{15}N$ and nitrate consumption are most tightly linked. This dominance of the nitrate consumption signal in the early and mid-summer must be tested in future work by sampling at these times of year.

Departure from the current mode of seasonality in past climates (e.g., a more extended or intense ammonium recycling period during ice ages) would complicate the inference of nitrate consumption from downcore changes in fossil foraminifer $\delta^{15}N$. However, all PON in surface waters ultimately derives from the assimilation of nitrate, such that the productivity of the seasons with distinct N cycling probably scale with the amount of nitrate consumed. If so, there would be limited capacity for the $\delta^{15}N$ of foraminifera shells accumulated in deep sea sediments to be decoupled from the isotope dynamics of nitrate assimilation. Nevertheless, a more complete view of how the different seasons contribute to the annual, flux-weighted $\delta^{15}N$ of foraminifera is needed to better gauge the importance of the "non-nitrate" signal.

The ecological diversity among planktic foraminifer species could hold the key to disentangling changes in nitrate consumption from changes in the seasonal cycle. Since different species occupy specific (sometimes overlapping) depth, seasonal and trophic niches in their environment, there is potential for detailed reconstructions from multi-species foraminifer-bound $\delta^{15}N$ records. Tapping into this capability would require a comprehensive understanding of both the common and species-specific $\delta^{15}N$ signals recorded in foraminifer shell-bound organic matter. More field studies akin to the present one would serve this goal. Among the aspects called for in such future work is a great need to sample the Southern Ocean for foraminifera during the early-to-mid-summer productive period, rather than after it, as was the case in this study.

6. Acknowledgements

7. References

Altabet, M.A. 1988. Variations in nitrogen isotopic composition between sinking and suspended particles: Implications for nitrogen cycling and particle transformation in the open ocean. *Deep-Sea Res. Pt I*, **35**, 535–554.

Altabet, M.A., & François, R. 1994. Sedimentary nitrogen isotopic ratio as a recorder for surface ocean nitrate utilization. *Global Biogeochem. Cycles*, **8**(1), 103–116.

Altabet, M.A., & François, R. 2001. Nitrogen isotope biogeochemistry of the Antarctic Polar Frontal Zone at 170°W. *Deep-Sea Res. Pt II*, **48**, 4247–4273.

Altabet, M.A., & McCarthy, J.J. 1986. Vertical patterns in ^{15}N natural abundance in PON from the surface waters of warm-core rings. *J. Mar. Res.*, **44**, 185–201.

Altabet, M.A., & Small, L.F. 1990. Nitrogen isotopic ratios in fecal pellets produced by marine zooplankton. *Geochim. Cosmochim. Acta*, **54**, 155–163.

Altabet, M.A., Deuser, W.G., Honjo, S., & Stienen, S. 1991. Seasonal and depth-related changes in the source of sinking particles in the N. Atlantic. *Nature*, **354**, 136–139.

Anderson, O.R., Spindler, M., Bé, A.W.H., & Hemleben, C. 1979. Trophic activity of planktonic foraminifera. *J. Mar. Biol. Assoc. U. K.*, **59**(3), 791–799.

Bé, A.W.H. 1977. *Oceanic Micropaleontology*. Vol. 1. Academic Press, London. Chap. An ecological, zoogeographic and taxonomic review of recent planktonic foraminifera., page 1–100.

Bé, A.W.H., & Hemleben, C. 1970. Calcification in a living planktonic foraminifer, Globigerinoides sacculifer (BRADY). *N. Jb. Geol. Paläont. Abh.*, **134**(3), 221–234.

Bé, A.W.H., Hemleben, C., Anderson, O.R., Spindler, M., Hacunda, J., & Tuntivate-Choy, S. 1977. Laboratory and Field Observations of Living Planktonic Foraminifera. *Micropaleontology*, **23**(2), 155–179.

Bé, A.W.H., Hemleben, C., Anderson, O.R., & Spindler, M. 1979. Chamber formation in planktonic Foraminifera. **25**(3), 294–307.

Belkin, I.M., & Gordon, A.L. 1996. Southern Ocean fronts from the Greenwich meridian to Tasmania. *J. Geophys. Res.*, **101**(C2), 3675–3696.

Bird, C., Darling, K.F., Russell, A.D., Davis, C.V., Fehrenbacher, J., Free, A., Wyman, M., & Ngwenya, B.T. 2017. Cyanobacterial endobionts within a major marine planktonic calcifier (Globigerina bulloides, Foraminifera) revealed by 16S rRNA metabarcoding. *Biogeosciences*, **14**, 901–920.

Bird, C., Darling, K.F., Russell, A.D., Fehrenbacher, J.S., Davis, C.V., Free, A., & Ngwenya, B.T. 2018. 16S rRNA gene metabarcoding and TEM reveals different ecological strategies within the genus Neogloboquadrina (planktonic foraminifer). *PLoS ONE*, **13**(1), e0191653.

Braman, R.S., & Hendrix, S.A. 1989. Nanogram nitrite and nitrate determination in environmental and biological materials by Vanadium(III) reduction with chemiluminescence detection. *Anal. Chem.*, **61**, 2715–2718.

Buitenhuis, E.T., Vogt, M. and, Moriarty R., Bednaršek, N., Doney, S.C., Leblanc, K., Le Quéré, C., Y.-W., Luo, O'Brien, C., O'Brien, T., Peloquin, J., Schiebel, R., & Swan, C. 2013. MAREDAT: towards a world atlas of MARine Ecosystem DATa. *Earth Syst. Sci. Data*, **5**, 227–239.

Campbell, E. 2016. *Where Three Oceans Meet: Nitrate Isotope Measurements from the South Atlantic Along 34.5°S*. Senior Thesis.

Casciotti, K.L., Sigman, D.M., Galanter Hastings, M., Böhlke, J.K., & Hilkert, A. 2002. Measurement of the Oxygen Isotopic Composition of Nitrate in Seawater and Freshwater Using the Denitrifier Method. *Anal. Chem.*, **74**, 4905–4912.

Checkley, D.M., & Miller, C.A. 1989. Nitrogen isotope fractionation by oceanic zooplankton. *Deep-Sea Res. Pt A*, **36**, 1449–1456.

Darling, K.F., & Wade, C.M. 2008. The genetic diversity of planktic foraminifera and the global distribution of ribosomal RNA genotypes. *Mar. Micropaleontol.*, **67**, 216–238.

de Boyer Montégut, C., Madec, G., Fischer, A.S., Lazar, A., & Iudicone, D. 2004. Mixed layer depth over the global ocean: An examination of profile data and a profile-based climatology. *J. Geophys. Res.*, **109**(C12003).

Decelle, J., Colin, S., & Foster, R.A. 2015. *Marine Protists*. Springer, Tokyo. Chap. Photosymbiosis in Marine Planktonic Protists, pages 465–500.

DiFiore, P.J., Sigman, D.M., Trull, T.W., Lourey, M.J., Karsh, K., Cane, G., & Ho, R. 2006. Nitrogen isotope constraints on Subantarctic biogeochemistry. *J. Geophys. Res.*, **111**(C08016).

DiFiore, P.J., Sigman, D.M., Karsh, K.L., Trull, T.W., Dunbar, R.B., & Robinson, R.S. 2010. Poleward decrease in the isotope effect of nitrate assimilation across the Southern Ocean. *Geophys. Res. Lett.*, **37**(L17601).

Elskens, M., Baeyens, W., Cattaldo, T., Dehairs, F., & Griffiths, B. 2002. N uptake conditions during summer in the Subantarctic and Polar Frontal Zones of the Australian sector of the Southern Ocean. *Journal of Geophysical Research Oceans*, **107**(11), 3182.

Faber, W.W., Anderson, O.R., Lindsey, J.L., & Caron, D.A. 1988. Algal-foraminiferal symbiosis in the planktonic foraminifer Globigerinella aequilateralis: I. Occurrence and stability of two mutually exclusive chrysophyte endosymbionts and their ultrastructure. *J. Foramin. Res.*, **18**, 334–343.

François, R., Altabet, M.A., & Burckle, L.H. 1992. Glacial to interglacial changes in surface nitrate utilization in the Indian sector of the Southern Ocean as recorded by sediment δ^{15}N. *Paleoceanography*, **7**(5), 589–606.

François, R., Altabet, M.A., Yu, E.F., Sigman, D.M., Bacon, M.P., Frank, M., Bohrmann, G., Bareille, G., & Labeyrie, L.D. 1997. Contribution of Southern Ocean surface-water stratification to low atmospheric CO_2 concentrations during the last glacial period. *Nature*, **389**, 929–935.

Fripiat, F., Martínez-García, A., Fawcett, S.E., Kemeny, P.C., Studer, A.S., Smart, S.M., Rubach, F., Oleynik, S., Sigman, D.M., & Haug, G.H. 2019. The isotope effect of nitrate assimilation in the Antarctic Zone: Improved estimates and paleoceanographic implications. *Geochimica et Cosmochimica Acta*.

Garcia, H. E., Locarnini, R.A., Boyer, T.P., Antonov, J.I., Baranova, O.K., Zweng, M.M., Reagan, J.R., & Johnson, D.R. 2014. World Ocean Atlas 2013, Volume 4: Dissolved Inorganic Nutrients (phosphate, nitrate, silicate). S. Levitus, Ed., A. Mishonov Technical Ed.; NOAA Atlas NESDIS 76, 25 pp.

Gastrich, M. D. 1987. Ultrastructure of a new intracellular symbiotic alga found within planktonic foraminifera. *J. Phycol.*, **23**, 623–632.

Glibert, P.M., Biggs, D.C., & McCarthy, J.J. 1982. Utilization of ammonium and nitrate during austral summer in the Scotia Sea. *Deep Sea Res. Part I*, **29**, 837–850.

Granger, J., & Sigman, D.M. 2009. Removal of nitrite with sulfamic acid for nitrate N and O isotope analysis with the denitrifier method. *Rapid Commun. Mass Spectrom.*, **23**, 3753–3762.

Gruber, N., & Sarmiento, J.L. 1997. Global patterns of marine nitrogen fixation and denitrification. *Global Biogeochem. Cycles*, **11**(2), 235–266.

Hannides, C.C.S., Popp, B.N., Choy, C.A., & Drazen, J.C. 2013. Midwater zooplankton and suspended particle dynamics in the North Pacific Subtropical Gyre: A stable isotope perspective. *Limnol. Oceanogr.*, **58**(6), 1931–1946.

Hemleben, C., Spindler, M., Breitinger, I., & Deuser, W.G. 1985. Field and laboratory studies on the ontogeny and ecology of some globorotaliid species from the Sargasso Sea off Bermuda. *J. Foramineferal Res.*, **15**(4), 254–272.

Hemleben, C., Spindler, M., & Anderson, O.R. 1989. *Modern Planktonic Foraminifera*. Springer-Verlag.

Holliday, N.P., & Read, J.F. 1998. Surface oceanic fronts between Africa and Antarctica. *Deep-Sea Res. Pt I*, **45**, 217–238.

Honjo, S., Francois, R., Manganini, S., Dymond, J., & Collier, R. 2000. Particle fluxes to the interior of the Southern Ocean in the Western Pacific sector along 170°W. *Deep Sea Res. Part II*, **47**, 3521– 3548.

Joubert, W.R., Thomalla, S.J., Waldron, H.N., Lucas, M.I., Boye, M., Le Moigne, F.A.C., Planchon, F., & Speich, S. 2011. Nitrogen uptake by phytoplankton in the Atlantic

sector of the Southern Ocean during late austral summer. *Biogeosciences*, **8**, 2947–2959.

Kemeny, P.C., Weigand, M.A., Zhang, R., Carter, B.R., Karsh, K.L., Fawcett, S.E., & Sigman, D.M. 2016. Enzyme-level interconversion of nitrate and nitrite in the fall mixed layer of the Antarctic Ocean. *Global Biogeochem. Cycles*, **30**, 1069–1085.

Kemeny, P.C., Kast, E.R., Hain, M.P., Fawcett, S.E., Fripiat, F., Studer, A.S., Martínez-García, A., Haug, G.H., & Sigman, D.M. 2018. A Seasonal Model of Nitrogen Isotopes in the Ice Age Antarctic Zone: Support for Weakening of the Southern Ocean Upper Overturning Cell. *Paleoceanography and Paleoclimatology*.

King, A.L., & Howard, W.R. 2001. Seasonality of foraminiferal flux in sediment traps at Chatham Rise, SW Pacific: Implications for paleotemperature estimates. *Deep Sea Res. Part I*, **48**, 1687– 1708.

King, A.L., & Howard, W.R. 2003. Planktonic foraminiferal flux seasonality in Subantarctic sediment traps: A test for paleoclimate reconstructions. *Paleoceanography*, **18**(1), 1019.

King, K., Jr., & Hare, P.E. 1972. Amino Acid Composition of the Test as a Taxonomic Character for Living and Fossil Planktonic Foraminifera. *Micropaleontology*, **18**(3), 285–293.

Knapp, A.N., Sigman, D.M., & Lipschultz, F. 2005. N isotopic composition of dissolved organic nitrogen and nitrate at the Bermuda Atlantic Time-series Study site. *Global Biogeochem. Cycles*, **19**, 1–15.

Knox, F., & McElroy, M.B. 1984. Changes in atmospheric CO_2: influence of the marine biota at high latitude. *J. Geophys. Res.*, **89**, 4629–4637.

Koike, I., Holm-Hansen, O., & Biggs, D.C. 1986. Inorganic nitrogen metabolism by Antarctic phytoplankton with special reference to ammonium cycling. *Mar. Ecol. Prog. Ser.*, **30**, 105–116.

Kovesi, P. 2015. Good Colour Maps: How to Design Them. *CoRR*, **abs/1509.03700**.

Lehmann, M.F., Bernasconi, S.M., Barbieri, A., & McKenzie, J.A. 2002. Preservation of organic matter and alteration of its carbon and nitrogen isotope composition during simulated and in situ early sedimentary diagenesis. *Geochim. Cosmochim. Acta*, **66**(20), 3573–3584.

Lourey, M.J., Trull, T.W., & Sigman, D.M. 2003. Sensitivity of $\delta^{15}N$ of nitrate, surface suspended and deep sinking particulate nitrogen to seasonal nitrate depletion in the Southern Ocean. *Global Biogeochem. Cycles*, **17**(3), 1–18.

Lutjeharms, J.R.E., & Valentine, H.R. 1984. Southern Ocean thermal fronts south of Africa. *Deep-Sea Research*, **31**, 1461–1475.

Martin, J.H. 1990. Glacial-interglacial CO_2 Change: The Iron Hypothesis. *Paleoceanography*, **5**(1), 1–13.

Martínez-García, A., Sigman, D.M., Ren, H., Anderson, R.F., Straub, M., Hodell, D.A., Jaccard, S.L., Eglinton, T.I., & Haug, G.H. 2014. Iron Fertilization of the Subantarctic Ocean During the Last Ice Age. *Science*, **343**, 1347–1350.

Martiny, A.C., Vrugt, J.A., & Lomas, M.W. 2014. Concentrations and ratios of particulate organic carbon, nitrogen, and phosphorus in the global ocean. *Sci. Data*, **1**(140048).

McCartney, M.S. 1977. *A Voyage of Discovery: George Deacon 70th Anniversary Volume*. Supplement to Deep-Sea Research. Pergamon Press, Oxford. Chap. Subantarctic Mode Water, pages 103–119.

McNeil, B.I., Matear, R.J., & Tilbrook, B. 2001. Does carbon 13 track anthropogenic CO_2 in the Southern Ocean? *Global Biogeochem. Cycles*, **15**, 597–613.

Meilland, J., Siccha, M., Weinkauf, M.F.G., Jonkers, L., Morard, R., Baranowski, U., Baumeister, A., Bertlich, J., Brummer, G.-J., Debray, P., Fritz-Endres, T., Groeneveld, J., Magerl, L., Munz, P., Rillo, M.C., Schmidt, C., Takagi, H., Theara, G., & Kucera, M. 2019. Highly replicated sampling reveals no diurnal vertical migration but stable species-specific vertical habitats in planktonic foraminifera. *J. Plankton Res.*, **0**(0), 1–15.

Minagawa, M., & Wada, E. 1984. Stepwise enrichment of 15N along food chains: Further evidence and the relation between d15N and animal age. *Geochim. Cosmochim. Acta*, **48**, 1135–1140.

Möbius, J. 2013. Isotope fractionation during nitrogen remineralization (ammonification): Implications for nitrogen isotope biogeochemistry. *Geochim. Cosmochim. Acta*, **105**, 422–432.

Mortyn, P.G., & Charles, C.D. 2003. Planktonic foraminiferal depth habitat and $\delta^{18}O$ calibrations: Plankton tow results from the Atlantic sector of the Southern Ocean. *Paleoceanography*, **18**(2), 1–14.

Nodder, S.D., & Northcote, L.C. 2001. Episodic particulate fluxes at southern temperate midlatitudes (42–45°S) in the Subtropical Front region, east of New Zealand. *Deep Sea Res. Part I*, **48**(3), 833–864.

Nowlin, W.D., & Klinck, J.M. 1986. The Physics of the Antarctic Circumpolar Current. *Rev. Geophys.*, **24**(3), 469–491.

Nydahl, F. 1978. On the peroxodisulphate oxidation of total nitrogen in waters to nitrate. *Water Res.*, **12**, 1123–1130.

Pennock, J.R., Velinsky, D.J., Ludlam, J.M., Sharp, J.H., & Fogel, M.L. 1996. Isotope fractionation of ammonium and nitrate during their uptake by Skeletonema Costatum: Implications for the δ^{15}N dynamics under bloom conditions. *Limnol. Oceanogr.*, **41**(3), 451–459.

Qi, H., Coplen, T.B., Geilmann, H., Brand, W.A., & Böhlke, J.K. 2003. Two new organic reference materials for δ^{13}C and δ^{15}N measurements and a new value for the δ^{13}C of NBS 22 oil. *Rapid Commun. Mass Spectrom.*, **17**, 2483–2487.

Rafter, P.A., Sigman, D.M., Charles, C.D., Kaiser, J., & Haug, G.H. 2012. Subsurface tropical Pacific nitrogen isotopic composition of nitrate: Biogeochemical signals and their transport. *Global Biogeochem. Cycles*, **26**(GB1003), 1–14.

Rafter, P.A., DiFiore, P.J., & Sigman, D.M. 2013. Coupled nitrate nitrogen and oxygen isotopes and organic matter remineralization in the Southern and Pacific Oceans. *J. Geophys. Res.*, **118**, 4781–4794.

Ren, H., Sigman, D.M., Meckler, A.N., Plessen, B., Robinson, R.S., Rosenthal, Y., & Haug, G.H. 2009. Foraminiferal Isotope Evidence of Reduced Nitrogen Fixation in the Ice Age Atlantic Ocean. *Science*, **323**, 244–248.

Ren, H., Sigman, D.M., Thunell, R.C., & Prokopenko, M.G. 2012. Nitrogen isotopic composition of planktonic foraminifera from the modern ocean and recent sediments. *Limnol. Oceanogr.*, **57**(4), 1011–1024.

Robinson, R.S., Brunelle, B.G., & Sigman, D.M. 2004. Revisiting nutrient utilization in the glacial Antarctic: evidence from a new diatom-bound N isotope method. *Paleoceanography*, **19**(PA3001), 1–13.

Saino, T., & Hattori, A. 1980. ^{15}N natural abundance in oceanic suspended particulate matter. *Nature*, **283**, 752–754.

Sambrotto, R.N., & Mace, B.J. 2000. Coupling of biological and physical regimes across the Antarctic Polar Front as reflected by nitrogen production and recycling. *Deep Sea Res. Part II*, **47**(15-16), 3339–3367.

Sandrock, C., & Afshari, S. 2016. Plot ternary diagrams in MATLAB. [Data set].

Sarmiento, J.L., & Toggweiler, J.R. 1984. A new model for the role of the oceans in determining atmospheric pCO$_2$. *Nature*, **308**, 621–624.

Schiebel, R. 2002. Planktic foraminiferal sedimentation and the marine calcite budget. *Global Biogeochem. Cycles*, **16**(4), 1–21.

Schiebel, R., & Hemleben, C. 2017. *Planktic Foraminifers in the Modern Ocean*. Springer-Verlag Berlin Heidelberg.

Schiebel, R., Waniek, J., Zeltner, A., & Alves, M. 2002. Impact of the Azores Front on the distribution of planktic foraminifers, shelled gastropods, and coccolithophorids. *Deep-Sea Res. Pt II*, **49**, 4035–4050.

Siccha, M., Schiebel, R., Schmidt, S., & Howa, H. 2012. Short-term and small-scale variability in planktic foraminifera test flux in the Bay of Biscay. *Deep-Sea Res. Pt I*, **64**, 146–156.

Siegenthaler, U., & Wenk, T. 1984. Rapid atmospheric CO$_2$ variations and ocean circulation. *Nature*, **308**, 624–626.

Sigman, D.M., Altabet, M.A., McCorkle, D.C., François, R., & Fischer, G. 1999a. The δ^{15}N of nitrate in the Southern Ocean: Consumption of nitrate in surface waters. *Global Biogeochem. Cycles*, **13**(4), 1149–1166.

Sigman, D.M., Altabet, M.A., François, R., McCorkle, D.C., & Gaillard, J.F. 1999b. The isotopic composition of diatom-bound nitrogen in Southern Ocean sediments. *Paleoceanography*, **14**(2), 118–134.

Sigman, D.M., Altabet, M.A., McCorkle, D.C., François, R., & Fischer, G. 2000. The δ^{15}N of nitrate in the Southern Ocean: Nitrogen cycling and circulation in the ocean interior. *J. Geophys. Res.*, **105**(C8), 19599–19614.

Sigman, D.M., Casciotti, K.L., Andreani, M., Barford, C., Galanter, M., & Böhlke, J.K. 2001. A Bacterial Method for the Nitrogen Isotopic Analysis of Nitrate in Seawater and Freshwater. *Anal. Chem.*, **73**, 4145–4153.

Sinyanya, K.Y., Parrott, R.G., Flynn, R.F., Walker, D.R., Ryu, Y., Sigman, D.M., & Fawcett, S.E. 2020 (February). *The Agulhas Current enhances the productivity of the subtropical*

Indian Ocean: evidence from coupled flow cytometry-high sensitivity nitrogen isotope analysis. Ocean Sciences Meeting. American Geophysical Union.

Smart, S.M. 2014. *Wintertime nitrate isotope dynamics in the Atlantic sector of the Southern Ocean*. M.Phil. thesis, University of Cape Town, South Africa.

Smart, S.M., Fawcett, S.E., Thomalla, S.J., Weigand, M.A., Reason, C.J.C., & Sigman, D.M. 2015. Isotopic evidence for nitrification in the Antarctic winter mixed layer. *Global Biogeochem. Cycles*, **29**.

Smart, S.M., Ren, H., Fawcett, S.E., Schiebel, R., Conte, M., Rafter, P.A., Ellis, K.K., Weigand, M.A., Sigman, D.M., & Haug, G.H. 2018. Ground-truthing the planktic foraminifer-bound nitrogen isotope paleo-proxy in the Sargasso Sea. *Geochim. Cosmochim. Acta*, **235**, 463–482.

Speer, K., Rintoul, S.R., & Sloyan, B. 2000. The diabatic Deacon cell. *J. Phys. Oceanogr.*, **30**, 3212–3222.

Spero, H. 1987. SYMBIOSIS IN THE PLANKTONIC FORAMINIFER, ORBULINA UNIVERSA, AND THE ISOLATION OF ITS SYMBIOTIC DINOFLAGELLATE, GYMNODINIUM BÉII SP. NOV.1. *J. Phycol.*, **23**, 307–317.

Spero, H.J. 1988. Ultrastructural examination of chamber morphogenesis and biomineralization in the planktonic foraminifer Orbulina universa. *Mar. Biol.*, **99**(1), 9–20.

Spero, H.J., & Angel, D.L. 1991. Planktonic sarcodines: microhabitat for oceanic dinoflagellates. *J. Phycol.*, **27**, 187–195.

Spindler, M., Hemleben, C., Salomons, J., & Smit, L. 1984. Feeding behavior of some planktonic foraminifers in laboratory cultures. *J. Foramin. Res.*, **14**(4), 237–249.

Stoecker, D.K., Johnson, M.D., de Vargas, C., & Not, F. 2009. Acquired phototrophy in aquatic protists. *Aquat. Microb. Ecol.*, **57**(3), 279–310.

Stoecker, D.K., Hansen, P.J., Caron, D.A., & Mitra, A. 2017. Mixotrophy in the Marine Plankton. *Annual Reviews of Marine Science*, **9**, 311–335.

Studer, A.S., Sigman, D.M., Martínez-García, A., Benz, V., Winckler, G., Kuhn, G., Esper, O., Lamy, F., Jaccard, S.L., Wacker, L., Oleynik, S., Gersonde, R., & Haug, G.H. 2015. Antarctic Zone nutrient conditions during the last two glacial cycles. *Paleoceanography*, **30**(7), 845–862. 2014PA002745.

Studer, A.S., Sigman, D.M., Martínez-García, A., Thöle, L.M., Michel, E., Jaccard, S.L., Lippold, J.A., Mazaud, A., Wang, X.T., Robinson, L.F., Adkins, J.F., & Haug, G.H.

147

2018. Increased nutrient supply to the Southern Ocean during the Holocene and its implications for the pre-industrial atmospheric CO_2 rise. *Nat. Geosci.*

Takagi, H., Kimoto, K., Fujiki, T., Saito, H., Schmidt, C., Kucera, M., & Moriya, K. 2019. Characterizing photosymbiosis in modern planktonic foraminifera. *Biogeosciences*.

Thomalla, S.J., Waldron, H.N., Lucas, M.I., Read, J.F., Ansorge, I.J., & Pakhomov, E. 2011. Phytoplankton distribution and nitrogen dynamics in the southwest Indian subtropical gyre and Southern Ocean waters. *Ocean Sci.*, **7**, 113–127.

Thunell, R.C., Sigman, D.M., Muller-Karger, F., Astor, Y., & Varela, R. 2004. Nitrogen isotope dynamics of the Cariaco Basin, Venezuela. *Global Biogeochem. Cycles*, **18**(GB3001), 1–13.

Toole, J. M. 1981. Sea ice, winter convection, and the temperature minimum layer in the Southern Ocean. *Journal of Geophysical Research Oceans*, **86**(C9), 8037–8047.

Trull, T., Bray, S., Manganini, S., Honjo, S., & François, R. 2001. Moored sediment trap measurements of carbon export in the Sub-Antarctic and Polar Frontal zones of the Southern Ocean, south of Australia. *J. Geophys. Res.*, **106**(C12), 31489–31509.

Trull, T.W., Davies, D., & Casciotti, K. 2008. Insights into nutrient assimilation and export in naturally iron-fertilized waters of the Southern Ocean from nitrogen, carbon and oxygen isotopes. *Deep-Sea Res. Pt II*, **55**, 820–840.

Uhle, M.E., Macko, S.A., Spero, H.J., Engel, M.H., & Lea, D.W. 1997. Sources of carbon and nitrogen in modern planktonic foraminifera: the role of algal symbionts as determined by bulk and compound specific stable isotopic analyses. *Org. Geochem.*, **27**(3/4), 103–113.

Uhle, M.E., Macko, S.A., Spero, H.J., Lea, D.W., Ruddiman, W.F., & Engel, M.H. 1999. The fate of nitrogen in the Orbulina universa foraminifera–symbiont system determined by nitrogen isotope analyses of shell-bound organic matter. *Limnol. Oceanogr.*, **44**(8), 1968–1977.

Wada, E., & Hattori, A. 1978. Nitrogen isotope effects in the assimilation of inorganic nitrogenous compounds by marine diatoms. *Geomicrobiol. J.*, **1**(1), 85–101.

Wang, X.T., Prokopenko, M.G., Sigman, D.M., Adkins, J.F., Robinson, L.F., Ren, H., Oleynik, S., Williams, B., & Haug, G.H. 2014. Isotopic composition of carbonate-bound organic nitrogen in deep-sea scleractinian corals: A new window into past biogeochemical change. *Earth Planet. Sci. Lett.*, **400**, 243–250.

Wang, X.T., Sigman, D.M., Prokopenko, M.G., Adkins, J.F., Robinson, L.F., Hines, S.K., Chai, J., Studer, A.S., Martínez-García, A., Chen, T., & Haug, G.H. 2017. Deep-sea coral evidence for lower Southern Ocean surface nitrate concentrations during the last ice age. *Proceedings of the National Academy of Sciences*, **114**(13), 3352–3357.

Waser, N.A.D., Harrison, P.J., Nielsen, B., Calvert, S.E., & Turpin, D.H. 1998. Nitrogen Isotope Fractionation During the Uptake and Assimilation of Nitrate, Nitrite, Ammonium, and Urea by a Marine Diatom. *Limnol. Oceanogr.*, **43**(2), 215–224.

Weigand, M.A., Foriel, J., Barnett, B., Oleynik, S., & Sigman, D.M. 2016. Updates to instrumentation and protocols for isotopic analysis of nitrate by the denitrifier method. *Rapid Commun. Mass Spectrom.*, **30**(12), 1365–1383. RCM-15-0493.R1.

Wessel, P., Smith, W.H.F., Scharroo, R., Luis, J., & Wobbe, F. 2013. Generic Mapping Tools: Improved Version Released. *Eos, Transactions American Geophysical Union*, **94**(45), 409–410.

Weyl, P.K. 1978. Micropaleontology and ocean surface climate. *Science*, **202**, 475–481.

Wu, J., Calvert, S.E., & Wong, C.S. 1997. Nitrogen isotope variations in the subarctic northeast Pacific: relationships to nitrate utilization and trophic structure. *Deep-Sea Res.*, **44**(2), 287–314.

7. Supplementary Information

7.1 Supplementary Text: Method testing for foraminifer tissue analysis

Our analyses were carried out in three laboratory sessions in 2016, 2017 (at Princeton University, USA) and 2018 (at the Max Planck Institute for Chemistry (MPIC), Germany). Altogether, we tested two different protocols for the pre-oxidation processing (i.e., rinsing, transferring and crushing) and three different persulfate oxidizing reagent (POR) "recipes" for the oxidation of tissue samples. We describe each protocol in turn below.

7.1.1 Tissue pre-processing

In 2016 and 2017, specimens (i.e., foraminifer shells with cytoplasm) were briefly rinsed with deionized water (loosening detritus and diluting any remnant nitrate or formalin), transferred to a 12 mL pre-combusted Wheaton vial and crushed open with an ethanol-cleaned spatula. Any residue left on the spatula was rinsed off into the vial with 0.5 mL of Milli-Q. Vials were capped and stored overnight until oxidation (without drying). In 2018, specimens were, transferred to a 4 mL pre-combusted Wheaton vial, and briefly rinsed with 1 mL of Milli-Q inside the vial. After pipetting off the supernatant liquid, samples were dried in a dessicator (with silica gel) for 10-16 h, and then crushed with an ethanol-cleaned spatula. Any dry residue left on the spatula after tapping inside the vial ($7\pm4\%$ of the total sample weight; $n = 9$) was discarded. While the former protocol (used in 2016 and 2017) minimizes handling and loss of material, it led to more variable (and generally lower) $\delta^{15}N$ values (i.e., larger standard deviations for replicate oxidations), possibly due to the effect of the 0.5 mL Milli-Q left in the vial or interactions between the organic N (foraminifer tissue), water, and atmospheric N such as ammonia. Indeed, repeat testing in 2018 suggests improved reproducibility for all three POR recipes when remnant rinse-water was removed from sample vials.

7.1.2 Tissue oxidation

The quantities of potassium persulfate and sodium hydroxide dissolved per 100 mL Milli-Q were varied as follows: 2 g and 1.2 g, respectively, in 2016; 2 g and 0.7 g, respectively, in 2017; and 1 g and 0.7 g, respectively, in 2018. The combination of pre-processing steps and the POR recipe used in 2017 appears to have led to a high rate of "failed" or incomplete oxidations, where samples required repeat POR additions. While we have not conclusively identified the

cause of these failed oxidations, the 2018 protocol was the most successful in avoiding such occurrences.

7.2 Supplementary Figures
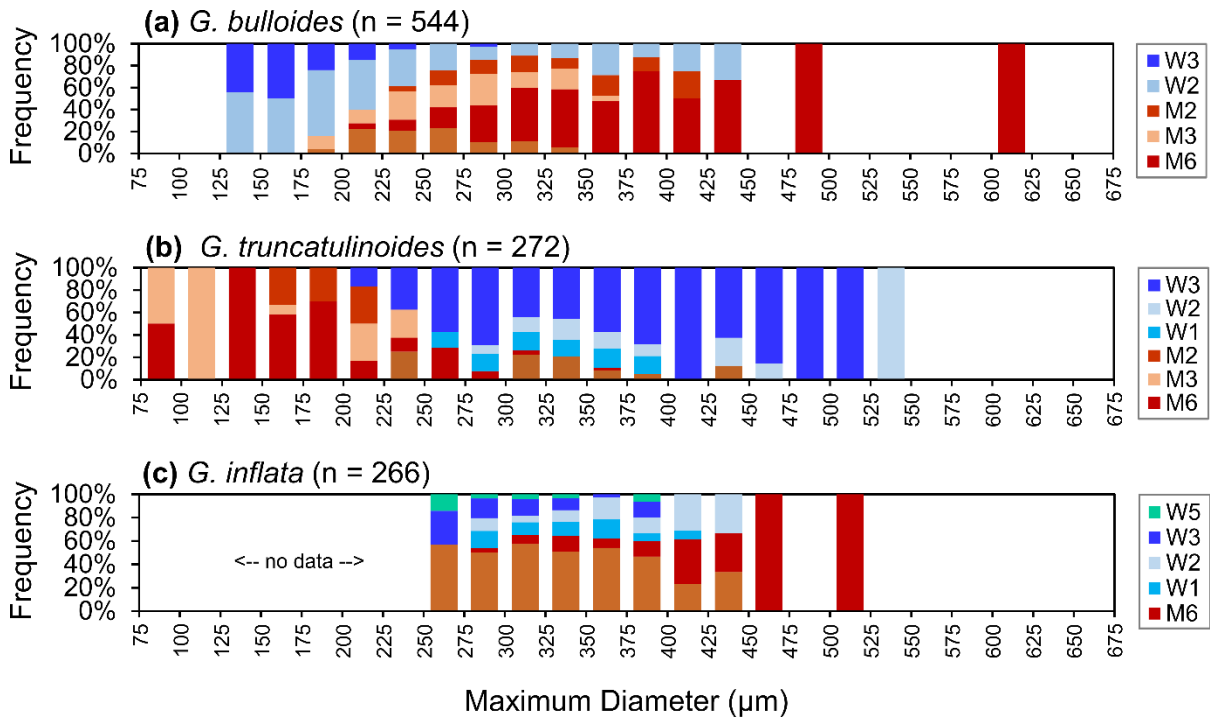
Fig. S3.1: Detailed specimen-size distributions for (a*) G. bulloides*, (b) *G. truncatulinoides*, and (c) *G. inflata* specimens from morphometric analyses undertaken in 2018.

151
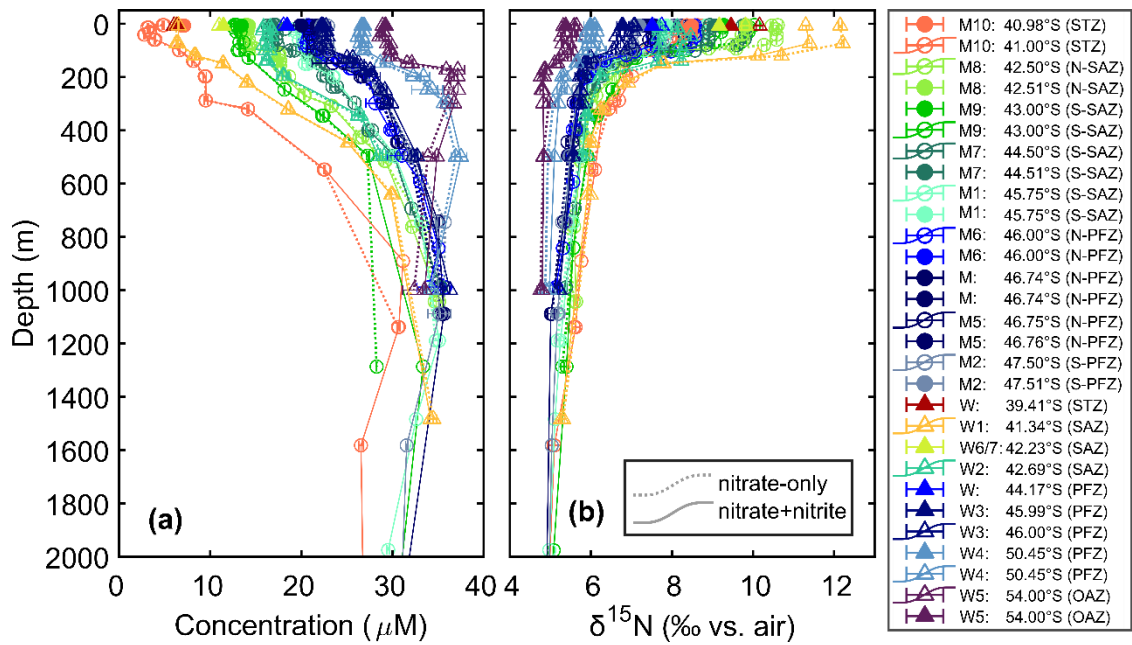
Fig. S3.2: Water-column nitrate+nitrite compared with nitrate-only. Depth profiles (open symbols) and surface (filled symbols) measurements of the (a) concentration (in μM) and (b) δ^{15}N (in ‰ versus N_2 in air) for nitrate+nitrite (solid lines) and nitrate-only (dotted lines) from the upper 2000 m in winter (triangles) and late summer (circles) south of Africa. Data are coloured by latitude zone, with the Subtropical Zone (STZ) and Subtropical Front (STF) in warm colours, the Subantarctic Zone (SAZ) in greens, Polar Frontal Zone (PFZ) in blues and the Open Antarctic Zone (OAZ) in purple. Error bars indicate the measurement standard deviation (n ≥ 2).
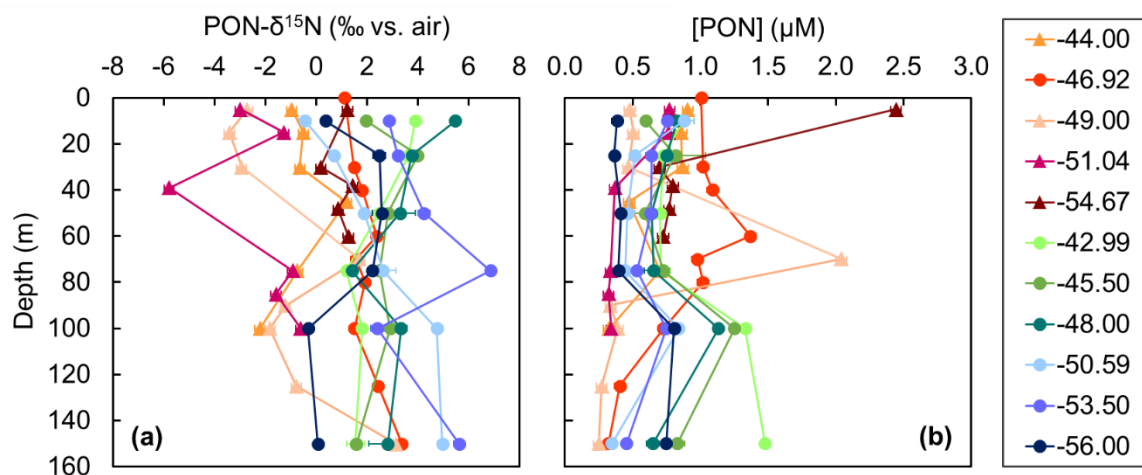
Fig. S3.3: Depth profiles of bulk (>0.7 µm) suspended PON (a) δ^{15}N and (b) concentration in the PFZ/SAZ south of Africa in midsummer 2016/2017 (profiles between 0 and 40°E; warm colours) and in winter 2017 (profiles along 30°E; cool colours). Circles denote collections from the Indian Sector and triangles denote those from the Atlantic Sector.

7.3 Supplementary Tables

Table S3.1: Net tow station details from the winter 2015 and late summer 2016 cruises in the Southern Ocean south of Africa.

Tow ID	Cruise	Date	Start time (GMT)	End time (GMT)	Depth (m)	Latitude (°S)	Longitude (°E)
W1	Winter 2015	2015-07-27	12:00	13:30	60	41.35	9.88
W2	Winter 2015	2015-07-28	11:49	13:19	40	42.70	8.74
W3	Winter 2015	2015-07-30	11:20	12:50	80	45.98	5.54
W4	Winter 2015	2015-08-01	11:13	12:43	90	50.46	1.00
W5	Winter 2015	2015-08-04	1:20	2:50	30	53.99	0.05
W6	Winter 2015	2015-08-06	19:21	20:51	30	42.22	0.04
W7	Winter 2015	2015-08-06	21:16	22:46	30	42.22	0.09
M1	Late summer 2016	2016-04-17	10:56	12:26	60	45.76	37.27
M2	Late summer 2016	2016-04-19	11:45	13:14	35	47.51	37.28
M5	Late summer 2016	2016-04-20	17:12	18:42	60	46.74	37.48
M6	Late summer 2016	2016-04-29	21:36	23:06	25	46.00	37.98
M7	Late summer 2016	2016-05-04	1:52	3:22	30	44.52	35.57
M8	Late summer 2016	2016-05-04	16:13	17:46	70	42.52	33.66
M9	Late summer 2016	2016-05-08	12:24	13:54	60	43.00	28.36
M10	Late summer 2016	2016-05-09	7:16	8:46	60	40.96	26.83

CHAPTER 4: The nitrate assimilation isotope effect in the Subantarctic Zone: Revised estimates from a seasonal model of the Southern Ocean

Presentation of a research paper in preparation

This paper is in preparation for submission to the research journal *Journal of Geophysical Research: Oceans*. The previously published Antarctic model (upon which our Subantarctic model is based) was built by P.C. Kemeny and co-authors (Kemeny et al., 2018). I was personally responsible for adapting and building onto the original model code (with the guidance of P.C. Kemeny and F. Fripiat), calibrating the model to field observations, interpreting the model output and writing the first draft of the manuscript. The observational data used for calibration come from a global nitrate isotope database compiled by D. Marconi. Samples from cruises P18 and IO8S were measured by F. Fripiat. D.M. Sigman, A. Martínez-García and S.E. Fawcett conceptualized this study. G.H. Haug provided resources and support. P.C. Kemeny, F. Fripiat and D.M. Sigman revised and/or gave feedback on the text.

ABSTRACT

The isotope effect of nitrate assimilation (the degree of isotope discrimination during nitrate uptake by phytoplankton) is one of the key parameters for inferring past biological nitrate consumption from the N isotope composition (δ^{15}N) of organic matter in the sedimentary record. Quantifying the isotope effect in the Subantarctic Zone (SAZ), the northernmost domain of the Southern Ocean, is challenging due to its complex circulation and seasonally varying nitrate supply regime. Furthermore, previous estimates were based on acidified seawater samples (from which nitrite is lost), which have been shown to overestimate the isotope effect in the Antarctic Zone (AZ). We present a multi-annual, seasonally resolved geochemical box model of the Southern Ocean for estimating the SAZ isotope effect based on non-acidified samples (nitrate+nitrite measurements) from the Indo-Pacific sector. Our basic version of the model re-creates the main features of seasonal nitrate drawdown and replenishment in the upper water column and produces a rate and δ^{15}N for annual N export

(172 mmol.m^{-2} and 1.7‰, respectively) within the range of observations from the SAZ. In order to fit the observed upper-ocean nitrate and export δ^{15}N, the basic model requires an isotope effect of 8.3±1.8‰ for nitrate assimilation in the SAZ. This is in line with previous estimates, despite their derivation from acidified samples. If this finding holds with better-resolved upper-water-column evolution and SAZ-specific biology, it confirms the previous suggestion that the SAZ hosts an isotope effect range for nitrate assimilation that is higher than the AZ and other studied nitrate-rich regions such as the equatorial Pacific and the subarctic North Pacific.

1. Introduction

The Southern Ocean is widely recognized as an important conduit of past, and potentially future, global climate change through its physical and biological controls on atmospheric carbon dioxide (CO_2) levels (Sarmiento & Toggweiler, 1984; Knox & McElroy, 1984; Siegenthaler & Wenk, 1984). Paleoceanographic records suggest that the Subantarctic Zone (SAZ; the northernmost domain of the Southern Ocean) contributed substantially to the ice-age decline in atmospheric CO_2 through an iron-fertilization-driven increase in the efficiency of the biological pump (the export of carbon to the deep ocean by biology) (Martin, 1990; Martínez-García et al., 2011). The evidence for enhanced major-nutrient consumption (and thus carbon drawdown) comes from the nitrogen (N) isotope composition, or δ^{15}N (where δ^{15}N = {[(^{15}N/^{14}N)$_{sample}$/(^{15}N/^{14}N)$_{N2\ in\ air}$] − 1} × 1000; in units of per mil, ‰), of organic matter in seafloor sediments, specifically, the fossil shells of planktic foraminifera (Martínez-García et al., 2014).

When nitrate (NO_3^-, a major nutrient) is taken up by phytoplankton, the lighter ^{14}N isotope is favored, causing an increase in the ratio of ^{15}N relative to ^{14}N in remaining nitrate; the extent to which the light ^{14}N isotope is favored over the heavy ^{15}N isotope is known as the isotope effect (ε), quantified using the ratio of reaction rates (k) of the two isotopes ($\varepsilon = [(^{14}k/^{15}k) − 1] \times 1000$). In turn, phytoplankton (and thus also bulk particulate organic N; PON) δ^{15}N also increases as nitrate consumption proceeds (Wada & Hattori, 1978; Pennock et al., 1996; Waser et al., 1998; Sigman et al., 1999a). In this way, PON sinking to the seafloor carries with it the isotopic fingerprint of nitrate consumption in surface waters (François et al., 1992; Altabet & François, 1994). However, bulk sedimentary PON is often compromised by bacterial

155

diagenesis, particularly in low-flux environments like the Southern Ocean where organic matter is buried more slowly (Altabet & François, 1994; Ren et al., 2009; Meckler et al., 2011; Robinson et al., 2012; Straub et al., 2013; Martínez-García et al., 2014). Microfossil-bound N offers an alternative, physically protected reservoir of organic N for paleo-reconstructions (Sigman et al., 1999b; Robinson et al., 2004; Ren et al., 2009). The $\delta^{15}N$ of organic matter trapped in the tests of diatoms (siliceous phytoplankton) and, under certain conditions, foraminifera (calcareous zooplankton) also track the $\delta^{15}N$ of nitrate consumed in surface waters (Sigman et al., 1999b; Studer et al., 2015; Ren et al., 2009; Ren et al., 2012). While the $\delta^{15}N$ of planktic foraminifera is also influenced by N cycling that modifies the $\delta^{15}N$ of their PON food sources on a seasonal basis, the ultimate origin of PON from the assimilation of nitrate likely ties foraminiferal $\delta^{15}N$ to the isotope dynamics of nitrate assimilation in the Southern Ocean (see Chapter 4, this thesis). In the SAZ, elevated foraminifer-bound $\delta^{15}N$ in glacial-aged sediments, has been interpreted as a higher $\delta^{15}N$ for nitrate consumed by phytoplankton, leading to the conclusion that nitrate drawdown was more complete during ice ages (Martínez-García et al., 2014). However, an alternative interpretation for the glacial $\delta^{15}N$ rise is a decrease in the isotope effect of nitrate assimilation, i.e., weaker discrimination against the incorporation of the heavy ^{15}N isotope into biomass.

Under conditions of complete nitrate drawdown, both of the N isotopes (^{14}N and ^{15}N) are completely transferred to the product and isotope discrimination is no longer expressed (i.e., the $\delta^{15}N$ of the accumulated PON pool converges on that of the nitrate originally supplied). In such settings (e.g., a subtropical gyre), fossil-bound $\delta^{15}N$ is viewed as a record of the source nitrate $\delta^{15}N$ (Altabet, 1988; Altabet & François, 1994; Ren et al., 2012; Wang et al., 2014; Wang et al., 2016). In a region like the Southern Ocean, where nitrate is only partially consumed in surface waters, fossil-bound $\delta^{15}N$ reflects not only the source nitrate $\delta^{15}N$, but also the degree of nitrate consumption (with higher $\delta^{15}N$ values indicating more-complete consumption) and the isotope effect of nitrate assimilation (the larger the isotope effect, the larger the $\delta^{15}N$ difference between nitrate and fossil-bound N) (François et al., 1992; Altabet & François, 1994). Therefore, disentangling changes in the isotope effect from changes in nutrient consumption is at the heart of the application of the $\delta^{15}N$ paleo-proxy in nitrate-replete environments.

The assumption of a constant nitrate assimilation isotope effect through glacial-interglacial cycles can be tested by estimating and mapping the isotope effect across different modern-

ocean environments (Sigman et al., 1999a; Altabet & François, 2001; Karsh et al., 2003; DiFiore et al., 2006; DiFiore et al., 2010) as a "metaphor" for changing climate at a single location. The isotope effect is typically estimated from hydrographic data using one of two simple isotope models: (1) the Rayleigh model (Mariotti et al., 1981), or (2) the steady-state model. The first describes a closed system, where nitrate is not resupplied during consumption. The second describes an open system, where nitrate is constantly supplied and removed (at the same rate) during consumption. In both cases, the isotope effect can be approximated from the slope of the line in isotope-*vs*.-concentration space (Mariotti et al., 1981; Hayes, 2004), i.e., describing the size of the δ^{15}N increase for a given [NO_3^-] decrease. In the SAZ, understanding of the circulation implies that neither model is adequate. Specifically, SAZ nitrate isotope dynamics are complicated by multiple (and seasonally varying) supply routes, and the fact that the two main nitrate sources have markedly different [NO_3^-]-to-δ^{15}N properties (Sigman et al., 1999a; DiFiore et al., 2006).

In spring and summer, surface warming and freshening (from sea-ice melt) leads to shoaling mixed layers across the Southern Ocean, particularly in the Antarctic Zone (AZ; south of the Polar Front). Improving light conditions (due to stratification and increased insolation) trigger phytoplankton blooms, causing the rapid drawdown (and δ^{15}N increase) of mixed-layer nitrate (Lourey et al., 2003). Equatorward Ekman transport within this upper layer (driven by the Westerly winds that drive the upwelling of Circumpolar Deep Water; CDW) and eddy-induced mixing carry partially consumed (and δ^{15}N-elevated) nitrate from the AZ, across the Polar Frontal Zone (PFZ) and into the SAZ where it undergoes further consumption. In winter, enhanced vertical mixing between the SAZ mixed-layer and the underlying thermocline introduces nitrate with a relatively low δ^{15}N for its [NO_3^-]. Unlike the polar source waters, the SAZ thermocline is influenced by isopycnal mixing (i.e., mixing along constant density surfaces) with the low-latitude thermocline, which is, in turn, a product of vertical mixing between the underlying pycnocline and overlying subtropical surface waters. The effect of this communication with subtropical waters is to lower the [NO_3^-] of the SAZ thermocline without raising its δ^{15}N (Sigman et al., 1999a; Sigman et al., 2000). It follows that the derived SAZ isotope effect can vary widely (from ~5‰ to ~11‰) depending on which model is used (Rayleigh or steady-state) and which nitrate source (or what ratio of the two sources) is assumed to best represent "start-of-summer conditions" (Sigman et al., 1999a; DiFiore et al., 2006). Such uncertainty for the isotope effect is problematic for interpreting a glacial-

157

interglacial δ^{15}N signal with an amplitude of ~4‰ (Robinson & Sigman, 2008; Martínez-García et al., 2014).

To address this problem, DiFiore et al. (2006) developed a time-dependent, one-box geochemical model to simulate the evolution of the SAZ mixed layer from the onset of spring to the peak of summertime production (a 90-day period), based on salinity, nitrate (δ^{15}N and [NO$_3^-$]), and sinking PON δ^{15}N measurements from the Australian sector. They concluded that an isotope effect of ~8-9‰ best fit their observations, which is higher than estimated for the AZ (~4-8‰; Sigman et al., 1999a; Karsh et al., 2003; DiFiore et al., 2009; DiFiore et al., 2010). This led to the conclusion that the isotope effect is spatially variable (decreasing poleward), and possibly correlated with mixed-layer depth, which would complicate interpretation of paleo-δ^{15}N records (DiFiore et al., 2006; DiFiore et al., 2010). Subsequently, the common practice of acid-preserving seawater nitrate samples has been called into question, at least for applications regarding the isotope effect. The addition of hydrochloric acid removes nitrite, which is present in low concentrations (typically <1% of total nitrate+nitrite) but can have a very low δ^{15}N in the Southern Ocean mixed layer, and thus significantly lower the δ^{15}N of the combined nitrate+nitrite pool (Rafter et al., 2013; Smart et al., 2015; Kemeny et al., 2016). The low δ^{15}N of nitrite is thought to derive from the large equilibration isotope effect expressed during nitrate-nitrite interconversion in the late-summer euphotic zone (Kemeny et al., 2016). Given the exchange between nitrate and nitrite, nitrate+nitrite is arguably more representative of the N available for consumption by phytoplankton, and thus more appropriate for quantifying the assimilation isotope effect (Fripiat et al., 2019). Using nitrate-only instead of nitrate+nitrite δ^{15}N can, therefore, lead to overestimation of the isotope effect of nitrate assimilation. Revised estimates from across the AZ (from the continental shelves of Antarctica to the Polar Front) have yielded lower and less variable estimates ($\varepsilon = 5.5 \pm 0.6$‰) for the isotope effect of nitrate assimilation than derived using acidified (nitrate-only) samples ($\varepsilon = 7.9 \pm 1.5$‰) (Fripiat et al., 2019). In contrast to Kemeny et al. (2016), in the revised estimates, the AZ isotope effect of nitrate assimilation was uncorrelated with mixed-layer depth, motivating reappraisal of the data underlying DiFiore et al. (2010).

Our goal is to provide improved estimates for the isotope effect of nitrate assimilation in the SAZ, using nitrate+nitrite data. We approach this using a multi-annual, seasonally resolved, four-box geochemical model of the Southern Ocean, consisting of surface and subsurface layers for the AZ and SAZ. Unlike the fixed inputs of the DiFiore et al. (2006) model, this

model accounts for the coupled seasonal evolution of AZ mixed-layer nitrate and its varying effect on the SAZ. This approach has the additional advantage of allowing mixed-layer and thermocline properties to develop over multiple seasonal cycles (rather than a single growing season), meaning that the model resolves the multi-annual steady-state conditions characterizing annual integrals. The two-layer structure of our model allows us to better resolve the influence of subtropical waters on the SAZ, both directly via surface mixing across the subtropical front (STF) and indirectly via mixing between the SAZ thermocline and the low-latitude pycnocline. In addition to informing reconstructions of past nitrate assimilation from SAZ paleo-δ^{15}N records (by providing more robust estimates for the isotope effect), this model could enable us to generate maps of the predicted sinking flux δ^{15}N for the modern Southern Ocean, a useful parameter that has proven difficult to measure in the field.

2. Methods

2.1 Model description

Our Southern Ocean model is built upon the two-layer AZ model of Kemeny et al. (2018), which simulates seasonal changes in the concentration and δ^{15}N of N in nitrate+nitrite, ammonium, phytoplankton (diatoms and non-diatoms) and zooplankton in the upper water column, calibrated to modern conditions in the Pacific sector. Using a series of differential equations (solved in MATLAB using the *ode15s* function), the model tracks net changes in ^{14}N for each N pool in each box at every time step based on fixed rates of ocean circulation and mixing, and varying rates for biogeochemical processes. Fluxes of ^{15}N are calculated based on ^{14}N fluxes, taking into account any associated isotopic fractionation and the abundance of both isotopes in the substrate. The model is run continuously until approximate steady state is reached (normally ~150 years), when there are no longer notable changes in the seasonal cycle from one model year to the next. Below, we outline relevant aspects of the model and modifications made for our application to the SAZ. Unless otherwise stated, the input parameters given in the text are those used for the "basic" model case.
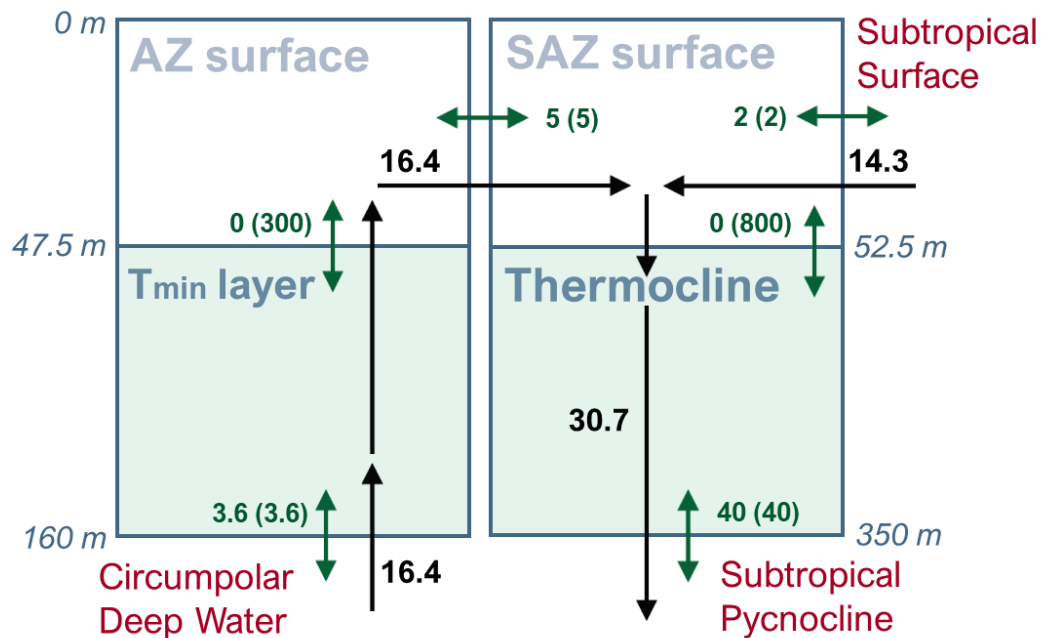
2.1.1 Structure

The original model of Kemeny et al. (2018) has two boxes: the Antarctic surface (which constitutes the mixed-layer in summer) and the temperature minimum layer, hereafter "T_{min}"

159

(the remnant winter mixed layer that underlies the summer mixed layer). In winter, the two layers are homogenized by vigorous mixing to become the new winter mixed layer. We have added another two boxes to represent the SAZ (which includes the PFZ): the Subantarctic surface (the mixed layer in summer) and the Subantarctic thermocline below it (Fig. 4.1). In the model SAZ (as for the AZ), wintertime mixed-layer deepening is simulated as vigorous mixing that homogenizes the thermocline and summer-mixed-layer boxes. The depths of summer and winter mixing vary zonally around the Southern Ocean, especially within the SAZ; we set the depths of the model boxes based on the water column structure of the sampling region used for calculating input values (i.e., water mass properties) and target outputs (i.e., upper-ocean averages from observations). Mixed-layer depth is obtained from the Argo-based monthly climatologies of Dong et al. (2008). For our basic model, the AZ surface layer is 47.5 m deep, with the base of the T_{min} at 160 m, while the SAZ surface layer is 52.5 m deep, with the base of the thermocline at 350 m. We base this version of the model on observations from the Indo-Pacific sector of the Southern Ocean, where winter mixing down to ~300-400 m essentially homogenizes the SAZ surface and thermocline layers (DiFiore et al., 2006). The Atlantic sector appears to experience less-deep winter mixing (such that SAZ surface and thermocline nitrate properties remain distinct during winter; Smart et al., 2015; this thesis, Chapter 3, Fig. 3.3). The data from the Atlantic sector will be considered in subsequent work.

2.1.2 Physics

Physical fluxes are modelled after the residual circulation of Karsten & Marshall (2002) for the zonally averaged Southern Ocean. Residual circulation (shown by one-way arrows in Fig. 4.1) is the net transport of water (given in Sverdrups, where 1 Sv = 10^6 $m^3.s^{-1}$) that results from the combination of wind-driven Ekman flow and eddy transfer. The westerly winds that drive upwelling of CDW through the base of the T_{min} / winter mixed layer and into the AZ surface also impart an equatorward flow (16.4 Sv) to surface water across the Polar Front. Convergence with poleward flow (14.3 Sv) from the subtropical surface leads to subduction (30.7 Sv, the sum of the two) of SAZ surface and thermocline waters into the subtropical pycnocline. While the net transport terms are held constant during the model year (for the duration of the run), mixing terms (denoted by double-headed arrows in Fig. 4.1) are allowed to vary seasonally. Mixing between the upper and lower layers of the model is more vigorous during winter (300 Sv in the AZ, 800 Sv in the SAZ; the minimum exchanges required to homogenize the two layers of each zone by the end of winter), but set to zero (0 Sv for both the AZ and SAZ) in

160

summer to simulate stratification of the water column. Two-way exchange at the model boundaries is held constant through the year: 3.6 Sv between the T_{min} and CDW (targeting a total CDW supply of 20 Sv from Ekman upwelling plus basal mixing; Kemeny et al., 2018), 40 Sv between the SAZ thermocline and the low-latitude pycnocline, and 2 Sv between SAZ surface and subtropical surface waters. Mixing is also allowed between the AZ and SAZ surface boxes (5 Sv in winter and summer).

Fig. 4.1: Model structure and physical fluxes (in Sverdrups, Sv). Black arrows and numbers indicate the direction and magnitude of the transport terms (residual circulation), which are held constant throughout the model year. Green arrows and numbers show the amount of mixing between boxes or across boundaries during summer (winter). Boundary water masses are labelled in red. Note that box depths are not to scale.

2.1.3 Biogeochemistry

The model contains two dissolved nutrient pools, nitrate+nitrite (which we refer to as nitrate for simplicity) and ammonium, plus three biological reservoirs – diatoms, non-diatom phytoplankton and zooplankton. The diatom pool is further subdivided into biomass (bulk tissue) N and frustule-bound N, to account for the lack of remineralization of the latter (discussed further below). As a starting point, we allow SAZ biology to mimic that of the AZ, using the same biogeochemical rates (determined by calibration to the modern Pacific AZ (Kemeny et al., 2018), given in text below) for both AZ and SAZ (Fig. 4.2).

161
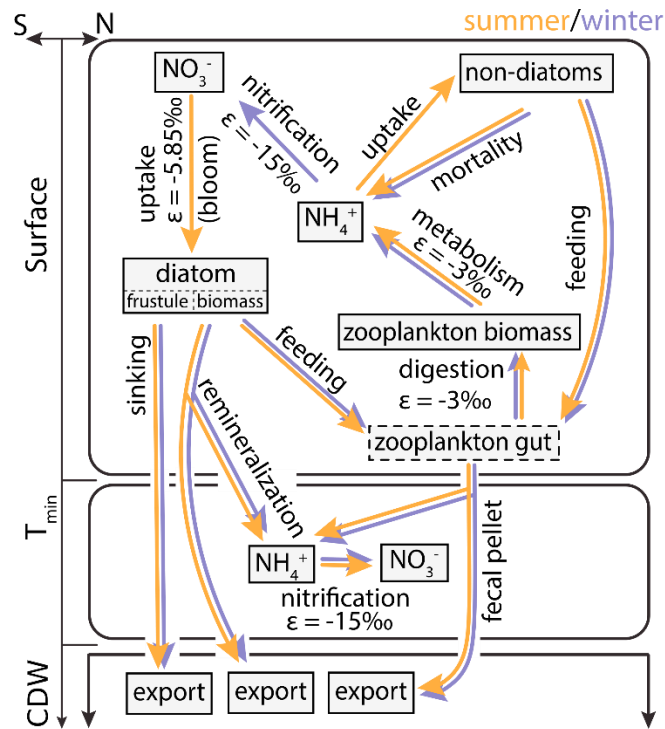
Fig. 4.2: Biogeochemical fluxes active in the model's Antarctic Zone during winter (purple) and summer (yellow). Associated N isotope effects (ε) are shown for fractionating processes. The same biogeochemistry is applied to the Subantarctic Zone (SAZ) in our "basic" model, except for the isotope effect of nitrate assimilation, which we modify to best fit SAZ nitrate observations [Figure adapted from Kemeny et al., 2018].

Nitrate is supplied via two main routes: upwelling plus basal mixing across the T_{min}-CDW boundary (with $[NO_3^-]$ of 32.7 µM and $\delta^{15}N$ of 5.05‰) and mixing between the SAZ thermocline and the subtropical pycnocline (with $[NO_3^-]$ of 29.3 µM and $\delta^{15}N$ of 6.17‰). Subtropical surface waters are appropriately approximated as being nitrate-free, such that any cross-frontal transport/exchange has a dilution effect (lowering $[NO_3^-]$) without altering nitrate $\delta^{15}N$ in the SAZ. The three boundary water masses (CDW, the low-latitude pycnocline and subtropical surface waters) are treated as infinite reservoirs, such that their $[NO_3^-]$ and $\delta^{15}N$ are fixed for the duration of the model simulation. The nitrate properties used for these water masses are the volume-integrated averages of Fripiat et al. (*in prep.*) from a global nitrate isotope database, where measurements are weighted by their representative area and depth ranges. In calculating $\delta^{15}N$ averages, measurements were additionally weighted by their respective nitrate+nitrite concentrations. In the model, ammonium is generated solely by internal N cycling and not supplied from external source waters. Ammonium is excreted by zooplankton and is also a product of biomass decomposition (remineralization of

162

phytoplankton and zooplankton fecal pellets) (Checkley & Miller, 1989; Lehmann et al., 2002). Ammonium is oxidized to nitrate via nitrification (5%/day with an isotope effect of −15‰; Casciotti et al., 2003), which occurs continuously in the subsurface layer of the model, but only during winter within the surface layer (Smart et al., 2015).

During the first 90 days of summer, diatoms take up nitrate following Monod kinetics (Sarthou et al., 2005), where nitrate is consumed at the maximum daily rate (57 µmol.m^{-3}.d^{-1}, with half saturation constant 500 µmol.m^{-3}; Capone et al., 2008) until day 91. This phase represents the iron-replete conditions of the spring bloom. Based on observations of the time progression of summertime nitrate drawdown (Altabet & François, 2001; Johnson et al., 2017), it is assumed that diatom growth stops in mid-summer, such that non-diatoms overtake them as the dominant phytoplankton group during the second phase of summer (days 91-182). Rather than nitrate, non-diatoms assimilate ammonium (at a rate of 40%/day), leading to a switch from new production to recycled production that occurs under the iron-limited conditions of late-summer surface waters (Sambrotto & Mace, 2000; Tagliabue et al., 2014). Every day of the model year, zooplankton consume a set percentage of each phytoplankton group (3% of diatoms and 17% of non-diatoms), 95% of which is incorporated into zooplankton biomass (with an isotope effect of −3‰; Altabet & Small, 1990), and the rest is released in the form of fecal pellets. In turn, 50% of zooplankton biomass N is converted to ammonium each day (with an isotope effect of −3‰; Checkley & Miller, 1989) to simulate excretion. During all seasons, 3% of the diatom pool and 100% of fecal pellets is exported daily from the surface. Ten percent of exported material (fecal pellets and diatom biomass, but not frustules) undergoes remineralization to ammonium (with an isotope effect of 0‰) and potentially nitrate within the sub-surface layer. The remainder is exported to the deep ocean, along with the diatom frustules. Non-diatom phytoplankton are assumed to be remineralized to ammonium within the surface ocean (3%/day without fractionation) and, therefore, do not contribute directly to the export flux. All N pools can be mixed or advected into, out of, or between the model boxes.

2.2 Model calibration to observations

We take an iterative approach to tuning the model, starting with the basic physical transports (Karsten & Marshall, 2002) and varying only the supply terms (mainly mixing) to reach the approximate baseline [NO$_3^-$] observed in each upper-ocean layer. Biogeochemical terms (rates, isotope effects etc.) in both the AZ and SAZ are kept the same as in the original model of Kemeny et al. (2018). Provided that the model output δ^{15}N values are also realistic (i.e., within

163

the range of upper-ocean nitrate and export observations; given below), we can offer a provisional estimate for the SAZ isotope effect of nitrate assimilation with this basic version of the model. In the second phase of tuning, we plan to modify SAZ biogeochemistry to better describe the biology and upper-ocean particle dynamics of the region; this will be called the "standard" model.

2.2.1 Upper-ocean nitrate targets

We calculate target [NO$_3^-$] and nitrate δ^{15}N for the model boxes from two hydrographic transects: P18 in the eastern Pacific sector (Dec 2016-Jan 2017) and GOSHIP IO8S in the eastern Indian sector (Feb-Mar 2016). These cruises were chosen for their non-acidified collections (i.e., nitrate+nitrite measurements) as well as their high depth-resolution sampling and broad latitudinal coverage. Based on previous observations of seasonal nitrate drawdown in the SAZ/PFZ (Lourey & Trull, 2001; Lourey et al., 2003), we take October 1st to represent the start of summer (day 1 in the model). In this context, the mid-cruise date of P18 corresponds to day 88 in the model (peak summer) and IO8S corresponds to model day 148 (near the end of summer), which are key timepoints for constraining the seasonal cycle. Using the actual time-point from the shipboard observations is a new complexity relative to previous AZ and SAZ N isotope models, which often use marine observations as broadly representative of seasonal trends without intra-season resolution. By accounting for the actual day of sampling for the calibration targets, this model is a better representation of seasonality in the Southern Ocean.

2.2.2 Bulk and diatom-bound N export targets

In addition to the constraints from upper-ocean nitrate observations, measurements of sinking and recently deposited sediments provide a means to evaluate the feasibility of different model scenarios, including different SAZ isotope effects. The annual flux of bulk sinking δ^{15}N has been measured from sediment traps to be −0.1-1.7‰ in the AZ (at 60°S, 63°S and 66°S; (Altabet & François, 2001), 0.9-1.6‰ in the PFZ (at 54°S (Lourey et al., 2003) and 57°S (Altabet & François, 2001)), and 2.0-3.0‰ in the SAZ (at 47°S; Lourey et al., 2003). We, therefore, target a modelled annual export δ^{15}N of ~0-2‰ for the AZ and ~1-3‰ for the SAZ. We simulate bulk sinking δ^{15}N by accumulating all exported particulate N pools (mostly diatom biomass and zooplankton fecal pellets, with a minor contribution from diatom frustules) during the model year (i.e., annual export) or season (e.g., summer export). Measurements of

164

diatom-bound $\delta^{15}N$ from seafloor sediments are ~2-3‰ in the AZ (Studer et al., 2015) and generally increase northwards to ~2-6‰ in the PFZ and higher in the SAZ (Robinson & Sigman, 2008). In the model, we assume diatom frustules to be 2.8‰ higher in $\delta^{15}N$ than their biomass (Kemeny et al., 2018), based on field observations of a 2-3‰ offset (Robinson et al., 2004; Brunelle et al., 2007; Morales et al., 2013; Morales et al., 2014).

3. Results & Discussion

3.1 The basic model

3.1.1 Seasonality in the upper water column

In this basic version of the model, AZ and SAZ nitrate follow the same seasonal trends but with different baseline $[NO_3^-]$ and $\delta^{15}N$ values (Fig. 4.3a&c), determined by those of the nitrate sources (i.e., boundary water masses and adjacent boxes) and their relative contributions (supplied by mixing and transport). Concentrations of the other biogeochemical N pools (phytoplankton, zooplankton and ammonium) are almost identical between the AZ and SAZ (Fig. 4.3b&d), with minor differences stemming from the dependence of diatom growth on $[NO_3^-]$ (with the lower $[NO_3^-]$ of the SAZ supporting a slightly smaller diatom population), and the knock-on effect of zooplankton growth on diatom abundance, and ammonium-assimilating phytoplankton on zooplankton excretion. Here we describe the seasonal progression in concentration and $\delta^{15}N$ of the model's main N reservoirs after interannual steady state has been reached.

165
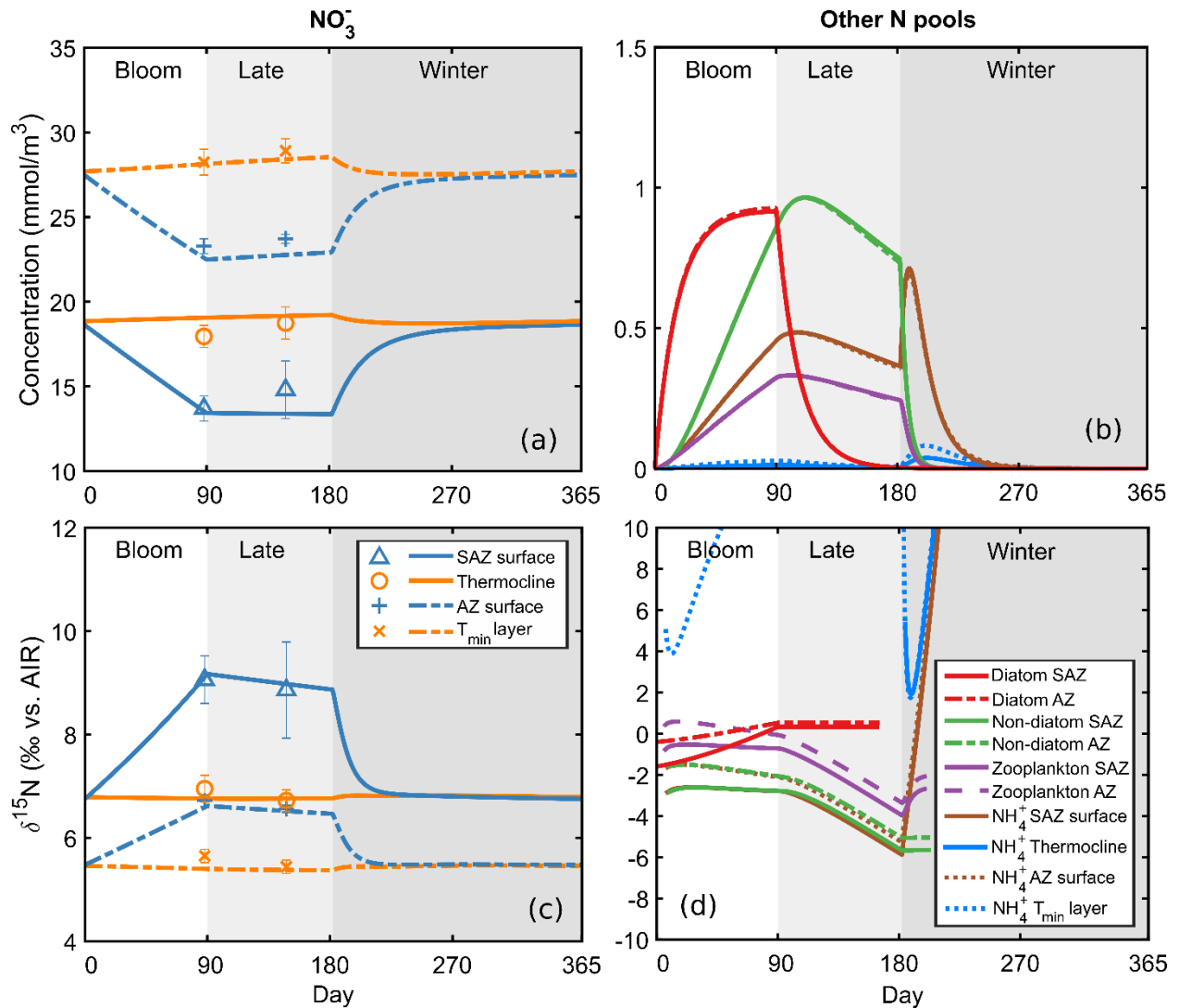
Fig. 4.3: Results for the model's steady-state year. Seasonality in the concentration and $\delta^{15}N$ of the main N reservoirs of the model (lines, all panels), with target nitrate properties from observations overlaid (symbols, left panels). Solid lines represent the SAZ and dashed/dotted lines represent the AZ. $\delta^{15}N$ is not shown for pools smaller than 0.01 mmol.m^{-3}.

On the first day of summer, diatoms begin assimilating nitrate, lowering [NO$_3^-$] and raising the $\delta^{15}N$ of both nitrate and diatoms in surface waters. Zooplankton feed on the growing diatom population, producing high-$\delta^{15}N$ fecal pellets (which are exported) and excreting low-$\delta^{15}N$ ammonium (which accumulates in surface waters). Rising ammonium concentrations support non-diatom phytoplankton growth, providing another (lower-$\delta^{15}N$) food source for zooplankton. Therefore, zooplankton $\delta^{15}N$ increases initially with the rise in diatom $\delta^{15}N$ but decreases thereafter as their diet shifts towards non-diatom phytoplankton.

166

In mid-summer, diatoms stop consuming nitrate, allowing surface $[NO_3^-]$ to rise and $\delta^{15}N$ to fall as the transports of CDW into the AZ and of AZ surface waters into the SAZ (which occur year-round) are no longer compensated by nitrate assimilation. Diatom concentration drops sharply as they are consumed, exported, or remineralized (in the surface or subsurface) without replenishment. Without the input of new production (from nitrate), zooplankton, ammonium and non-diatom phytoplankton concentrations decline, and their $\delta^{15}N$ decreases as ^{15}N is preferentially exported to the sub-surface (in the form of sinking fecal pellets) and ^{14}N is preferentially recycled within the late-summer mixed layer.

Throughout the summer (bloom and late phases), stratification prevents the T_{min} layer from mixing with overlying surface waters, but upwelling and basal mixing continue at the T_{min}-CDW boundary. These work together with the remineralization of sinking organic matter to raise the concentration and lower the $\delta^{15}N$ of T_{min} nitrate during summer. Although surface-subsurface mixing is also set to zero in the summertime SAZ, subduction continues to supply relatively low $[NO_3^-]$, high $\delta^{15}N$ surface nitrate to the SAZ thermocline. This is approximately compensated by continuous mixing with the subtropical pycnocline (which adds comparatively high-$[NO_3^-]$, low-$\delta^{15}N$ nitrate). The net result of these plus in situ remineralization and nitrification is a very weak $[NO_3^-]$ increase and $\delta^{15}N$ decrease in the SAZ thermocline during summer.

In winter, vigorous mixing homogenizes surface and subsurface layers, causing their nitrate properties to converge. As the larger reservoir (i.e., thicker layer) with a higher $[NO_3^-]$, the former summer subsurface layer (T_{min} or thermocline) dominates the resulting winter mixed-layer nitrate properties. In the AZ, a slight $[NO_3^-]$ increase and $\delta^{15}N$ decrease occurs through the winter due to the continued supply of CDW from below. Non-diatom phytoplankton concentrations drop sharply into the winter as they stop assimilating ammonium and are preyed upon or remineralized without replacement. With a shrinking food source, the zooplankton population also declines. The combined result is an initial accumulation of ammonium in surface waters, but the pool is diluted by mixing with subsurface waters and consumed by nitrification in the winter mixed layer.

3.1.2 Fitting observations and estimating the isotope effect

The basic model does fairly well at meeting the upper-ocean nitrate targets (symbols overlaid on Fig. 4.3a&c) calculated from modern observations in the Indo-Pacific sector. To achieve this fit, we have varied only the physical supply terms of the original model (Kemeny et al., 2018) and the SAZ isotope effect of nitrate assimilation. We begin with fitting the AZ, as its nitrate properties affect those of the SAZ. The 20 Sv total exchange (upwelling plus basal mixing) between the T_{min} and underlying CDW yields higher $[NO_3^-]$ and lower $\delta^{15}N$ than our target values for the AZ upper water column. There are two different ways to combat this in the basic model: (1) reducing the supply of CDW (to ~14 Sv), or (2) allowing mixing (~5 Sv) between AZ and SAZ surface waters. The first has the effect of raising the $\delta^{15}N$ of exported particles (bulk and diatom-bound N), as the reduced nitrate supply (with the same assimilation rate) leads to greater fractional nitrate utilization, raising the $\delta^{15}N$ of surface nitrate and thus also the diatoms that consume it. The second has a similar effect on export $\delta^{15}N$, as any exchange with the SAZ surface lowers the $[NO_3^-]$ and raises the $\delta^{15}N$ of AZ surface nitrate. Under both scenarios, annual N export is ~156 mmol.m^{-2}, within the range of observations from the Pacific sector (100-500 mmol.m^{-2}; Rubin et al., 1998) with a $\delta^{15}N$ of ~2.1‰, just above the 0-2‰ target range for the AZ. Modelled diatom-bound $\delta^{15}N$ is ~2.9‰ in both cases, at the high end of the observed ~2-3‰ range. Therefore, while we cannot distinguish between mechanisms (1) and (2) with the current information, the choice does not seem to affect how well the model simulates observed AZ nitrate or export properties. We choose to proceed with (2), as ~20 Sv of CDW supply and ~5 Sv of mixing across the Polar Front (PF) are more in line with existing estimates (Abernathey et al. (2016) and Dufour et al. (2015), respectively).

In the basic model, the baseline $[NO_3^-]$ of the upper-ocean SAZ is determined by inputs from the AZ surface (via 16.4 Sv northward Ekman transport and 5 Sv cross-PF mixing), the subtropical pycnocline (through mixing only) and subtropical surface waters (via 14.3 Sv southward transport and mixing across the STF). Without any supply of nitrate from the subtropical pycnocline, surface and thermocline $[NO_3^-]$ would be ~10 µM too low in the SAZ, and bulk export $\delta^{15}N$ would be ~3.6‰, which is higher than measured from SAZ sediment traps (~1-3‰). SAZ $[NO_3^-]$ targets can be met equally well by 35 Sv pycnocline mixing and 0 Sv subtropical surface mixing, as by 40 Sv pycnocline mixing and 2 Sv subtropical surface mixing. Both cases yield an annual N export of ~172 mmol.m^{-2}, with export $\delta^{15}N$ values within the range of observations. Much larger mixing terms, while still able to meet the SAZ baseline

168

[NO_3^-] and export targets, result in a surface [NO_3^-] decline from peak summer to late summer, which is not supported by upper-ocean nitrate measurements. We choose to proceed with the case of 40 Sv pycnocline mixing and 2 Sv subtropical surface mixing, as there is unlikely to be zero mixing across the STF.

The slope of the winter-to-midsummer rise in surface nitrate δ^{15}N (Fig. 4.3c) depends on the size of the nitrate assimilation isotope effect. Therefore, we can vary the SAZ isotope effect and determine which value best fits the observations. Choosing a small isotope effect, $\varepsilon = -5$‰, causes surface nitrate δ^{15}N to increase more gradually in early summer, underestimating peak nitrate δ^{15}N by ~1.3‰ and overestimating bulk export δ^{15}N by at least 0.9‰ (as weaker discrimination against the heavy isotope allows more ^{15}N to end up in biomass). Choosing a large isotope effect, $\varepsilon = -10$‰, causes surface nitrate δ^{15}N to increase more rapidly in early summer, overestimating peak nitrate δ^{15}N by ~0.8‰ and underestimating bulk export δ^{15}N by at least 0.7‰. We find that $\varepsilon = -8.3$‰ best fits the upper-ocean nitrate targets (determined by least squares) and simultaneously produces export δ^{15}N in line with observations from the Indo-Pacific SAZ/PFZ; ~1.5‰ for bulk δ^{15}N (within the observed range, 1-3‰) and ~2.4‰ for diatom-bound δ^{15}N (within but at the low end of observations, 2-6‰ or higher). Using a Monte Carlo approach based on the error (±0.5‰) in the target nitrate δ^{15}N for the mid-summer SAZ surface (the observation that determines the slope of the spring-to-midsummer δ^{15}N rise in SAZ nitrate in Fig.4.3c, and thus the isotope effect in the basic model) we estimate a standard deviation of ±1.8‰ for the isotope effect.

In isotope-*vs.*-log-concentration space (Fig. 4.4), larger isotope effects produce steeper slopes between surface and subsurface nitrate. The choice of SAZ isotope effect also has a slight influence on the modelled AZ nitrate "profiles" because of the cross-PF mixing allowed by the basic model. Unlike traditional methods of estimating the isotope effect (e.g., the Rayleigh model), ours does not assume a single, unchanging nitrate source for the duration of nitrate consumption. Therefore, a slope of -8 in isotope-*vs.*-log-concentration space (thin black line in Fig. 4.4) does not correspond exactly to the slope of the model SAZ with $\varepsilon = -8$‰ (solid orange line Fig. 4.4). Our best isotope effect estimate of ~8‰ from the basic model falls in the mid-range of early estimates based on simple isotope models (Rayleigh and steady state; Sigman et al., 1999a) and is in agreement with more recent estimates from a time-dependent one-box model (DiFiore et al., 2006), despite the use of acidified samples in previous studies. This suggests that nitrite removal by sample acidification may be less problematic for the SAZ

169

than for the AZ, where revised isotope effects (using nitrate+nitrite) are ~2‰ lower than those based on nitrate-only (Fripiat et al., 2019). Indeed, the δ^{15}N-difference between nitrate and nitrite may be smaller in the SAZ than in more polar waters (this thesis, Chapter 3, section 3.1).
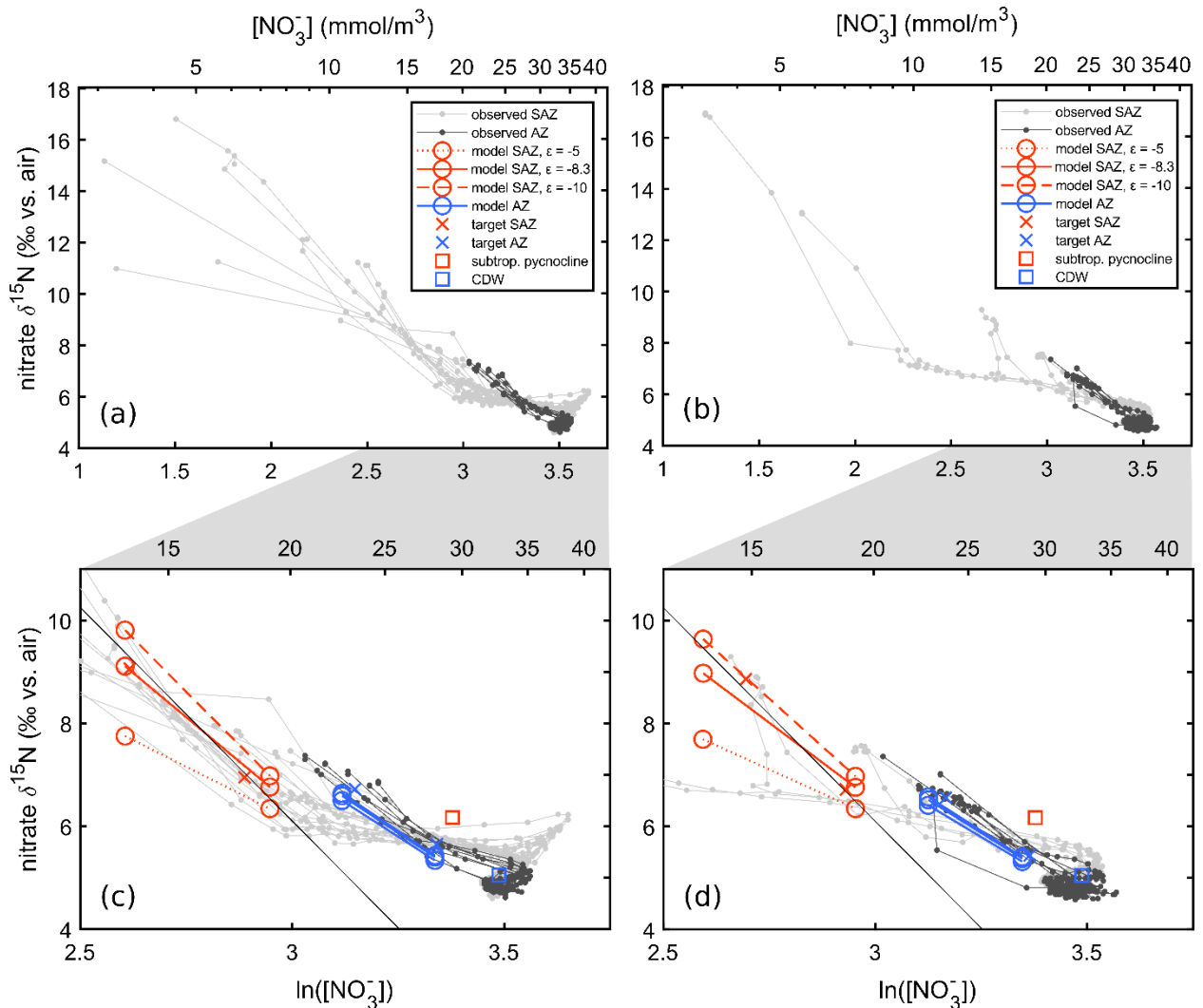
Fig. 4.4: Nitrate δ^{15}N *vs.* the natural logarithm of concentration in the Southern Ocean in (a, c) midsummer and (b, d) late summer. The upper panels (a, b) show depth profiles from cruises in the Indo-Pacific AZ (dark grey) and SAZ (light grey). In the lower panels (c, d), the same cruise profiles are compared with upper-ocean nitrate from the modelled AZ (blue circles) and SAZ (orange circles), zooming into the relevant portion of the upper panels. The composition of Circumpolar Deep Water (CDW) and subtropical pycnocline nitrate are indicated by squares (blue and orange, respectively). Model results are shown for three different SAZ isotope effects: ε = −5‰ (dotted orange line), ε = −8.3‰ (solid orange line), and ε = −10‰ (dashed orange line). The solid black line shows the slope of a hypothetical nitrate utilization trend that would result from simple Rayleigh consumption with ε = −8.3‰.

3.1.3 Limitations and short-comings

In general, the basic model does well to capture the main features of nitrate seasonality in the Southern Ocean. The clearest exception is the [NO_3^-] rise in the SAZ surface from midsummer to late summer, which the observations show but the model does not. A possible explanation for this misfit is that the basic model does not realistically simulate seasonal changes in upper-ocean water column structure (i.e., mixed-layer depth) and/or water transport. First, in the real in the ocean, surface mixed-layer deepening begins in late summer (not suddenly at the end of summer / start of winter), gradually mixing in some of the higher-[NO_3^-], lower-$\delta^{15}N$ waters of the underlying thermocline before winter begins in earnest. Second, the basic model does not account for seasonal variation in northward Ekman transport, which is estimated to be ~10 Sv larger in summer than in winter due to strengthening of the circumpolar winds (Döös, 1996). Therefore, increased summertime transport of polar-sourced nitrate into the SAZ could also contribute to the [NO_3^-]-decrease and $\delta^{15}N$-increase apparent in SAZ surface waters during late summer (when its effect is no longer masked by diatom nitrate assimilation; Fig. 4.3a).

Another discrepancy is that the modelled T_{min} and SAZ thermocline nitrate display weaker seasonality than observed. This may well be corrected by implementing seasonally varying transport and intra-seasonally varying mixed-layer depth (as explained above). If not, another possibility, at least for the SAZ, is that late-summer remineralization of organic matter in the thermocline is underestimated. Indeed, the basic model applies the biogeochemical rates of the AZ to the SAZ, which limits the total accumulation of PON in the surface layer to 1 mmol.m^{-3}. In the SAZ, suspended PON concentrations are typically higher, around 1.5-2 mmol.m^{-3} (Martiny et al., 2014). To allow biomass pools to build to higher concentrations requires modifying the rates of nutrient uptake by phytoplankton, predation by zooplankton, mortality and particle sinking. Tailoring these rates to the SAZ is the focus of the second phase of this project. For now, we discuss how SAZ biogeochemistry may differ from the AZ and how we expect these differences to affect our estimation of the isotope effect.

The PFZ, which is encompassed by the model SAZ, represents an important transition zone for biology in the Southern Ocean. In silicate-rich waters of the PFZ and further south, phytoplankton assemblages are dominated by diatoms. North of the PFZ, the phytoplankton community is typically flagellate-dominated, with a larger fractional contribution from carbonate-forming phytoplankton like coccolithophores (Hasle, 1969; Wright et al., 1996; Eynaud et al., 1999). The transition is also seen in the sinking flux as a northward shift from

171

biogenic silica- to carbonate-dominated export (Trull et al., 2001; Honjo, 2004). This raises questions about (1) the basic model's use of diatoms as the only agent of nitrate assimilation in the SAZ, and (2) the modelled ratio of diatoms to non-diatoms in the SAZ (determined by the biological rates listed above).

Concerning question (1), coccolithophores appear to be less dominant in the Pacific sector than in the Atlantic (Eynaud et al., 1999). South of the Subantarctic Front (which divides the PFZ from the SAZ), diatoms still dominate the assemblage. North of the Subantarctic Front, diatoms and coccolithophores are similarly abundant, each contributing less than 10% to total phytoplankton biomass in the Australian SAZ (Trull et al., 2018). Nevertheless, it is perhaps more appropriate to refer to the two phytoplankton groups in the basic model as "nitrate-assimilators" and "ammonium-assimilators" rather than "diatoms" and "non-diatoms". In reality, most phytoplankton are capable of both nitrate and ammonium assimilation (Waser et al. (1998); Glibert et al. (2016) and references therein), and we plan to build this capability into future versions of the model. Regarding question (2), the ratio of nitrate- to ammonium-assimilation specialists may be lower in the SAZ than in the AZ. If this is the case, higher nitrate assimilation rates may be required for a smaller population of nitrate-assimilators to cause the same degree of nitrate drawdown. Such modifications to SAZ biological rates are likely to affect the concentration and δ^{15}N of surface ocean biomass and export. However, we do not expect our isotope effect estimate to change substantially. The reason for this is that the size of the isotope effect is dictated by the nitrate observations, specifically, the δ^{15}N-difference between the modelled winter mixed-layer nitrate (largely set by the preceding SAZ thermocline δ^{15}N, measured in late summer) and the observed mid-summer surface nitrate.

4. Conclusions & Future Directions

This study provides proof of concept for estimating the SAZ isotope effect of nitrate assimilation from a seasonal model of the Southern Ocean. Our initial estimate of 8.3±1.8‰ is in agreement with that of DiFiore et al. (2006), despite their use of acidified samples. This suggests that nitrite removal by sample acidification may not have compromised isotope effect estimation in the SAZ to the same degree as in the AZ (Fripiat et al., 2019). Nonetheless, the difference between nitrate-only- *vs.* nitrate+nitrite-based estimates of the isotope effect may become discernable as we improve the accuracy and precision of our model input and target

values. Such a high isotope effect of ~8‰ sets the SAZ apart from other nitrate-rich regions, including the adjacent AZ (Sigman et al., 1999a; DiFiore et al., 2009; Fripiat et al., 2019), the subarctic North Pacific (Wu et al., 1997; Brunelle, 2009) and the equatorial Pacific (Altabet, 2001; Rafter & Sigman, 2016). Explaining this apparent deviation is important for understanding the controls on the isotope effect of nitrate assimilation, and thus determining how likely it is that such conditions have changed through glacial-interglacial cycles. An example of how a temporally variable isotope effect could influence interpretation of Subantarctic foraminifer-bound δ^{15}N records is as follows: a smaller isotope effect during glacial periods would yield particulate N (and thus also foraminifera) that have a higher δ^{15}N than those deriving from the same degree of nitrate consumption but a larger isotope effect (because of weaker discrimination against ^{15}N-containing nitrate under glacial conditions). Assuming a constant isotope effect through climate transitions would, therefore, lead to overestimation of Subantarctic nitrate (and thus CO_2) drawdown associated with ice-age peaks in foraminifer-bound δ^{15}N.

In future, we plan to incorporate more of the global nitrate isotope database to yield more robust mean Southern Ocean and sector-specific estimates for the SAZ isotope effect. The addition of oxygen isotopes to the model will provide additional constraints on biogeochemical rates like nitrification (which affects the N and O isotopes of nitrate differently). Next steps include sensitivity testing (to identify the input parameters most important to constrain), evaluating model uncertainty (using a Monte Carlo approach), and implementing a scoring system (to more objectively minimize differences between model outputs and observations). By reducing uncertainty regarding this key parameter of SAZ nutrient dynamics, this study contributes to improving paleo-reconstructions from the δ^{15}N archives of the Southern Ocean.

5. Acknowledgements

6. References

Abernathey, R.P., Cerovecki, I., Holland, P.R., Newsom, E., Mazloff, M., & Talley, L.D. 2016. Water-mass transformation by sea ice in the upper branch of the Southern Ocean overturning. *Nat. Geosci.*, **9**(8), 596–601.

Altabet, M.A. 1988. Variations in nitrogen isotopic composition between sinking and suspended particles: Implications for nitrogen cycling and particle transformation in the open ocean. *Deep-Sea Res. Pt I*, **35**, 535–554.

Altabet, M.A. 2001. Nitrogen isotopic evidence for micronutrient control of fractional NO_3^- utilization in the equatorial Pacific. *Limnol. Oceanogr.*, **46**(2), 368–380.

Altabet, M.A., & François, R. 1994. Sedimentary nitrogen isotopic ratio as a recorder for surface ocean nitrate utilization. *Global Biogeochem. Cycles*, **8**(1), 103–116.

Altabet, M.A., & François, R. 2001. Nitrogen isotope biogeochemistry of the Antarctic Polar Frontal Zone at 170°W. *Deep-Sea Res. Pt II*, **48**, 4247–4273.

Altabet, M.A., & Small, L.F. 1990. Nitrogen isotopic ratios in fecal pellets produced by marine zooplankton. *Geochim. Cosmochim. Acta*, **54**, 155–163.

Bard, E., & Rickaby, R.E.M. 2009. Migration of the subtropical front as a modulator of glacial climate. *Nature*, **460**, 380–384.

Brunelle, B.G. 2009. *Nitrogen isotope constraints on the biogeochemistry and paleoclimatology of the subarctic North Pacific*. Ph.D. thesis, Princeton University, USA.

Brunelle, B.G., Sigman, D.M., M.S., Cook, Keigwin, L.D., Haug, G.H., Plessen, B., Schettler, G., & Jaccard, S.L. 2007. Evidence from diatom-bound nitrogen isotopes for subarctic

174

Pacific stratification during the last ice age and a link to North Pacific denitrification changes. *Paleoceanography*, **22**, PA1215.

Capone, D.G., Bronk, D.A., Mulholland, M.R., & Carpenter, E.J. (eds). 2008. *Nitrogen in the marine environment*. Burlington, MA: Academic Press.

Casciotti, K.L., Sigman, D.M., & Ward, B.B. 2003. Linking Diversity and Stable Isotope Fractionation in Ammonia-Oxidizing Bacteria. *Geomicrobiol. J.*, **20**, 335–353.

Checkley, D.M., & Miller, C.A. 1989. Nitrogen isotope fractionation by oceanic zooplankton. *Deep-Sea Res. Pt A*, **36**, 1449–1456.

DiFiore, P.J., Sigman, D.M., Trull, T.W., Lourey, M.J., Karsh, K., Cane, G., & Ho, R. 2006. Nitrogen isotope constraints on Subantarctic biogeochemistry. *J. Geophys. Res.*, **111**(C08016).

DiFiore, P.J., Sigman, D.M., & Dunbar, R.B. 2009. Upper ocean nitrogen fluxes in the Polar Antarctic Zone: Constraints from the nitrogen and oxygen isotopes of nitrate. *Geochemistry Geophysics Geosystems*, **10**(Q11016).

DiFiore, P.J., Sigman, D.M., Karsh, K.L., Trull, T.W., Dunbar, R.B., & Robinson, R.S. 2010. Poleward decrease in the isotope effect of nitrate assimilation across the Southern Ocean. *Geophys. Res. Lett.*, **37**(L17601).

Dong, S., Sprintall, J., Gille, S.T., & Talley, L. 2008. Southern Ocean mixed-layer depth from Argo float profiles. *J. Geophys. Res.*, **113**(C06013), 1–12.

Döös, K. 1996. The meridional circulation in the Southern Ocean and its seasonal variability as seen by the fine resolution Antarctic model. *J. Geophys. Res.*, **101**(C3), 6393– 6407.

Dufour, C.O., Griffies, S.M., de Souza, G.F., Frenger, I., Morrison, A.K., J.B., Palter, Sarmiento, J.L., Galbraith, E.D., Dunne, J.P., Anderson, W.G., & Slater, R.D. 2015. Role of Mesoscale Eddies in Cross-Frontal Transport of Heat and Biogeochemical Tracers in the Southern Ocean. *J. Phys. Oceanogr.*, **45**, 3057–3081.

Eynaud, F., Giraudeau, J., Pichon, J.-J., & Pudsey, C.J. 1999. Sea-surface distribution of coccolithophores, diatoms, silicoflagellates and dinoflagellates in the South Atlantic Ocean during the late austral summer 1995. *Deep Sea Res. Part I*, **46**, 451–482.

François, R., Altabet, M.A., & Burckle, L.H. 1992. Glacial to interglacial changes in surface nitrate utilization in the Indian sector of the Southern Ocean as recorded by sediment δ^{15}N. *Paleoceanography*, **7**(5), 589–606.

Fripiat, F., Martínez-García, A., Fawcett, S.E., Kemeny, P.C., Studer, A.S., Smart, S.M., Rubach, F., Oleynik, S., Sigman, D.M., & Haug, G.H. 2019. The isotope effect of nitrate assimilation in the Antarctic Zone: Improved estimates and paleoceanographic implications. *Geochimica et Cosmochimica Acta*.

Glibert, P.M., Wilkerson, F.P., Dugdale, R.C., Raven, J.A., Dupont, C.L., Leavitt, P.R., Parker, A.E., Burkholder, J.M., & Kana, T.M. 2016. Pluses and minuses of ammonium and nitrate uptake and assimilation by phytoplankton and implications for productivity and community composition, with emphasis on nitrogen-enriched conditions. *Limnol. Oceanogr.*, **61**, 165–197.

Hasle, G.R. 1969. An analysis of the phytoplankton of the Pacific Southern Ocean: abundance, composition and distribution during the Brategg Expedition 1947-1948. *Halvaradets Skr. Science of Royal Marine Biology Research*, **52**, 1–168.

Hayes, J.M. 2004. *An introduction to isotopic calculations*. Woods Hole, MA: Woods Hole Oceanographic Institution.

Honjo, S. 2004. Particle export and the biological pump in the Southern Ocean. *Antarct. Sci.*, **16**(4), 501–516.

Johnson, K.S., Plant, J.N., Dunne, J.P., Talley, L.D., & Sarmiento, J.L. 2017. Annual nitrate drawdown observed by SOCCOM profiling floats and the relationship to annual net community production. *J. Geophys. Res. Oceans*, **122**, 6668–6683.

Karsh, K.L., Trull, T.W., Lourey, M.J., & Sigman, D.M. 2003. Relationship of nitrogen isotope fractionation to phytoplankton size and iron availability during the Southern Ocean Iron RElease Experiment (SOIREE). *Limnol. Oceanogr.*, **48**(3), 1058–1068.

Karsten, R.H., & Marshall, J. 2002. Constructing the residual circulation of the ACC from observations. *J. Phys. Oceanogr.*, **32**(12), 3315–3327.

Kemeny, P.C., Weigand, M.A., Zhang, R., Carter, B.R., Karsh, K.L., Fawcett, S.E., & Sigman, D.M. 2016. Enzyme-level interconversion of nitrate and nitrite in the fall mixed layer of the Antarctic Ocean. *Global Biogeochem. Cycles*, **30**, 1069–1085.

Kemeny, P.C., Kast, E.R., Hain, M.P., Fawcett, S.E., Fripiat, F., Studer, A.S., Martínez-García, A., Haug, G.H., & Sigman, D.M. 2018. A Seasonal Model of Nitrogen Isotopes in the Ice Age Antarctic Zone: Support for Weakening of the Southern Ocean Upper Overturning Cell. *Paleoceanography and Paleoclimatology*.

Knox, F., & McElroy, M.B. 1984. Changes in atmospheric CO_2: influence of the marine biota at high latitude. *J. Geophys. Res.*, **89**, 4629–4637.

Lehmann, M.F., Bernasconi, S.M., Barbieri, A., & McKenzie, J.A. 2002. Preservation of organic matter and alteration of its carbon and nitrogen isotope composition during simulated and in situ early sedimentary diagenesis. *Geochim. Cosmochim. Acta*, **66**(20), 3573–3584.

Lourey, M.J., & Trull, T.W. 2001. Seasonal nutrient depletion and carbon export in the Subantarctic and Polar Frontal Zones of the Southern Ocean south of Australia. *J. Geophys. Res.*, **106**(C12), 31463–31487.

Lourey, M.J., Trull, T.W., & Sigman, D.M. 2003. Sensitivity of $\delta^{15}N$ of nitrate, surface suspended and deep sinking particulate nitrogen to seasonal nitrate depletion in the Southern Ocean. *Global Biogeochem. Cycles*, **17**(3), 1–18.

Mariotti, A., Germon, J.C., Hubert, P., Kaiser, P., Letolle, R., Tardieux, A., & Tardieux, P. 1981. Experimental determination of nitrogen kinetic isotope fractionation: Some principles; illustration for the denitrification and nitrification processes. *Plant Soil*, **62**, 413–430.

Martin, J.H. 1990. Glacial-interglacial CO_2 Change: The Iron Hypothesis. *Paleoceanography*, **5**(1), 1–13.

Martínez-García, A., Rosell-Melé, A., Geibert, W., Gersonde, R., Masqué, P., Gaspari, V., & Barbante, C. 2009. Links between iron supply, marine productivity, sea surface temperature, and CO_2 over the last 1.1 Ma. *Paleoceanography*, **24**(PA1207).

Martínez-García, A., Rosell-Melé, A., Jaccard, S.L., Geibert, W., Sigman, D.M., & Haug, G.H. 2011. Southern Ocean dust–climate coupling over the past four million years. *Nature*, **476**, 312–315.

Martínez-García, A., Sigman, D.M., Ren, H., Anderson, R.F., Straub, M., Hodell, D.A., Jaccard, S.L., Eglinton, T.I., & Haug, G.H. 2014. Iron Fertilization of the Subantarctic Ocean During the Last Ice Age. *Science*, **343**, 1347–1350.

Martiny, A.C., Vrugt, J.A., & Lomas, M.W. 2014. Concentrations and ratios of particulate organic carbon, nitrogen, and phosphorus in the global ocean. *Sci. Data*, **1**(140048).

Meckler, A.N., Ren, H., Sigman, D.M., Gruber, N., Plessen, B., Schubert, C.J., & Haug, G.H. 2011. Deglacial nitrogen isotope changes in the Gulf of Mexico: evidence from bulk sedimentary and foraminifera-bound nitrogen in Orca Basin sediments. *Paleoceanography*, **26**(PA4216), 1–13.

Morales, L.V., Sigman, D.M., Horn, M.G., & Robinson, R.S. 2013. Cleaning methods for the isotopic determination of diatom-bound nitrogen in non-fossil diatom frustules. *Limnol. Oceanogr. Methods*, **11**(2), 101–112.

Morales, L.V., Granger, J., Chang, B.X., Prokopenko, M.G., Plessen, B., Gradinger, R., & Sigman, D.M. 2014. Elevated ^{15}N/^{14}N in particulate organic matter, zooplankton, and diatom frustule-bound nitrogen in the ice-covered water column of the Bering Sea eastern shelf. *Deep Sea Res. Part II*, **109**, 100–111. Understanding Ecosystem Processes in the Eastern Bering Sea III.

Pennock, J.R., Velinsky, D.J., Ludlam, J.M., Sharp, J.H., & Fogel, M.L. 1996. Isotope fractionation of ammonium and nitrate during their uptake by Skeletonema Costatum: Implications for the δ^{15}N dynamics under bloom conditions. *Limnol. Oceanogr.*, **41**(3), 451–459.

Rafter, P.A., & Sigman, D.M. 2016. Spatial distribution and temporal variation of nitrate nitrogen and oxygen isotopes in the upper equatorial Pacific Ocean. *Limnol. Oceanogr.*, **61**, 14–31.

Rafter, P.A., DiFiore, P.J., & Sigman, D.M. 2013. Coupled nitrate nitrogen and oxygen isotopes and organic matter remineralization in the Southern and Pacific Oceans. *J. Geophys. Res.*, **118**, 4781–4794.

Ren, H., Sigman, D.M., Meckler, A.N., Plessen, B., Robinson, R.S., Rosenthal, Y., & Haug, G.H. 2009. Foraminiferal Isotope Evidence of Reduced Nitrogen Fixation in the Ice Age Atlantic Ocean. *Science*, **323**, 244–248.

Ren, H., Sigman, D.M., Thunell, R.C., & Prokopenko, M.G. 2012. Nitrogen isotopic composition of planktonic foraminifera from the modern ocean and recent sediments. *Limnol. Oceanogr.*, **57**(4), 1011–1024.

Robinson, R.S., & Sigman, D.M. 2008. Nitrogen isotopic evidence for a poleward decrease in surface nitrate within the ice age Antarctic. *Quat. Sci. Rev.*, **27**, 1076–1090.

Robinson, R.S., Brunelle, B.G., & Sigman, D.M. 2004. Revisiting nutrient utilization in the glacial Antarctic: evidence from a new diatom-bound N isotope method. *Paleoceanography*, **19**(PA3001), 1–13.

Robinson, R.S., Kienast, M., Albuquerque, A.L., Altabet, M., Contreras, S., De Pol Holz, R., Dubois, N., François, R., Galbraith, E., Hsu, T-C., Ivanochko, T., Jaccard, S., Kao, S-J, Kiefer, T., Kienast, S., Lehmann, M., Martinez, P., McCarthy, M., Möbius, J., Pedersen, T., Quan, T.M., Ryabenko, E., Schmittner, A., Schneider, R., Schneider-Mor, A., Shigemitsu, M., Sinclair, D., Somes, C., Studer, A., Thunell, R., & Yang, J-Y. 2012. A review of nitrogen isotopic alteration in marine sediments. *Paleoceanography*, **27**(PA4203).

Rubin, S.I., Takahashi, T., D.W., Chipman, & Goddard, J.G. 1998. Primary productivity and nutrient utilization ratios in the Pacific sector of the Southern Ocean based on seasonal changes in seawater chemistry. *Deep Sea Res. Part I*, **45**(8), 1211–1234.

Sambrotto, R.N., & Mace, B.J. 2000. Coupling of biological and physical regimes across the Antarctic Polar Front as reflected by nitrogen production and recycling. *Deep Sea Res. Part II*, **47**(15-16), 3339–3367.

Sarmiento, J.L., & Toggweiler, J.R. 1984. A new model for the role of the oceans in determining atmospheric pCO_2. *Nature*, **308**, 621–624.

Sarthou, G., Timmermans, K.R., Blain, S., & Tréguer, P. 2005. Growth physiology and fate of diatoms in the ocean: A review. *J. Sea Res.*, **53**(1–2), 25–42.

Siegenthaler, U., & Wenk, T. 1984. Rapid atmospheric CO_2 variations and ocean circulation. *Nature*, **308**, 624–626.

Sigman, D.M., Altabet, M.A., McCorkle, D.C., François, R., & Fischer, G. 1999a. The $\delta^{15}N$ of nitrate in the Southern Ocean: Consumption of nitrate in surface waters. *Global Biogeochem. Cycles*, **13**(4), 1149–1166.

Sigman, D.M., Altabet, M.A., François, R., McCorkle, D.C., & Gaillard, J.F. 1999b. The isotopic composition of diatom-bound nitrogen in Southern Ocean sediments. *Paleoceanography*, **14**(2), 118–134.

Sigman, D.M., Altabet, M.A., McCorkle, D.C., François, R., & Fischer, G. 2000. The $\delta^{15}N$ of nitrate in the Southern Ocean: Nitrogen cycling and circulation in the ocean interior. *J. Geophys. Res.*, **105**(C8), 19599–19614.

Smart, S.M., Fawcett, S.E., Thomalla, S.J., Weigand, M.A., Reason, C.J.C., & Sigman, D.M. 2015. Isotopic evidence for nitrification in the Antarctic winter mixed layer. *Global Biogeochem. Cycles*, **29**.

Straub, M., Sigman, D.M., Ren, H., Martínez-García, A., Nele Meckler, A., & Haug, G.H. 2013. Changes in North Atlantic nitrogen fixation controlled by ocean circulation. *Nature*, **501**, 200–204.

Studer, A.S., Sigman, D.M., Martínez-García, A., Benz, V., Winckler, G., Kuhn, G., Esper, O., Lamy, F., Jaccard, S.L., Wacker, L., Oleynik, S., Gersonde, R., & Haug, G.H. 2015. Antarctic Zone nutrient conditions during the last two glacial cycles. *Paleoceanography*, **30**(7), 845–862. 2014PA002745.

Tagliabue, A., Sallée, J.B., Bowie, A.R., Lévy, M., Swart, S., & Boyd, P.W. 2014. Surface-water iron supplies in the Southern Ocean sustained by deep winter mixing. *Nat. Geosci.*, **7**(4), 314–320.

Trull, T., Bray, S., Manganini, S., Honjo, S., & François, R. 2001. Moored sediment trap measurements of carbon export in the Sub-Antarctic and Polar Frontal zones of the Southern Ocean, south of Australia. *J. Geophys. Res.*, **106**(C12), 31489–31509.

Trull, T.W., Passmore, A., Davies, D.M., Smit, T., Berry, K., & Bronte Tilbrook, B. 2018. Distribution of planktonic biogenic carbonate organisms in the Southern Ocean south of Australia: a baseline for ocean acidification impact assessment. *Biogeosciences*, **15**, 31–49.

Wada, E., & Hattori, A. 1978. Nitrogen isotope effects in the assimilation of inorganic nitrogenous compounds by marine diatoms. *Geomicrobiol. J.*, **1**(1), 85–101.

Wang, X.T., Prokopenko, M.G., Sigman, D.M., Adkins, J.F., Robinson, L.F., Ren, H., Oleynik, S., Williams, B., & Haug, G.H. 2014. Isotopic composition of carbonate-bound organic nitrogen in deep-sea scleractinian corals: A new window into past biogeochemical change. *Earth Planet. Sci. Lett.*, **400**, 243–250.

Wang, X.T., Sigman, D.M., Cohen, A.L., Sinclair, D.J., Sherrell, R.M., K.M., Cobb, Erler, D.V., Stolarski, J., Kitahara, M.V., & Ren, H. 2016. Influence of open ocean nitrogen supply on the skeletal ä^1^5N of modern shallow-water scleractinian corals. *Earth Planet. Sci. Lett.*, 125–132.

Waser, N.A.D., Harrison, P.J., Nielsen, B., Calvert, S.E., & Turpin, D.H. 1998. Nitrogen Isotope Fractionation During the Uptake and Assimilation of Nitrate, Nitrite, Ammonium, and Urea by a Marine Diatom. *Limnol. Oceanogr.*, **43**(2), 215–224.

Wright, S.W., Thomas, D.P., Marchant, H.J., Higgins, H.W., Mackey, M.D., & Mackey, D.J. 1996. Analysis of phytoplankton of the Australian sector of the Southern Ocean: Comparison of microscopy and size frequency data with interpretations of pigment HPLC data using the 'CHEMTAX' matrix factorization program. *Mar. Ecol. Prog. Ser.*, **144**(1), 285–298.

Wu, J., Calvert, S.E., & Wong, C.S. 1997. Nitrogen isotope variations in the subarctic northeast Pacific: relationships to nitrate utilization and trophic structure. *Deep-Sea Res.*, **44**(2), 287–314.

CHAPTER 5: Conclusions & Future Directions

The work presented in this thesis confirms the utility of planktic foraminifera as recorders of upper-ocean N dynamics. At the same time, it reveals that the $\delta^{15}N$ of organic matter in modern foraminifer shells is set by the complex interplay of a number of processes, rather than by a singular, direct dependence on nitrate. This more nuanced picture of the foraminifer-bound $\delta^{15}N$ proxy afforded by modern-ocean observations presents both a challenge and an opportunity for its interpretation from the sedimentary archive. Encouragingly, ground-truthing the foraminifer-bound $\delta^{15}N$ paleo-proxy in two contrasting nutrient regimes of the modern ocean has independently led to several of the same conclusions. First, living foraminifera exhibit a close relationship between bulk tissue and shell-bound $\delta^{15}N$, supporting the interpretation of shell-bound $\delta^{15}N$ (at least the original composition, before sinking) as a measure of the $\delta^{15}N$ of the living organism. Second, foraminifer $\delta^{15}N$ is more closely tied to the $\delta^{15}N$ of particulate N than to that of dissolved nitrate, consistent with foraminifera acquiring most (if not all) of their N from their diet. Third (as a consequence of the second), foraminifer $\delta^{15}N$ is influenced by upper-ocean N recycling and therefore has the potential to stray from the present-day relationships with nitrate $\delta^{15}N$ in both subtropical and subpolar environments.

In the present-day Sargasso Sea, several factors appear to work together to cause the $\delta^{15}N$ of dinoflagellate-bearing foraminifer species to approximate the $\delta^{15}N$ of the modern nitrate supply: (a) their dinoflagellate symbionts weakening their $\delta^{15}N$ elevation relative to their diet, (b) the lowering of particulate $\delta^{15}N$ due to ammonium recycling in late-summer surface waters, (c) their diet consisting of zooplankton and eukaryotic phytoplankton, the main components of the subtropical export flux, and (d) the complete consumption of nitrate in surface waters (such that $\delta^{15}N$ export $\approx \delta^{15}N$ supply). This balance could change if ammonium-based production (factor (b), above) were more or less important relative to nitrate-based production.

In the modern Southern Ocean, seasonal changes in the $\delta^{15}N$ of bulk particles and the foraminifera that feed upon them reflect late-summer ammonium recycling (lowering $\delta^{15}N$) and wintertime particle decomposition (raising $\delta^{15}N$). The effect of the former outweighs the latter in terms of its influence on the $\delta^{15}N$ of foraminifera sinking to the seafloor each year, yet both signals are likely weak compared to the productive spring/mid-summer, which dominates the present-day sinking flux (evident from previously reported sediment trap data). Therefore, if the current mode of seasonality were maintained through past climate cycles, downcore

183

changes in foraminifer $\delta^{15}N$ would closely approximate changes in the $\delta^{15}N$ of nitrate consumed in surface waters (which varies with the degree of nitrate assimilation) since bulk particle $\delta^{15}N$ and nitrate consumption are tightly linked during spring/mid-summer. If, on the other hand, the seasonal cycle were different in the past, this could complicate interpretation of high-latitude fossil-bound $\delta^{15}N$ records. For example, an extended winter season in the ice-age Southern Ocean might lead to a larger proportion of high-$\delta^{15}N$ shells (from foraminifera with a diet of more-degraded particles) in glacial sediments, which could be mistaken for more complete nitrate consumption in surface waters. However, the availability of wintertime PON is ultimately tied to biological production in the spring and summer seasons. Thus, the representation of the high-$\delta^{15}N$ winter signal in the foraminifera flux to the sediment likely scales with the spring+midsummer production signal (and, thus, the degree of nitrate drawdown), holding steady the ratio of spring+midsummer to winter shells. If such seasonal scaling effects apply more broadly (e.g., tying late-summer ammonium-based production to spring+midsummer nitrate-based production), it would limit the capacity for foraminifera-bound $\delta^{15}N$ records to become decoupled from the isotope dynamics of nitrate assimilation during climate transitions. This idea remains to be tested.

The ecological diversity among planktic foraminifer species could hold the key to disentangling changes in nitrate utilization from any changes in the seasonal cycle. Differences in the timing of peak abundances among species cause their shells to represent upper-ocean conditions at different times of year. Similarly, differences in depth habitat and dietary preferences cause different species to record different components of seasonal production (e.g., nitrate- *vs.* ammonium-supported production, or living prey *vs.* detrital material). In this way, coupled $\delta^{15}N$ measurements of complementary foraminifer species (e.g., spring- *vs.* summer-peaking, or surface- *vs.* deep-dwelling) from the same sediment core could enable the reconstruction of the ocean's past N cycle in unprecedented detail. Tapping into this capability calls for a comprehensive understanding of both the common and species-specific $\delta^{15}N$ signals recorded in foraminifer shell-bound organic matter.

The finding of a weak $\delta^{15}N$ increase (by ~0.6‰) in sinking shells within the upper 500 m of the subtropical water column compared to near-surface tow-caught shells (proposed to be the result of partial dissolution) requires further investigation. Measurements of foraminifer-bound $\delta^{15}N$ from multi-depth net tows and sediment traps from a range of environments would help to determine whether this observation is robust and widespread. In addition, emerging

184

techniques for analysing the isotopic composition of specific compounds (e.g., amino acids) and mapping the distributions of organic matter within single foraminifer shells offer a means to test the hypotheses presented in this work, including the partial dissolution of shells (or shell portions) mentioned above. Such techniques, applied to field-collected and laboratory-cultured foraminifera, promise to provide new insight into questions of organic N incorporation and preservation.

An overarching concern for all $\delta^{15}N$ paleo-proxies is uncertainty regarding the magnitude of the isotope effect of nitrate assimilation and whether it has changed through past climate cycles. This concern is especially warranted for the Subantarctic Ocean, where even the modern-day isotope effect is elusive and poorly constrained (to between ~5‰ and ~11‰). This thesis approaches the problem using a multi-annual, seasonally resolved geochemical box model of the Southern Ocean, which is better suited than traditional isotope models to deal with the complex nitrate supply and consumption regime of the region. Initial results from the model study suggest a nitrate assimilation isotope effect of ~8‰ for the Subantarctic Zone, which is >2‰ higher than that determined for its polar neighbour, the Antarctic Zone. It is not yet clear what could cause the isotope effect to be higher in the Subantarctic than in other nitrate-rich regions, but it may be related to the deeper mixed layer that characterizes this zone and/or the relationship of the mixed layer with euphotic depth.

If further testing and model improvements verify the finding of a spatially variable nitrate assimilation isotope effect, this would imply that a temporally variable isotope effect cannot be ruled out. An example of how such a time-varying isotope effect could affect interpretation of Subantarctic foraminifer-bound $\delta^{15}N$ records is as follows: a lower isotope effect during ice ages (whether due to a northward shift of Antarctic waters over the core site, or a local change in Subantarctic mixed-layer and/or euphotic depth) would yield particles (and therefore also foraminifera) that are higher in $\delta^{15}N$ than those resulting from the same degree of nitrate consumption but with a larger isotope effect (due to weaker discrimination against ^{15}N-bearing nitrate in the ice-age case). Not accounting for such changes in the isotope effect but instead assuming it has been constant through time (a fairly common practice in paleoceanographic studies) could lead one to misinterpret the glacial peaks in foraminifer-bound $\delta^{15}N$ through the record as reflecting more-complete nitrate consumption, supporting the role of the Subantarctic as a reinforcing actor in the ice-age drawdown of CO_2 when this may not have been the case.

Now more than ever, a mechanistic comprehension of the internal feedbacks that regulate our planet's climate system is called for. Recognizing and understanding the physical and biogeochemical changes that have accompanied major climatic transitions of the past will better equip us to navigate the high-CO_2 world ahead.